CARL VON OSSIETZKY universität OLDENBURG

Activation mechanism of photoreceptor membrane bound Guanylate Cyclase

Von der Fakultät für Medizin und Gesundheitswissenschaften
der Carl von Ossietzky Universität Oldenburg
Zur Erlangung des Grades und Titels eines

Doktors der Naturwissenschaften (Dr. rer. nat.)

angenommene Dissertation

von
Manisha Kumari Shahu
geboren am 20.03.1991 in Imphal, Manipur, India

Betreuender Gutachter: Prof. Dr. Karl-Wilhelm Koch
Zweitgutachter: Prof. Dr. Michael Winklhofer
Tag der Disputation: 02.10.2025

Table of Contents

Abstract

The guanylate cyclase (GC) system in photoreceptor cells is a cornerstone of phototransduction, providing the biochemical processes that allow adaptation to fluctuating light conditions through the regulated synthesis of guanosine-3',5'-cyclic monophosphate (cGMP) controlled by intracellular calcium-sensor proteins known as guanylate cyclase activating proteins (GCAPs). These sensors respond to fluctuations in intracellular Ca^{2+} levels by switching between an inhibitory Ca^{2+}-bound state and a stimulatory Mg^{2+}-bound form, thereby fine-tuning the activity of guanylate cyclase-E (GC-E), a membrane-bound, retinal specific isoform of GC. Disruptions in this feedback mechanism, often caused by mutations in the gene encoding GC-E or GCAPs, are associated with various inherited retinal dystrophies.

Despite considerable progress, the precise molecular mechanisms underlying GC-E activation remain incompletely understood, largely due to structural complexity and experimental limitations. This thesis investigates the molecular processes that transition GC-E from an inactive to an active state. A combination of biochemical assays and computational modelling was used to evaluate the hypothesis of conformational modulation via rotation of transmembrane domains and catalytic domain rearrangement. Contrary to the hypothesis that a helical rotation mediates activation (prevailing in hormone-sensitive GC-A), our data did not support the presence of an α-helical rotation mechanism in GC-E.

A major focus of this work was the characterization of the disease-associated V902L GC-E mutant, which showed constitutive activation in the absence of GCAPs. Through kinetic and structural analyses, it was found that the mutation mimics the GCAP-stabilized active state; rather than rotational movements, activation appears to involve a swinging motion in the dimerization domain, which serves as a critical conformational switch. Futhermore, the V902L mutant demonstrated a Ca^{2+}-dependent modulation of cyclase activity, independent of GCAP mediation, consistent with a two-metal ion catalytic mechanism involving competitive interactions between Mg^{2+} and Ca^{2+} at the active site.

Additional mutagenesis studies targeting a conserved helix-turn-helix motif at residue L804 further revealed a long-range allosteric communication pathway within the GC-E protein. Alteration in this motif modulated enzyme catalytic efficiency without abolishing function, highlighting how long-range structural coupling contributes to enzymatic control. Computational connectivity analysis underscored the altered allosteric network in the V902L mutant compared to wild-type, offering a mechanistic explanation for its gain-of-function phenotype.

Complementing this work, structural characterization of GCAP5 expressed in the zebrafish retina provides insight into the dimerization behavior and metal-ion sensitivity of GCAP5 and homologous regulatory proteins. Using NMR and EPR-DEER spectroscopy, we resolved the structure of GCAP5 in its activating state and identified specific hydrophobic and electrostatic interactions stabilizing the dimer. Notably, the two non-conserved cysteine residues in GCAP5

enable Fe^{2+}-binding, potentially linking metal ion availability to cyclase regulation in species-specific contexts.

Taken together, these findings advance our understanding of the diverse structural and regulatory mechanisms that govern photoreceptor guanylate cyclases and their modulators. They offer valuable insights into the conformational transitions that underlie enzymatic activation and shed light on molecular dysfunctions that contribute to inherited retinal diseases. By integrating biochemical, structural, and computational modelling this work provides a more comprehensive framework for elucidating the fine regulation of cGMP signaling in visual transduction, under both physiological and pathological conditions.

Zusammenfassung

Das Guanylatzyklase (GC)-System in Photorezeptorzellen ist ein Eckpfeiler der visuellen Phototransduktion. Es stellt die biochemischen Prozesse bereit, die die Anpassung an schwankende Lichtbedingungen durch die regulierte Synthese von Guanosin-3',5'-zyklisches Monophosphat (cGMP) ermöglichen, die von intrazellulären Kalzium-Sensorproteinen, den so genannten Guanylatzyklase-aktivierenden Proteinen (GCAPs), gesteuert wird. Diese Sensoren reagieren auf Schwankungen des intrazellulären Ca^{2+}-Spiegels, indem sie zwischen einem hemmenden Ca^{2+}-gebundenen Zustand und einer stimulierenden Mg^{2+}-gebundenen Form wechseln und so die Aktivität der Guanylatzyklase-E (GC-E), einer membrangebundenen, retinaspezifischen Isofrom der GC, fein abstimmen. Störungen in diesem Rückkopplungsmechanismus, die häufig durch Mutationen in den GC- oder GCAP-Genen verursacht werden, sind mit verschiedenen vererbten Netzhautdystrophien verbunden.

Trotz erheblicher Fortschritte sind die genauen molekularen Mechanismen, die der GC-E-Aktivierung zugrunde liegen, nach wie vor unvollständig verstanden, was vor allem auf die strukturelle Komplexität und experimentellen Beschränkungen zurückzuführen ist. In dieser Arbeit werden die molekularen Prozesse untersucht, die GC-E von einem inaktiven in einen aktiven Zustand überführen. Die Hypothese einer Konformationsmodulation durch Rotation der Transmembrandomänen und Umlagerung der katalytischen Domäne wurde mit Hilfe einer Kombination aus biochemischen Assays und computergestützter Modellierung untersucht. Im Gegensatz zu der Hypothese, dass eine helikale Rotation die Aktivierung vermittelt (vorherrschend bei der hormonsensitiven GC-A), unterstützen unsere Daten nicht das Vorhandensein eines α-helikalen Rotationsmechanismus in GC-E.

Ein Hauptaugenmerk dieser Arbeit lag auf der Charakterisierung der krankheitsassoziierten V902L GC-E-Mutante, die in Abwesenheit von GCAPs eine konstitutiv aktiv ist. Durch kinetische und strukturelle Analysen wurde festgestellt, dass die Mutation den GCAP-stabilisierten aktiven Zustand nachahmt; anstelle von Rotationsbewegungen scheint die Aktivierung eine Schwingungsbewegung in der Dimerisierungsdomäne zu beinhalten, die als kritischer Konformationsschalter dient. Darüber hinaus zeigte die V902L-Mutante eine Ca^{2+}-abhängige Modulation der Cyclase-Aktivität, unabhängig von der GCAP-Vermittlung, was mit einem katalytischen Zwei-Metallionen-Mechanismus übereinstimmt, der kompetitive Wechselwirkungen zwischen Mg^{2+} und Ca^{2+} am aktiven Zentrum beinhaltet.

Zusätzliche Mutagenese-Studien, die auf ein konserviertes Helix-Turn-Helix-Motiv am Rest L804 abzielten, deckten einen weitreichenden allosterischen Kommunikationsweg innerhalb des GC-E-Proteins auf. Die Veränderung dieses Motivs modulierte die katalytische Effizienz des Enzyms, bei prinzipieller Erhaltung der Funktion. Diese Ergebnisse deuteten an, dass eine strukturelle Kopplung über große Abstände im Protein zur enzymatischen Kontrolle beiträgt. Computergestützte Konnektivitätsanalysen unterstrichen das veränderte allosterische Netzwerk in der V902L-Mutante im Vergleich zum Wildtyp und boten eine mechanistische Erklärung für den Phänotyp der Funktionssteigerung.

Ergänzend zu dieser Arbeit gibt die strukturelle Charakterisierung von GCAP5 aus der Zebrafischretina Aufschluss über das Dimerisierungsverhalten und die Empfindlichkeit von GCAP5 und homologer regulatorischer Proteine gegenüber Metallionen. Mithilfe von NMR- und EPR-DEER-Spektroskopie konnten wir die Struktur von GCAP5 in seinem aktivierenden Zustand auflösen und spezifische hydrophobe und elektrostatische Wechselwirkungen identifizieren, die das Dimer stabilisieren. Insbesondere die beiden nicht konservierten Cysteinreste in GCAP5 ermöglichen eine Fe^{2+}-Bindung, was möglicherweise eine Verbindung zwischen der Verfügbarkeit von Metallionen und der Regulierung der Zyklase in artspezifischen Zusammenhängen herstellt.

Zusammengenommen verbessern diese Ergebnisse unser Verständnis der vielfältigen strukturellen und regulatorischen Mechanismen, die Photorezeptor-Guanylatcyclasen und ihre Modulatoren steuern. Sie bieten wertvolle Einblicke in die Konformationsübergänge, die der enzymatischen Aktivierung zugrunde liegen, und werfen ein Licht auf molekulare Fehlfunktionen, die zu erblichen Netzhauterkrankungen beitragen. Durch die Integration biochemischer, struktureller und computer-gestützter Modellierungen bietet diese Arbeit einen umfassenderen Rahmen für die Aufklärung der Feinregulierung der cGMP-Signalübertragung bei der visuellen Transduktion sowohl unter physiologischen als auch pathologischen Bedingungen.

Abbreviations

°C	Degree(s) Celsius
Ca^{2+}	Calcium
$[Ca^{2+}]$	Calcium concentration
Fe^{2+}	Iron
Mg^{2+}	Magnesium
µ	Micro
α	Alpha
α	Anti
aa	Amino acid
AC	Amacrine cells
ADP	Adenosine diphosphate
AEC	Anion exchange chromatography
AMP	Adenosine monophosphate
Amp	Ampicillin
ANP	Atrial natriuretic peptide
APS	Ammonium persulfate
ATP	Adenosine triphosphate
b	Bovine
BC	Bipolar cells
Bidest	Double distilled
BNP	Brain natriuretic peptide
bp	Base pair
BSA	Bovine serum albumin
c	Centi
C	Cones
cAMP	Adenosine-3',5'-cyclic monophosphate
CCD	Cyclase catalytic domain
cGMP	Guanosine-3',5'-cyclic monophosphate
CNG channel	Cyclic-nucleotide-gated cation channel
CORD6	Cone-rod dystrophy 6 (related to *GUCY2D* mutations)
CRD	Cone rod dystrophy
C-terminus	Carboxyl-terminus
CV	Column volume
Cys	Cysteine
Da	Dalton
DC	Double cone
DD	Dimerization domain
DMSO	Dimethyl sulfoxide
DNA	Deoxyribonucleic acid
dNTP	Deoxyribose nucleotide triphosphate
dpf	days post fertilization
DTT	Dithiothreitol
EC_{50}	Effective concentration
ECD	Extra cellular domain

ER	Endoplasmic reticulum
E. coli	Escherichia coli
EDTA	Ethylenediaminetetraacetic acid
FCS	Fetal calf serum
FPLC	Fast protein liquid chromatography
g	Gravity equivalent (centrifugation)
g	Gram
G418	Geneticin
GC	Guanylate cyclase
GC-D	Guanylate cyclase D
GC-E	Guanylate cyclase E (GC1)
GC-F	Guanylate cyclase F (GC2)
GC-G	Guanylate cyclase G
GCL	Ganglion cell layer
GCAP-1	Guanylate cyclase activating protein 1
GCAP-2	Guanylate cyclase activating protein 2
GCAP-3	Guanylate cyclase activating protein 3
GCAP-5	Guanylate cyclase activating protein 5
GCAPs	Guanylate cyclase activating proteins
GDP	Guanosine diphosphate
GMP	Guanosine monophosphate
GPCR	G protein coupled receptor
gt	Goat
GTP	Guanosine triphosphate
GUCA1A	gene for GCAP1
GUCA1B	gene for GCAP2
GUCA1C	gene for GCAP3
GUCY2D	gene for guanylate cyclase E
GUCY2F	gene for guanylate cyclase F
h	Human
h	hour
HC	Horizontal cells
HCl	Hydrochloric acid
HEK293	Human embryonic kidney cells
HEPES	2-(4-(2-Hydroxyethyl)-1-piperazinyl) ethane sulfonic acid
His	Histidine (H)
HPLC	High pressure liquid chromatography
HRP	Horseradish peroxide
IC_{50}	Inhibitory concentration
IEC	Ion exchange chromatography
IgG	Immunoglobulin G
INL	Inner nuclear layer
IPL	Inner plexiform layer
IPTG	Isopropyl β-D-1-thiogalactopyranoside
IS	Inner segment
JMD	Juxta membrane domain
k	Kilo
k_a	Association rate constant

K_{cat}	Catalytic constant
Kan	Kanamycin
k_d	Dissociation rate constant
K_D	Dissociation constant
kDa	Kilodalton
KHD	Kinase homology domain
Km	Michaelis-Menten constant
L	Liter
LB	Lysogeny broth
LCA	Leber congenital amaurosis
LCA 1	Leber congenital amaurosis type 1
LCA12	Leber congenital amaurosis type 12
M	Molar
m	Milli
mA	Milli Ampere
mg	Milli gram
$MgCl_2$	Magnesium chloride
min	Minutes
mL	Milliliter
mM	Millimolar
mPIC	Mammalian Protease Inhibitor Cocktail
ms	Mus musculus
mT	Milli Tesla
MWCO	Molecular weight cut-off
myr	Myristoylated
n	Nano
NaCl	Sodium chloride
NaOH	Sodium hydroxide
NCBI	National center for biotechnology information
NCS	Neuronal calcium sensor
NDS	Normal donkey serum
ng	Nano gram
Ni-NTA	Nickel nitrilotriacetic acid
nm	non-myristoylated
NPRA	Natriuretic peptide receptor ANP
NPRB	Natriuretic peptide receptor BNP
N-terminus	Amino-terminus
OD	Optical density
OGP	Octyl ß-D-glucopyranoside
ONL	Outer nuclear layer
OPL	Outer plexiform layer
OS	Outer segment
p	Pico
PBS	Phosphate buffer saline
PCR	Polymerase chain reaction
PDB	Protein Data Bank
PDE	Phosphodiesterase
POD	Peroxidase

R	Rods
rb	Rabbit
RD3	Retinal degeneration 3 protein
RGC	Retinal ganglion cells
RNA	Ribonucleic acid
ROS	Rod outer segment
rpm	Revolutions per minute
rt	Rat
RT	Room temperature
SDS	Sodium dodecyl sulfate
SDS-PAGE	Sodium dodecyl sulfate polyacrylamide gel electrophoresis
SEC	Size exclusion chromatography
TEMED	Tetramethyl ethylenediamine
TM	Transmembrane domain
TRIS	2-Amino-2-(hydroxymethyl) propane-1,3-diol
Trp	Tryptophan (W)
UV	Ultraviolet
V	Volt
WT	Wild type

Single-letter amino acid code:

A	Alanine	**Ala**		**M**	Methionine	**Met**
C	Cysteine	**Cys**		**N**	Asparagine	**Asn**
D	Aspartic acid	**Asp**		**P**	Proline	**Pro**
E	Glutamic acid	**Glu**		**Q**	Glutamine	**Gln**
F	Phenylalanine	**Phe**		**R**	Arginine	**Arg**
G	Glycine	**Gly**		**S**	Serine	**Ser**
H	Histidine	**His**		**T**	Threonine	**Thr**
I	Isoleucine	**Ile**		**V**	Valine	**Val**
K	Lysine	**Lys**		**W**	Tryptophan	**Trp**
L	Leucine	**Leu**		**Y**	Tyrosine	**Tyr**

List of Figures and Tables

Table

Chapter 1: Introduction

The human sensory system is a remarkable tapestry of organs and neural pathways that collectively facilitate our understanding of and interaction with the world. Among the traditional senses- smell, hearing, taste, and touch- vision is one of the primary sensory modalities through which humans navigate and interact with their environment. The sensory organ responsible for this remarkable feat, the eye, is a sophisticated optical instrument composed of specialized tissues such as retina, and cells that detect and convert light stimuli into neural signals. Through intricate physiological processes, visual information is absorbed by the retina and transmitted to the brain for interpretation, ultimately culminating in the perception of the surrounding world. Thus, in daily life, we rely heavily on proper visual function. However, multiple factors, including aging, smoking, and exposure to UV light, can impair vision stimuli by damaging retinal tissues. In addition, inherited retinal diseases contribute to multiple eye disorders. Retinal dystrophies depict both phenotypically and genotypically heterogeneous group of disorders, with no universal treatment currently available. Recent pharmacological and technological innovations, such as gene therapy approaches, retinal cell transplantation derived from stem cell, and electronic devices, have revolutionized the management of retinal diseases. To fully harness these advancements, a deeper understanding of the vision process is essential. Decades of research suggest that the complexity of vision and its signaling events pose significant challenges, necessitating further exploration. The aim of my PhD research is to investigate the signaling cascade of GC-GCAP system (GC- guanylate cyclase and GCAP- guanylate cyclase activating protein) involved in phototranduction with main focus on elucidating the activity control mechanism of membrane bound guanylate cyclase in phototransduction.

1.1 Vision

The eye comprises several structurally distinct components, each playing a crucial role in the visual process. The process begins with light passing through the optical components of the eye, such as the cornea and lens, which collectively refract incoming light to form a sharp image on a sheet of photoreceptors called the retina, much like a camera lens focuses light onto a film or sensor (Dowling, 2012). The vertebrate retina, positioned at the back of the eye, then takes over as the site of sensory transduction. During development, the retina undergoes a precisely orchestrated process of neurogenesis to produce diverse cell types in an organized manner. This process is regulated by a network of transcription factors, and disruptions in these regulatory mechanisms can result in severe eye disorders (Stenkamp, 2015). The retina consists of six major classes of neuronal cells: retinal ganglion cells (RGCs), amacrine cells (ACs), bipolar cells (BCs), horizontal cells (HCs), and two types of photoreceptor cells- rods (R) and cones (C) (Iribarne & Masai, 2017), an overview of the architecture is depicted in Figure 1. In addition to that, Müller glial cells are mainly responsible for providing metabolic and homeostatic support to retinal neurons (Hoon et al., 2014; Wässle, 2004).

The retinal tissue is arranged into distinct layers, each contributing to the encoding and processing of visual information. Light detection begins in photoreceptor cells, which convert light into changes in membrane potential. This triggers alternations in the release of the neurotansmitter glutamate, which mediated communication with second-order glutamatergic bipolar cells in the outer plexiform layer (OPL), where horizontal cells mediate synaptic transmission. Two subtypes of bipolar cells exist: rod bipolar cells, which exclusively function as ON-bipolar cells, depolarizing in response to light, and cone bipolar cells, which can be either ON or OFF types, responding to light increments or decrements, respectively.

In the inner plexiform layer (IPL), cone bipolar cells form synapses with retinal ganglion cells and amacrine cells. The IPL is further divided into two sublayers: the inner lamina, where ON-bipolar cells synapse with amacrine cells and the outer lamina, where OFF- bipolar cells interact with amacrine and retinal ganglion cells. Amacrine cells modulate the activity of retinal ganglion cells either by direct inhibition at their dendrites or by feedback inhibition at bipolar cell terminals. Retinal ganglion cells serves as the output neurons of the retina, transmitting visual signals to higher brain regions, including the visual cortex (Hoon et al., 2014).

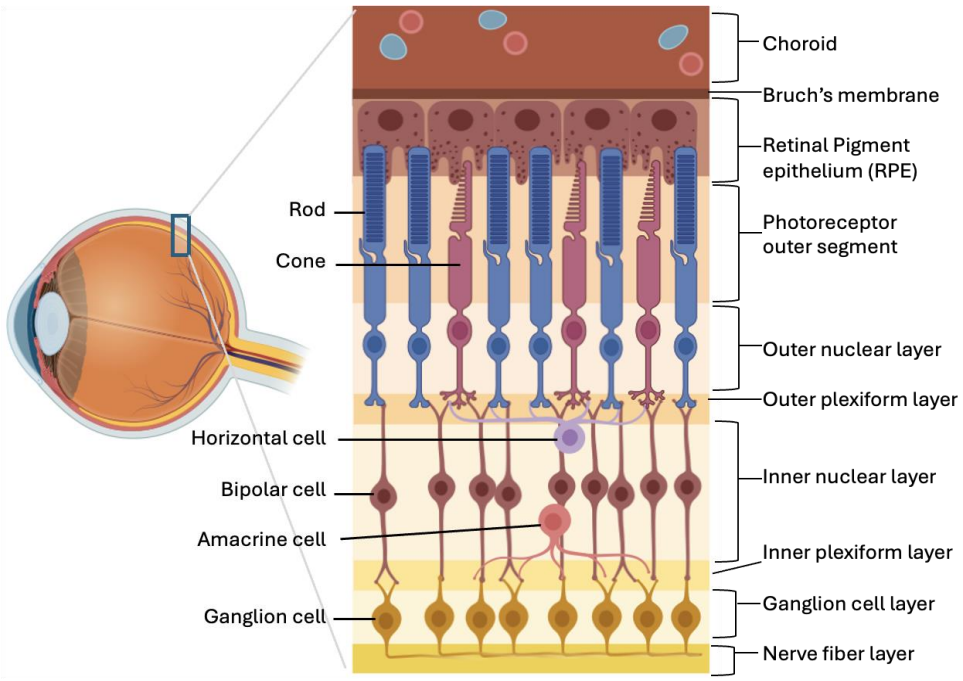

Figure 1: Schematic overview of the retina showing different layers and the main retinal cell types.
The figure illustration was taken by Biorender (biorender.com) and further modified.

1.1.1 Photoreceptor cells

Vertebrates rely on two types of photoreceptor cells: rod cells and cone cells (Walls, 1942). These photoreceptors are highly sensitive light detectors, capable of responding to single photons and mediating sensory input across an astonishing range of 10 orders of magnitude in light intensity (Koch, 2023). Rod cells are extremely sensitive to light, detecting single photons, and are essential for vision in dim light (Rieke, 2000). In contrast, cone cells, though less

sensitive, exhibit faster response times, making them indispensable for bright light vision, high visual acuity, and color perception (Dowling, 1987; Hoon et al., 2014). Together, these features underscore the intricate architecture and functionality of the vertebrate retina, tailored to meet the visual demands of different species as reviewed by Stenkamp (2015). For instance, the compositions of photoreceptors vary significantly among species. Mice harbor two cone types that co-express both opsins in varying proportions depending on retinal location, with short-wavelength-sensitive (S-opsins) dominating ventral retina (80-90%) and middle-wavelength-sensitive (M-opsins) dominating dorsal retina (80-90%) (Applebury et al., 2000). Humans, by contrast, possess three cone types sensitive to red, green, and blue light, enabling trichromatic vision. Zebrafish exhibit even greater diversity, with an additional UV-sensitive cone type (Iribarne & Masai, 2017). The average human retina constitutes ~92 million rods, with cones accounting for the remaining 4-5 million (Curcio et al., 1990).

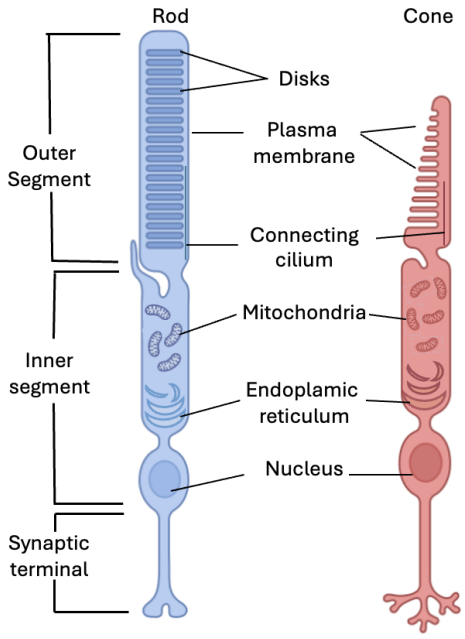

Figure 2: Schematic description of a rod and a cone photoreceptor cell.
Photoreceptors are subdivided in an outer segment, consisting of a stack of disk membrane, which house the protein machinery necessary for phototransduction, an inner segment harboring the cell organelles necessary for basal cellular function and a synaptic terminal that communicates to downstream retinal neurons. Outer and inner segment are connected via cilium.

Rods and cones are composed of an outer segment (OS), an inner segement (IS), cell body and a synaptic terminal (Figure 2). The OS is connected to the IS through a thin connecting cilium. The outer segment is filled with a dense stack of membrane discs, spaced at intervals of about 28nm. The OS carry the visual pigment (rhodopsin in rods and opsin for cones) and all other phototransduction components. The size and shape of both photoreceptor cells differ significantly like for example the OS of mouse rods (which are broadly similar to primate photoreceptors) is about 1.4 µm in diameter and 24 µm in length, and about 1.2 µm and 13 µm respectively for cones (Fu & Yau, 2007). Interestingly in rod OS (ROS), the discs are separate and enclosed by the plasma membrane, whereas in cone discs remain as invagination of the

plasma membrane. The IS contains mitochondria, endoplasmic reticulum and other organelles necessary for the cellular metabolism. The synaptic terminal transmits light signal further to other neurons in the retina (Cote, 2006) before signals reach the brain.

1.1.2 Phototransduction

Phototransduction is a biochemical process by which light, captured by a visual pigment (rhodopsin in rods and opsin for cones) molecule in the OS, generates an amplified electrochemical signal via a 'G-protein signalling cascade'- a sequence of reaction initiated by a G- protein coupled receptors (GPCR) and a cyclic nucleotide-gated (CNG) channel as downstream target that is directly regulated by the second messenger guanosine -3',5'-cyclic monophosphate (cGMP) (Koch, 2023; Koch et al., 2002; Koch & Dell'Orco, 2015; Nakatani et al., 2002; Pugh & Lamb, 2000).

From as early as the 1940s, to the modern era of mouse genetics, our understanding of phototransduction has evolved through several key experimental approaches. Initial psychophysical experiments by Hecht et al. (1942), first suggested that human retina rods can detect single photons. These findings were confirmed and extended by suction pipette recordings in the late 1970s (Baylor et al., 1979). Advancements in mouse genetics allowed to knocked out, overexpress or mutate specific genes in rods, which further accelerated our understanding of the molecular and cellular processes in rod cells. While the mechanisms underlying light detection in rods and cones share similarities, the intensive research focus on rods has provided a comprehensive understanding of their phototransduction, whereas cones remain relatively less explored (Koch & Dell'Orco, 2015).

As such, this PhD project continues to focus on rod phototransduction, leveraging its well-established physiological and biochemical framework to gain deeper insights into its mechanisms and functions.

Phototransduction begins when a photon of light strikes the photoreceptor, it is absorbed by the chromophore of a seven-transmembrane domain receptor Rhodopsin, causing a change in the structure of the chromophore from its 11-cis-retinal form to an all-trans configuration, which triggers a conformational change in rhodopsin activating the photopigment to an active form, known as metarhodopsin II (Rh*). Activated Rh* then catalyses the activation of heterotrimeric G protein transducin (T) by causing GDP/GTP exchange on the α-subunit. The GTP bound α-subunit dissociates from the ß/γ subunit and in turn activates its effector phosphodiesterase (PDE6), leading to the hydrolysis of second messenger cGMP to 5'-GMP. cGMP represents one of the two important second messengers found in the photoreceptor cells. In dark adapted state the cytoplasmic free cGMP level is relatively high ~ 5 μM keeping a fraction of cyclic nucleotide-gated (CNG) channels open. Hence a constant influx of positively charged ions Ca^{2+}, Na^{+} into the cell takes place. Ca^{2+} represents the other important second messenger in photoreceptors. Flow of Ca^{2+} into the cell is balance by continuous operation of a Na^{+} / Ca^{2+}, K^{+} exchanger, which removes the intracellular Ca^{2+}, maintaining the intracellular free [Ca^{2+}] at a resting level of 500-600 nM. Light induced hydrolysis of cGMP leads to closure of the CNG channel, thus reducing the influx of cations into the outer segment. However,

because of the extrusion of the Ca^{2+} by the exchanger leads to a decrease of free [Ca^{2+}] to a level below 100 nM (Hwang et al., 2003; Koch & Dell'Orco, 2015; Peshenko & Dizhoor, 2006). The closure of CNG channel therefore leads to membrane hyperpolarization. As a result this hyperpolarization decreases the amount of glutamate release at the synaptic terminal. The signaling information is transferred to attached retinal neurons and via the optic nerve to the brain. The phototransduction cascade in rod outer segments is illustrated briefly in Figure 3.

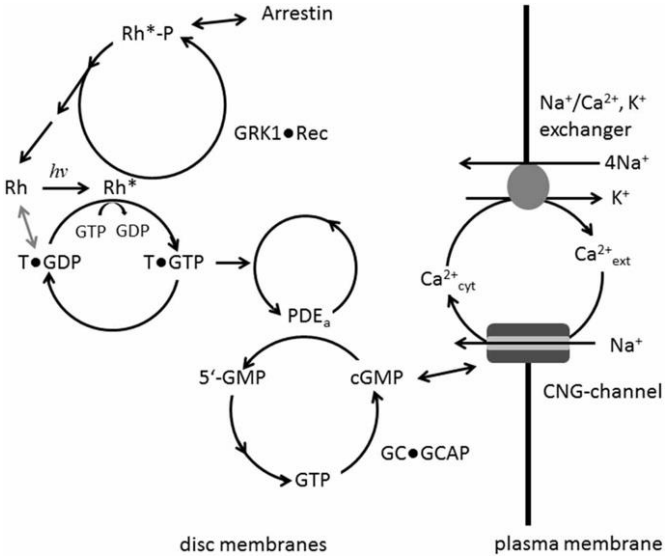

Figure 3: Overview of the phototransduction cascade in the rod photoreceptor cell.
Photoactivation of rhodopsin (Rh to Rh*) triggers GDP/GTP exchange in transducing (T), activating PDE, which in turn hydrolyzes cGMP. The reduction in cGMP causes closure of CNG channels, lowering intracellular Ca^{2+}. This drop is sensed by Ca^{2+} binding proteins including GCAPs, leading to increased cGMP synthesis via GC activation. Recoverin dissociates from the GRK1 allowing it to phosphorylate Rh*. Arrestin therefore binds to the phosphorylated Rh* preventing further transducin activation. The restored cGMP levels reopen CNG channels, resetting the cascade (taken from Koch & Dell'Orco, 2015).

Following light activation and hyperpolarization, a timely recovery of the photoreceptor cell is essential inorder to prepare them for new light stimuli, which requires the efficient shut off of all the exciting steps in the phototransduction cascade as well as rapid restoration of the exhausted cGMP concentration. The significant reduction in cytoplasmic [Ca^{2+}] is sensed by neuronal calcium sensor proteins (NCS), Recoverin and GCAPs which loses their bound Ca^{2+} ions and act in a Ca^{2+} mediated feedback system. Termination of activated Rh* is a two step process. First, Recoverin upon losing its bound Ca^{2+}, dissociates from the rhodopsin kinase (GRK1) thereby allowing GRK1 to phosphorylate Rh*. Second, the protein called arrestin binds to the phosphorylated Rh, blocking it from further activating transducin. Further, transducin achieves its inactive state by its intrinsic GTPase activity, which hydrolyses attached GTP to GDP. Once transducin is inactivated, it dissociates from PDE6, thus restoring the low basal activity controlled by its small inhibitory γ subunits, and thus GPCR signalling cascade stops. Further depending on the intracellular [Ca^{2+}] GCAPs activate GCs which then convert GTP to cGMP, resulting in restoration of cGMP level (Palczewski et al., 2004) and reopening of the CNG channel leading to repolarization of the cell and the photoreceptor's dark state is restored (Burns & Pugh, 2010; Fu & Yau, 2007; Koch & Dell'Orco, 2015).

1.1.3 GC-GCAP System

A critical element enabling photoreceptors to adapt to changing light conditions is the GC-GCAP complex system. The GC-GCAP complex regulates cGMP synthesis, counteracting its decrease upon illumination through a Ca^{2+} mediated negative feedback loop, thereby facilitating the restoration to the photoreceptor's initial dark-adapted state (Figure 4).

When cytoplasmic Ca^{2+} levels fall following light exposure, GCAPs undergo a conformational change that relieves their inhibition of GCs. This allows GCs to resume cGMP synthesis, promoting the reopening of CNG channels and helping the cell return to the dark adapted state (Pugh & Lamb, 2000). The importance of this GC-GCAP system for restoring photoreceptor cell function following illumination is well demonstrated in the study by Mendez et. al. (2001), where mice lacking GCAPs, exhibited a delayed recovery of photoresponse. Without GCAP-mediated regulation, the timely restoration of cGMP is impaired, prolonging the unresponsive state of the cell. This highlights the crucial role of the GC-GCAP system not only in restoring ion balance, but also in ensuring that photoreceptors are rapidly ready to detect new light stimuli-a critical feature for continuous visual perception.

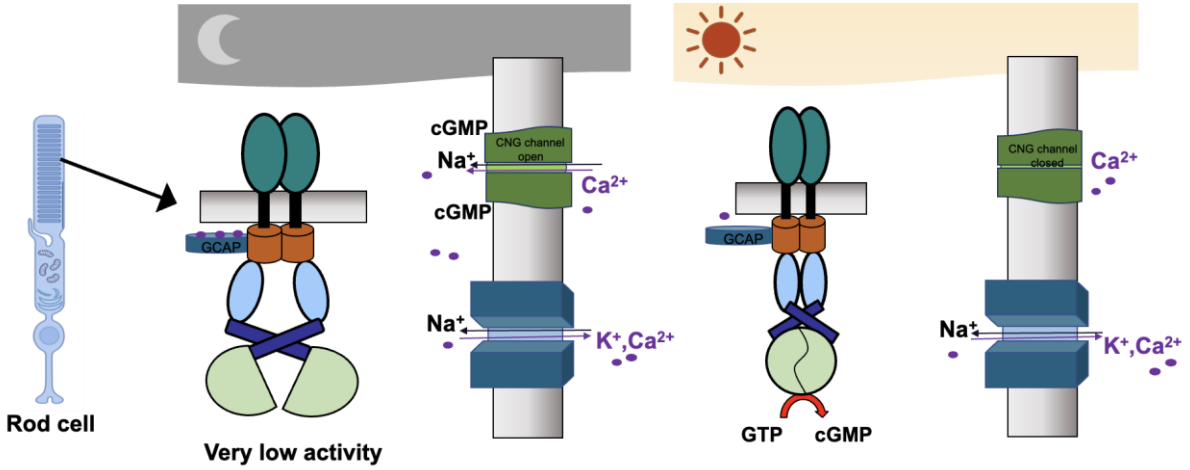

Figure 4: GC -GCAP system in ROS
In the dark, when GCAP is in its Ca^{2+} loaded form, the GCAPs interact with GC in a way that GC remains in its inactive form. Upon light activation, when GCAP start losing Ca^{2+} and turn into Ca^{2+} free/Mg^{2+} bound state, it stabilizes the GC transition in a way that GC reach to an active state, thereby re-synthesizing cGMP to return to the dark-adapted state.

Two to eight different isoforms of GCAP exist, in species from fish to human. The apparently redundant expression of different GCAPs raised questions about the physiological meaning. Although GCAP1 and GCAP2 form similar three-dimensional structures (Ames et al., 1999; Stephen et al., 2007), they nevertheless display remarkable differences in their regulatory properties as shown in a detailed biochemical study of the bovine system concerning activation profiles of GCAP1 and GCAP2 (Hwang et al., 2003). Apparently, the catalytic efficiency of ROS-GC1 (K_{cat}/K_M) is enhanced by both GCAPs. However, the presence of a myristoyl group in GCAP1 significantly impacts its regulation of GC with a catalytic efficiency increasing 25-

fold, compared to just a 3.4-fold increase with nonmyristoylated GCAP1. In contrast myristoylation of GCAP2 has only a minor effect on catalytic efficiency, resulting in a 10 to 13-fold increase regardless of whether GCAP2 is myristoylated or not. Additionally, GCAP1 and GCAP2 impact distinct Ca^{2+} sensitivity to GC. Activation by GCAP1 is half-maximal (IC_{50}) at 707 nM free [Ca^{2+}], while activation by GCAP2 at 100 nM respectively.

The differential regulation of GC by GCAP1 and GCAP2 is a result of their sensitivity to distinct levels of free intracellular Ca^{2+} (Figure 5). The Ca^{2+} relay model has been proposed by Koch and Dell'Orco (2013) to describe this coordinated regulation of GC by GCAPs. Studies using physiological and biochemical data from mice (Peshenko et al., 2011), and from native bovine and purified recombinant samples (Helten et al., 2007; Hwang & Koch, 2002) have provided strong evidence supporting the Ca^{2+} relay mechanism. It links the differential Ca^{2+} sensitivities of GCAPs to a sequential activation pattern for phototransduction regulation. GCAPs operate in a calcium relay system, namely, to make gradual responses to small changes in Ca^{2+}. Briefly, after illumination when the free [Ca^{2+}] begins to fall, GCAP1 becomes active and when the free [Ca^{2+}] further decreases the GCAP2 starts acting on GC. This step-by-step mechanism of different GCAP isoforms on GC regulation provide a molecular basis for light adaptation in the vertebrate retina.

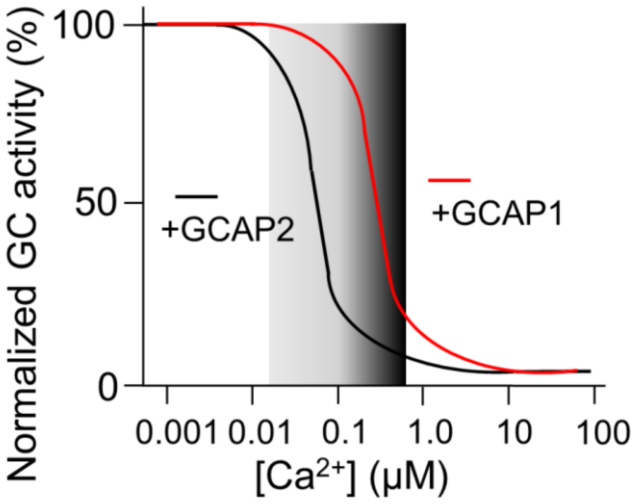

Figure 5: Ca^{2+} dependent activation profile of GC
The grey bar in the back indicates the cytoplasmic Ca^{2+} in the physiological range that changes from high (dark grey) to a low value (light grey). Activation of GC by GCAP1 (red line) and GCAP2 (black line) occurs in different range of free Ca^{2+} indicating the differential regulation of GCAPs following Ca^{2+} relay system (adapted from Koch & Dell'Orco, 2013).

The significance of this GC-GCAP system is of utmost importance as mutations in both GCAP1 and GCs that disrupt the Ca^{2+} dependent cyclase activation are genetically linked to retinal degenerative diseases (Behnen et al., 2010; Dell'Orco et al., 2010; Payne, 1998; Sokal et al., 1998; Wilkie et al., 2001). Therefore, elucidating its tightly regulated mechanism is essential.

1.1.4 The cGMP cycle in photoreceptor cells

The discovery of cyclic nucleotides cGMP and cAMP traces back to 1963 when Ashman et al. (1963) first identified these molecules in rat urine. These small but powerful molecules have been recognized as critical second messengers that orchestrate a wide range of cellular functions, from growth, differentiation, muscle relaxation to contractility, vasodilation and cell viability. Acting as intracellular messenger, they translate external signals into precise physiological responses (Kuhn, 2016).

Cyclic nucleotides are synthesized from ATP or GTP by specific enzymes: adenylate cyclases (ACs) for cAMP and guanylate cyclases (GCs) for cGMP. In mammals, researchers have uncovered nine membrane-bound isoforms of AC (AC1-AC9) along with a soluble AC (sAC). Similarly, GCs exist in soluble (sGC) and particulate, i.e. membrane (pGC) forms, which convert Mg^{2+} bound GTP into cGMP + pyrophosphate (PPi) as detailed in Figure 6. This delicate synthesis, coupled with their hydrolysis by phosphodiesterases (PDEs), allows dynamic changes in intracellular cAMP and cGMP level, finely tuning their cellular effects.

In the retina, the identity of cGMP was resolved in 1985 when Fesenko et al. (1985) discovered cyclic GMP-gated channels in frog rod outer segments, establishing its central and indispensable role in the phototransduction cascade, however the contribution of cAMP to phototransduction is still elusive. Some studies suggest that cAMP might influence the activity of PDE6 (Astakhova et al., 2012; Erofeeva et al., 2023), and as reviewed by Erofeeva N et al. (2023) emphasizes that cAMP levels in the retina exhibit circadian fluctuations, aligning with natural light cycles. Additionally, cAMP concentrations can undergo rapid, localized changes in response to transient light variations, suggesting its role in both long-term and immediate retinal adaptations.

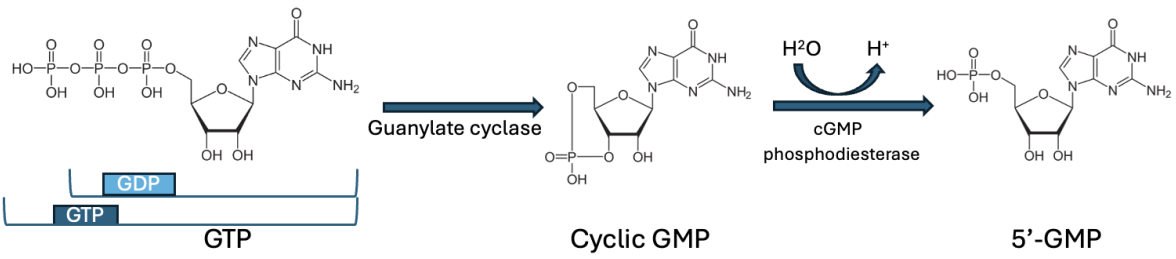

Figure 6: cGMP cycle in photoreceptor.
cGMP plays a central role in phototransduction, where it is hydrolyzed by PDE6 to 5'GMP. The resulting 5'GMP is either further degraded to guanosine or recycled back to GTP through enzymatic steps. The regenerated GTP is then used by the GC to produce cGMP for the dark-adapted state restoration.

1.2 Guanylate cyclases

The mammalian genome encodes multiple isoforms of GCs, broadly categorized into soluble (sGC) and membrane bound (particulate) (mGC) cyclases. Both soluble and particulate GCs share the catalytic function of generating cGMP but differ in their activation mechanisms,

cellular localization, and physiological roles. The soluble cyclases form heterodimers comprising of two subunits (α and ß) (Derbyshire & Marletta, 2012; Russwurm & Koesling, 2002). A heme group is bound to each subunit (Stone & Marletta, 1995), and the cyclase is activated by the binding of nitric oxide (NO) to the heme group (Bredt & Snyder, 1994; Katsuki et al., 1977) with major function in vasodilation and cardiac regulation. The membrane bound cyclases are homodimeric comprising of seven different forms of proteins GC-A to GC-G, which are further subdivided into two subfamilies: the natriuretic peptide-activated family, whose members are activated by the binding of atrial naturetic peptide (ANP) or a related peptide to an extracellular domain, and the calcium activated subfamily, whose members are activated by one or more calcium binding proteins that interact with intracellular domains of the cyclase. The mGCs are transmembrane receptors which share a unique topology comprising of an extracellular domain (ECD), and an intracellular domain (ICD) separated by a single transmembrane domain (TMD). GC-A serves as receptor for ANP, BNP (brain natriuretic peptide) regulating blood pressure/volume and energy balance. GC-B serves as a receptor for C-type natriuretic peptide (CNP) stimulating endochondral ossification in an autocrine way. GC-C binds to peptides (uro)guanylin and mediate electrolyte and water transport in the gut (Kuhn, 2016). GC-E and GC-F are expressed in photoreceptor cells which has a pivotal role in phototransduction and visual recovery (Koch & Dell'Orco, 2015). Finally, in mice two olfactorial GCs, GC-D and GC-G are expressed that respond to low concentrations of CO_2, guanylins and cold temperatures (Chao et al., 2015; Kuhn, 2016).

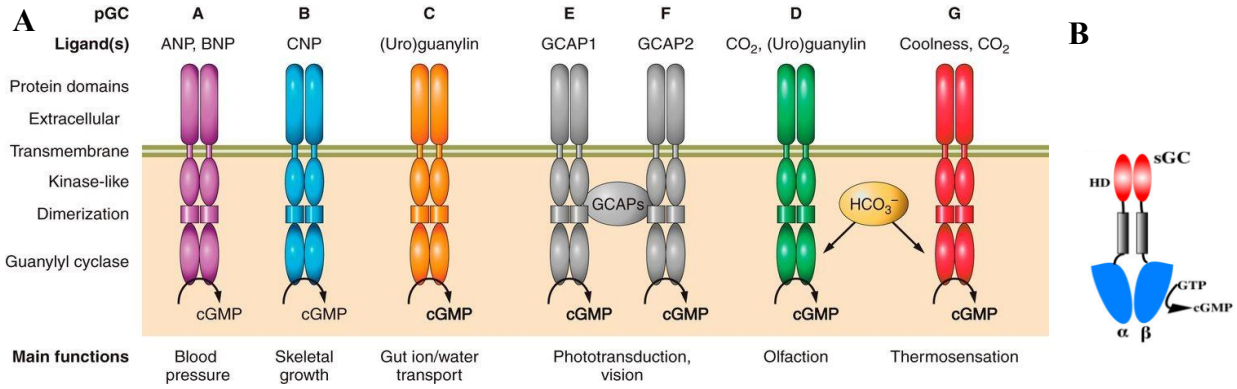

Figure 7: Illustration of the general structure and main regulatory functions of membrane bound guanylate cyclases (A) and soluble guanylate cyclase (B).
(A) GC-A (ANP/BNP) and GC-B (CNP) serve as receptors for the respective natriuretic peptide, while GC-C functions as receptor for (Uro) guanylin. GC-E and GC-F act as the retinal guanylate cyclase and regulated by GCAPs. GC-D and GC-G act as olfactorial and thermosensation receptors (Figure taken from Kuhn, 2016). **(B)** Soluble guanylate cyclase lacks an extracellular domain and is activated by nitric oxide binding to the heme binding domain (HD) (Figure taken from Fitzpatrick et al., 2006).

1.2.1 The retinal guanylate cyclase

In vertebrate retina the GC is expressed in two isoforms ROS-GC1 and ROS-GC2 (Dizhoor, 1994; Lowe et al., 1995), outside the retina the ROS-GC1 are expressed in pineal gland and olfactory bulb (Duda & Koch, 2002; Duda & Sharma, 2004), in the auditory nerve and the organ of Corti (Seebacher et al., 1999) in the anterior portion of gustatory epithelium (Duda & Sharma, 2004) and in the sperm (Jankowska et al., 2014), whereas ROS-GC2 was exclusively

expressed in the retina. ROS-GC1 and ROS-GC2 are referred to the bovine forms and their counter parts retGC1 and retGC2, and GC-E and GC-F are referred to human and rat forms respectively as stated in Table 1. Therefore, irrespective of their species- specificity, these Ca^{2+} modulated mGCs are chosen as GC-E and GC-F for further description. *GUCY2D* and *GUCY2F* are the genes that encodes GC-E and GC-F, respectively.

Table 1: Nomenclature of different membrane guanylate cyclases used historically with respect to their origin. (Modified from Pugh et al., 1997)

Name	Structural analogue of	Species	Localization
ROS-GC1	RetGC1, GC-E	Bovine	Rod outer segment [1]
RetGC1	ROS-GC1, GC-E	Human	Photoreceptor layer of retina[2]
GC-E	RetGC1, ROS-GC1	Rat	Retina[3]
ROS-GC2	RetG2, GC-F	Bovine	Retina[4]
RetGC2	ROS-GC2, GC-F	Human	Photoreceptor layer of retina[5]
GC-F	ROS-GC2, RetGC2	Rat	Retina[3]

[1]Goraczniak *et al*., 1994.
[2]Shyjan *et al*., 1992.
[3]Yang *et al*., 1995.
[4]Goraczniak *et al*., 1997.
[5]Lowe *et al*., 1995.

These GCs are multidomain transmembrane protein with a theoretical mass of 110-120 kDa. In 1991, the first purification of photoreceptor GC was done from bovine rod outer segments (ROS) by two independent groups (Hayashi & Yamazaki, 1991; Koch, 1991). The GC-E gene was cloned shortly after its protein purification and shows that native GC-E is glycosylated at its N-terminus (Goraczniak et al., 1994; Koch et al., 1994). In contrast, to GC-E, the sequence of GC-F indicates that it is not glycosylated at the N-terminus (Goraczniak et al., 1997; Lowe et al., 1995). Among all membrane GCs cloned to date, GC-E is the only one identified based on part of its protein sequence. The gene that encodes GC-E is *GUCY2D* and in humans, located on chromosome 17p13.1 (Oliveira et al., 1994). Interestingly, in the same time frame Koch and Stryer reported evidence that the exquisite sensitivity of photoreceptor GC to Ca^{2+} was conferred by a soluble protein (Koch & Stryer, 1988) followed by cloning of the GC regulators named GCAP1 and GCAP2 (Dizhoor et al., 1995; Palczewski et al., 1994). Collectively, these investigations paved the way for in-depth studies on retinal GCs and their activating proteins (Sharma & Duda, 2012).

1.2.2 Structure of Guanylate cyclase

GC-E is a single transmembrane spanning homodimer protein which is divided into two main parts, the extracellular domain (ECD) and intracellular domain (IcD), separated by the transmembrane domain (TMD). The IcD consists of a juxtamembrane (JMD), a kinase homology (KHD), a dimerization (DD), and a catalytic (CD) domain. The classification, structure, and molecular characterization of IcD subdomains in GC-E have undergone significant advancements in recent years.

- **Extracellular domain (ECD)**- Located at the N-terminus, this domain resides in the intradiscal space (lumen) of photoreceptor rod outer segments. To date, no ligand has been identified that's binds to it to regulate GC-E activity, as the GC-E activity is primarily controlled intracellularly. Studies using heterologous expression systems have shown that the entire ECD of GC-E can be removed without affecting its enzymatic activity or its regulation by GCAPs (Laura et al., 1996; Peshenko et al., 2010), suggesting ECD is not necessary for cGMP synthesis. While its exact function remains unclear, a point mutation (S248W) in the ECD of GC-E leads to congenital blindness (LCA1) in human (Jacobson et al., 2013), indicating this domain is crucial for proper vision. It may contribute to protein trafficking, stabilization of GC-E homodimers, or interactions with other proteins (Karan et al., 2010).
- **Transmembrane domain (TMD)**- TMD is a single spanning transmembrane domain that divides GC-E into two segments EXD and IcD. A mutation study addressing different regions demonstrated that TMD is essential for stabilizing the CD and ensuring proper alignment of successive modular domain (JMD, KHD, DD and CCD) for efficient catalysis. Thus, TMD plays a crucial role in maintaining basal catalytic activity by anchoring GC-E in the membrane (Ravichandran, 2017).
- **Juxtamembrane domain and kinase homology domain (JMD/KHD)**- The JMD was initially considered part of KHD. However, sequence analysis reveals that this 115-amino-acid region is highly conserved between GC-E and GC-F but shares only ~7% homology with peptide receptor guanylate cyclases such as NPR-A, NPR-B, and STaR (Lange et al., 1999) and therefore renamed as separate region JMD. The JMD connects directly to the TMD and connects the extracellular and intracellular region. JMD is followed by KHD and the CD. The KHD probably harbours a kinase activity for autophosphorylation (Aparicio & Applebury, 1996) as well as ATP and Mg^{2+} binding sites. The autophosphorylation is independent of GCAPs or upstream phototransduction activity, although an intact KHD is essential for GC-E activity (Bereta et al., 2010).
- **Dimerization domain (DD)**- DD connects the KHD to the CD, further it links the catalytic center of two domains to form a catalytic center. This linker region adopts a coiled-coil (Ramamurthy et al., 2001) or alpha helical structure (Saha et al., 2009; Zägel et al., 2013), necessary for GCAP dependent regulation.
- **Catalytic domain** (**CD)**- CD is located C-terminal to the DD. The two CD from both subunits of GC forms a catalytic center in which GTP binds and is converted to cGMP. The GTP substrate binding sites are the four residues Asp890, Arg981, Ala1013 and Lys1051. There is strong homology between adenylate cyclase and guanylate cyclase catalytic domains and so far, no complete crystal structure of mGCs or of the CD is known. However, the CD of a soluble GC derived from *Chlamydomonas reinhardtii* (Winger et al., 2008), of human sGC (Allerston et al., 2013) and adenylate cyclase (Tesmer et al., 1997) was solved. These structural studies reveal that the CD consists of β-strands and α-helices, forming a homodimer wherein the two monomers are arranged in an antiparallel orientation, with their N- and C- termini oriented oppositely. (Duda et al., 2012; Venkataraman et al., 2008).

- **C-terminal extension (CTE)-** The CD is followed by an additional CTE (Goraczniak et al., 1994). This region contains binding sites for two calcium sensor proteins, GCAP2 and S100B, which play crucial roles in GC-E regulation (Duda et al., 2002, 2005).

Multiple regions of photoreceptor GC-E are involved in binding and/or regulation by GCAPs (Peshenko et al., 2015; Sulmann et al., 2017; Zägel et al., 2013), yet the exact interaction mechanism and the precise locations of the binding sites in target GCs remain under debate (Peshenko et al., 2015; Sulmann et al., 2017). The vast domain organization of GC-E and the involvement of all its regions in proper functioning raise important questions about the mechanism underlying its activation. Does GCAP induce a conformational transition in GC-E or does GC-E itself undergo some form of rotation in its TMD, transitioning from an inactive to an active state, similar to the TMD rotation involved in the activation of its isoform GC-A (Parat et al., 2010)? Alternatively, as described by Maruyama (2015), all cell surface receptors seem to follow a common rotational activation mechanism, but whether this mechanism operates in for GC-E is unclear. Understanding these mechanisms could provide crucial insights into the broader regulatory principles governing GC and their role in signaling, therefore, my first approach was to investigate whether GC-E activation involves a rotation mechanism.

1.2.3 The rotational mechanism in cell surface receptors

Transmembrane, cell-surface receptors often transmit extracellular signals across plasma membrane to the cytoplasm via a TMD. A characteristic feature of such receptor is receptor dimerization upon ligand binding leading to its activation (Endres et al., 2014). However, many receptors do exist in constitutively dimeric form prior to ligand binding but in an inactive state. This leads to the question how does a preformed dimeric receptor becomes activated by ligand binding?

Unlike soluble proteins, membrane-bound proteins are anchored to the membrane by TMD. Since the plasma membrane consists of lipid bilayers, these receptors are therefore constrained to the bilayer and might function while their TMD is restricted to four principal motions: translation, piston, pivot and rotation (Matthews et al., 2006). During transmembrane signaling, TMD rotation is energetically more favorable than their lateral movement against the lipid bilayer barrier. As reviewed by Maruyama (2015) many receptors like receptor tyrosine kinases (RTKs), cytokine receptors and other cell-surface receptors such as GC-A (also known as NPRA) from the guanylate cyclase family, utilize a rotational mechanism for activation. In the proposed ‘‘rotation model’’ ligand binding to the ECD initiates some form of rotation in the TMD, which then reorganizes or stabilizes the IcD. This structural shift facilitates the receptor’s transition from an inactive to an active state (Figure 8), suggesting that rotation is a common mechanism for cell-surface receptor activation.

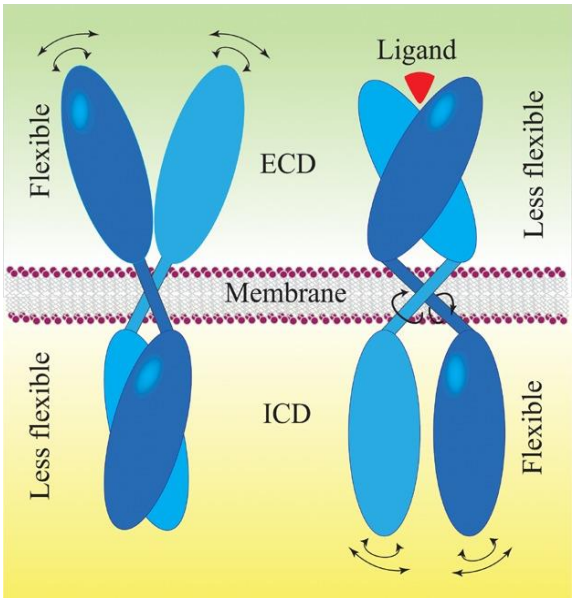

Figure 8: ‘‘Rotation model’’ as a common mechanism for cell-surface receptor activation
Prior to ligand binding, the receptor exists in dimeric form and in an inactive state on the cell surface. Ligand binding induces a change in conformation of ECD which in turn induces or allow a rotation of the TMD, which then rearranges the IcD, making it to become active for downstream signaling (taken from Maruyama, 2015).

More than 140 mutations in the *GUCY2D* gene, which encodes photoreceptor GC-E, have been linked to various retinal disorders, including Leber’s congenital amaurosis (LCA1) and cone-rod dystrophies (CRD), often resulting in blindness or severe visual impairment (Sharon et al., 2018). To thoroughly investigate the correlation between different regions of GC-E and its catalytic mechanism, a deep understanding of its conformational changes is essential. However, the lack of native GC-E structural data has made this challenging. Recently, Rehkamp et al. (2021) presented the 3D structural analysis of full-length GC-E from bovine retina using cross-linking mass spectrometry combined with computational modeling, providing valuable insights into its conformation. Rehkamp et al, modified the previously known IcD by suggesting a novel domain organization formed of a KHD, an α-helical domain (αHD), and the cyclase catalytic domain (CCD). This αHD links the KHD to the CD and featuress a highly conserved helix-turn-helix motif at its N-terminal extension found in topologically related proteins (Gajiwala & Burley, 2000). It also contains the formally assigned DD, which play a cruicial role in dimerization and is proposed to serve as a GCAP binding interface or regulatory control module (Peshenko et al., 2015; Zägel et al., 2013).

Notably, several amino acid residues within this region are mutated in GC-E of patients with autosomal dominant cone-rod dystrophy (adCRD), making it a key ‘‘hot spot’’ for retinal diseases (Sharon et al., 2018). Moreover, mutations in GC-E are found across all domains, with functional studies often showing a substantial decline in GC-E activity due to point mutations, with an exception for V902L mutant, causing CRD, which leads to constitutively active GC-E exhibiting high activity (Wimberg et al., 2018). Therefore the structural evidences provided by Rehkamp et al. (2021), has been used as a cruial tool for my thesis on understanding the activity control of GC-E.

1.2.4 Retinal GC is a part of multi-protein complex

GCs have been found to be associated with Triton X-100 insoluble cytoskeletal protein axonemes (Fleischman & Denisevich, 1979). A co-immunoprecipitation study demonstrated interaction of GC with Actin (Hallett et al., 1996) and another direct study showed further that GC-E, the alpha subunit of tubulin, and GCAP1 form a complex (Schrem et al., 1999), which potentially controls the light dependent translocation of transducin (Rosenzweig et al., 2009). Additionally, GC-E was found to be a major component of a multi-protein complex in rod, but not cone, photoreceptors, assembled by glutamic-acid-rich proteins (GARPs) (Körschen et al., 1999). Two proteins RGS9 (regulators of G protein signaling) (Seno et al., 1998) and RD3 (retinal degeneration protein) (Peshenko et al., 2011 b) act as a negative regulators, which inhibit GC-E cyclase activity. RD3 also found to be necessary for correct translocation and cellular localization of GC-E (Azadi et al., 2010; Wimberg et al., 2018; Zulliger et al., 2015)

GCs are regulated by Ca^{2+} sensor proteins GCAPs, upon encountering changes in cytoplasmic Ca^{2+} as a Ca^{2+} feedback loop system. Apart from GCAPs other calcium sensors proteins Neurocalin δ (Venkataraman et al., 2008) and S100ß (Duda et al., 1996) target to bind GC and regulate GC activity opposite to GCAP, in a calcium dependent manner modulating the signal transmission in cone ON-bipolar cells (Wen et al., 2012).

1.3 Guanylate cyclase activating protein (GCAP)

GCAPs are a class of neuronal calcium sensor (NCS) proteins, a subclass of the calmodulin superfamily of proteins. GCAPs play a crucial role in photoreceptor signaling (Ames & Lim, 2012) and have similar structures like recoverin, which is also a part of the negative feedback loop in photoreceptor cells (see above and Figure 3).

In higher mammals, two predominant GCAP isoforms- GCAP1 and GCAP2 are expressed in photoreceptor cells. GCAP1 is encoded by the *GUCA1A* gene, mapped to chromosome 6p21.1 (Subbaraya et al., 1994), while GCAP2 is encoded by the *GUCA1B* gene. Using PCR analysis and sequencing Surguchov et al. (1997), showed that these two genes are arranged in a tail-to-tail array on the short arm of chromosome 6. In addition, GCAP3, encoded by *GUCA1C gene*, (Haeseleer et al., 1999) is a cone specific isoform found in primates and some fish species but is absent in mice. Zebrafish retina on the other hand expresses a total of six GCAP variants (zGCAP1, 2, 3, 4, 5 and 7). The diversity of GCAPs isoforms could be an advantage allowing natural selection to refine and optimize the photoreceptor response to light stimuli (Wen et al., 2014).

GCAPs are expressed in both rods and cones, but their subcellular localization differs between isoforms. GCAP1 is predominantly localized in the outer segments of rods and cones, as well as in synaptic terminals, and some cone somata, as shown in bovine and primate retinas (Frins et al., 1996; Gorczyca et al., 1995). In contrast, GCAP2 is mainly found in the inner segments, cell bodies, and synaptic terminals, particularly of cone photoreceptors. In bovine retina,

GCAP2 labeling is strongest in rod inner segments and cone myoids, while signal in the outer segment is weak—correlating with low GCAP2 content detected in rod outer segment (ROS) fractions (Gorczyca et al., 1995; Otto-Bruc et al., 1997). Interestingly, GCAP2's distribution appears more dynamic and possibly regulated, suggesting distinct functional roles beyond GC regulation. These findings point toward complementary roles for GCAP1 and GCAP2 within distinct subdomains of the photoreceptor cell. Moreover, GCAP translocation to the outer segment has been reported to depend on its binding affinity for GCs, potentially acting as a targeting mechanism from inner to outer segment (López-Begines et al., 2018).

Functionallly, GCAPs act as Ca^{2+} sensitive regulators, responding to intracellular Ca^{2+} fluctuations through conformational change that modulate GC activity (Koch & Dell'Orco, 2013). They activate photoreceptor GCs at low Ca^{2+} concentrations and physiological Mg^{2+} levels and inhibit it at high Ca^{2+} levels, allowing photoreceptors to adapt effectively to changes in light intensity (Peshenko & Dizhoor, 2006).

On a molecular level, GCAPs contain EF-hand motifs, which are specialized helix-loop-helix structures that facilitate Ca^{2+} and Mg^{2+} binding. Among the four EF-hands present in GCAPs, three (EF-hands 2, 3, and 4) are functionally active in Ca^{2+} binding, while EF-hand 1 does not bind Ca^{2+}. The exact nature of Mg^{2+} binding remain debated, with some studies suggesting that all three EF-hands bind both Ca^{2+} and Mg^{2+} (Peshenko & Dizhoor, 2006), while it has been proposed that GCAP1 binds functionally to Mg^{2+} at EF2 which is required for GC-E activation (Lim et al., 2009). Additional insights into these regulatory states have come from structural studies, where Marino et al. (2015) demonstrated that Mg^{2+} binding significantly influences the conformational and functional states of GCAPs. Specifically, Mg^{2+} binding stabilizes a compact, GC-activating conformation of GCAP1 under low Ca^{2+} state, emphasizing its role in photoreceptor light adaptation.

1.3.1 Ca^{2+}-myristoyl switch

The Ca^{2+}-myristoyl switch, a mechanism observed in some neuronal calcium sensor (NCS) proteins like recoverin, involves a conformational change where the myristoyl group is exposed in the Ca^{2+}-bound state and buried in the Ca^{2+}-free state (Ames et al., 1997). This myristoyl switch could be an important regulatory step in phototransduction. The N-terminal consensus sequence recognized by N-terminal myristoyl transferase (NMT) enables posttranslational modification with small fatty acids, such as myristic acid, in guanylate cyclase-activating proteins (GCAPs) (Bereta & Palczewski, 2011). However, while guanylate cyclase-activating proteins (GCAPs) and recoverin variants share structural similarities, a classical Ca^{2+}-myristoyl switch is absent in most GCAPs and zebrafish recoverin variants (Elbers et al., 2018; Hwang & Koch, 2002; Olshevskaya et al., 1997). Instead, GCAP1 exhibits a "Ca^{2+}-myristoyl tug" mechanism that influences Ca^{2+} sensitivity and target regulation (Peshenko et al., 2012), whereas GCAP2 interacts with lipid bilayers, though its Ca^{2+}-dependent conformational changes remain unclear (Theisgen et al., 2011). Myristoylation also affects GCAPs subcellular localization, with unmyristoylated GCAP1 largely retained in the inner segment, while GCAP2 still localizes to rod outer segments, albeit less efficiently (López-Begines et al., 2018). Unlike recoverin, GCAP1 and GCAP2 maintain their myristoyl groups inside a hydrophobic pocket

regardless of Ca^{2+} binding, which plays a role in modulating their interaction with GC-E and influences their physiological function (Hwang & Koch, 2002).

1.3.2 Ca^{2+} sensitive regulation and dimer formation

GCAPs exhibit distinct Ca^{2+} sensitivity in regulating GC activity and binding Ca^{2+}, forming the molecular foundation of the Ca^{2+}-relay model, where GCAP1 activates the target GC at higher Ca^{2+} concentration, while GCAP2 takes over as Ca^{2+} level drop (Hwang et al., 2003; Koch & Dell'Orco, 2013; Mendez et al., 2001; Vinberg et al., 2018). GCAP3 has been shown to activate GC-E similarly to GCAP1 but with lower maximal efficiency (Avesani et al., 2022). However, conflicting studies on bovine GCAP1 and human GCAP3 leave its precise physiological role uncertain (Haeseleer et al., 1999).

GCAP1 and GCAP2 regulate GC activity through a monomer-dimer equilibrium that is influenced by Ca^{2+} and Mg^{2+} levels. GCAP1 has a significantly higher propensity for dimerization in the Ca^{2+}-bound state, than in the Ca^{2+}-free/Mg^{2+}-bound state, because the monomers exhibit about 5–8 times higher affinities when forming dimers (Bonì et al., 2020). The dimerization interface in GCAP1 is primarily hydrophobic, stabilized by key residues such as H19, Y22, F73, V77, and W94. It is suggested that GCAP1 dimerization facilitates the formation of a high-affinity 2:2 complex with GC, stabilizing its activity. However, some evidence indicates that GC binding may interfere with GCAP1 dimerization due to overlapping interaction sites (Ames, 2021; Koch, 2023; Peshenko et al., 2010).

In contrast, GCAP2 also forms dimers (Ermilov et al., 2001), but its dimerization interface consists mainly of charged and polar residues, including K98, L167, R175, and D188, which stabilize the dimer through salt bridges and hydrogen bonds (Pettelkau et al., 2013). These intermolecular polar contacts in the GCAP2 dimer are not conserved in the other GCAPs and the overall quaternary structure of the GCAP2 dimer is very different from that of GCAP1. The interaction with the target GC plays a crucial role in shifting the monomer-dimer equilibrium (Ames, 2021). However, it remains under debate whether GCAP1 and GCAP2 bind to overlapping or distinct interaction sites on GC-E (Peshenko et al., 2015; Sulmann et al., 2017).

1.3.3 The Zebrafish GCAPs system

The zebrafish is one of the most valuable model organisms used for investigating genetic and functional aspects in sensory cells, due to its rapid development from a transparent embryo to an adult fish within three months (Bilotta & Saszik, 2001), in addition the larvae respond to visual stimuli as early as 3-5 days post fertilization (dpf). In zebrafish rod and cone cells express a total of three sensory GCs (zGC1, zGC2 and zGC3) and six different GCAP isoforms. Transcription of zGC3 and four GCAPs (zGCAP3, 4, 5 and 7) are shown exclusively found in cones (Imanishi et al., 2004; Rätscho et al., 2009) and protein level expression has been demonstrated for zGCAP3 (Fries et al., 2012). The zGCAP1 and zGCAP2 isoforms, are however expressed in rods and UV cones. This vast variety of transcription and protein expression pattern of zGCs and zGCAPs might indicate adaptation to the specific challenges of the aqueous habitat (Rätscho et al., 1/2010b).

These six zGCAP isoforms can be grouped in two categories of different Ca^{2+} sensitivities, zGCAP4, 5 and 7 regulating GC activation profile at higher Ca^{2+} (≈ 400nM) and zGCAP1-3 at low Ca^{2+} (≈ 30nM) (Koch, 2013; Scholten & Koch, 2011). This differential Ca^{2+} regulation of zGCs activity agrees with the Ca^{2+} relay model discussed above.

Notably, the zGCAP5 isoform differs from the other variants in several aspects. Compared to other GCAPs regulatory property of GCAPs activating GC, zGCAP5 has a low potency to activate the GC in a Ca^{2+} dependent manner (Scholten & Koch, 2011). Unlike GCAP1 and GCAP2, GCAP5 can activate GC in both Ca^{2+} free and Ca^{2+} bound states, though with lower potency.

It has a more divergent amino acid sequence among other zGCAPs, containing non-conserved cysteine residue (Cys15 and Cys17) that enable Fe^{2+} and Mg^{2+} binding. The GCAP5 was found to exist in dimer form in solution in both Fe^{2+} free and Fe^{2+}- bound state (Lim et al., 2017). A structural model determined by an NMR-guided homology modeling approach exhibited Fe^{2+} bound GCAP5. A single Fe^{2+} ion binds two GCAP5 molecules into a dimeric complex. This Fe^{2+} binding seems to trigger a switch in the GCAP5 dimer, transitioning it from the Fe^{2+} free/activator state to the inactivate state, suggesting GCAP5 may function as an Fe^{2+} sensor in phototransduction (Lim et al., 2017).

The dimeric structure of GCAP5 is similar to that of GCAP1 dimer (Lim et al., 2018), as both proteins contain key hydrophobic amino acids in the monomer-monomer interface. Mutations in the dimer interface of GCAP1 (H19R, Y22D, F73E and V77E) abolish protein dimerization affecting regulation of GC activity (Lim et al., 2018; Peshenko et al., 2014). It is therefore interesting to determine whether the preformed GCAP5 dimer does affect cyclase activity in a similar manner.

1.4 Retinal degeneration protein (RD3)

Retinal degeneration protein 3 (RD3) is a 23 kDa protein encoded by the *RD3* gene (formally the *C1orf36* gene) (Lavorgna et al., 2003). The name derives from the fact that truncation or mutation on it can cause photoreceptor degeneration and severe early-onset vision loss in Leber congenital amaurosis 12 (LCA 12) patients. Results from animal models like the rd3 mouse (Friedman et al., 2006) and the rcd2 collie (Kukekova et al., 2009) highlighting the crucial role of RD3 in the survival of photoreceptor cells. Co-localization and immunoprecipitation studies revealed that RD3 co-localizes, and directly interacts with GC-E and GC-F in the retina and plays a crucial role in their stable expression and membrane trafficking from inner to outer segments in rod and cone photoreceptors (Azadi et al., 2010). These findings shed light on the molecular mechanisms underlying photoreceptor degeneration in LCA12 patients and rd3 mouse.

RD3 is a high affinity allosteric modulator of the cyclase, which inhibits GC activity at submicromolar concentrations and act as a negative regulator of GC, ensuring proper guanylate

cyclase function by preventing premature cGMP synthesis in photoreceptor cells (Peshenko et al., 2011), however it does not change the Ca^{2+} sensitivity regulation of GC-E by GCAPs.

Although it has been observed that RD3 compete with GCAPs for regulating GC activity (Peshenko et al., 2011, Figure 2), the precise nature of this competition between GCAPs and RD3 for the same target remains unresolved and the exact RD3 binding site on GC-E is still unknown. Evidence suggests that the binding sites for GCAPs and RD3 overlap in the three-dimensional GC-E structure, as mutations in the KHD domain disrupt both interactions (Peshenko et al., 2016). With the growing evidence of RD3 function in photoreceptor and GC-E trafficking process, a thorough understanding of its mechanism and their interaction study of whether GCAPs and RD3 compete/overlap for same target site is much needed.

Previously in the Division of Biochemistry (University of Oldenburg), Dr. Hanna Wimberg investigated the effects of negative GC regulator RD3 on GC-E mutants. Interestingly, while GCAP activated GC-E was completely inhibited by RD3 at concentrations above 100 nM, with an IC_{50} value (the Ca^{2+} concentration required for half-maximal inhibition of GC-E activity) of 68 nM, the mutant V902L exhibited a significantly higher IC_{50} value of 250 nM compared to the wildtype (Wimberg et al., 2018). This suggests a possible alteration in RD3 binding affinity or regulatory dynamics in the mutant, warranting further investigation.

Objectives

Main Objective

Although guanylate cyclase (GC) is the key enzyme playing role in phototransduction, there is little known about its in-depth mechanism. In order to ascribe a certain function of it, it is important to first elucidate the activity control of membrane bound guanylate cyclase i.e. the mechanism behind its transition from an inactive to an active state. Accordingly, my thesis is an attempt to understand the activation mechanism of photoreceptor guanylate cyclase in the phototransduction, with an emphasis on its structural conformation changes and functional dynamics, and the involvement of allosteric communication between various region or domains.

1. **How does photoreceptor guanylate cyclase reach from an inactive state to an active state?**

Maruyama (2015) hypothesize a common mechanism of α-helix rotation for membrane-bound receptors for an active cyclase, which has been experimentally proven by Parat et al. (2010) for GC-A. Based on this hypothesis, we applied a similar experimental approach in our study to simulate a rotational switch in the transmembrane domain. Therefore, a combination of experiments was conducted with heterologous protein expression in HEK293T cell, which aimed to:

- Generation of GC-E mutants by poly-alanine insertion into GC-E in positions that seem critical for a rotational activation step, e.g. near the transmembrane region.
- Test on whether poly alanine mutants of GC-E are constitutively active (indicative of a rotational mechanism). The results are presented in Chapter 2 presenting a published manuscript.

2. **Does the mutation V902L in GC-E causing constitutive activation to stabilize the transition state?**

After disproving the initial hypothesis, we extended the project by comparing conformational changes in GC-E with those in GC-E carrying a point mutation (V902L). This mutation, is found in patients suffering from retinal cone-rod dystrophy and leads to a constitutively active state of GC-E. This thesis aimed to:

- Perform enzymatic kinetic analysis of GC-E and V902L mutant
- Understanding protein dynamics using Molecular dynamics simulations approach.

The computational approach based on all-atom molecular dynamics simulations was done by collaborating with Fabian Schuhmann and Prof. Ilia Solov'yov from the Institute of Physics (quantbiolab) at University of Oldenburg. The results are presented in Chapter 2.

3. **Deeper investigation of the GC-E mutant V902L concerning Ca^{2+} dependency and allosteric communication**

Upon discovering that the swinging motion of the dimerization domain of GC-E is a key conformational switch regulating cyclase going from the low-to-high activity state and preliminary findings as indicative of Ca^{2+} effect on the constitutively active V902L mutant in the absence of its regulator GCAPs, we further elaborate our study which aimed to:

- Determine the Ca^{2+} dependency of V902L in the absence of its regulator GCAPs.
- Further to study the possible allosteric effects in V902L within its interacting subunits and comparing it with wild type. The results are presented in Chapter 3.

4. **Pursuing the V902L study triggered a project to bring the mutant by additional mutation its original native-like state.**

Restoring GC-E to its basal activity state would be a key step in phototransduction paving a way in the therapeutic industry for the development of therapeutics to inherited retinal diseases. The conformational changes observed in the αHD suggest a dynamic transition between low and high activity states. To explore this further, we sought to modify or disrupt a critical residue in the αHD to elucidate the plausible effect, for this we aimed to:

- Generate a double mutant (L804P/V902L), which was introduced at the background of V902L cDNA and check for cyclase activity through functional assays.
- Further incorporate the double mutant into structural models to perform computational analyses of its conformational and connectivity changes. The results are presented in Chapter 3.

Secondary objective

During the investigation of GC-E regulation with and without GCAPs as described above, a side project had emerged, regarding GCAP- dependent control of guanylate cyclase activity.

- Characterizing the conformational dynamics of GCAP5 (a GCAP homologue from zebrafish).
- Studying the role of GCAP5 dimerization in GC activation.

The GCAP5 dimerization is required for the guanylate cyclase activation, so I was involved to characterize the activity of GC-E in the presence of different GCAP5 mutants, which were located at the dimer interface and designed to disrupt the dimerization of GCAP5. In a joint manuscript with the group of Prof. Jim Ames (UC Davies, California, USA), we successfully published the results presented in Chapter 4 (Figure 6).

These objectives outlined above were addressed in three publications- Chapter 2, 3 and 4 presenting a published manuscript. In addition, the thesis consists of a part with unpublished methods and results which may be relevant for future research.

Declaration:

Hereby I confirm that, Ms. Manisha Kumari Shahu contributed to the aforementioned studies as stated below:

Article:

The Transition of Photoreceptor Guanylate Cyclase Type 1 to the Active State.

Manisha Kumari Shahu, Fabian Schuhmann, Alexander Scholten, Ilia A. Solv'yov, Karl-Wilhelm Koch

Published in: *Int. J. Mol. Sci.* **2022**, *23*(7), 4030

Author contributions:
Conceptualization, K.-W.K. and M.K.S.; methodology, M.K.S., A.S., and F.S.; software, F.S. and I.A.S.; validation, K.-W.K., M.K.S., F.S., A.S., and I.A.S.; formal analysis, M.K.S. and F.S.; investigation, M.K.S. and F.S.; resources, K.-W.K. and I.A.S.; data curation, M.K.S. and F.S.; writing—original draft preparation, K.-W.K.; writing—review and editing, M.K.S., F.S., A.S., I.A.S., and K.-W.K.; visualization, M.K.S. and F.S.; supervision, I.A.S. and K.-W.K.; project administration, K.-W.K.; funding acquisition, K.-W.K. and I.A.S. All authors have read and agreed to the published version of the manuscript.

Article:

Allosteric Communication of the Dimerization and the Catalytic Domain in Photoreceptor Guanylate Cyclase

Manisha Kumari Shahu, Fabian Schuhmann, Siu Ying Wong, Ilia A. Solov'yov, and Karl-Wilhelm Koch

Published in: *Biochemistry* **2024**, 63, 17, 2131–2140

Author Contributions:
M.K.S.: conceptualization, methodology, validation, investigation, writing-original draft, visualization. F.S.: conceptualization, software, formal analysis, investigation, writing-original draft. S.Y.W.: software, validation, formal analysis, writing-original draft. I.A.S.: resources, data curation, writing-review and editing, supervision, funding acquisition K.-W.K.: conceptualization, resources, data curation, writing-review and editing, supervision, funding acquisition.

Article:

NMR and EPR-DEER Structure of a Dimericc Guanylate Cyclase Activator Protein-5 from Zebrafish Photoreceptors

Diana Cudia, Graham P. Roseman, Tufa E. Assafa, Manisha Kumari Shahu, Alexander Scholten, Sarah-Karina Menke-Sell, Hiroaki Yamada, Karl-W. Koch, Glenn Milhauser and James B. Ames

Published in: *Biochemistry* **2021,** 60,41, 3058-3070

Author contributions:

J.B.A. designed research and, with input from other authors, wrote the paper; D.E.A., G.R., T.A., M.K.S., A.S, S.-K.Z., H.Y., K.W.K., G.M. and J.B.A. performed research; D.E.A., G.R, T.A, A.S and J.B.A. analyzed data.

Chapter 2 : The transition of photoreceptor guanylate cyclase type 1 to the active state.

Manisha Kumari Shahu[1], Fabian Schuhmann[2], Alexander Scholten[1], Ilia A. Solov'yov[2], Karl-Wilhelm Koch[1,3#]

[1]Division of Biochemistry, Department of Neuroscience, University of Oldenburg, Oldenburg 26111, Germany. manisha.kumari.shahu1@uni-oldenburg.de (M.K.S.) alexander.scholten@uni-oldenburg.de (A.S.); karl.w.koch@uni-oldenburg.de (K.W.K.)

[2]Institute of Physics, University of Oldenburg, Oldenburg 26111, Germany. ; fabian.schuhmann@uni-oldenburg.de (F.S.); ilia.solovyov@uni-oldenburg.de (I.A.S.)

[3]Research Centre for Neurosensory Science, University of Oldenburg, Oldenburg 26111, Germany.

*To whom correspondence should be addressed: karl.w.koch@uni-oldenburg.de

Running title: Active state of photoreceptor guanylate cyclase

Keywords: guanylate cyclase, cGMP, calcium-binding proteins, phototransduction, retinal degeneration, vision, retina, GCAP, molecular dynamics simulation, protein geometry

Abstract

Membrane-bound guanylate cyclases (GCs), which synthesize the second messenger guanosine-3′, 5′-cyclic monophosphate, differ in their activation modes to reach the active state. Hormone peptides bind to the extracellular domain in hormone-receptor type GCs and trigger a conformational change in the intracellular, cytoplasmic part of the enzyme. Sensory GCs that are present in rod and cone photoreceptor cells have intracellular binding sites for regulatory Ca2+-sensor proteins, named guanylate cyclase-activating proteins. A rotation model of activation involving an α-helix rotation was described as a common activation motif among hormone-receptor GCs. We tested whether the photoreceptor GC-E undergoes an α-helix rotation when reaching the active state. We simulated experimentally such a transitory switch by integration of alanine residues close to the transmembrane region and compared the effects of alanine integration with the point mutation V902L in GC-E. The mutation V902L is found in patients suffering from retinal cone-rod dystrophies and leads to a constitutively active state of GC-E. We analyzed enzymatic catalytic parameters of wildtype and mutant GC-E. Our data shows no involvement of an α-helix rotation when reaching the active state indicating a difference to hormone receptor GCs. To characterize the protein conformations that represent the transition to the active state, we investigated the protein dynamics by a computational approach based on all-atom molecular dynamics simulations. We detected a swinging movement of the dimerization domain in the V902L mutant as the critical conformational switch in the cyclase going from the low-to-high activity state.

Introduction

Membrane-bound guanylate cyclases (GCs) are single-pass transmembrane proteins and operate as key enzymes in diverse physiological processes by synthesizing the second messenger guanosine-3′, 5′-cyclic monophosphate (cGMP). The functional state of the enzyme requires a homodimeric topology and the different GC sub-groups are built from a similar molecular domain structure consisting of an extracellular domain (ECD), a transmembrane domain (TM), a kinase homology domain (KHD), a dimerization domain (DD) and a catalytic domain (CCD). GC-subgroups, however, differ remarkably in their regulatory features. Extracellular ligands as natriuretic peptides activate hormone receptor GCs and regulate blood pressure, skeletal growth, and water transport. A second subgroup operates in sensory cells mediating phototransduction, chemosensation and thermosensation [1-3]. GC-E and GC-F (also dubbed ROS-GC1/2, retGC1/2) are expressed in vertebrate rod and cone photoreceptor cells. Both enzymes are not activated by external ligands; they are instead regulated at the cytoplasmic part by guanylate cyclase-activating proteins (GCAPs) in response to changes in free cytoplasmic [Ca^{2+}]. GCAPs operate in a gradual step-by-step activation pattern shaping, thereby the photoreceptor light response [4-8]. Several regions in photoreceptor GC-E participate in binding and /or regulation by GCAPs [9-11], but the interaction mode and the location of binding sites in the target GCs are still a matter of discussion [10, 11]. Mammalian photoreceptor GCs further bind to several other signalling proteins (for review [12]), including the retinal degeneration protein 3 (RD3) that has a strong inhibitory effect and is involved in GC trafficking [13, 14]. The molecular mechanism of these control steps is unknown so far.

Membrane-bound hormone-regulated GCs are in a preformed dimeric, but inactive state prior to ligand binding or before receiving a triggering activation signal. A rotation mechanism was proposed for the natriuretic peptide-receptor A (GC-A) involving the juxtamembrane region that is located between the TM and KHD regions (for review [15, 16]). This hypothesis of an activating rotation mechanism was experimentally investigated by testing mutants of GC-A for GC activity by successive integration of up to five alanine residues close to the N-terminal end of the TM region. The main conclusion of this work was that binding of the natriuretic peptide ligand triggers an α–helix rotation in the TM domain, which is further transmitted to the CCD [17]. By this mechanism, GC-A switches from the inactive to the active form. However, it is unknown whether all membrane GCs or even all transmembrane cell-surface receptors operate via this mechanism [16].

Sensory GCs like GC-E and GC-F are not activated by external ligands. Switching these GCs to the active state requires a change in free [Ca^{2+}] that is detected by guanylate cyclase-

activating proteins (GCAPs) acting as intracellular Ca^{2+}-sensor proteins and activity regulators of GC-E and GC-F [2, 4, 5-8]. This activation step differs fundamentally from those triggered by the binding of extracellular ligands. Further, photoreceptor GC-E can interact with mutant GCAP1 variants forming a constitutively active state under physiological free [Ca^{2+}] that persist even under conditions of non-physiologically high free [Ca^{2+}]. These mutations in GCAP1 correlate with forms of retinal diseases and are discussed as the molecular cause of visual impairment diagnosed in affected patients [18-26]. More recently, Wimberg et al. (2018) described a valine/leucine point mutation in human GC-E in amino acid position 902 (V902L mutant) [27]. The amino acid substitution leads to a constitutively active GC-E showing only a small additional activation by GCAP1 or GCAP2. The point mutation apparently facilitates a conformational change to the active state of GC-E that does not need the stabilizing regulatory interaction with either one or two of the GCAP Ca^{2+}-sensors. This conformational transition appears like the results obtained with the alanine mutants of GC-A, in which the integration of four alanine residues enforces a helix rotation leading to constitutive GC activation [17].

In the present study, we discuss whether the rotation model of activation is a common activation motif among membrane-bound GCs or not. We have tested whether one can induce a similar constitutive activation of GC-E by integration of alanine residues close to the TM region. We compared the effects of alanine integration with the point mutation V902L in GC-E, which leads to a constitutively active state of GC-E and correlates with cone-rod dystrophy in a patient [27]. We further analyzed the impact of the point mutation by molecular dynamics simulations using three-dimensional structural data of bovine GC-E.

Results

Test of the rotation model in GC-E activation process

Integration of one alanine residue in an α–helical secondary structural region would induce a helix rotation of 100°. Therefore, a complete 360° rotation could originate from four alanine inserted into the primary sequence. If a rotation of the TM region or other domains in the GC-E structure is an essential step for transition to the active state, we expect a constitutive activity of GC-E in the absence of GCAPs (Figure 1A). Further, we predict no Ca^{2+}-dependency of the GC-E activity. To challenge our hypotheses, we cloned GC-E constructs that harbored up to five additional alanine residues (Figure 1B) and tested the heterologous expression of the recombinant GC-E mutants in HEK293 cells. All GC-E variants expressed in the HEK293 cells and are suitable for subsequent functional tests. The expression was probed employing immunoblotting with anti-GC-E antibodies in the HEK293 cell membrane preparations (Supplementary Figure S1).

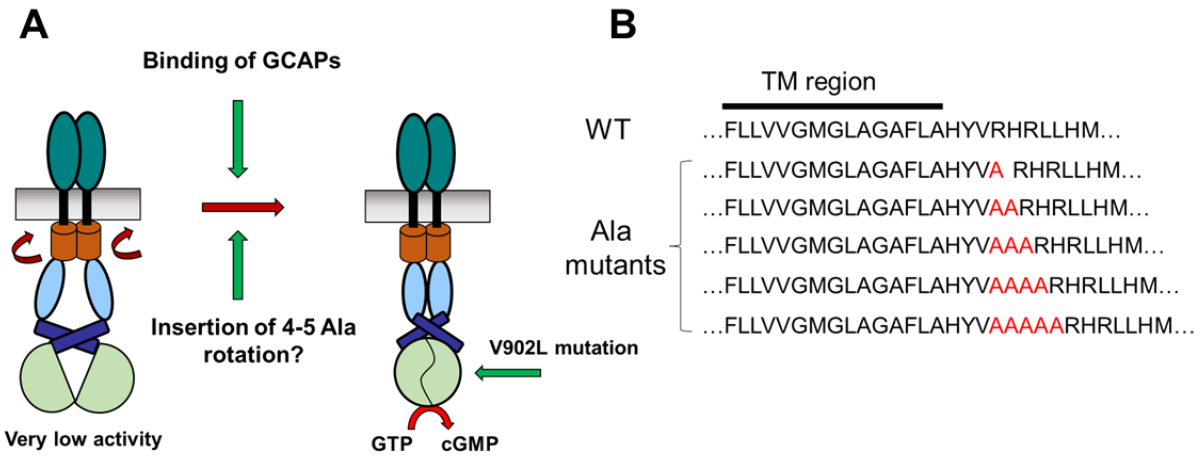

Figure 1. Hypothesis about photoreceptor GC-E reaching the active state. (**A**) Activation of GC-E by GCAPs could trigger a rotation in the cytoplasmic part of GC-E, leading to the active state. The point mutation V902L leads to a constitutively active state of human GC-E [27]. (**B**) Insertion of Ala residues (red) after the TM region of human GC-E.

Enzymatic GC assays were performed in the presence and absence of GCAP1 and GCAP2 at high and low [Ca^{2+}]. GC activities were compared with those obtained with wildtype (WT) GC-E. Figure 2 summarizes the activity profiles of GC-E variants and the regulatory impact of GCAP1 and GCAP2 on the WT and the alanine mutants at low (grey bars) and high (black bars) free [Ca^{2+}]. First, the activity of WT GC-E showed a strong dependency on free [Ca^{2+}] and GCAP1, but it was less sensitive to GCAP2 (Figure 2A and B, notice different scaling), which agreed with previous observations [18, 19, 27]. Integration of more than one alanine residue caused a 30-50% decrease in GCAP1 sensitivity without having a significant effect on the Ca^{2+}-inhibited state (Figure 2A). Testing the alanine mutants in the presence of GCAP2 resulted in a similar outcome. A low activation rate of WT GC-E by GCAP2 was observed when alanine mutants were incubated with GCAP2, yielding either identical (1Ala in Figure 2B) or 50-70% lower activation levels (Figure 2B). Comparing WT and mutant GC activities in the absence of GCAPs (only in the presence of the incubation buffer) showed nearly similar basal GC activities at a very low level (Figure 2C).

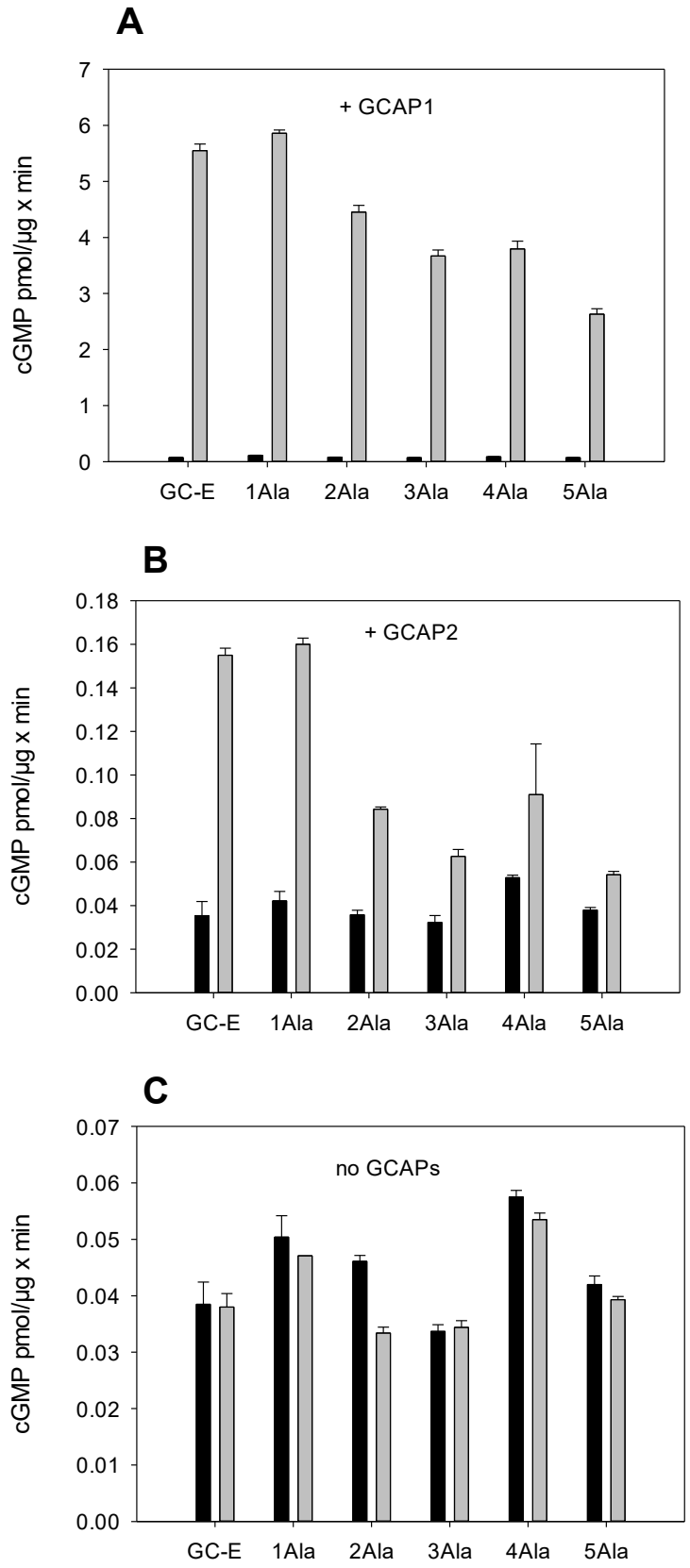

Figure 2. GC activities of Ala mutants and WT human GC-E. (**A**) Ala mutants were incubated at low (< 10 nM, grey bars) and high (33 µM, black bars) free [Ca^{2+}] in the presence of 5 µM human GCAP1 (n = 3). Control incubation of WT GC-E with GCAP1. (**B**) Similar to **A**,

GCAP2 was present instead of GCAP1 (n = 3). (**C**) Incubation of Ala mutants and WT GC-E in the absence of GCAPs at high and low [Ca^{2+}] (n = 3). Results show basal GC activities that indicate no activating effect by the insertion of Ala residues.

In summary, the data in Figure 2 showed that none of the alanine mutants exhibited a constitutive activity of GC-E indicating that the activation mechanism of GC-E appears different from that hypothesized for natriuretic peptide receptor A (GC-A).

Kinetic analysis of the constitutively active GC-E mutant V902L

The point mutation V902L in human GC-E causes cone-rod dystrophy (CRD) and so far is unique among mutations correlating with CRD in patients [27, 28]. The mutation turns GC-E into a constitutively active state, which displays only limited GCAP sensitivity. To gain more insight into this active state and the mechanism underlying its transition, we have performed a series of enzymatic assays. We tested the GC activity of WT and V902L mutants as a function of the substrate (Mg-GTP) concentration, both in the presence and absence of GCAP1 and GCAP2. Direct plots of GC activity versus [Mg-GTP] showed in all cases a sigmoidal curve indicating a cooperative process (Figure 3). Activation rates of GC-E in the presence of GCAP1 saturated above a substrate concentration of 1 mM GTP, reaching a V_{max} of 11.33 pmol/µg × min (Figure 3A). Similar results were obtained for the V902L mutant (Figures 3C and D). WT GC-E showed a 10-fold lower activation rate by GCAP2 (Figure 3B, note different scaling) in agreement with previous reports [18, 19, 27], and the curve did not reach saturation over the tested concentration range of Mg-GTP. All other activation curves saturated at the V_{max} values between 7 and 11 pmol/min/µg of protein. Figure 3E demonstrated the constitutively active state of the V902L mutant in the absence of GCAPs reaching half-maximal saturation at 0.37 mM GTP (Table 1). Fitting of the curves to a Hill model (see methods) yielded values for V_{max}, half-maximal saturation (EC_{50}) and the apparent Hill coefficient as listed in Table 1.

Table 1. Catalytic parameters of WT GC-E and V902L

Sample	**Vmax** (pmol/µg×min)	**EC_{50}** (mM)	**K_M** (mM)	**Kcat** (s^{-1})	**Kcat/K_M** ($10^3 M^{-1} \times s^{-1}$)	**Hill parameter h**
WT GC-E+GCAP1	11.33	0.37	0.34	0.8	2.35	2.07
WT GC-E+GCAP2	-	3.45	-	-	-	-
V902L+GCAP1	9	0.20	0.20	0.8	4	1.75
V902L+GCAP2	7.32	0.36	0.31	0.7	2.2	1.76
V902L no GCAPs	7.36	0.37	0.34	0.7	2.1	1.58

We tested the results of V_{max} and EC_{50} (equivalent to an apparent K_M) by analysis in Lineweaver-Burk plots. Due to the cooperativity of substrate binding, one can weigh the x-axis 1/[S] with a corresponding Hill coefficient n ($1/[S]^n$) to yield straight lines (Figure 4). The

analysis revealed apparent K_M values for WT and the V902L mutant, which were nearly identical to the determination of the corresponding EC_{50} values (Table 1). We limited the analysis to WT GC-E + GCAP1 and the mutant V902L + GCAP1/GCAP2, because human WT GC-E showed very low activation rates by GCAP2 (Figure 3B, and [27]), and we reached no saturation with the substrate in a reasonable concentration range. Analysis of results in Figure 3B, however, revealed a half-maximal saturation (EC_{50}) at 3.45 mM GTP, which was at least 10-fold higher than the K_M determined for the combination of WT GC-E with GCAP1, V902L with GCAP1 or GCAP2 and V902L without GCAPs (Table 1). This result confirms the much lower activation rate of human WT GC-E by GCAP2, which could originate from a 10-fold lower affinity of human WT GC-E for the Mg-GTP substrate.

The analysis showed further that the constitutively active state of the V902L mutant does not differ significantly from the active state of WT GC-E with respect to the catalytic parameters V_{max}, K_M, and k_{cat} yielding similar catalytic efficiencies between 2000 and 4000 $M^{-1}\times sec^{-1}$ (expressed in k_{cat}/K_M, Table 1, Figure 3 and 4).

We conclude from these results that the active state of the V902L mutant originates from a protein conformation that is like the conformation of WT GC-E in the active state stabilized by GCAP1 interaction. To gain more insight into the protein conformations that represent the transition to the active state, we undertook a computational approach based on all-atom molecular dynamics (MD) simulations.

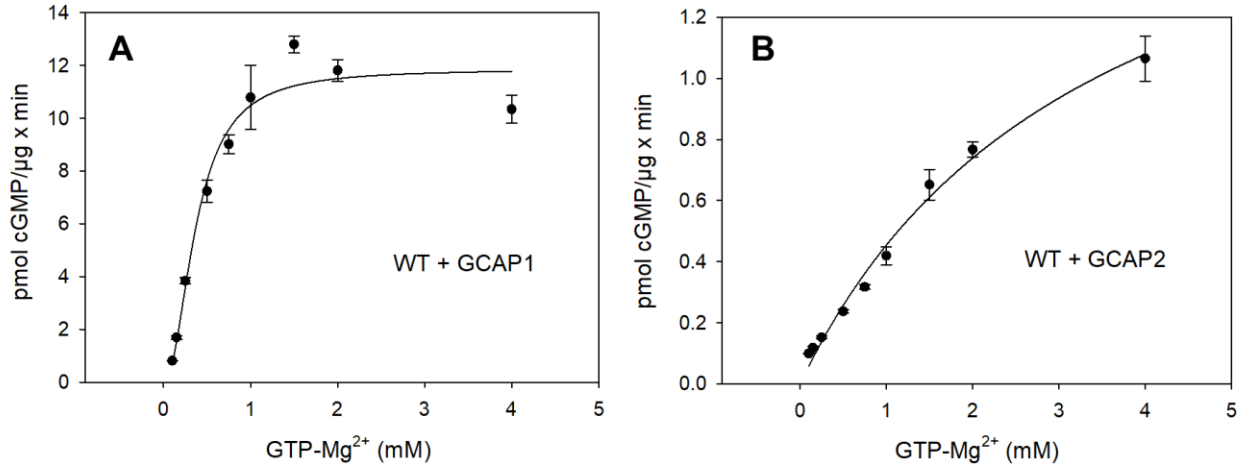

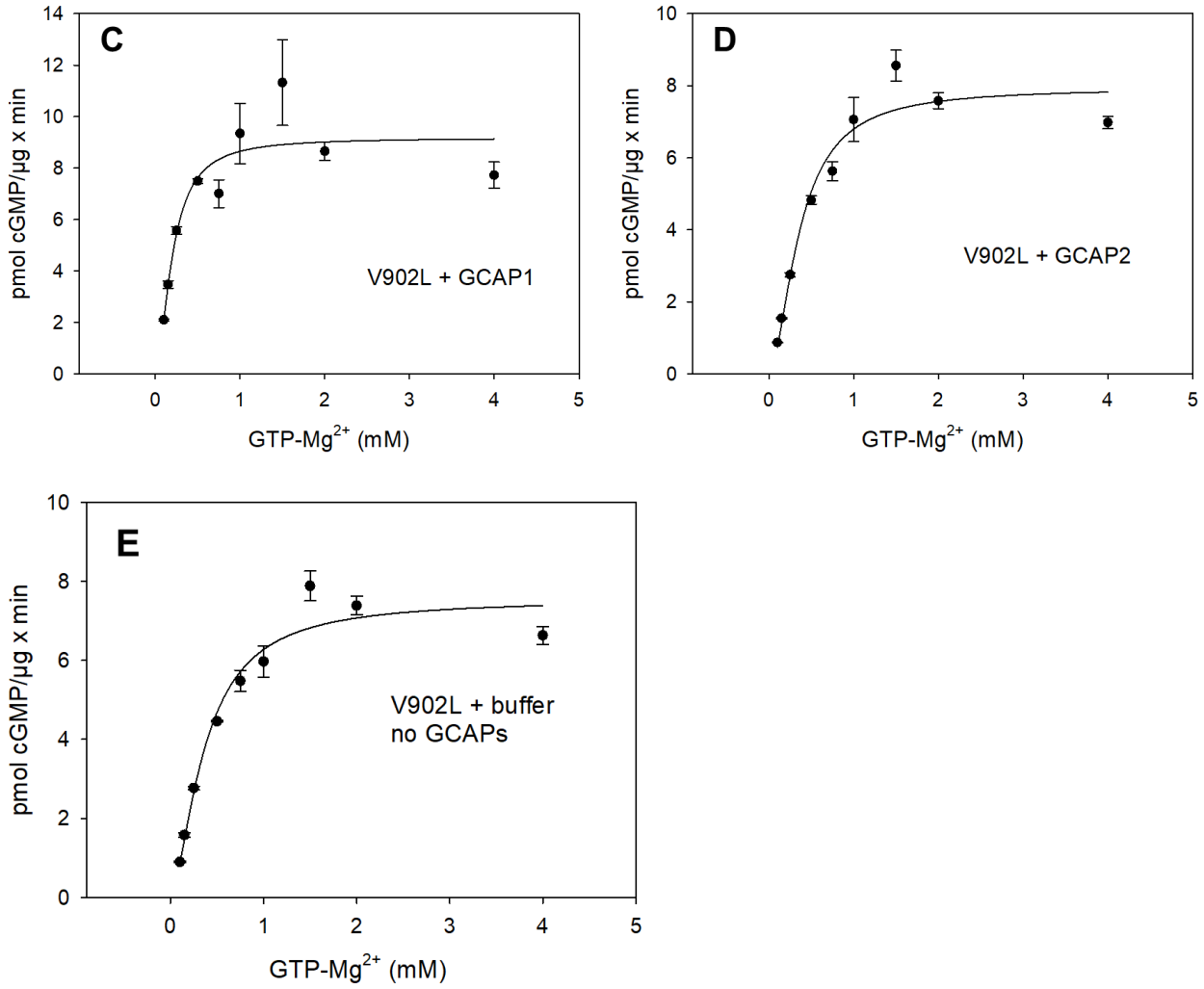

Figure 3. Functional analysis of WT and V902L mutant of human GC-E. Human GC-E variants were expressed in HEK293 cells and incubated with GCAP1 or GCAP2 at increasing Mg-GTP concentrations (in mM). Activities of WT GC-E in the presence of 5 µM GCAP1 (**A**) or 5 µM GCAP2 (**B**) (n = 3). (**C**) and (**D**) are the corresponding data sets obtained with the V902L mutant. (**E**) Constitutive activity of V902L in the absence of GCAPs. (n = 3)

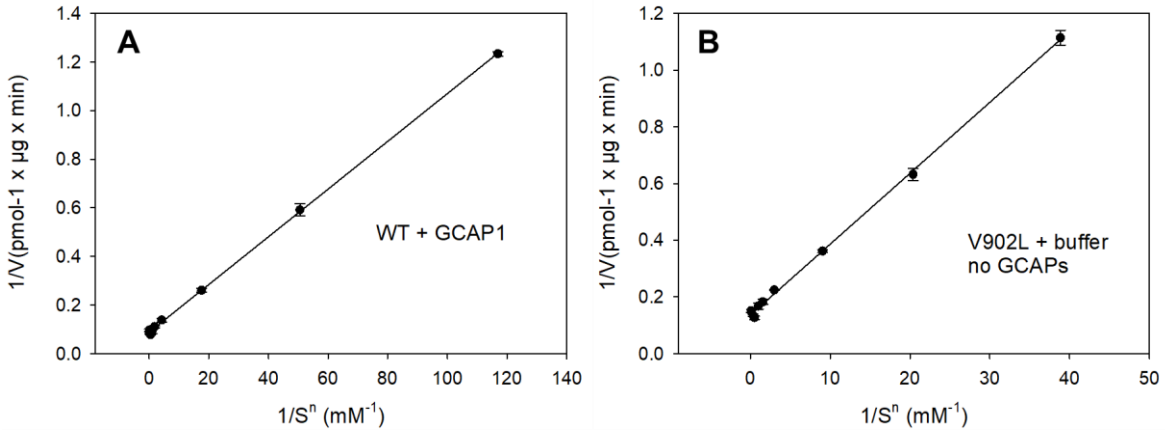

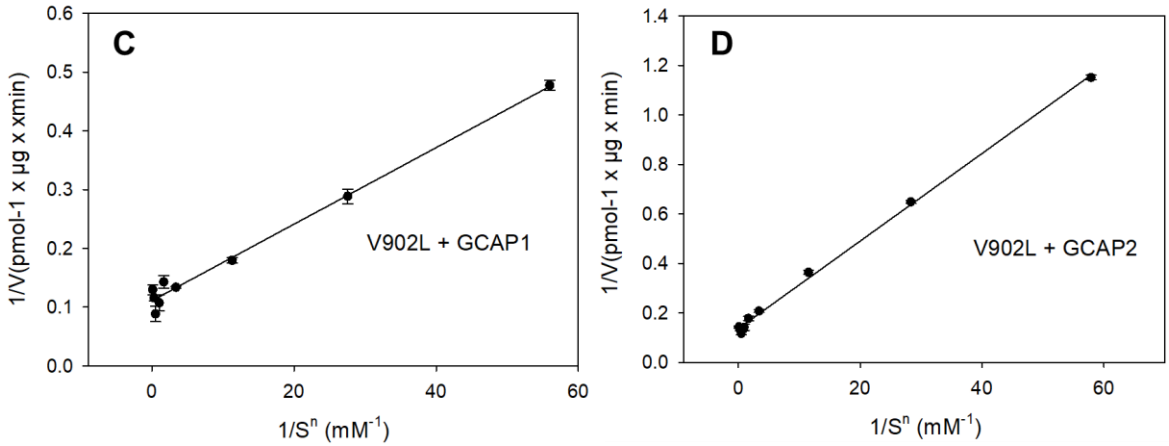

Figure 4. Lineweaver Burk plot analysis of GC activities. GC-E variants were analyzed as indicated: WT GC-E in the presence of GCAP1 (**A**) and mutant V902L (**B**) in the absence of GCAPs. V902L mutant in the presence of GCAP1 (**C**) and GCAP2 (**D**). Reciprocal substrate GTP concentration 1/S is given in (mM^{-1}). Kinetics, as shown in Figure 3, showed deviations from an ideal Michaelis-Menten model. We linearized the plots by using apparent Hill coefficients as h = 2.07 (WT + GCAP1), h = 1.58 (V902L + buffer, no GCAPs), h = 1.75 (V902L + GCAP1), h = 1.76 (V902L + GCAP2).

Molecular dynamics simulations

The amino acid residue at position 902 is in the catalytic domain and the mutation might cause a significant reorganization of the dimeric arrangement in this domain. Simulations were based on the structural information recently reported by Rehkamp et al. [29] for bovine GC-E. Human and bovine orthologues share a high sequence identity/ homology, and the corresponding valine is in position 907 (mutant V907L in the MD approach, amino acid numbering of the modelled structure refers to the bovine orthologue). Previous work identified the GCAP1 binding sites in the juxtamembrane and kinase homology region of mammalian GC-E [10, 11, 30, 31] indicating a movement or conformational change of the catalytic domain relative to the kinase homology domain during the activation process. To probe for the catalytic domain movement, the kinase homology domain of WT bovine GC-E had to be aligned to the structure of the mutant (see Methods for details). Photoreceptor GC-E exists as a homodimer [32]. The two residues in position 818 are located just before the alpha-helical dimerization domain. The residues were taken as a reference point, and the structure was translated such that the middle between the two residues 818 coincides with the origin of the coordinate system used for analysis (see Figure 5). For each MD snapshot, the geometric center of the catalytic domain was calculated and used to define the catalytic domain's position. The line segment connecting

the origin to the geometric center describes the tilting of the alpha-helical and catalytic domain relative to the kinase homology domain. To show the changes arising during bovine GC-E dynamics, the endpoints of the line segments were projected onto a plane, as visualized in Figure 5 and 6.

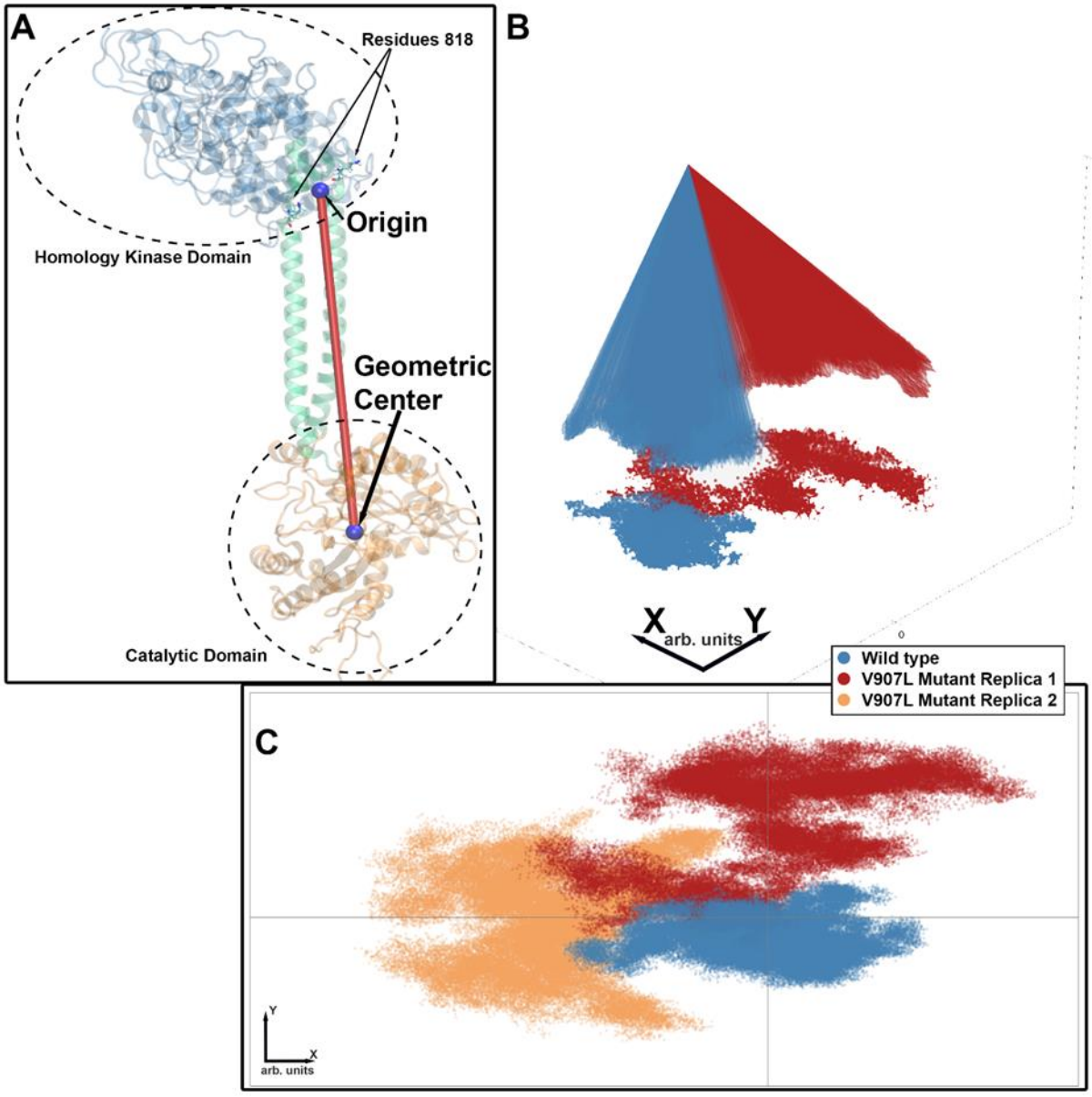

Figure 5. Visualization of bovine GC-E orientation through the plane projection. (A) The two residues at position 818 in the GC-E dimer are located at the beginning of the alpha-helical dimerization domain (green). The protein structure is translated such that the origin (0,0,0) is just in the middle between the two residues 818 (measured from the first carbon in the backbone). For each MD snapshot, the line segment between the origin and the geometric center of the catalytic domain is considered as indicated by the red line in panel A. (B) The endpoints of the line segments are then projected to the (xy)-plane. The projection describes the area, in which the catalytic domain moves relatively to the kinase homology domain during the simulation. (C) The last panel shows the top view of the projected area, including the results for both mutant replica simulations. One notices that the wildtype rather remains in its original position, while both replicas move away, although in different directions.

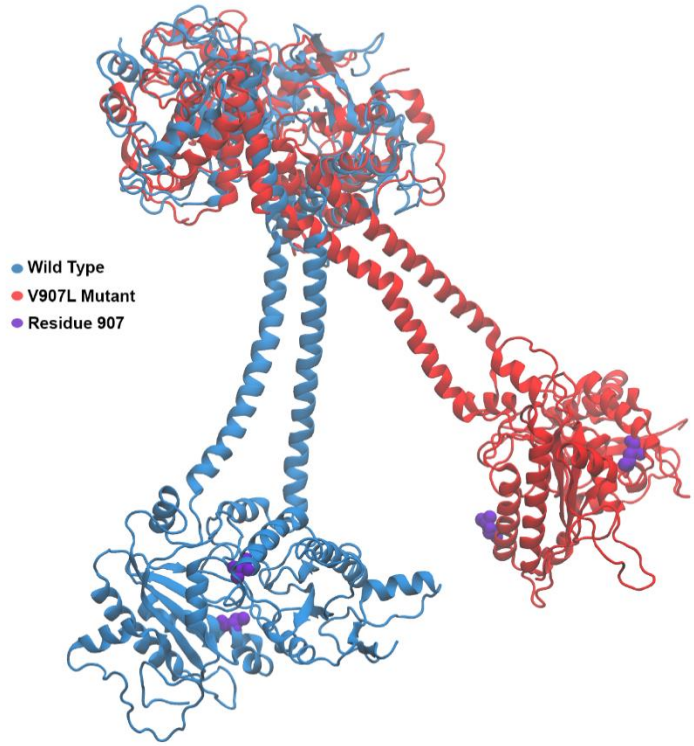

Figure 6. Bovine GC-E protein structure. Starting from the top, the kinase homology domain is shown, which is followed by the alpha-helical dimerization domain and concludes in the catalytic domain. The wildtype structure is shown in blue, the V907L mutant is shown in red. Residues 907 are shown in purple.

Difference Distance Matrix

The GTP substrate binding site in photoreceptor GC-E is supposed to comprise residues Asp890, Arg981, Ala1013, and Lys1051 in the cyclase catalytic domain [33, 34]. The alignment process was repeated, aligning the whole structure, and hence not excluding the catalytic domain. Difference distance matrices were computed following the approach outlined earlier [35], where every residue was described through the first backbone carbon atom, and the distance to all other seven binding site residues was measured. These calculated distances were averaged over the duration of the MD simulation. The process was repeated for the WT and the V907L mutant of GC-E. This analysis results in two 8×8 matrices containing the pairwise averaged distances with zero diagonal elements. The element-wise difference of the two matrices yields a difference distance matrix, which shows the positional changes of the residue relative to the other trajectory (Figure 7), which makes the conformational change measurable.

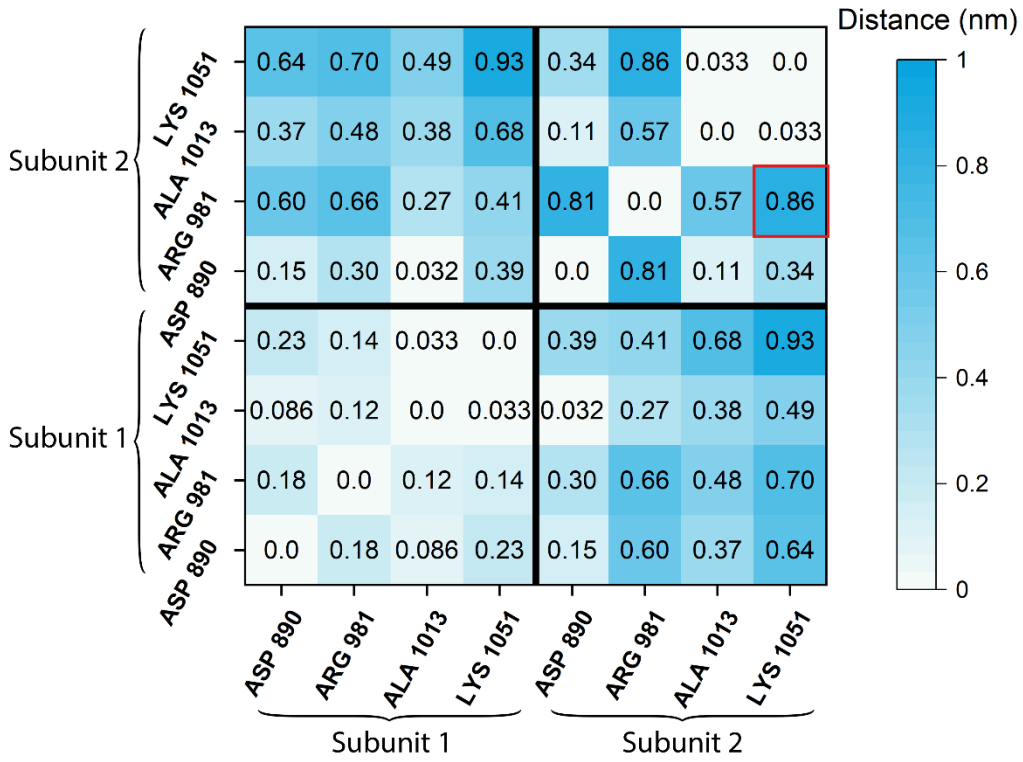

Figure 7. Difference distance matrix for binding site residues. The eight residues comprising the binding site are shown in a symmetric difference distance matrix, which quantifies the change in distance throughout the simulation duration between the wildtype and the V907L mutant of the bovine GC-E. The first four residues belong to the first subunit, while the last four belong to the second. The lower left and upper right submatrix compare distances within a subunit, while the bottom right shows the differences beyond the individual subunits. For instance, the highlighted entry (red square) indicates that the average change in distance from Lys1051 to Arg981 from the second subunit is 0.86 nm comparing the wildtype to the mutant.

Data in the difference distance matrix indicated that the residues in one subunit move very little relative to each other after the mutation, while the other subunit experiences profound changes. Especially Lys1051 changes its position drastically (visually shown in Figure 8). Furthermore, the distance between the two sets of four residues changes noticeably. It came as a surprise that the point mutation V907L has asymmetric effects on the structure of the catalytic domain.

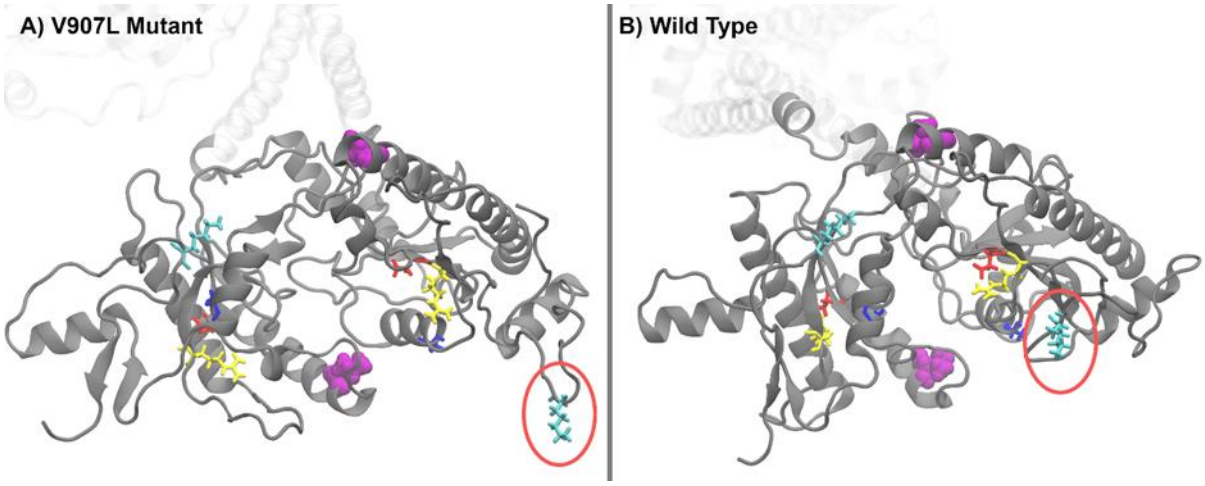

Figure 8. Critical amino acid positions in the putative GTP substrate-binding site in GC-E. Panels A and B show the catalytic domain for the V907L mutant and WT GC-E, respectively. The residues comprising the binding site are highlighted in sticks representation and colored according to their type (blue=Ala, lime=Arg, red=Asp, cyan=Lys). In one of the subunits of the GC-E structure, Lys1051 exhibits significant movement as it swings out (red ellipsoid). Residues 907 are highlighted in purple.

Discussion

Membrane-bound GCs reach the active state by different interaction processes. Hormone receptor GC types bind hormone peptides at the extracellular domain, whereas photoreceptor GCs have intracellular binding sites for Ca^{2+}-sensor proteins, named GCAPs. However, despite these apparent differences, membrane-bound GCs could reach the active state by similar conformational transitions since membrane-bound GCs share a similar structural topology. Experimental support for a ligand-induced rotation mechanism exists for GC-A [17]. We used the same experimental approach as Parat et al. [17] by inserting alanine residues close to the TM region (Figure 1) and tested the functional consequences. Since we did not observe any constitutive activation of GC-E, we interpret our results as that successive insertion of alanine residues did not cause a conformational transition to the active state. In fact, the alanine point mutants displayed some minor disturbances in basal and GCAP-dependent activity, pointing to a mechanism that does not involve a rotational repositioning of the TM or juxtamembrane region.

This result leaves the question about the conformational dynamics exhibited by photoreceptor GCs in their transit to the active state. We took advantage of the point mutation V902L in human GC-E that was characterized as permanently active without the on-off control operated by the GCAP Ca^{2+}-sensor. So far, the V902L mutation in GC-E is the only point mutation

known so far in human GC-E that leads to a constitutive activation in the absence of GCAPs. Other point mutations in GC-E causing visual impairment show drastically reduced activities or a change in Ca^{2+}-sensitive GCAP regulation [28], and not an increase of basal enzyme activity. Thus, we took this mutant as a tool to investigate the mechanism of GC-E activation. Previous work on V902L focused on the effects of changing Ca^{2+} and GCAP concentrations but not on the substrate dependency and the catalytic efficiency expressed in k_{cat}/K_M. We determined these values as listed in Table 1, showing that k_{cat}/K_M for the mutant V902L with GCAP1 and without GCAPs is like the parameter analyzed for WT with GCAP1. The constitutive activity of the V902L mutant could, therefore, not originate from a higher catalytic efficiency. In fact, rod and cone photoreceptor GCs are low-efficiency enzymes with k_{cat}/K_M of 1.9×10^4 - 1.6×10^5 $M^{-1}sec^{-1}$ as noted previously for the bovine and mice orthologues [5, 6]. The parameter k_{cat}/K_M is equivalent to the association rate constant of the substrate binding to the enzyme. Taking structural information as visualized for the bovine orthologue in Figure 8, the V907L mutation causes a flexible movement of a Lys in position 1051 swinging away from the dimer interface. This movement or higher flexibility might facilitate reaching the transition state in the catalytic center. GCAPs probably activate photoreceptor GCs by stabilizing the transition state [36]. In the constitutively active state of GC-E, the stabilization must be realized by the point mutation and its structural consequences. Figure 6 illustrates how the swinging movement of the alpha-helical domain connected to the catalytic domain leads to a different orientation of the residues in position 907. In WT GC-E, both valines are close to the dimer interface and opposite to each other. In the mutant, Leu907 is more exposed on the protein surface. Leu contains one additional methylene group in the side chain. The side chain is longer and more hydrophobic than in Val. This might have caused a repulsion between the leucines leading to a different dimer interface.

Constitutive activation of human GC-E is a consequence of several point mutations that cause retinal dystrophies in patients suffering from visual impairment [28]. Most of these mutations are, however, found in the regulatory Ca^{2+}-sensor GCAP1. Point mutations in GCAP1 very often cause lower affinities for Ca^{2+}, and GCAP1 mutants thereby display a shift in Ca^{2+}sensitive GC regulation to free [Ca^{2+}], which is outside of the physiologically relevant range between 50 and 500 nM leading to permanent activity of the GCAP1/GC-E complex [18-26]. Retinal disease-related point mutations in the alpha-helical dimerization domain of human GC-E also correlate in some cases with a disturbance of Ca^{2+}-sensitive control by GCAPs [9] and for review [28]. The alpha-helical dimerization domain has been discussed as a Ca^{2+}-sensitive control module in this context, which is influenced by Ca^{2+}-dependent conformational

changes in GCAPs but is not a Ca^{2+}-sensor itself [9]. The swinging movement of the dimerization domain in the V902L mutant, as illustrated in Figure 6, might represent the critical conformational switch in the cyclase going from the low-to-high activity state. In the case of the WT, the switch is triggered by interaction with GCAP1; in the case of the V902L mutant, the amino acid exchange is sufficient for the transition. Our results show a principal difference in the activation modus between hormone receptor GCs and sensory GCs, which is relevant for understanding the molecular basis of retinal diseases.

Materials and Methods

Cloning of polyalanine GC-E mutants

To create the five desired polyalanine GC-E mutants, the WT GC-E sequence was cloned into a pIRES2-eGFP vector and used as a template [9]. Site-directed mutagenesis was achieved by introducing one to five alanines at the C-terminal site of the transmembrane region (Figure 1B) in the GC-E sequence by polymerase chain reaction (PCR) using KOD (Hot start DNA Polymerase Novagen®) enzyme. Instructions according to the manufacturer's protocol were followed. The primers used to produce the mutants are listed in Supplementary Table S1. GC-E polyalanine mutants are abbreviated **1Ala, 2Ala, 3Ala, 4Ala, 5Ala**. Since the cloning strategy failed for creating 4Ala, we used a different approach. The isolated 1Ala cDNA was used instead of GC-E cDNA to introduce four alanine residues at the site of interest employing the primer set *b* as mentioned in Supplementary Table S1. The obtained clones were verified by full-length sequencing of the GC-E coding region. Vector encoding V902L mutant sequence [27] was retransformed into XL-1 Blue cells for DNA isolation and for further expressing mutant protein transiently in HEK 293 cells.

Heterologous expression of GC-E, polyalanine mutants and V902L mutant

For further functional studies, the HEK293 cell line was transiently transfected with GC-E WT cDNA and the respective mutant forms. Transfection was performed using Polyethylemine (PEI) at 60-70% of confluency of 100 mm plates. Eight µg DNA were mixed with 32 µg PEI in DMEM without supplements and incubated at room temperature (RT) for 15 min. Subsequently, sample mix was added to the respective cell plates and incubated in the incubator at 37°C, 5% CO_2. Cells were harvested between 72-96h of incubation post transfection by centrifugation for 5min at 500×g. Cell pellets were washed with PBS, transferred in 1.5 ml tube respectively, and centrifuged again for 5 min at 12,000×g. The pellets were frozen at -80°C until further use.

Electrophoresis and western blotting

Sodium dodecyl-sulfate polyacrylamide gel electrophoresis (SDS-PAGE) and western blotting were performed according to established procedures in the laboratory [9, 37] with the following modification, the protein transfer was done via tank transfer method. The blot was then incubated in TBST buffer (Tris-buffered saline/0.05% Tween 20) with 1X ROTI®Block (ROTH) solution for 1 hour. Primary antibody GC1 # 3 directed against bovine GC-E [5, 9] recognized human GC-E and was used at a dilution of 1:10,000. Incubation with the primary antibody was done overnight at 4°C. A goat anti-rabbit peroxidase-conjugated antibody (Dianova, Germany) at a concentration of 50% in glycerol was used as a secondary antibody at a dilution of 1:5000.

Guanylate cyclase assay and enzyme kinetics

To analyze GC-E activity for a possible effect of subunit rotation, the enzymatic activity of the polyalanine mutants compared to WT GC-E was measured. Transfected HEK cell pellets were resuspended in 1 ml, 10 mM Hepes/KOH pH 7.4 with 1 mM DTT and a protease inhibitor cocktail. The suspension was incubated on ice for 30 min followed by cell lysis using a syringe with a 0.7 mm needle. After centrifugation at 13,000×g for 8 min at 4°C, the cell pellet was resuspended in 100 µl of 50 mM Hepes/KOH pH 7.4, 50 mM KCl, 20 mM NaCl, 1 mM DTT and a protease inhibitor cocktail. Twenty µl of a GCAP1 or GCAP2 solution (5 µM) or water, which were previously adjusted to different free Ca^{2+} concentrations using a Ca^{2+} / EGTA buffer system, exactly as described previously [5, 9, 38]. For each sample, 10 µl of respective membrane suspensions were mixed and pre-incubated for 5min at room temperature. Reaction started by adding 20 µl of 2.5×GC buffer (75 mM Mops/KOH pH 7.2, 150 mM KCl, 10 mM NaCl, 2.5 mM DTT, 8.75 mM $MgCl_2$, 2.5 mM GTP, 0.75 mM, and 0.4 mM Zaprinast). The reaction mixtures were incubated for 10 min at 30°C and stopped by adding 50 µl 0.1 M EDTA incubating at 95°C for 5 min. Samples were centrifuged for 10 min at 13,000 ×*g*. Supernatants were analyzed for produced cGMP by reversed-phase HPLC using a LiChrospher® 100 RP-18 (5µm) column (Merck, Darmstadt, Germany) exactly as described [5, 9, 38].

For the analysis of enzyme kinetics of WT GC-E and the mutant V902L, we followed basically our previous protocol [5]. Briefly, GC-E variants were reconstituted with 5 µM of purified myristoylated forms of human GCAP1 and human GCAP2. Incubations containing V902L were also done in the absence of GCAPs. Guanylate cyclase activity was assayed at 2 mM EGTA ($\leq$ 10 nM free Ca^{2+}) as a function of the substrate GTP (concentration range between 0 and 4 mM). Analysis of data was performed as previously reported [5]. Plots of activity versus Mg-GTP concentration were fitted to a Hill model (f = a*x^h/(c^h+x^h) using SigmaPlot 13.0.

Expression and purification of GCAP1 and GCAP2

Human myristoylated GCAP1 and GCAP2 were expressed in *E.coli* and purified to homogeneity by anion exchange chromatography and size exclusion chromatography as previously reported [5, 38]. Myristoylation of GCAPs during bacterial expression was accomplished by co-transforming *E.Coli* cells with N-myristoyl-transferase from yeast and supplementation with myristic acid as reported previously [5]. We modified the expression of GCAP1 for obtaining the protein in a soluble fraction using 0.1mM IPTG at 30°C for 2 hours.

Expression of the catalytic domain of GC

A fusion construct consisting of the catalytic domain of GC-E and the maltose-binding protein (MBP) was expressed and purified as previously reported [11] but adding a further purification step using Ni-NTA column. A fraction containing the GC-E construct was loaded on a Ni-NTA column that was pre-equilibrated with 20 mM Tris/HCl pH 7.5, 150 mM NaCl, 5% (v/v) glycerol, 10 mM imidazole, 5 mM β-mercaptoethanol. After loading, the column was washed with the same buffer before the construct was eluted using 20 mM Tris/HCl pH 7.5, 200 mM NaCl, 5% glycerol, 250 mM imidazole, 5mM β-mercaptoethanol. Eluted protein fractions were stored in aliquots at -80°C until further use.

Chemiluminescence detection and quantification of polyalanine mutants

Expression of polyalanine mutants: 5 µg protein of each variant were analyzed by SDS-PAGE and western blotting as described above. After transfer to the blot membrane, blots were incubated with Western Bright ECL reagent 1 and 2 (advansta) and protein bands were detected using Azure c400 Gel Imaging System by Azure Biosystems. The intensity of protein bands was determined using the device-specific software AzureSpot (Supplement Figure S1). The difference in the protein expression level of mutant proteins was normalized to WT GC-E. Normalization of varying amounts in protein expression level was considered while calculating the final cGMP level.

Quantification of WT GC-E and V902L mutant

The fusion construct MBP-CD consisting of the catalytic domain of GC-E and MBP was used for creating a calibration curve. For this purpose, increasing amounts of purified MBP-CD (20-400 ng) were applied on SDS polyacrylamide gels. Membrane suspensions of 2.5 µg and 5 µg of total membrane protein containing GC-E or V902L were applied on the same gels and analyzed by SDS-PAGE. After electrophoresis, proteins were blotted, and band intensity was detected and determined as described above using Azure c400 and AzureSpot. Varying amount of MBP-CD were used for calibration and the amount of cyclase GC-E and V902L was obtained from the calibration curve (Supplement Figure S2).

Molecular dynamics simulation

In a recent study [29] the bovine guanylate cyclase 1 protein from the rod outer segment membrane bovine GC-E was modeled. The resulting published structure serves as a base for the following all-atom molecular dynamics MD protocol.

The studied structure contains the kinase homology domain, the alpha-helical domain, and the catalytic domain, while the extracellular, transmembrane domain and juxtamembrane domain are missing. Additionally, residues 608 to 617 are missing in the structure, but the sequence for these residues is known. The structure of bovine GC-E was used to study the behavior of its human counterpart, as it is in close resemblance with a sequence identity of 87% in the existing parts. Due to a slight shift in sequence comparing the bovine to the human GC-E protein, all residues are off by five. Hence, assuming one is looking for residue 902 in human GC-E, one would choose residue 907 in bovine GC-E. All simulations were carried out using the bovine GC-E structure.

All simulations were run using NAMD [39, 40], and the interatomic interactions were described using the CHARMM36 force field with CMAP corrections [41-48]. Simulations were set up using the online platform VIKING [49].

Pep McConst [35] was used to reconstruct the missing residues, which was followed by structure minimization in vacuum, where all residues except the newly added ones were restrained to allow the newly added part to relax to a feasible conformation. Following energy minimization, the structure was first equilibrated with a simulation timestep of 0.25 fs, which was increased to 1.0 fs once a stable conformation was achieved. The equilibrated structure was solvated in a water box and neutralized. 4 mM NaCl and 3.5 mM $MgCl_2$ were added to neutralize and ionize the system. The system was then equilibrated further and subsequently simulated extensively at a temperature of 310 K and atmospheric pressure of 1 bar in an NVT (constant number of particles, volume, and temperature) ensemble. In total, the structure was equilibrated for over 140 ns.

The alignment was conducted by an iterative scheme employing the Kabsch-algorithm successfully applied in an earlier study [50]. The simulated trajectory was aligned to the first snapshot as a reference and then iteratively aligned to the new average structure until the overall root mean square deviation dropped below a threshold value.

Two replica simulations, in which the valine residue at position 907 in bovine GC-E was mutated to leucine (V902L), were initiated. The wildtype simulation was also continued. The mutations were conducted using the Mutator plugin of VMD [51]. The three simulations (WT,

two replicas of V907L) were conducted for 400 ns each. The resulting trajectories were prepared for analyses using the MDTraj package [52].

Supplementary Materials: The following supporting information can be downloaded at: www.mdpi.com/xxx/s1, Figure S1: Western blot for verification and quantification of poly alanine mutants; Figure S2: Quantification of GC-E and V902L in HEK293 cell membranes. Table S1: Oligonucleotide sequences used in the present study.

Author Contributions: Conceptualization, K.W.K. and M.K.S.; methodology, M.K.S., A.S., F.S.; software, F.S. and I.A.S..; validation, K.W.K., M.K.S., F.S., A.S. and I.A.S.; formal analysis, M.K.S. and F.S..; investigation, M.K.S. and F.S..; resources, K.W.K. and I.A.S.; data curation, M.K.S. and F.S.; writing—original draft preparation, K.W.K.; writing—review and editing, M.K.S., F.S., A.S., I.A.S. and K.W.K.; visualization, M.K.S. and F.S.; supervision, I.A.S. and K.W.K.; project administration, K.W.K.; funding acquisition, K.W.K. and I.A.S.. All authors have read and agreed to the published version of the manuscript.

Funding: This research was funded by DFG (Deutsche Forschungsgemeinschaft) grant numbers GRK1885/2 and SFB 1372 (to K.W.K and I.A.S.). I.A.S. thanks the Volkswagen Foundation (Lichtenberg Professorship) and MWK (SMART).

Institutional Review Board Statement: Not applicable

Data Availability Statement: Data are stored on institutional (university operated) devices; they are available upon request from the corresponding authors.

Acknowledgments: Computational resources for the simulations were provided by the CARL Cluster at the Carl-von-Ossietzky University of Oldenburg and the North German Supercompu-ting Alliance (HLRN).

Conflicts of Interest: The authors declare no conflict of interest. The funders had no role in the design of the study; in the collection, analyses, or interpretation of data; in the writing of the manuscript, or in the decision to publish the results.

References

1. Pichlo, M.; Bungert-Plümke, S.; Weyand, I.; Seifert, R.; Bönigk, W.; Strünker, T.; Kashikar, N.D.; Goodwin, N.; Müller, A.; Pelzer, P.; et al. High density and ligand affinity confer ultrasensitive signal detection by a guanylyl cyclase chemoreceptor. *J Cell Biol* **2014**, *206*, 541-57, doi: 10.1083/jcb.201402027.

2. Sharma, R.K.; Duda, T.; Makino, C.L. Integrative Signaling Networks of Membrane Guanylate Cyclases: Biochemistry and Physiology. *Front Mol Neurosci* **2016**, *9,83*, doi: 10.3389/fnmol.2016.00083.
3. Kuhn, M. Molecular Physiology of Membrane Guanylyl Cyclase Receptors. *Physiol Rev* **2016,** *96, 751-804*, doi: 10.1152/physrev.00022.2015.
4. Mendez, A.; Burns, M.E.; Sokal, I.; Dizhoor, A.M.; Baehr, W.; Palczewski, K.; Baylor, D.A.; Chen, J. Role of guanylate cyclase-activating proteins (GCAPs) in setting the flash sensitivity of rod photoreceptors. *Proc Natl Acad Sci U S A* **2001,** *98, 9948-53*, doi: 10.1073/pnas.171308998.
5. Hwang, J.Y.; Lange, C.; Helten, A.; Höppner-Heitmann, D.; Duda, T.; Sharma, R.K.; Koch, K.W. Regulatory modes of rod outer segment membrane guanylate cyclase differ in catalytic efficiency and Ca(2+)-sensitivity. *Eur J Biochem* **2003**, *270, 3814-3821*, doi: 10.1046/j.1432-1033.2003.03770.x.
6. Peshenko, I.V.; Olshevskaya, E.V.; Savchenko, A.B.; Karan, S.; Palczewski, K.; Baehr, W.; Dizhoor, A.M. Enzymatic properties and regulation of the native isozymes of retinal membrane guanylyl cyclase (RetGC) from mouse photoreceptors. *Biochemistry* **2011** *50, 5590-5600*, doi: 10.1021/bi200491b.
7. Makino, C.L.; Wen, X.H.; Olshevskaya, E.V.; Peshenko, I.V.; Savchenko, A.B.; Dizhoor, A.M. Enzymatic relay mechanism stimulates cyclic GMP synthesis in ro; photoresponse: biochemical and physiological study in guanylyl cyclase activating protein 1 knockout mice. *PLoSOne* **2012**, 7, e47637. doi: 10.1371/journal.pone.0047637.
8. Koch, K.W.; Dell'Orco, D. A calcium-relay mechanism in vertebrate phototransduction. *ACS Chem Neurosci* **2013**, *4*, 909-917, doi:10.1021/cn400027z
9. Zägel, P.; Dell'Orco, D.; Koch, K.W. The dimerization domain in outer segment guanylate cyclase is a Ca^{2+}-sensitive control switch module. *Biochemistry* **2013** 52, 5065-5074. doi: 10.1021/bi400288p.
10. Peshenko, I.V.; Olshevskaya, E.V.; Dizhoor, A.M. Evaluating the role of retinal membrane guanylyl cyclase 1 (RetGC1) domains in binding guanylyl cyclase-activating proteins (GCAPs). *J Biol Chem* **2015**, *290, 6913-6924*, doi: 10.1074/jbc.M114.629642.
11. Sulmann, S.; Kussrow, A.; Bornhop, D.J.; Koch, K.W. Label-free quantification of calcium-sensor targeting to photoreceptor guanylate cyclase and rhodopsin kinase by backscattering interferometry. *Sci Rep* **2017**, *7, 45515*, doi: 10.1038/srep45515.
12. Koch, K.W.; Dell'Orco, D. Protein and Signaling Networks in Vertebrate Photoreceptor Cells. *Front Mol Neurosci* **2015**, *8*, 67, doi:10.3389/fnmol.2015.00067

13. Azadi, S.; Molday, L.L.; Molday, R.S. RD3, the protein associated with Leber congenital amaurosis type 12, is required for guanylate cyclase trafficking in photoreceptor cells. *Proc Natl Acad Sci U S A* **2010**, *107, 21158-21163*, doi: 10.1073/pnas.1010460107.
14. Peshenko, I.V.; Olshevskaya, E.V.; Azadi, S.; Molday, L.L.; Molday, R.S.; Dizhoor, A.M. Retinal degeneration 3 (RD3) protein inhibits catalytic activity of retinal membrane guanylyl cyclase (RetGC) and its stimulation by activating proteins. *Biochemistry* **2011**, *50, 9511-9519*, doi: 10.1021/bi201342b.
15. Misono, K.S.; Philo, J.S.; Arakawa, T.; Ogata, C.M.; Qiu, Y.; Ogawa, H.; Young, H.S. Structure, signaling mechanism and regulation of the natriuretic peptide receptor guanylate cyclase. *FEBS J* **2011**, *278, 1818-1829*, doi: 10.1111/j.1742-4658.2011.08083.x.
16. Maruyama, I.N. Activation of transmembrane cell-surface receptors via a common mechanism? The "rotation model". *Bioessays* **2015**, *37, 959-967*, doi: 10.1002/bies.201500041.
17. Parat, M.; Blanchet, J.; De Léan, A. Role of juxtamembrane and transmembrane domains in the mechanism of natriuretic peptide receptor A activation. *Biochemistry* **2010**, *49, 4601-4610,* doi: 10.1021/bi901711w.
18. Dell'Orco, D.; Dal Cortivo, G. Normal GCAPs partly compensate for altered cGMP signaling in retinal dystrophies associated with mutations in GUCA1A. *Sci Rep* **2019**, *9, 20105,* doi:10.1038/s41598-019-56606-5.
19. Avesani, A.; Marino, V.; Zanzoni, S.; Koch, K.W.; Dell'Orco, D. Molecular properties of human guanylate cyclase-activating protein 2 (GCAP2) and its retinal dystrophy-associated variant G157R. *J Biol Chem* **2021**, *296, 100619*, doi: 10.1016/j.jbc.2021.100619.
20. Kitiratschky, V.B.; Behnen, P.; Kellner, U.; Heckenlively, J.R.; Zrenner, E.; Jagle, H.; Kohl, S.; Wissinger, B.; Koch, K.W. Mutations in the GUCA1A gene involved in hereditary cone dystrophies impair calcium-mediated regulation of guanylate cyclase. *Hum Mutat* **2009**, *30, E782-796*, doi:10.1002/humu.21055.
21. Dizhoor, A.M.; Boikov, S.G.; Olshevskaya, E.V. Constitutive activation of photoreceptor guanylate cyclase by Y99C mutant of GCAP-1. Possible role in causing human autosomal dominant cone degeneration. *J Biol Chem* **1998**, 273, 17311-17314. doi: 10.1074/jbc.273.28.17311.
22. Sokal, I.; Li, N.; Surgucheva, I.; Warren, M.J.; Payne, A.M.; Bhattacharya, S.S.; Baehr, W.; Palczewski, K. GCAP1 (Y99C) mutant is constitutively active in autosomal dominant cone dystrophy. *Mol Cell* **1998**, *2, 129-133,* doi: 10.1016/s1097-2765(00)80121-5.
23. Biasi, A.; Marino, V.; Dal Cortivo, G.; Maltese, P.E.; Modarelli, A.M.; Bertelli, M.; Colombo, L.; Dell'Orco, D. A Novel GUCA1A Variant Associated with Cone Dystrophy Alters cGMP

Signaling in Photoreceptors by Strongly Interacting with and Hyperactivating Retinal Guanylate Cyclase. *Int J Mol Sci* **2021**, *22*, doi:10.3390/ijms221910809.

24. Marino, V.; Dal Cortivo, G.; Oppici, E.; Maltese, P.E.; D'Esposito, F.; Manara, E.; Ziccardi, L.; Falsini, B.; Magli, A.; Bertelli, M., et al. A novel p.(Glu111Val) missense mutation in GUCA1A associated with cone-rod dystrophy leads to impaired calcium sensing and perturbed second messenger homeostasis in photoreceptors. *Hum Mol Genet* **2018**, *27*, 4204-4217, doi:10.1093/hmg/ddy311.
25. Vocke, F.; Weisschuh, N.; Marino, V.; Malfatti, S.; Jacobson, S.G.; Reiff, C.M.; Dell'Orco, D.; Koch, K.W. Dysfunction of cGMP signalling in photoreceptors by a macular dystrophy-related mutation in the calcium sensor GCAP1. *Hum Mol Genet* **2017**, *26*, 133-144, doi:10.1093/hmg/ddw374.
26. Peshenko, I.V.; Cideciyan, A.V.; Sumaroka, A.; Olshevskaya, E.V.; Scholten, A.; Abbas, S.; Koch, K.W.; Jacobson, S.G.; Dizhoor, A.M. A G86R mutation in the calcium-sensor protein GCAP1 alters regulation of retinal guanylyl cyclase and causes dominant cone-rod degeneration. *J Biol Chem* **2019**, *294*, 3476-3488, doi:10.1074/jbc.RA118.006180.
27. Wimberg, H.; Lev, D.; Yosovich, K.; Namburi, P.; Banin, E.; Sharon, D.; Koch, K.W. Photoreceptor Guanylate Cyclase (GUCY2D) Mutations Cause Retinal Dystrophies by Severe Malfunction of Ca2+-Dependent Cyclic GMP Synthesis. *Front Mol Neurosci* **2018,** *11, 348*, doi: 10.3389/fnmol.2018.00348.
28. Sharon, D.; Wimberg, H.; Kinarty, Y.; Koch, K.W. Genotype-functional-phenotype correlations in photoreceptor guanylate cyclase (GC-E) encoded by GUCY2D. *Prog Retin Eye Res* **2018**, *63, 69-91,* doi: 10.1016/j.preteyeres.2017.10.003.
29. Rehkamp, A.; Tänzler, D.; Tüting, C.; Kastritis, P.L.; Iacobucci, C.; Ihling, C.H.; Kipping, C.; Koch, K.-W.; Sinz, A. First 3D-Structural Data of Full-Length Guanylyl Cyclase 1 in Rod-Outer-Segment Preparations of Bovine Retina by Cross-Linking/Mass Spectrometry. *J Mol Biol* **2021**, *433, 166947*, doi: org/10.1016/j.jmb.2021.166947.
30. Lange, C.; Duda, T.; Beyermann, M.; Sharma, R.K.; Koch, K.W. Regions in vertebrate photoreceptor guanylyl cyclase ROS-GC1 involved in Ca(2+)-dependent regulation by guanylyl cyclase-activating protein GCAP-1. *FEBS Lett* **1999**, *460, 27-31*. doi: 10.1016/s0014-5793(99)01312-5.
31. Krylov, D.M.; Hurley, J.B. Identification of proximate regions in a complex of retinal guanylyl cyclase 1 and guanylyl cyclase-activating protein-1 by a novel mass spectrometry-based method. *J Biol Chem* **2001**, *276, 30648-30654,* doi: 10.1074/jbc.M104121200.

32. Yang, R.B.; Garbers, D.L. Two eye guanylyl cyclases are expressed in the same photoreceptor cells and form homomers in preference to heteromers. *J Biol Chem* **1997**, *272, 13738-13742,* doi: 10.1074/jbc.272.21.13738.
33. Tucker, C.L.; Hurley, J.H.; Miller, T.R.; Hurley, J.B. Two amino acid substitutions convert a guanylyl cyclase, RetGC-1, into an adenylyl cyclase. *Proc Natl Acad Sci U S A* **1998** *95, 5993-5997,* doi: 10.1073/pnas.95.11.5993.
34. Liu, Y.; Ruoho, A.E.; Rao, V.D.; Hurley, J.H. Catalytic mechanism of the adenylyl and guanylyl cyclases: modeling and mutational analysis. *Proc Natl Acad Sci U S A* **1997**, *94,13414-13419,* doi: 10.1073/pnas.94.25.13414.
35. Schuhmann, F.; Korol, V.; Solov'yov, I. A. Introducing Pep McConst—A user-friendly peptide modeler for biophysical applications. *J Comput Chem* **2021**, *42, 572– 580*, DOI: 10.1002/jcc.26479
36. Koch, K.W. Target recognition of guanylate cyclase by guanylate cyclase-activating proteins. *Adv Exp Med Biol* **2002**, *514, 349-60*, doi: 10.1007/978-1-4615-0121-3_21.
37. Scholten, A.; Koch, K.W. Differential calcium signaling by cone specific guanylate cyclase-activating proteins from the zebrafish retina. *PLoSOne*. **2011**, *6, e23117.* doi: 10.1371/journal.pone.0023117.
38. Koch, K.W.; Helten, A. Guanylate cyclase-based signaling in photoreceptors and retina. In *Signal Transduction in the Retina.*, Taylor and Francis CRC Press: 2008; pp. 121-143
39. Phillips, J. C.; Braun, R.; Wang, W.; Gumbart, J.; Tajkhorshid, E.; Villa, E.; Chipot, C.; Skeel, R. D.; Kalé, L.; Schulten, K. Scalable Molecular Dynamics with NAMD. *J Comput Chem* **2005**, *26, 1781–1802,* DOI: 10.1002/jcc.20289.
40. Phillips, J. C.; Hardy, D. J.; Maia, J. D.; Stone, J. E.; Ribeiro, J. V.; Bernardi, R. C.; Buch, R.; Fiorin, G.; Hénin, J.; Jiang, W. Scalable Molecular Dynamics on CPU and GPU Architectures with NAMD. *J Chem Phys* **2020**, *153, 044130*, DOI: 10.1063/5.0014475.
41. Foloppe, N.; MacKerell, A. D. All-Atom Empirical Force Field for Nucleic Acids: I. Parameter Optimization Based on Small Molecule and Condensed Phase Macromolecular Target Data. *J Comput Chem* **2000**, *21, 86–104*, DOI: 10.1002/(sici)1096-987x(20000130)21:2<86::aid-jcc2>3.0.co;2-g.
42. Best, R. B.; Zhu, X.; Shim, J.; Lopes, P. E. M.; Mittal, J.; Feig, M.; MacKerell, A. D. Optimization of the Additive CHARMM All-Atom Protein Force Field Targeting Improved Sampling of the Backbone ϕ, ψ and Side-Chain $\chi1$ and $\chi2$ Dihedral Angles. *J Chem Theory Comput* **2012**, *8, 3257–3273,* DOI: 10.1021/ct300400x.

43. Hart, K.; Foloppe, N.; Baker, C. M.; Denning, E. J.; Nilsson, L.; MacKerell, A. D. Optimization of the CHARMM Additive Force Field for DNA: Improved Treatment of the BI/BII Conformational Equilibrium. *J Chem Theory Comput* **2012**, *8, 348–362,* DOI: 10.1021/ct200723y.
44. Pavelites, J. J.; Gao, J.; Bash, P. A. A Molecular Mechanics Force Field for NAD+ , NADH, and the Pyrophosphate Groups of Nucleotides. *J Comput Chem* **1997**, *18, 221–239,* DOI: 10.1002/(SICI)1096-987X(19970130)18:2<221::AID-JCC7>3.0.CO;2-X.
45. MacKerell, A. D.; Banavali, N. K. All-Atom Empirical Force Field for Nucleic Acids: II. Application to Molecular Dynamics Simulations of DNA and RNA in Solution. *J Comput Chem* **2000**, *21, 105–120,* DOI: 10.1002/(sici)1096-987x(20000130)21:2<105::aid-jcc3>3.0.co;2-p.
46. Denning, E. J.; Priyakumar, U. D.; Nilsson, L.; MacKerell, A. D. Impact of 20-Hydroxyl Sampling on the Conformational Properties of RNA: Update of the CHARMM All-Atom Additive Force Field for RNA. *J Comput Chem* **2011**, *32, 1929–1943,* DOI: 10.1002/jcc.21777.
47. MacKerell, A. D.; Feig, M.; Brooks, C. L. Improved Treatment of the Protein Backbone in Empirical Force Fields. *J Am Chem Soc* **2004**, *126, 698–699*, DOI: 10.1021/ja036959e.
48. MacKerell, A. D.; Bashford, D.; Bellott, M.; Dunbrack, R. L.; Evanseck, J. D.; Field, M. J.; Fischer, S.; Gao, J.; Guo, H.; Ha, S. et al. All-atom Empirical Potential for Molecular Modeling and Dynamics Studies of Proteins. *J Phys Chem B* **1998**, *102, 3586–3616*, DOI: 10.1021/jp973084f.
49. Korol, V.; Husen, P.; Sjulstok, E.; Nielsen, C.; Friis, I.; Frederiksen, A.; Salo, A. B.; Solov'yov, I. A. Introducing VIKING: A Novel Online Platform for Multiscale Modeling. ACS Omega 2020, 5, 1254– 1260, DOI: 10.1021/acsomega.9b03802.
50. Schuhmann, F.; Kattnig, D.R.; Solov'yov, I.A. Exploring Post-activation Conformational Changes in Pigeon Cryptochrome 4. *J Phys Chem B* **2021** *125, 9652-9659*, doi.org/10.1021/acs.jpcb.1c02795.
51. Humphrey, W.; Dalke, A.; Schulten, K. VMD: Visual Molecular Dynamics. *J Mol Graphics* **1996**, *14, 33–38,* DOI: 10.1016/0263-7855(96)00018-5.
52. McGibbon, R.T.; Beauchamp, K.A.; Harrigan, M.P.;Klein, C.; Hernández, C.X.; Schwantes, C.R.; Wang, L.P.; Lane, L.P.; Pande, V.S. MDTraj: A Modern Open Library for the Analysis of Molecular Dynamics Trajectories. *Biophys J* **2015**, *109, 1528,* doi: org/10.1016/j.bpj.2015.08.01.

2.1 Supplementary information

The transition of photoreceptor guanylate cyclase type 1 to the active state

Manisha Kumari Shahu[1], Fabian Schuhmann[2], Alexander Scholten[1], Ilia A. Solv'yov[2,3], Karl-Wilhelm Koch[1,3#]

[1]Division of Biochemistry, Department of Neuroscience, University of Oldenburg, Oldenburg 26111, Germany.

[2]Institute of Physics, University of Oldenburg, Oldenburg 26111, Germany.

[3]Research Centre for Neurosensory Science, University of Oldenburg, Oldenburg 26111, Germany.

*To whom correspondence should be addressed: karl.w.koch@uni-oldenburg.de

Table S1. Oligonucleotide sequences used in the present study.

Mutants	Oligonucleotide Sequence 5'-3'
1 Alanine (1Ala)	**FP**- 5'- AGG CAC CGG CTA CTT CAC ATG CAA ATG -3' **RP**- 5'- **AGC** CAC ATA ATG GGC CAG GAA GGC -3'
2 Alanine (2Ala)	**FP**- 5'- AGG CAC CGG CTA CTT CAC ATG CAA ATG -3' **RP** 5'- **TGC AGC** CAC ATA ATG GGC CAG GAA GGC -3'
3 Alanine (3Ala)	**FP** 5'- **GCC** AGG CAC CGG CTA CTT CAC ATG -3' **RP** 5'- **TGC AGC** CAC ATA ATG GGC CAG GAA GGC -3'
4 Alanine (4Ala) Set a	**FP** 5'- **GCC GCT** AGG CAC CGG CTA CTT CAC ATG -3' **RP** 5'- **TGC AGC** CAC ATA ATG GGC CAG GAA GGC -3'
4 Alanine (4Ala) Set b	**FP** 5'- **GCC GCT GCT** AGG CAC CGG CTA CTT CAC ATG -3' **RP**- 5'- **AGC** CAC ATA ATG GGC CAG GAA GGC -3'
5 Alanine (5Ala)	**FP** 5'- **GCC GCT GCT** AGG CAC CGG CTA CTT CAC ATG -3' **RP** 5'- **TGC AGC** CAC ATA ATG GGC CAG GAA GGC -3'

Figure S1

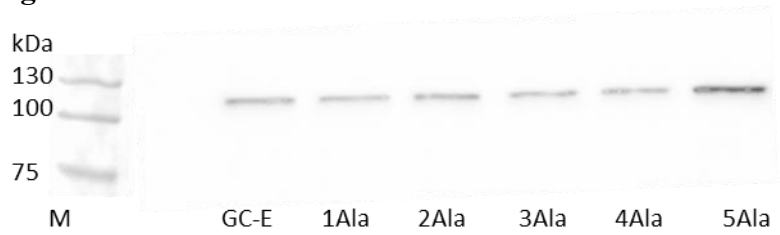

Figure S1. Western blot for verification and quantification of poly alanine mutants. Expression level of mutants was compared to that of GC-E wildtype in HEK293 cell membranes. Five µg of total protein amount for each sample was analysed by SDS-PAGE. The samples were detected by the specific antibody anti-GC1#3. The slight difference between each mutant band intensity was considered for the activity measurement of amount of cGMP synthesized with each sample.

Figure S2

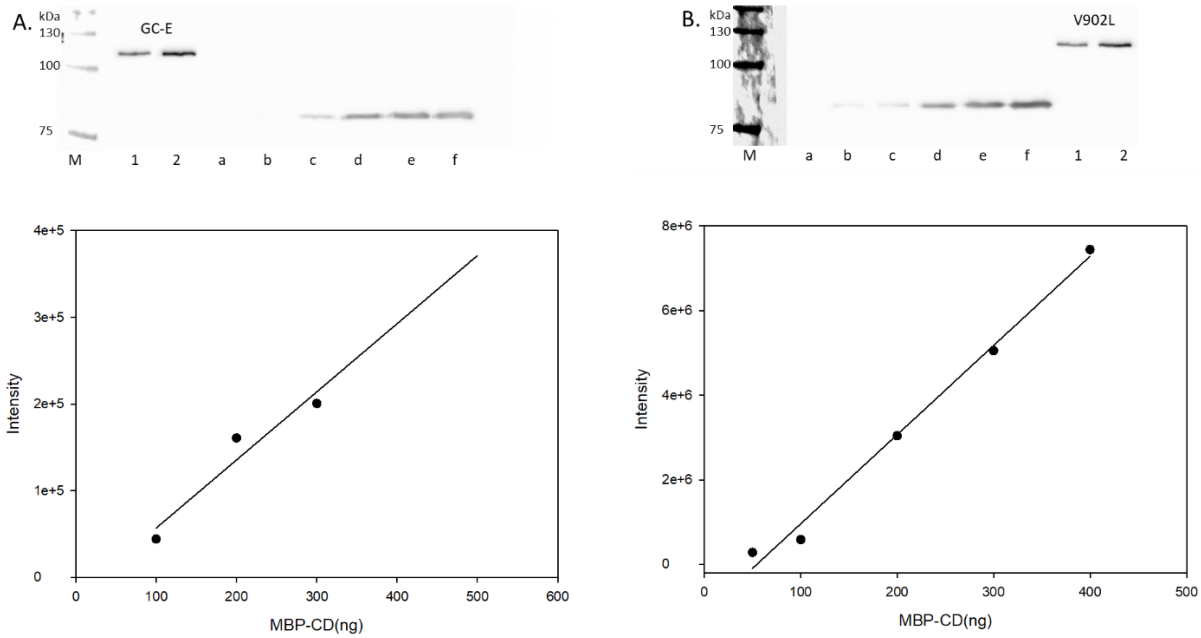

Figure S2. Quantification of GC-E and V902L in HEK293 cell membranes. Purified MBP-CD protein samples were electrophoresed and blotted in increasing amount (a- 20ng, b-50ng, c-100ng, d-200ng, e-300ng, f-400ng) were used to create a calibration curve along with a sample of wildtype GC-E (**A**) or V902L (**B**) present in HEK293 membrane fractions (1- 2.5 µg, 2- 5 µg). The samples were detected by GC1 # 3 antibody and ECL imaging. Band intensity was linear within the tested range for **B**, for **A** the plot was extended manually based on linearity. Quantification yielded for 5 µg membrane protein 292 ng of GC-E wildtype, and 212 ng of V902L, taking a purity of 73% into account.

Chapter 3 : Allosteric communication of the dimerization and the catalytic domain in photoreceptor guanylate cyclase

Manisha Kumari Shahu[1], Fabian Schuhmann[2,3], Siu Ying Wong[3], Ilia A. Solov'yov[3,4,5] and Karl-Wilhelm Koch[1,4,*]

[1]Carl von Ossietzky Universität Oldenburg, Department of Neuroscience, Carl-von-Ossietzky-Str. 9-11, Oldenburg, 26129, Germany.

[2]Niels Bohr International Academy, Niels Bohr Institute, University of Copenhagen, Blegdamsvej 17, 2100 Copenhagen, Denmark

[3]Carl von Ossietzky Universität Oldenburg, Institute of Physics, Carl-von-Ossietzky-Str. 9-11, Oldenburg, 26129, Germany.

[4]Carl von Ossietzky Universität Oldenburg, Research Centre for Neurosensory Science, Carl-von-Ossietzky-Str. 9-11, Oldenburg, 26129, Germany.

[5]Center for Nanoscale Dynamics (CENAD), Carl von Ossietzky Universität Oldenburg, Institute of Physics, Ammerländer Heerstr. 114-118, 26129 Oldenburg, Germany.

*Corresponding author: karl.w.koch@uol.de;

Keywords: guanylate cyclase, photoreceptor, retinal dysfunction, allosteric, connectivity analysis

Running title: activity control of photoreceptor guanylate cyclase

Abstract

Phototransduction in vertebrate photoreceptor cells is controlled by Ca^{2+}-dependent feedback loops involving the membrane-bound guanylate cyclase GC-E that synthesizes the second messenger guanosine-3',5'-cyclic monophosphate. Intracellular Ca^{2+}-sensor proteins named guanylate cyclase-activating proteins (GCAPs) regulate the activity of GC-E by switching from a Ca^{2+}-bound inhibiting to a Ca^{2+}-free/Mg^{2+}-bound activating state. The gene *GUCY2D* encodes for human GC-E, and mutations in *GUCY2D* are often associated with an imbalance of the Ca^{2+} and cGMP homeostasis causing retinal disorders. Here, we investigate the Ca^{2+}-dependent inhibition of the constitutively active GC-E mutant V902L. The inhibition is not mediated by GCAP variants but by Ca^{2+} replacing Mg^{2+} in the catalytic center. Distant from the cyclase catalytic domain is an α–helical domain containing a highly conserved helix-turn-helix motif. Mutating the critical amino acid position 804 from leucine to proline left the principal activation mechanism intact, but resulted in a lower level of catalytic efficiency. Our

experimental analysis of amino acid positions in two distant GC-E domains implied an allosteric communication pathway connecting the α–helical and the cyclase catalytic domains. A computational connectivity analysis unveiled critical differences between wildtype GC-E and the mutant V902L in the allosteric network of critical amino acid positions.

Introduction

Inherited retinal dystrophies (IRDs) are widespread and affect millions worldwide. They are both phenotypically and genotypically heterogeneous diseases (1-3) and include retinitis pigmentosa (RP), Leber Congenital amaurosis (LCA), and cone-rod dystrophy (CRD). Causes of retinal dysfunction are often pathological changes in the function and operation of the light-sensitive rod and/or cone photoreceptor cells. Photoreceptor cells mediate the sensory phototransduction process of the visual system by converting the absorbance of photons to electrical signals. Visual information is further transmitted via retinal neurons and decoded by the visual processing center of the brain. Phototransduction in vertebrate rod and cone cells depends critically on the homeostasis of two second messenger, guanosine-3', 5'-cyclic monophosphate (cGMP) and Ca^{2+}. The cytoplasmic concentrations of both messengers decrease after illumination and recover by deactivation and feedback processes (4-7). An imbalance of their cytoplasmic concentrations has detrimental effects and leads to visual dysfunction or even blindness in humans. According to a comprehensive list of data on RetNet (https://sph.uth.edu/retnet/), more than 300 genes are associated with IRDs and over 140 disease-causing mutations described so far were found in the *GUCY2D* gene (3). *GUCY2D* is the gene that encodes for photoreceptor guanylate cyclase GC-E (also known as ROS-GC1 or retGC1), a key enzyme in phototransduction that synthesizes the second messenger cGMP and returns the cell to its dark-adapted state in a Ca^{2+}-dependent negative feedback loop (5, 7).

Cytoplasmic Ca^{2+}-sensor proteins named guanylate cyclase-activating proteins (GCAPs) mediate this feedback on GC-E activity by activating GC-E at low Ca^{2+}-concentration [Ca^{2+}] when GCAPs switch to a Mg^{2+}-bound activating form. GC-E returns to the basal, low activity state, when GCAPs are saturated with Ca^{2+} (8-10). The functional state of the GC-E requires a homodimeric topology that consists of an extracellular (ECD), a transmembrane (TM), and an intracellular domain (IcD). The IcD consists of a juxtamembrane (JMD), a kinase homology (KHD), a dimerization (DD), and a catalytic (CCD) domain. Rehkamp et al. (11) presented the first 3D structural data for the IcD of GC-E, combining cross-linking and mass spectrometry of a native GC-E preparation with computational modelling. Rehkamp et al. (11) modified a previous division of the IcD by suggesting a novel domain organization formed of a KHD, an "α–helical domain" (αHD), and the cyclase catalytic domain (CCD). The αHD connects the KHD with the CCD and contains a highly conserved helix-turn-helix motif at its N-terminal extension found in topologically related proteins (12). It also includes the formally assigned DD. Structural studies on related soluble guanylate cyclases point to an intrinsic flexibility in the hinge motif of the αHD leading to various conformations. For example, a conformational change from a 90° kinked helix-turn-helix motif (PDB: 6PAS representing the inactive state) to a straight helix motif (PDB: 6PAT representing the active state) triggers the activation of the soluble guanylate cyclase from Manduca sexta (13). This high degree of flexibility is also

observed in the αHD of the GC-E (11) and, therefore, in the focus of current research. The domain is critical for dimerization and is suggested as a GCAP binding interface or regulatory control module (14, 15).

Several amino acid positions are mutated in the GC-E of human patients suffering from autosomal dominant cone-rod dystrophy (adCRD), making this a “hot spot” region for retinal diseases (3). In addition, mutations in GC-E are spread over all domains, and functional studies addressing the effects of point mutations often indicate a drastic decrease in GC-E activity. However, exceptions as we described for the point mutation V902L in GC-E lead to a constitutively active form exhibiting high activity in the absence and presence of GCAP1 thereby exceeding the suggested physiological level of cGMP synthesis rate (16). Patients carrying the point mutation V902L suffer from cone-rod dystrophy (16), which is probably caused by the impaired ability of the mutant GC-E to return to the low-activity state during recovery of the photoresponse.

Kinetic analysis of enzymatic parameters and molecular dynamics simulations of the V902L mutant suggested a swinging movement of the dimerization domain in the V902L mutant as the critical switch to transit to the GC-E active state (17). This indicates that a point mutation in the CD, such as V902L, triggers a movement upstream in the GC-E structure indicating a robust connectivity between the αHD and the CD.

These observations show that the precise responses of photoreceptors require tightly controlled conformational transitions in GC-E. Inspired by kinetic and structural studies on soluble guanylate cyclases (13, 18), we investigated this transition further using a combination of experimental enzymatic assays and molecular dynamics simulation. We investigated a double mutant with critical mutations in the helix-turn-helix motif (L804P) and the CD (V902L) to test the suggested allosteric communication between the αHD and the CD. We asked, how the GCAP-independent Ca^{2+}-sensitivity of the mutant V902L can be understood and how this relates to the active or inactive state in the catalytic centre. Finally, we performed a computational connectivity analysis to construct an amino acid interaction network operating in conformational transitions.

Results and Discussion

Effects of Ca^{2+} on the catalytic center

Our previous work indicated an allosteric communication pathway between the helix-turn-helix region in the αHD and the CD (17). The point mutant V902L appears as a useful tool for investigating the properties of this allosteric effect further. First, we analyzed whether the reduced efficiency of GCAP1 activating GC-E was observed with the other GCAP variant, GCAP3. Figure 1 shows the activity profiles of WT and mutant V902L in the presence of either GCAP1 or GCAP3 at high and low [Ca^{2+}]. The mutant V902L exhibited a high activity at high and low [Ca^{2+}] in the absence of any GCAP variant exceeding the basal activity 6 to16-fold (compare columns WT and V902L in Figure 1). An addition of GCAP1 has only a modest, however significant, effect on the activity of V902L in the presence and absence of Ca^{2+} (Figure 1, V902L vs. V902L-GCAP1). These results confirm our previous conclusion that the mutant V902L is a constitutively active GC-E (16). Interestingly, GCAP3 activated GC-E in a Ca^{2+}-dependent manner, but to a lesser degree than GCAP1, whereas the mutant V902L was almost

unaffected by GCAP3 (Figure 1). GC activities of V902L in the presence and absence of GCAP3 at high [Ca^{2+}] were almost the same (Figure 1). At low [Ca^{2+}], GCAP3 caused a slightly higher activity of V902L (Figure 1).

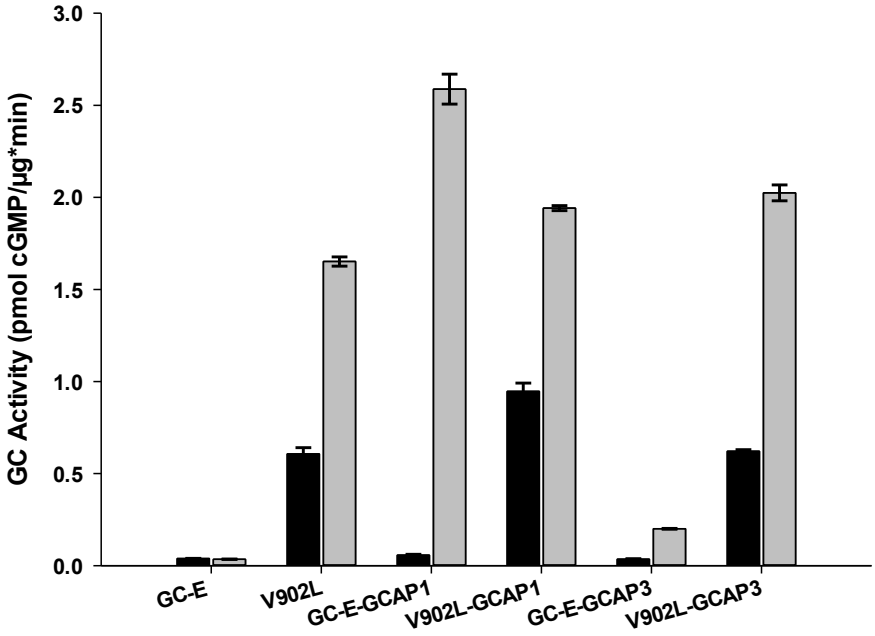

Figure 1. Activity profiles of GC-E variants. (A) WT and mutant V902L were activated with GCAP1 or GCAP3 at high (33 µM, black bars) or low (<10 nM, gray bars) free [Ca2+]. The x-fold activation of V902L without GCAPs is 2.7; in the presence of GCAP1, 2.0, and in the presence of GCAP3, it is 3.3. The x-fold activation of GC-E WT is 45.5-fold with GCAP1 and 5.6-fold with GCAP3. Error bars are s.d. (one example of technical triplicates out of three to four biological replicates, results of other biological replicates are in the Supporting Information, Figures S1-S3).

The activity profile of V902L in the absence of GCAPs (Figure 1) showed that the activity of the mutant V902L is Ca^{2+}-dependent, although no Ca^{2+}-sensor protein is present to mediate this effect. We measured the V902L activity at increasing free [Ca^{2+}] and observed a nearly constant activity of V902L up to 10 µM free [Ca^{2+}] (Figure 2A). Above 10 µM free [Ca^{2+}], the activity decreased and reached a plateau of lower activity at 100 µM free [Ca^{2+}] slightly below the activity observed at a free [Ca^{2+}] of 33 µM as in Figure 1. Half-maximal inhibition (IC_{50}) was observed between 16 and 19 µM free [Ca^{2+}] employing a sigmoidal four-parameter Hill model provided by the SigmaPlot 13.0 software, Systat Software, Inc., San Jose, CA, 2014, (two independent data sets in triplicates, see example in Figure 2A). The constitutive activity of the V902L mutant allowed us to dissect the Ca^{2+}-dependency of GC-E mediated by GCAPs from a direct Ca^{2+}-effect on the catalytic mechanism. Serfass et al. (18) previously analyzed a similar Ca^{2+}-dependent inhibition for the catalytic properties of soluble guanylate cyclase from bovine lung. The authors interpreted their finding as a two-metal ion catalytic mechanism involving two Mg^{2+}-ions similar to the catalytic mechanism observed in adenylate cyclases (19-21). One Mg^{2+} forms with GTP the substrate complex and one Mg^{2+} (in excess of the

substrate) is primarily bound to the cyclase in the catalytic center. Such a mechanism implies that Ca^{2+}-bound to the cyclase can be removed by increasing free Mg^{2+} in excess of the Mg^{2+}-GTP substrate. We performed an experiment to reverse the inhibition of Ca^{2+} at three different Mg^{2+}- concentrations (Figure 2B) and observed two effects: GC activity increased reaching a saturating profile at an excess of 5 mM Mg^{2+} and 100 µM Ca^{2+} were not sufficient for an inhibitory effect as seen in Figure 2A. Fitting data points in Figure 2B revealed IC_{50} at Ca^{2+}-concentrations of 64 µM, 82 µM and 91 µM for Mg^{2+}-concentrations of 2 mM, 3.5 mM and 5 mM, respectively. Differences were statistically significant for curves with 2 and 3.5 mM Mg^{2+} ($p < 0.01$; t-test), but not when comparing curves for 3.5 mM and 5 mM Mg^{2+} (n.s.).

A

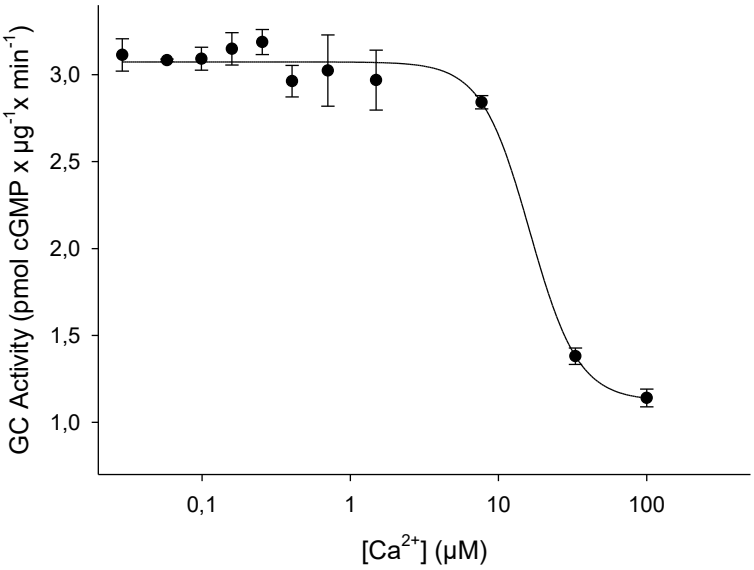

B

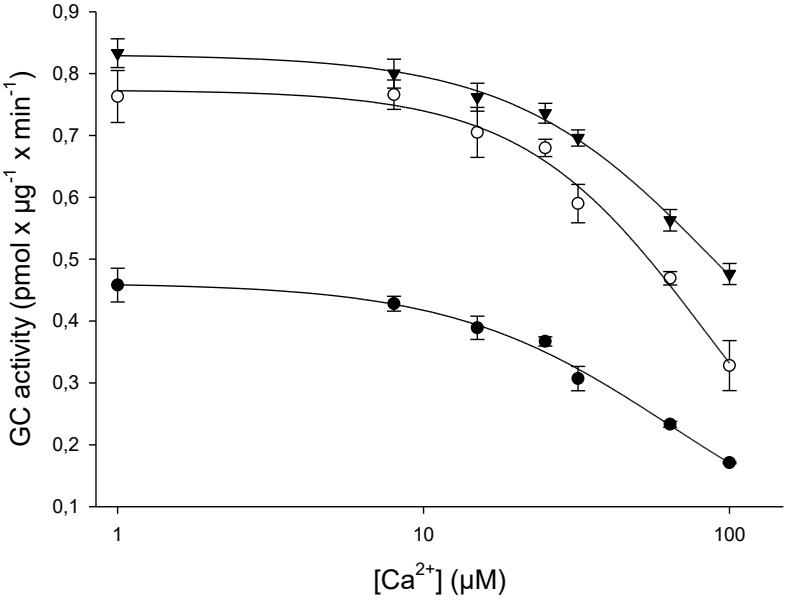

Figure 2. Ca^{2+}-dependent inhibition of the V902L mutant. **(A)** Incubation of V902L was performed in the absence of GCAP1 or GCAP3. Free [Ca^{2+}] was varied, as indicated and half-maximal inhibition was at 16.3 µM free [Ca^{2+}] (Error bars are s.d., one example of technical triplicates out of three biological replicates, see also Figure S4). **(B)** Increasing concentrations of free Mg^{2+} reverse the inhibitory effect of Ca^{2+}. Incubation was performed as in **(A)**. The Mg^{2+}-concentration was 2 mM (●, filled circles), 3.5 mM (○, open circles) and 5 mM (▼, filled triangles). We performed non-linear regression fitting using a sigmoidal Hill model provided by the SigmaPlot 13.0 software (three-parameter model for data with 2 and 3.5 mM Mg^{2+}; four-parameter model for 5 mM Mg^{2+}). Error bars are s.d. (technical triplicates). All curve fittings passed the Normality Test (Shapiro-Wilk) and the Constant Variance Test.

A critical mutation in the helix-turn-helix motif has an impact on the catalytic center

Switching GC-E back to the basal activity state is a decisive step in phototransduction. Our previous simulations pointed to a conformational change in the αHD required for GC-E to transit between low and high activity states. Since we located the structural trigger of the switch in the helix-turn-helix motif, we reasoned that changing or breaking a critical α–helix might impact the catalytic center. This suggestion is further supported by previous findings that locate a crucial regulatory control module in or near the dimerization domain (14, 15). Therefore, to evince our hypothesis, we substituted Leucine at position 804 with Proline in the V902L mutant creating the double mutant L804P/V902L (LP-VL) (Figure 3A).

A

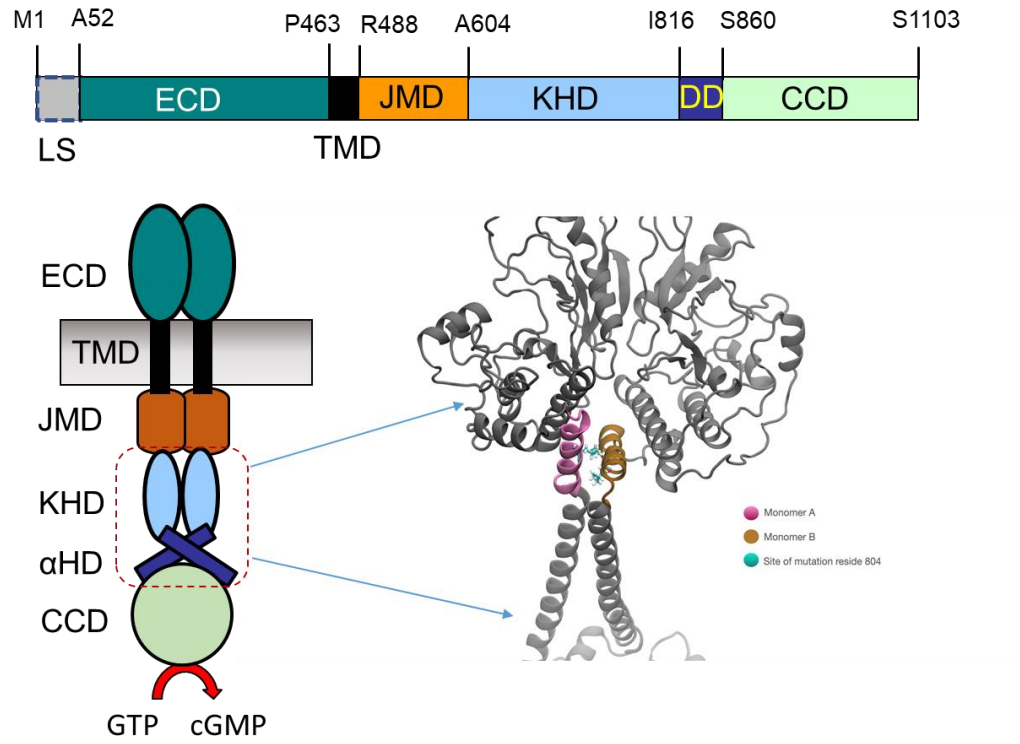

B

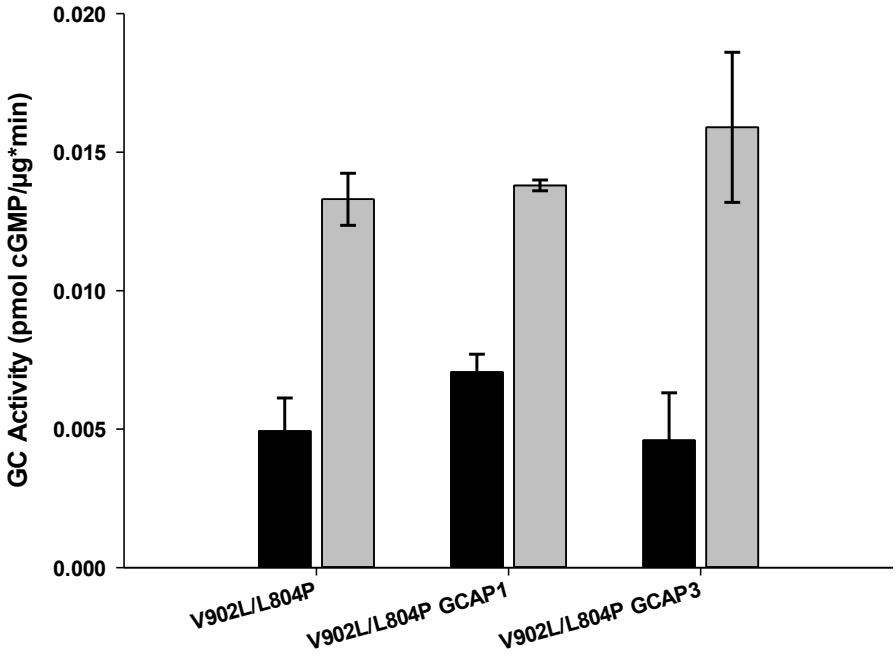

Figure 3. Activity profiles of GC-E variants. **(A)** Upper part, general topology of a GC-E monomer showing domain locations (LS, leader sequence; ECD, extracellular domain, TMD, transmembrane domain; JMD, juxtamembrane domain; KHD, kinase homology domain; DD, dimerization domain; CCD, cyclase catalytic domain). Amino acid positions indicate start of the respective domain, S1103 indicates the last amino acid of the primary sequence. Lower

part, location of the point mutation L804P in the helix-turn-helix motif. **(B)** Activity of the double mutant V902L/L804P in the absence and presence of GCAP1 at high (33 µM, black bars) or low (<10 nM, gray bars) free [Ca^{2+}]. The x-fold activation of the double mutant without GCAPs is 2.7, in the presence of GCAP1 2.0 and in the presence of GCAP3 it is 3.4. Comparing activities of the Ca^{2+}-bound states yielded no significant differences for all combinations (V902L/L804P vs. V902L/L804P + GCAP1, V902L/L804P + GCAP1 vs. V902L/L804P + GCAP3 and V902L/L804P vs. V902L/L804P + GCAP3). Error bars are s.d. (one example of technical triplicates out of three to four biological replicates, results of other biological replicates are in the Supporting Information, Figures S5-S7).

Subsequent testing of GC activities showed two main effects: a general decrease in activities in the absence and the presence of GCAPs (Figure 3B). The V902L/L804P mutant has a reduced basal activity in comparison to WT GC-E. The activity is 8-fold lower in the presence of Ca^{2+} and 3-fold lower in the presence of EGTA (comparison of Figure 1, data shown for *GC-E,* with Figure 3, data shown for V902L/L804P). Expression of V902L and the double mutant was identical as tested by western blotting and immunohistochemistry of transfected HEK 293 cells (supplement, Figure S8 and S9). However, biological replicates differ in expression yield of GC-E variants (see Supporting Information). Secondly, we compared the x-fold activation (activity at low [Ca^{2+}] divided by activity at high [Ca^{2+}]) of the mutant V902L with the double mutant and the WT (see legend of Figure 3B) yielding an x-fold activation for both mutants between 2 and 4 fold indicating that the principal activation mechanism remained intact, but at a lower level of catalytic efficiency. Comparing all Ca^{2+}-bound states with each other (double mutant V902L/L804P with GCAP1 or GCAP3) yielded no significant differences (Figure 3B). The same was observed for the Ca^{2+}-free states. Compared to WT GC-E (x-fold activation is more than 45-fold, Figure 1), we observed no recovery of the Ca^{2+}-sensitive GCAP effect in the double mutant but a substantial effect on the catalytic performance. Our results supported our hypothesis of a conformational pathway connection between the αHD and the CD.

Connectivity analysis

Our experimental analysis of critical amino acid positions in two distant GC-E domains implied a communication pathway connecting the αHD and the CD. To achieve a broader view of the allosteric regulatory impact, we carried out a computational connectivity analysis, as described in the method section.

The connectivity analysis utilizes two approaches, which probe separate attributes describing connectivity within a network derived from the locations of amino acid residues during molecular dynamics (MD) simulations. The *reach method* (22) values amino acids that reach the most other amino acids along the network edges as highly influential. On the other hand, the *betweenness method* (23) prefers amino acid residues, which are located at important network intersections throughout the protein structure.

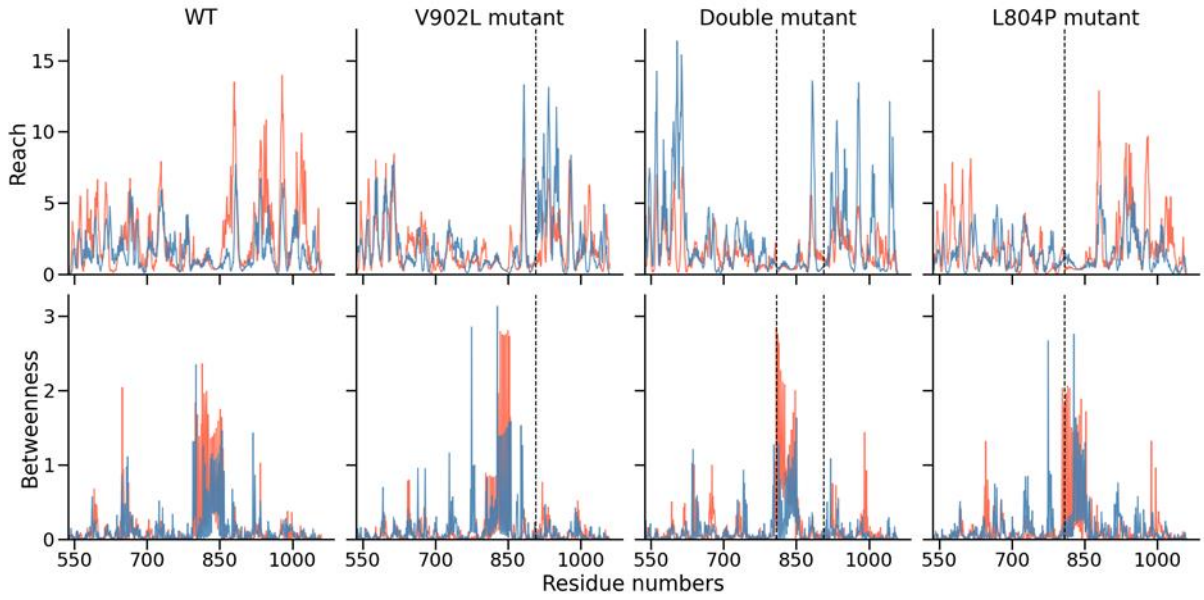

Figure 4. *Reach* and *betweenness* of the monomers for all residues. The graphs show the *reach* (first row) and the *betweenness* (second row) of the two monomers. The first monomer is coloured blue, the second red. The vertical dashed lines indicate mutated residues at positions 902 and 804. Noticeably, considering the introduction of further mutation (WT, V902L, Double mutant) the reach of the residues within the homology kinase domain increases with the introduction of more mutations, while the importance of the different monomers switches for the catalytic domain. Contrary to the *reach*, the *betweenness* picks up on the α-helical domain. Additionally, the *betweeness* is greater in the second monomer after the introduction of the single mutant. The effect is more diversified again in the double mutant, however, still leaning towards the red mutant. Interestingly, almost isolated signals can also be found in the two other domains. Furthermore, the second single mutant L804P remains similar to the wild type protein, except for a slight shift to a single monomer in the betweeness in the α-helical domain, which can also be observed in the double mutant.

The graphs in Figure 4 show the *reach* (first row) and the *betweenness* (second row) for the individual amino acid residues. The results align with the assumption that the residues with the highest *betweenness* are located in the α-helical domain, which connects the homology kinase and catalytic domain as all shortest paths from one domain to the other have to pass through these residues. The residues with the highest *reach* are located in the catalytic domain for the wildtype and the V902L mutant. For the double mutant, however, residues in the homology kinase domain have a similar *reach* to those in the catalytic domain. In particular, the residues with a high betweeness seem to shift towards a single monomer, while concentrated in the α-helical domain for the single mutant. While the effect is still visible in the double mutant, it is more diversified and reduced, particularly for residues in the middle of the α-helical domain. The L804P mutant is remarkably similar to the wildtype with a slight exception in the betweeness in the α-helical domain. Here, the high betweeness residues conglomerate in a single monomer, which can also be seen in the double mutant.

With these *betweenness* graphs (Figure 4) and averaging the two monomers, potential residues of importance can be singled out. The analysis was performed for the WT and the V902L mutant. The six residues with the most significant *reach* and *betweenness* (relative to each other) are shown in Figure 5. The *high betweenness* residues are located in the double

helix of the α-helical domain and do not differ significantly between the WT and the V902L mutant. The *reach*, however, paints a different picture. The residues with the most significant *reach* change from the WT to the V902L mutant. In the mutant, the highest *reach* residues are located at the N-terminal part of the homology kinase domain, almost at the juxtamembrane domain (not displayed and modeled). In the WT, the highest *reach* residues are even split across the homology kinase and the catalytic domain. Here, the residues are also closer to the α-helical domain.

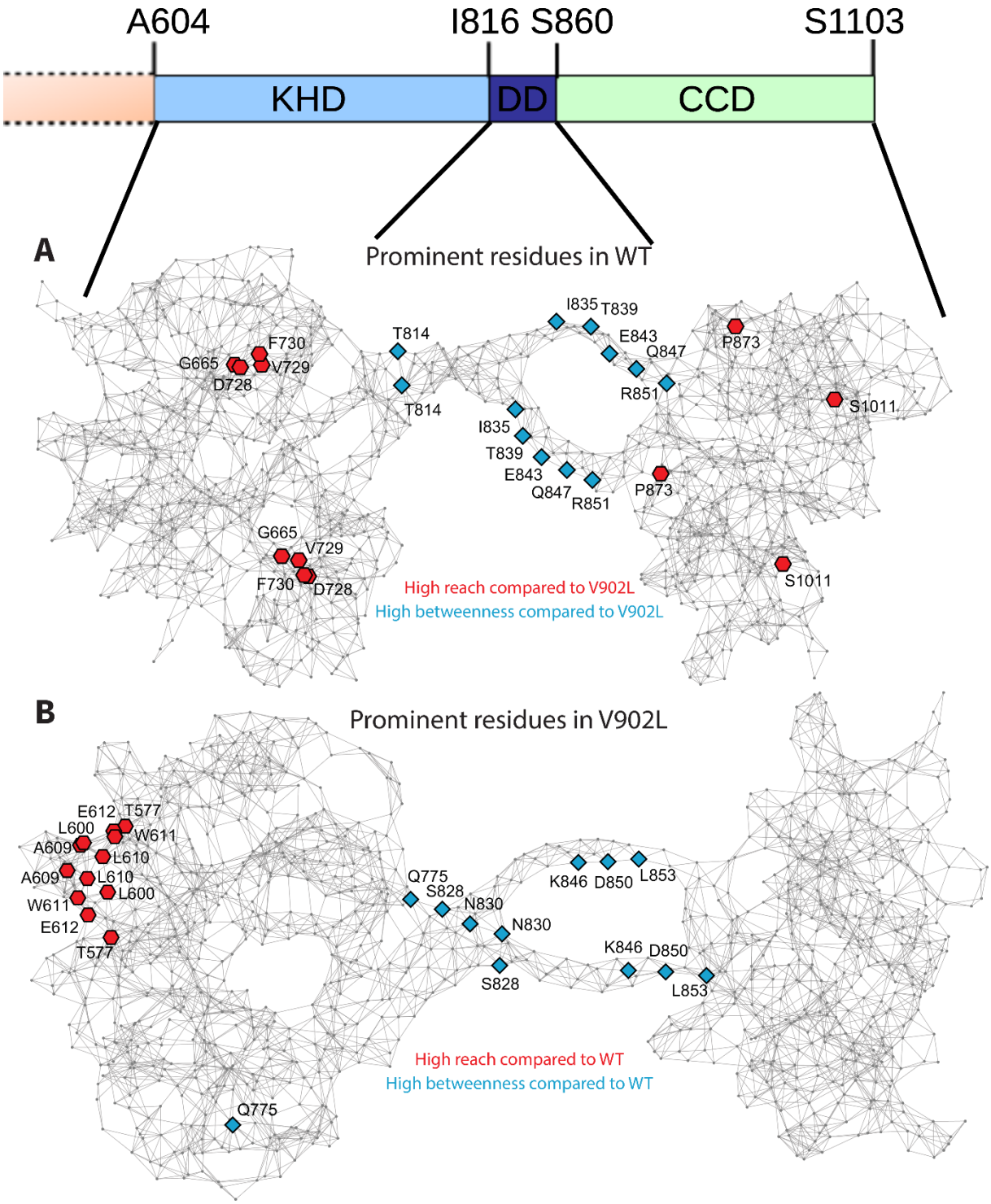

Figure 5. The graphical network representations of the WT (A) and V902L (B) proteins, plotted in grey using the spring embedding method in Wolfram Mathematica

(https://www.wolfram.com/mathematica). The six residues with the highest *reach* (red hexagons) and *betweenness* (blue diamonds) compared to the other protein version (WT and V902L mutant, respectively) are highlighted and labelled in each graph. Corresponding domains and amino acid positions are indicated on top.

Functional interpretation of the connectivity results

Marino and Dell'Orco (24) performed a structural network analysis of GCAP1 and described an allosteric information transfer from different cation binding states to amino acid residues in the GC-E target interface (24). The same authors extended the analysis to related neuronal Ca^{2+}-sensor proteins and uncovered conserved amino acid positions in three related Ca^{2+}-sensor proteins that point to an evolutionary conservation of molecular communication pathways (25).

Our analysis here focuses on the GCAP1 target GC-E and the amino acid network involved in the conformational transition process. For example, position S1011 in the CD is next to E1010, which forms a complex with Mg^{2+} and the pyrophosphate part of GTP (26). The loss of *high reach* in V902L (Figure 5B) might be the reason for the decrease or even loss of the allosteric regulation by GCAPs as seen in the functional properties of the V902L mutant (16, 17; this study). The remaining Ca^{2+}-sensitive control is located in the binding site of GTP in the catalytic center and might significantly impact the V902L mutant under certain conditions. For example, constitutive activation of the mutant V902L would create a high level of cytoplasmic cGMP in the photoreceptor cell, causing a higher influx of Ca^{2+} than average. However, an excessive local increase in concentrations of Ca^{2+} would then inhibit V902L by the direct binding of Ca^{2+}, bringing the cGMP synthesis back to low basal rates. This scenario would still differ from a healthy state since it has a shifted Ca^{2+}-cGMP homeostasis.

Two amino acid positions with a *high reach* in the WT compared to the V902L mutant (Figure 5) are mutated in patients suffering from retinal diseases. One is the point mutation D728N in the KHD causing autosomal recessive Leber congenital amaurosis (27, 28). The second is P873R, located in the CD and found in patients suffering from cone rod dystrophy (16). A functional analysis of the latter showed a complete loss of GC-E activity, indicating a severe impact on photoreceptor physiology (16). Functional analysis of the D728N mutant is lacking so far. Still, mutations in the KHD often correlate with either impaired basal GC activity or partial loss of activity regulation by GCAPs (for a summary, see ref. 3). Thus, our connectivity analysis highlighted amino acid positions that are critical for the allosteric control of GC-E activity and some of the positions presented in Figure 5 might carry point mutations that correlate with retinal diseases but are not detected so far.

Conclusion

Switching of photoreceptor GC-E from the inactive to the active state and *vice versa* is essential for the second messenger homeostasis in rod and cone cells. Here, we describe an allosteric communication pathway linking two distant domains of GC-E and identify a network of amino acid positions that seem critical for enzyme activity control. Our connectivity analysis identified point mutations at some of these positions found in patients suffering from retinal dysfunction. Thus, the analysis might be able to predict positions that could cause retinal diseases when mutated.

Methods

Generation of the double mutant by site-directed mutagenesis

The pIRES2-eGFP vector containing the GC-E mutant V902L sequence was used for amino acid substitution to generate the double mutant. Proline was introduced at position 804 to substitute Proline with Leucine (L804P) by site-directed mutagenesis which was achieved by the polymerase chain reaction (PCR) using a KOD (Hot start DNA Polymerase Novagen) enzyme. The PCR amplification was followed according to the manufacturer's protocol using Forward primer 5'-ATCAACAAGGGCCGGAAGACGAACATCATT-3' and reverse primer 5'-GTTCTTGAACGGGTCGAAGGTGTGGTCCAT-3'. The obtained clones were verified by full-length sequencing for the substitution of L804P.

Heterologous expression of V902L mutant and the L804P/V902L double mutant

The HEK293 cell line was transiently transfected with cDNA of GC-E mutants V902L and L804P/V902L using polyethylenimine (PEI) at 60-70% of confluency at 100 mm plates. Respective 8 µg of DNA was mixed with 32 µg of PEI in DMEM without supplements and incubated at room temperature (RT) for 20 min. The sample mix was then added to the respective cell plate and incubated in the incubator at 37°C with 5% CO_2. After transfection and 72-96 h incubation, the cells were harvested by centrifugation at 500x g for 5 min. The cell pellets were washed with PBS and centrifuged at 12000x g for 5 min. The pellets were frozen and stored at -80°C until further use.

Expression and purification of GCAP1

Human myristoylated GCAP1 was expressed in *Escherichia coli* and purified to homogeneity by anion exchange chromatography and size exclusion chromatography as previously described and reported (29). Myristoylation of GCAP1 during bacterial expression was accomplished by co-transforming *Escherichia coli* cells with N-myristoyl-transferase from yeast and supplementation with myristic acid, as reported previously (29).

Expression and purification of GCAP3

Human myristoylated GCAP3 was expressed in *Escherichia coli* and purified to homogeneity by anion exchange chromatography and size exclusion chromatography as previously described and reported (30). Myristoylation of GCAP3 during bacterial expression was accomplished by co-transforming *Escherichia coli* cells with N-myristoyl-transferase from yeast and supplementation with myristic acid, as reported previously. After the hGCAP3 protein was expressed in bacterial cells, the cell pellet was lysed, and inclusion bodies were resuspended in 6-M guanidinium hydrochloride for overnight solubilization. Next day protein was refolded by dialysis (20mM Tris-HCl pH-7.5, 2mM NaCl, 1mM DTT) and at first purified by anion exchange chromatography with HiTrap^{TM} Q HP equilibrated in 20mM Tris-HCl pH-7.5, 2mM $CaCl_2$ and 1mM DTT and then the protein was eluted with a salt gradient from 0.02 to 0.55 M of NaCl. Fractions containing the expressed hGCAP3 protein were further pooled and precipitated by ammonium sulfate and again purified by size exclusion chromatography

with Superdex 75 (HighLoad 26/60), which was equilibrated with 20mM Tris-HCl pH-7.5, 150mM NaCl, 2mM $CaCl_2$ and 1mM DTT. SDS-PAGE analyzed the purity of expressed protein, and samples were exchanged against 50mM ammonium hydrogen carbonate, lyophilized and stored at -80°C for further use.

Guanylate Cyclase activity Assay

The double mutant L804P/V902L activity was analyzed by comparing the enzymatic activity with that of V902L. Transiently transfected respective HEK cell pellets were resuspended in 1 ml, 10 mM Hepes/KOH pH 7.4 with 1 mM DTT and a protease inhibitor cocktail. The suspension was incubated for 30 min on ice and followed by cell lysis using a syringe with a 0.7 mm needle. After centrifugation at 13,000× g for 8 min at 4°C, the cell pellet was resuspended in 100 μl of 50 mM Hepes/KOH pH 7.4, 50 mM KCl, 20 mM NaCl, 1 mM DTT, and a protease inhibitor cocktail. Twenty μl of a GCAP1 solution (10 μM) or water (for the absence of GCAP1) that was previously adjusted to different free Ca^{2+} concentrations using a Ca^{2+} / EGTA buffer system exactly as described earlier (31, 32) were used in the assay. For each sample 10 μl (containing typically 60-100 µg protein) of respective membrane suspensions were mixed and pre-incubated for 5 min at room temperature. The reaction started by adding 20 μl of 2.5×GC buffer (75 mM Mops/KOH pH 7.2, 150 mM KCl, 10 mM NaCl, 2.5 mM DTT, 8.75 mM $MgCl_2$, 2.5 mM GTP, 0.75 mM, and 0.4 mM Zaprinast). The reaction mixtures were incubated for 10 min at 30°C. The reaction was stopped by adding 50 μl 0.1 M EDTA and incubating at 95°C for 5 min. Samples were centrifuged for 10 min at 13,000× g. Supernatants were analyzed for the amount of produced cGMP by reversed-phase HPLC using a LiChrospher® 100 RP-18 (5 μm) column (Merck, Darmstadt, Germany) exactly as described (17, 29, 31). The detection limit of the assay for cGMP is 2-5 pmol (ref. 31 and determination in the Biochemistry group). Measurements were done with three to four biological replicates, each set-in technical triplicates, if not stated otherwise, and were evaluated by using SigmaPlot 13.0. Differences in GC activities of biological replicates are due to differences in expression yields of heterologously expressed GC variants (Figures S1-S7 in Supporting Information).

To check the direct inhibitory effect of Ca^{2+} on GC-E activity, the GC activity assay was performed as mentioned above with the following modification. Half maximal inhibition of GC-E mutant V902L by Ca^{2+} was determined by setting the free Ca^{2+}-concentration ranging from 1 to 100 µM without an EGTA-buffer system. All other assay conditions are as described above. Variations of free Mg^{2+} concentration in the assay medium were calculated using the WEBMAXC STANDARD software with proper corrections for pH, salt and temperature. Incubation was performed in three free Mg^{2+} concentrations of 2 mM, 3.5 mM and 5 mM.

Protein determination, sodium dodecyl-sulfate polyacrylamide gel electrophoresis (SDS-PAGE) and Western blot Analysis

A modified Bradford assay employing octyl-β-D-glucopyranoside (OGP) to solubilize membrane-bound proteins is used for determination of protein concentration (33). Respective membrane suspensions of 5 μg, 10 μg, and 20 μg of total membrane protein containing V902L or L804P were applied to the gel. SDS-PAGE and western blotting were performed according

to established procedures in the laboratory. Primary antibody GC1#3 directed against bovine GC-E (34) recognized human GC-E, and can be used to detect GC-E mutants V902L and L804P. The dilution of the primary antibody was 1:10,000. Incubation was overnight at 4°C. A goat anti-rabbit peroxidase-conjugated antibody (Dianova, Germany) at a concentration of 50% in glycerol was used as a secondary antibody at a dilution of 1:5000. The band intensity was detected and determined using Azure c400 Gel Imaging System by Azure Biosystems as described recently.

Heterologous expression of GC-E and mutants in the HEK293 cells

Cells were grown on a poly-L-lysine coated 12 mm coverslip placed in a 24-well plate. After 24 h at a density of 50-70%, it is transiently transfected with respective 0.5µg of plasmid DNA with 2µg of PEI. After 48 h of incubation at 37°C, 5% CO_2, cells were washed three times (5min) in PBS (pH 7.4), fixed in 4% paraformaldehyde (PFA) in PBS for 20 min, and then again washed three times (5min) with PBS (pH 7.4). Then, the cells were incubated with a blocking solution of 5% donkey serum in PBS (pH 7.4) and 0.5% Triton X-100 for 1 h. One time (5 min), washed with PBS (pH 7.4) and then subsequently incubated with the primary antibodies in a similar blocking solution, with primary antibody GC1#3 (1:500), rabbit polyclonal IgG, anti-Calnexin [1:300, calnexin (E-10), sc-46669, mouse monoclonal IgG 2a (Santa Cruz Biotechnology)]. We routinely observed that heterologous expressed GC-E localizes mainly in the ER (colocalization with calnexin), and we measured guanylate cyclase activity in membrane suspensions containing ER (ref. 15).

The next day, cells were again washed three times (5 min) in PBS (pH 7.4) and were further incubated with secondary antibodies [1:200, Alexa Fluor™ 568 goat anti-rabbit IgG and 1:200, Alexa Fluor™ 647 donkey anti-mouse IgG] for 90 min at room temperature in blocking solution. The next step is a final washing (three times, 5 min) in PBS (pH 7.4), then the coverslips were sealed with Mowiol containing DAPI on a microscopic slide and stored at 4°C till further use. Visualization was done using a fluorescence microscope, Olympus iX2.

Molecular Dynamics Simulation

In the earlier study (17), molecular dynamics (MD) simulations were performed on GC-E for a wild type and a V902L structure (17). Employing the same protocol as the earlier study, a double mutant V902L/L804P was established and simulated. Simulations were based on the structural information provided by Rehkamp et al. (11) for bovine GC-E. Coordinates of the starting model were provided by Dr. Christian Tüting and Prof. Panagiotis L. Kastritis, both at Martin Luther University Halle-Wittenberg in Germany, upon request. We refer to the human orthologue with a high sequence identity/ homology with the bovine variant. The corresponding valine of bovine GC-E is in position 907, in humans at position 902. Analogously, the double mutant translates to a mutation L809P in the bovine GC-E. The connectivity analysis (see below) refers to positions independent of amino acid side chains. Numbering in Figures 4 and 5 relates to the human variant. The simulation was set up through the VIKING online platform (35) employing the simulation software NAMD (36, 37). The CHARMM36 force field with CMAP corrections was used (38-41).

The structure was equilibrated in three phases, gradually lifting harmonic restraints to ensure a stable simulation. For the equilibration protocol the default parameters of VIKING were chosen. In the first step, 1 ns was simulated with a simulation time step of 1 fs in an NPT (constant number of atoms, constant pressure, and constant temperature) ensemble. Only water and ions were considered free to move. In the second equilibration step, the restraints on the side chains of the protein structure were lifted, and a 2 ns simulation was conducted using the same parameters. In the final equilibration step, all restraints were released, and another 2 ns simulation was run in an NVT (constant number of atoms, constant volume, and constant temperature) ensemble with a pressure of 1.01325 bar.

The production simulation was run for 400 ns in an NVT ensemble with a simulation time step of 2 fs and rigid hydrogen bonds. The other simulation parameters were equal to those from the third equlibration phase. All simulations were performed at a temperature of 310 K.

Connectivity Analysis

Connectivity networks were constructed based on the final simulation snapshot of all three variants of the GC-E protein structure (Wildtype, V902L, L804P, V902L/L804P). Comparing the so-called amino acid interaction network (42) between the simulations can be used to identify a change in key residues and potentially suggest potential mutation sites.

The network is constructed from the final simulation snapshot for each GC-E structure variation. Representing the location of each residue by its backbone Cα atom position, the distances between all the residues were calculated. If the distance between two residues was found below a particular threshold value, the residues were assumed to be connected in the network. Here, a threshold of 8 Å was chosen based on the example of an earlier study (23). A binary adjacency matrix can be constructed for each simulation using the threshold. One was employed by Kattnig et al. (23), which describes the betweenness of nodes and identifies important hubs in the network (Betweenness approach). The second approach was used by Estrada et al. (22), which describes the connectivity and the reach of an amino acid residue in the network (Reach approach).

Betweenness approach

The betweenness is calculated for each residue in each monomer of the dimer, such that $\beta_k(i)$ describes the betweeness of residue i in monomer k. $\beta_k(i)$ is defined as

$$\beta_k(i) = \sum_{u \neq v \neq i} \frac{\sigma_{uv}(i)}{\sigma_{uv}},$$

where $\sigma_{uv}(i)$ is the number of shortest paths connecting nodes u and v which pass through the node corresponding to residue i, and σ_{uv} is the total number of shortest paths connecting u and v.

Residues with a high betweenness value might be important for pathways through the protein as they are located in strategic intersections throughout the protein and a mutation in these residues might have a devastating impact on the dynamic properties of the protein

structure. As the GC-E structure comprises two monomers and potential experimental validation of proposed mutants would always act on both monomers, the betweenness and the reach values need to be adequately averaged over the individual monomers.

For the network representation, the average betweenness $\beta(i)$ is calculated for the whole dimer from the individual monomer betweeness $\beta_1(i)$ and $\beta_2(i)$ for monomers 1 and 2. The final betweeness is then the defined as

$$\beta(i) = \frac{\beta_1(i) + \beta_2(i)}{2}.$$

Reach approach

The Reach approach can be applied to determine the number of other residues that a given residue can reach in n steps through the network for every amino acid residue. The more other residues can be reached with a smaller n, the higher the reach of the given amino acid residue becomes. Mathematically speaking the approach roots on the following theorem (43):

Theorem 1. *If A is an adjacency matrix with elements* a_{ij}*, and* A^k *is the matrix exponential, such that, if* $B = A^2$*, then the elements* b_{ij} *are given by* $b_{ij} = \sum_{k=1}^{n} a_{ik}\, a_{kj}$*. The element* $a_{jk}^{(k)}$ *in* A^k *is then the number of walks of exactly length* k *from the node* i *to the node* j *in the network described by the adjacency matrix* A *.*

The theorem can now be used to quantify the connectivity of all the residues in the protein complex, with weighting factors such that paths to distant residues have less contribution. The matrix exponential function is a perfect fit for the above purpose, given by

$$G = \exp(A) = \sum_{k=0}^{\infty} \frac{A^k}{k!}.$$

The equation above contains A^k in each summand which yields the adjacency matrices with the number of paths with length k, but also a scaling factor $1/k!$, which devalues longer paths.

The information obtained from G can be interpreted in the context of the protein structure as follows. As $a_{ij}^{(k)}$ describes the number of paths of lengths k from amino acid i to amino acid j through the connectivity network, a larger value of the element g_{ij} can be interpreted as more options to reach each amino acid j from amino acid i in shorter trips.

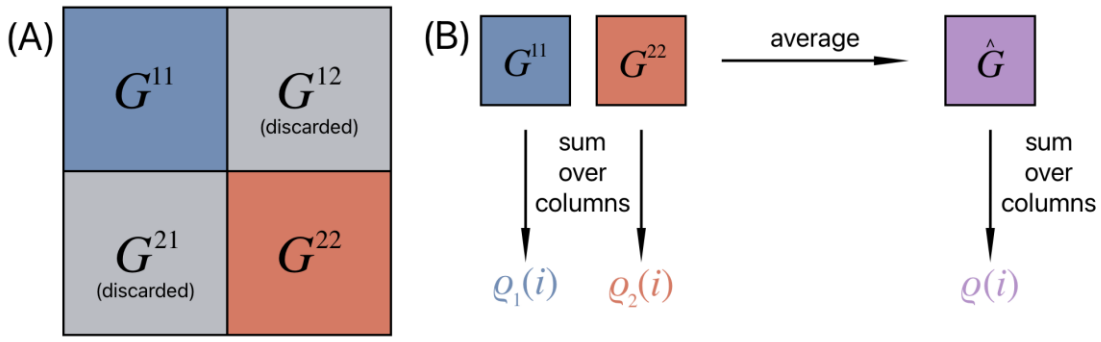

Figure 6: Panel A shows a schematic representation of the matrix G. Panel B visualizes the averaging process for the individual monomers of GC-E.

The reach value needs to be interpreted for each monomer for the network representation and an averaging procedure is applied. As each monomer contains 524 amino acid residues, the total protein contains 1048 residues, the exponential adjacency matrix G defining the network has the size 1048×1048. Subdividing the matrix into four blocks of size 524×524 yields two blocks on the diagonal corresponding to the individual monomers denoted by G^{11} and G^{22}. The other two blocks (G^{12} and G^{21}) describing the reach from one monomer to the other are discarded in the analysis. The process is schematically shown in Figure 6. The averaged reach matrix is then the element-wise summation as follows:

$$\bar{G} = \frac{1}{2}(G^{11} + G^{22})$$

Finally, the sum over column i of $\bar{G}$ is denoted with $\rho(i)$:

$$\rho(i) = \sum_j \bar{g}_{ij}.$$

$\rho(i)$ is called the reach of residue i. A larger value of $\rho(i)$ can be interpreted as a greater reach of amino acid i and it is subsequently assumed, that the amino acid residue has a greater impact on the overall structure. Conversely, a small reach value would indicate a more isolated residue.

Additionally, to look into residues in their original monomers, $\rho_k(i)$ describes the sum over the column of the matrices G^{kk}, with the process schematically shown in Figure 6.

Comparison between WT and V902L proteins

The reach and betweeness values are calculated individually for the WT and the V902L mutant. In order to extract the interesting residues from the two structures, the residues with the greatest differences in their values comparing the two version of the structure are considered.

We, therefore, consider not the absolute values of $\beta(i)$ and $\rho(i)$, but their differences between the WT and mutant proteins, defined as:

$$\Delta\beta(i) = \beta_{\mathrm{WT}}(i) - \beta_{\mathrm{V902L}}(i)$$

and

$$\Delta\rho(i) = \rho_{\mathrm{WT}}(i) - \rho_{\mathrm{V902L}}(i).$$

Considering the sign for the individual contributions, a positive values in $\Delta\beta(i)$ and $\Delta\rho(i)$ indicate a greater connectivity in the WT structure compared to the mutant, while a negative value shows a greater connectivity in the mutant compared to the WT. If one now considers the sorted list of residues, the first and last residues are particularly interesting.

Safety statement

No unexpected or unusually high safety hazards were encountered.

Supporting information

Figure S1. Activity profile of GC-E variants (biological replicate)

Figure S2. Activity profile of GC-E mutant V902L (biological replicate)

Figure S3. Activity profile of GC-E mutant V902L (biological replicate)

Figure S4. Ca^{2+}-dependent inhibition of the V902L mutant in the absence of GCAP1 or GCAP3 (biological replicates)

Figure S5. Activity profile of GC-E variants (biological replicate)

Figure S6. Activity profile of GC-E variant (biological replicate)

Figure S7. Activity profile of GC-E variant (biological replicate)

Figure S8. Expression of V902L and double mutant V902L/L804P in HEK293 cells.

Figure S9. Heterologous expression of GC-E and mutants (V902L, V902L/L804P) in HEK293 cells.

Accession Codes

GC-E, UniProt: Q02846.

GCAP1, NCBI Reference Sequence: NP_001371839.1

GCAP3, NCBI Reference Sequence: NP_005450.3

Author contribution

MKS: Conceptualization, Methodology, Validation, Investigation, Writing - Original Draft, Visualization. **FS**: Conceptualization, Software, Formal Analysis, Investigation, Writing - Original Draft. **SYW**: Software, Validation, Formal Analysis, Writing - Original Draft. **IAS**: Resources, Data Curation, Writing - Review & Editing, Supervision, Funding acquisition

KWK: Conceptualization, Resources, Data Curation, Writing - Review & Editing, Supervision, Funding acquisition

Acknowledgement.

The authors would like to thank the Volkswagen Foundation (Lichtenberg Professorship to IAS), the Deutsche Forschungsgemeinschaft (DFG; GRK1885/2: Molecular Basis of Sensory Biology and SFB 1372: Magnetoreception and Navigation in Vertebrates, project-number: 395940726), the Ministry for Science and Culture of Lower Saxony (Simulations Meet Experiments on the Nanoscale: Opening up the Quantum World to Artificial Intelligence (SMART) and Dynamik auf der Nanoskala: Von kohärenten Elementarprozessen zur Funktionalität (DyNano)) and Novo Nordisk Foundation (grant no NNF22OC0079182). The CARL Cluster at the Carl-von-Ossietzky University, Oldenburg, supported by the DFG and the Ministry for Science and Culture of Lower Saxony, provided computational resources for the simulations. The authors gratefully acknowledge the computing time granted by the Resource Allocation Board and provided on the supercomputer Lise and Emmy at NHR@ZIB and NHR@Göttingen as part of the NHR infrastructure. The calculations for this research were conducted with computing resources under the project nip00058.

References

1. Rivolta C, Sharon D, DeAngelis MM, Dryja TP. Retinitis pigmentosa and allied diseases: numerous diseases, genes, and inheritance patterns. Hum Mol Genet. (2002) 11(10):1219-27. doi: 10.1093/hmg/11.10.1219. Erratum in: Hum Mol Genet. 2003 12(5):583-4.

2. Hartong DT, Berson EL, Dryja TP. Retinitis pigmentosa. Lancet. (2006) 368(9549):1795-809. doi: 10.1016/S0140-6736(06)69740-7.

3. Sharon D, Wimberg H, Kinarty Y, Koch KW. Genotype-functional-phenotype correlations in photoreceptor guanylate cyclase (GC-E) encoded by GUCY2D. Prog Retin Eye Res. (2018) 63:69-91. doi: 10.1016/j.preteyeres.2017.10.003.

4. Luo DG, Xue T, Yau KW. How vision begins: an odyssey. Proc Natl Acad Sci U S A. (2008) 105(29):9855-9862. doi: 10.1073/pnas.0708405105.

5. Koch KW, Dell'Orco D. Protein and Signaling Networks in Vertebrate Photoreceptor Cells. Front Mol Neurosci. (2015) 8:67. doi: 10.3389/fnmol.2015.00067.

6. Lamb TD. Photoreceptor physiology and evolution: cellular and molecular basis of rod and cone phototransduction. J Physiol. (2022) 600(21): 4585-4601. doi: 10.1113/JP282058.

7. Dizhoor AM, Peshenko IV. Regulation of retinal membrane guanylyl cyclase (RetGC) by negative calcium feedback and RD3 protein. Pflugers Arch. (2021) 473(9): 1393-1410. doi: 10.1007/s00424-021-02523-4. Erratum in: Pflugers Arch. (2021) 5

8. Palczewski K, Sokal I, Baehr W. Guanylate cyclase-activating proteins: structure, function, and diversity. Biochem Biophys Res Commun. (2004) 322(4):1123-1130. doi: 10.1016/j.bbrc.2004.07.

9. Dizhoor AM, Olshevskaya EV, Peshenko IV. Mg2+/Ca2+ cation binding cycle of guanylyl cyclase activating proteins (GCAPs): role in regulation of photoreceptor guanylyl cyclase. Mol Cell Biochem. (2010) 334(1-2): 117-124. doi: 10.1007/s11010-009-0328-6.

10. Koch KW, Dell'Orco D. A calcium-relay mechanism in vertebrate phototransduction. ACS Chem Neurosci. (2013) 4(6): 909-917. doi: 10.1021/cn400027z.

11. Rehkamp A, Tänzler D, Tüting C, Kastritis PL, Iacobucci C, Ihling CH, Kipping M, Koch KW, Sinz A. First 3D-Structural Data of Full-Length Guanylyl Cyclase 1 in Rod-Outer-Segment Preparations of Bovine Retina by Cross-Linking/Mass Spectrometry. J Mol Biol. (2021) 433(10):166947. doi: 10.1016/j.jmb.2021.166947.

12. Gajiwala KS, Burley SK. Winged helix proteins. Curr Opin Struct Biol. (2000) 10(1):110-116. doi: 10.1016/s0959-440x(99)00057-3.

13. Horst BG, Yokom AL, Rosenberg DJ, Morris KL, Hammel M, Hurley JH, Marletta MA. Allosteric activation of the nitric oxide receptor soluble guanylate cyclase mapped by cryo-electron microscopy. Elife. (2019) 8:e50634. doi: 10.7554/eLife.50634.

14. Peshenko IV, Olshevskaya EV, Dizhoor AM. Dimerization Domain of Retinal Membrane Guanylyl Cyclase 1 (RetGC1) Is an Essential Part of Guanylyl Cyclase-activating Protein (GCAP) Binding Interface. J Biol Chem. (2015) 290(32):19584-19596. doi: 10.1074/jbc.M115.661371.

15. Zägel P, Dell'Orco D, Koch KW. The dimerization domain in outer segment guanylate cyclase is a Ca^{2+}-sensitive control switch module. Biochemistry. (2013) 52(30):5065-5074. doi: 10.1021/bi400288p.

16. Wimberg H, Lev D, Yosovich K, Namburi P, Banin E, Sharon D, Koch KW. Photoreceptor Guanylate Cyclase (GUCY2D) Mutations Cause Retinal Dystrophies by Severe Malfunction of Ca2+-Dependent Cyclic GMP Synthesis. Front Mol Neurosci. (2018) 11:348. doi: 10.3389/fnmol.2018.00348.

17. Shahu MK, Schuhmann F, Scholten A, Solov'yov IA, Koch KW. The Transition of Photoreceptor Guanylate Cyclase Type 1 to the Active State. Int J Mol Sci. (2022) 23(7):4030. doi: 10.3390/ijms23074030.

18. Serfass L, Carr HS, Aschenbrenner LM, Burstyn JN. Calcium ion downregulates soluble guanylyl cyclase activity: evidence for a two-metal ion catalytic mechanism. Arch Biochem Biophys. (2001) 387(1):47-56. doi: 10.1006/abbi.2000.2090.

19. Scholich K, Barbier AJ, Mullenix JB, Patel TB. Characterization of soluble forms of nonchimeric type V adenylyl cyclases. Proc Natl Acad Sci U S A. (1997) 94(7): 2915-2920. doi: 10.1073/pnas.94.7.2915. Erratum in: Proc Natl Acad Sci U S A (1997) 94(19):10485.

20. Hurley JH. Structure, mechanism, and regulation of mammalian adenylyl cyclase. J Biol Chem. (1999) 274(12):7599-7602. doi: 10.1074/jbc.274.12.7599.

21. Tesmer JJ, Sunahara RK, Johnson RA, Gosselin G, Gilman AG, Sprang SR. Two-metal-Ion catalysis in adenylyl cyclase. Science. (1999) 285(5428):756-760. doi: 10.1126/science.285.5428.756.

22. Estrada E. Topological analysis of SARS CoV-2 main protease. Chaos. (2020) 30(6): 061102. doi: 10.1063/5.0013029.

23. Kattnig DR, Nielsen C, Solov'yov, IA. Molecular dynamics simulations disclose early stages of the photo-activation of cryptochrome 4. New J. Phys. (2018) 20: 083018. DOI 10.1088/1367-2630/aad70f.

24. Marino V, Dell'Orco D. Allosteric communication pathways routed by Ca2+/Mg2+ exchange in GCAP1 selectively switch target regulation modes. Sci Rep. (2016) 6: 34277. doi: 10.1038/srep34277.

25. Marino V, Dell'Orco D. Evolutionary-Conserved Allosteric Properties of Three Neuronal Calcium Sensor Proteins. Front Mol Neurosci. (2019) 12: 50. doi: 10.3389/fnmol.2019.00050.

26. Liu Y, Ruoho AE, Rao VD, Hurley JH. Catalytic mechanism of the adenylyl and guanylyl cyclases: modeling and mutational analysis. Proc Natl Acad Sci U S A. (1997) 94(25):13414-1319. doi: 10.1073/pnas.94.25.13414.

27. Li L, Xiao X, Li S, Jia X, Wang P, Guo X, Jiao X, Zhang Q, Hejtmancik JF. Detection of variants in 15 genes in 87 unrelated Chinese patients with Leber congenital amaurosis. PLoS One. 2011;6(5):e19458. doi: 10.1371/journal.pone.0019458. Epub 2011 May 13. PMID: 21602930; PMCID: PMC3094346.

28. Xu Y, Xiao X, Li S, Jia X, Xin W, Wang P, Sun W, Huang L, Guo X, Zhang Q. Molecular genetics of Leber congenital amaurosis in Chinese: New data from 66 probands and mutation overview of 159 probands. Exp Eye Res. (2016) 149: 93-99. doi: 10.1016/j.exer.2016.06.019.

29. Abbas S, Marino V, Weisschuh N, Kieninger S, Solaki M, Dell'Orco D, Koch KW. Neuronal Calcium Sensor GCAP1 Encoded by GUCA1A Exhibits Heterogeneous Functional Properties in Two Cases of Retinitis Pigmentosa. ACS Chem Neurosci. (2020) 11(10):1458-1470. doi: 10.1021/acschemneuro.0c00111.

30. Avesani A, Bielefeld L, Weisschuh N, Marino V, Mazzola P, Stingl K, Haack TB, Koch KW, Dell'Orco D. Molecular Properties of Human Guanylate Cyclase-Activating Protein 3 (GCAP3) and Its Possible Association with Retinitis Pigmentosa. Int J Mol Sci. (2022) 23(6): 3240. doi: 10.3390/ijms23063240.

31. Koch, K.-W. and Helten, A. Guanylate cyclase-based signaling in photoreceptors and retina. Chapter 6 in Signal Transduction in the Retina (Fliesler, S. J. and Kisselev, O. G., Eds.) Taylor and Francis CRC Press (2008), pp. 121-143

32. Hwang JY, Lange C, Helten A, Höppner-Heitmann D, Duda T, Sharma RK, Koch KW. Regulatory modes of rod outer segment membrane guanylate cyclase differ in catalytic efficiency and Ca(2+)-sensitivity. Eur J Biochem. (2003) 270(18): 3814-3821. doi: 10.1046/j.1432-1033.2003.03770.x.

33. Fanger BO. Adaptation of the Bradford protein assay to membrane-bound proteins by solubilizing in glucopyranoside detergents. Anal Biochem. (1987) 162: 11-17. doi: 10.1016/0003-2697(87)90004-2.

34. Koch KW, Stecher P, Kellner R. Bovine retinal rod guanyl cyclase represents a new N-glycosylated subtype of membrane-bound guanyl cyclases. Eur J Biochem. (1994) 222(2):589-595. doi: 10.1111/j.1432-1033.1994.tb18901.x.

35. Korol V, Husen P, Sjulstok E, Nielsen C, Friis I, Frederiksen A, Salo AB, Solov'yov IA. Introducing VIKING: A Novel Online Platform for Multiscale Modeling. ACS Omega. (2019) 5(2): 1254-1260. doi: 10.1021/acsomega.9b03802.

36. Phillips JC, Braun R, Wang W, Gumbart J, Tajkhorshid E, Villa E, Chipot C, Skeel RD, Kalé L, Schulten K. Scalable molecular dynamics with NAMD. J Comput Chem. (2005) 26(16):1781-1802. doi: 10.1002/jcc.20289.

37. Phillips JC, Hardy DJ, Maia JDC, Stone JE, Ribeiro JV, Bernardi RC, Buch R, Fiorin G, Hénin J, Jiang W, McGreevy R, Melo MCR, Radak BK, Skeel RD, Singharoy A, Wang Y, Roux B, Aksimentiev A, Luthey-Schulten Z, Kalé LV, Schulten K, Chipot C, Tajkhorshid E. Scalable molecular dynamics on CPU and GPU architectures with NAMD. J Chem Phys. (2020) 153(4): 044130. doi: 10.1063/5.0014475.

38. Foloppe, N. and MacKerell, Jr., A.D. All-atom empirical force field for nucleic acids: I. Parameter optimization based on small molecule and condensed phase macromolecular target data. J. Comput. Chem. (2000) 21: 86-104.

39. Best RB, Zhu X, Shim J, Lopes PE, Mittal J, Feig M, Mackerell AD Jr. Optimization of the additive CHARMM all-atom protein force field targeting improved sampling of the backbone φ, ψ and side-chain χ(1) and χ(2) dihedral angles. J Chem Theory Comput. (2012) 8(9): 3257-3273. doi: 10.1021/ct300400x.

40. Best RB, Zhu X, Shim J, Lopes PE, Mittal J, Feig M, Mackerell AD Jr. Optimization of the additive CHARMM all-atom protein force field targeting improved sampling of the backbone φ, ψ and side-chain χ(1) and χ(2) dihedral angles. J Chem Theory Comput. (2012) 8(9): 3257-3273. doi: 10.1021/ct300400x.

41. MacKerell AD, Bashford D, Bellott M, Dunbrack RL, Evanseck JD, Field MJ, Fischer S, Gao J, Guo H, Ha S, Joseph-McCarthy D, Kuchnir L, Kuczera K, Lau FT, Mattos C, Michnick S, Ngo T, Nguyen DT, Prodhom B, Reiher WE, Roux B, Schlenkrich M, Smith JC, Stote R, Straub J, Watanabe M, Wiórkiewicz-Kuczera J, Yin D, Karplus M. All-atom empirical potential for molecular modeling and dynamics studies of proteins. J Phys Chem B. (1998) 102(18): 3586-3616. doi: 10.1021/jp973084f.

42. Gaci O. A topological description of hubs in amino Acid interaction networks. Adv Bioinformatics. (2010) 2010:257512. doi: 10.1155/2010/257512.

43. Matousek J, Nesetril J. Invitation to Discrete Mathematics (2. ed.). Oxford University Press 2009, ISBN 978-0-19-857042-4, pp. I-XVII, 1-443.

Acknowledgement.

The authors would like to thank the Volkswagen Foundation (Lichtenberg Professorship to IAS), the Deutsche Forschungsgemeinschaft (DFG; GRK1885/2: Molecular Basis of Sensory Biology and SFB 1372: Magnetoreception and Navigation in Vertebrates, project-number: 395940726), the Ministry for Science and Culture of Lower Saxony (Simulations Meet Experiments on the Nanoscale: Opening up the Quantum World to Artificial Intelligence

(SMART) and Dynamik auf der Nanoskala: Von kohärenten Elementarprozessen zur Funktionalität (DyNano)) and Novo Nordisk Foundation (grant no NNF22OC0079182). The CARL Cluster at the Carl-von-Ossietzky University, Oldenburg, supported by the DFG and the Ministry for Science and Culture of Lower Saxony, provided computational resources for the simulations. The authors gratefully acknowledge the computing time granted by the Resource Allocation Board and provided on the supercomputer Lise and Emmy at NHR@ZIB and NHR@Göttingen as part of the NHR infrastructure. The calculations for this research were conducted with computing resources under the project nip00058.

For Table of Contents use only (TOC graphic)

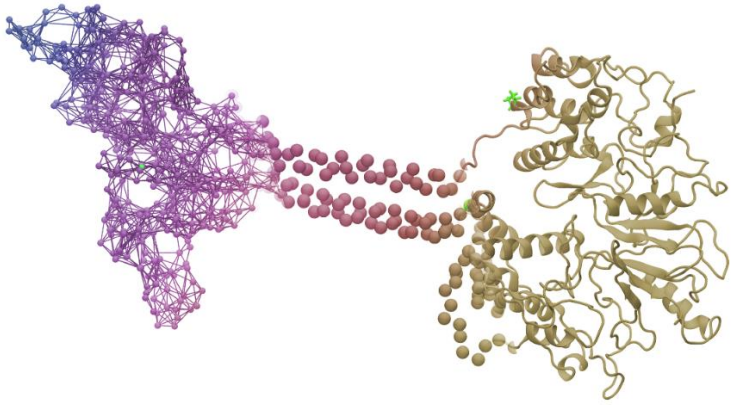

3.1 Supporting information

Allosteric communication of the dimerization and the catalytic domain in photoreceptor guanylate cyclase

Manisha Kumari Shahu[1], Fabian Schuhmann[2,3], Siu Ying Wong[3], Ilia A. Solov'yov[3,4,5] and Karl-Wilhelm Koch[1,4]

[1]Carl von Ossietzky Universität Oldenburg, Department of Neuroscience, Carl-von-Ossietzky-Str. 9-11, Oldenburg, 26129, Germany.

[2]Niels Bohr International Academy, Niels Bohr Institute, University of Copenhagen, Blegdamsvej 17, 2100 Copenhagen, Denmark

[3]Carl von Ossietzky Universität Oldenburg, Institute of Physics, Carl-von-Ossietzky-Str. 9-11, Oldenburg, 26129, Germany.

[4]Carl von Ossietzky Universität Oldenburg, Research Centre for Neurosensory Science, Carl-von-Ossietzky-Str. 9-11, Oldenburg, 26129, Germany.

[5]Center for Nanoscale Dynamics (CENAD), Carl von Ossietzky Universität Oldenburg, Institute of Physics, Ammerländer Heerstr. 114-118, 26129 Oldenburg, Germany.

Corresponding authors: karl.w.koch@uol.de

Figure S1

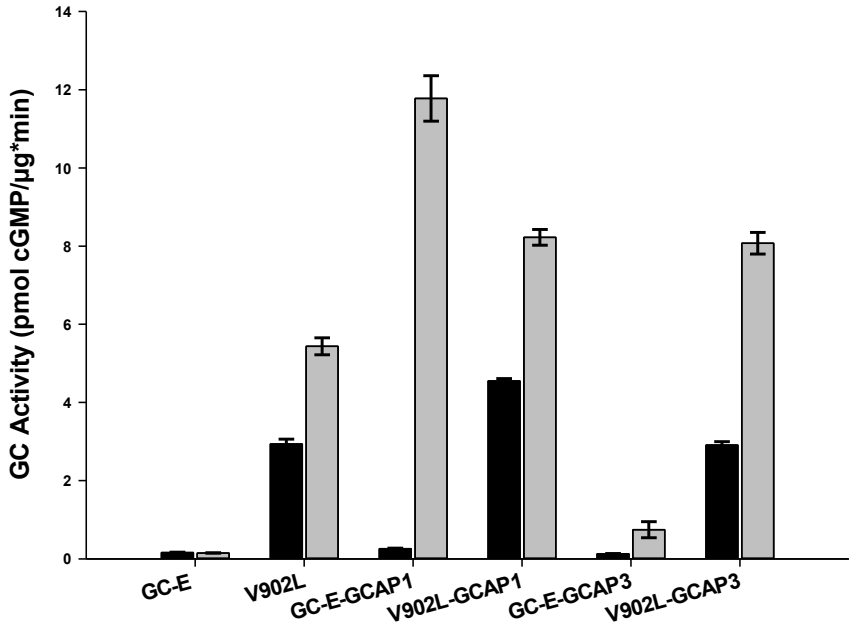

Figure S1. Activity profile of GC-E variants. WT and mutant V902L were activated with GCAP1 or GCAP3 at high (33 µM, black bars) or low (<10 nM, gray bars) free [Ca^{2+}]. The x-fold activation of GC-E WT with GCAP1 is 45.3 and with GCAP3 is 5.8. The x-fold activation of V902L without GCAPs is 1.9; in the presence of GCAP1 is 1.8 and with GCAP3 it is 2.8. Error bars are s.d of technical replicates.

Figure S2

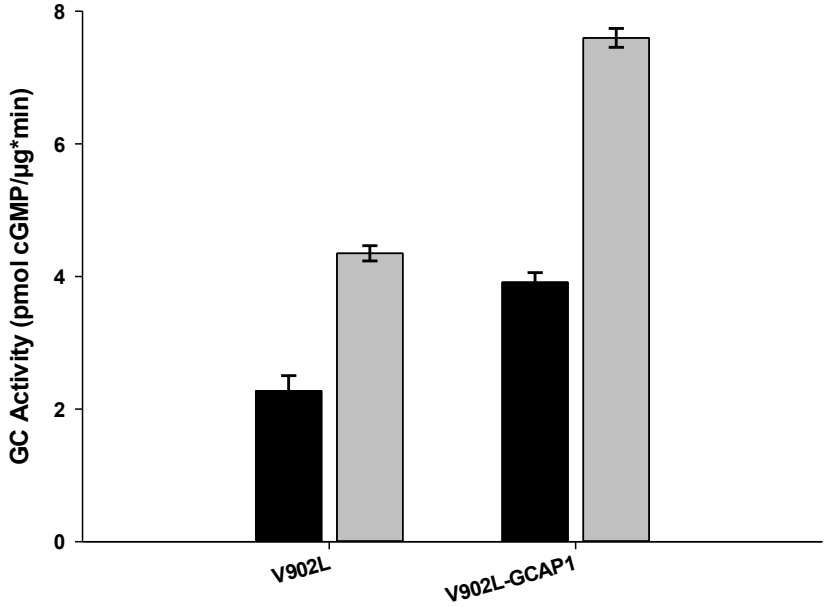

Figure S2. Activity profile of GC-E mutant V902L. Assay was done in the absence and presence of GCAP1 at high (33 µM, black bars) or low (<10 nM, gray bars) free [Ca^{2+}]. The

x-fold activation of V902L without GCAP1 is 1.9; in the presence of GCAP1 is 1.9. Error bars are s.d of technical replicates.

Figure S3

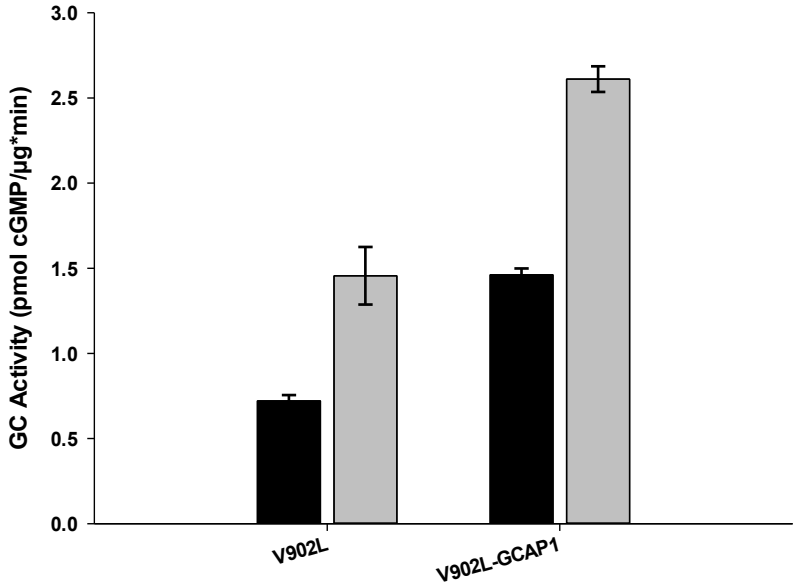

Figure S3. Activity profile of GC-E mutant V902L. Assay was done in the absence and presence of GCAP1 at high (33 µM, black bars) or low (<10 nM, gray bars) free [Ca^{2+}]. The x-fold activation of V902L without GCAP1 is 2; in the presence of GCAP1 is 1.8. Error bars are s.d of technical replicates.

Figure S4

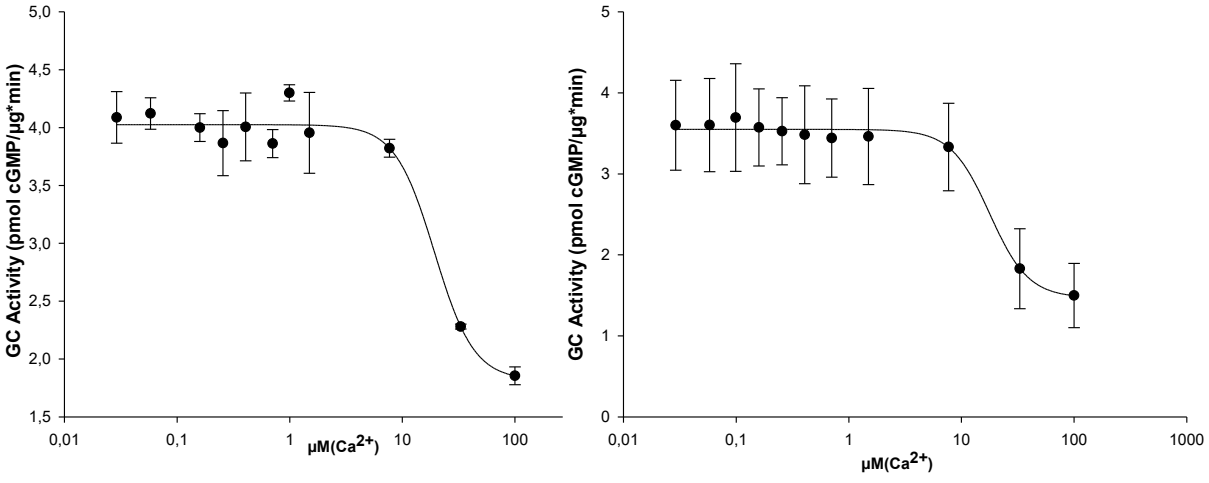

Figure S4. Ca^{2+}-dependent inhibition of the V902L mutant in the absence of GCAP1 or GCAP3. Free [Ca^{2+}] was varied as indicated and half-maximal inhibition was at 19.3 µM free [Ca^{2+}] (left graph) and 17.8 µM [Ca^{2+}] (right graph), (biological replicates, error bars are s.d.).

Figure S5

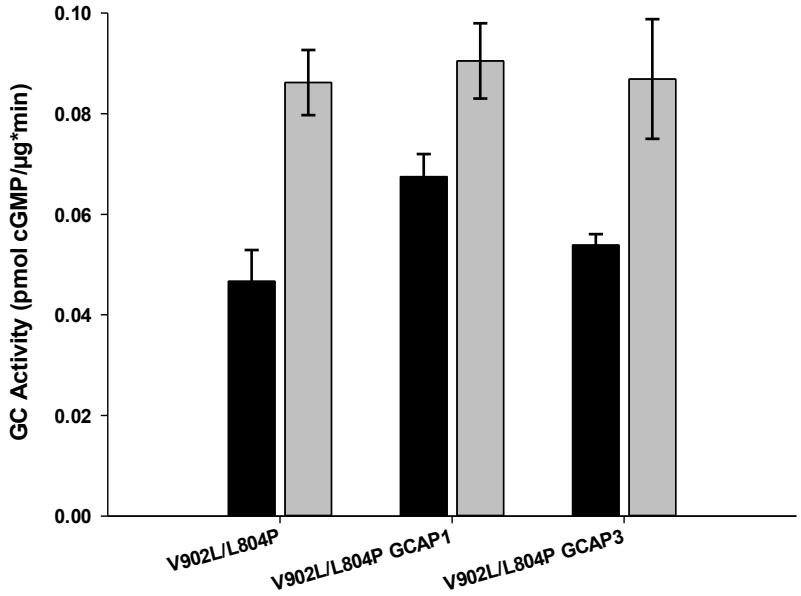

Figure S5. Activity profile of GC-E variants. Double mutant V902L/L804P was activated with GCAP1 or GCAP3 at high (33 µM, black bars) or low (<10 nM, gray bars) free [Ca^{2+}]. The x-fold activation of double mutant without GCAP1 is 1.8; in the presence of GCAP1 it is 1.3 and with GCAP3 it is 1.6. Error bars are s.d of technical replicates.

Figure S6

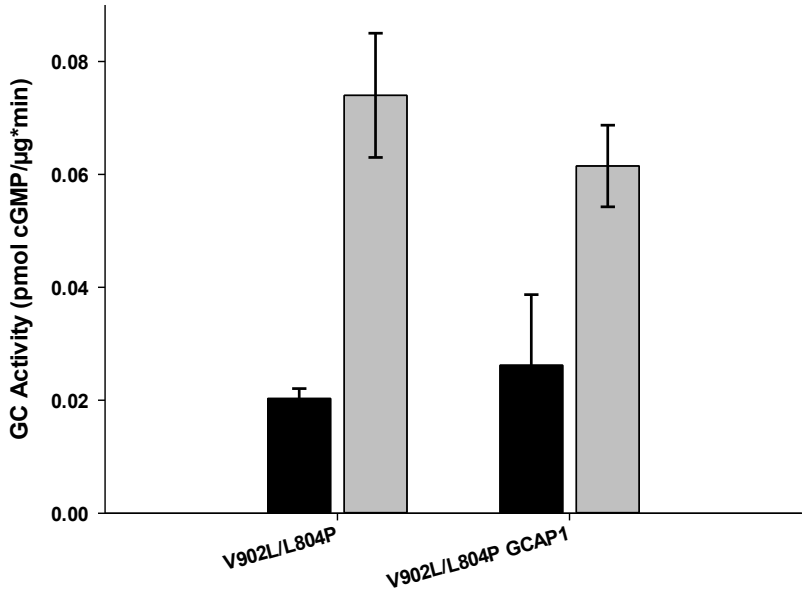

Figure S6. Activity profile of GC-E variant. Double mutant V902L/L804P was activated with GCAP1 at high (33 µM, black bars) or low (<10 nM, gray bars) free [Ca^{2+}]. The x-fold activation of double mutant without GCAP1 is 3.6 and is 2.3 in the presence of GCAP1. Error bars are s.d of technical replicates.

Figure S7

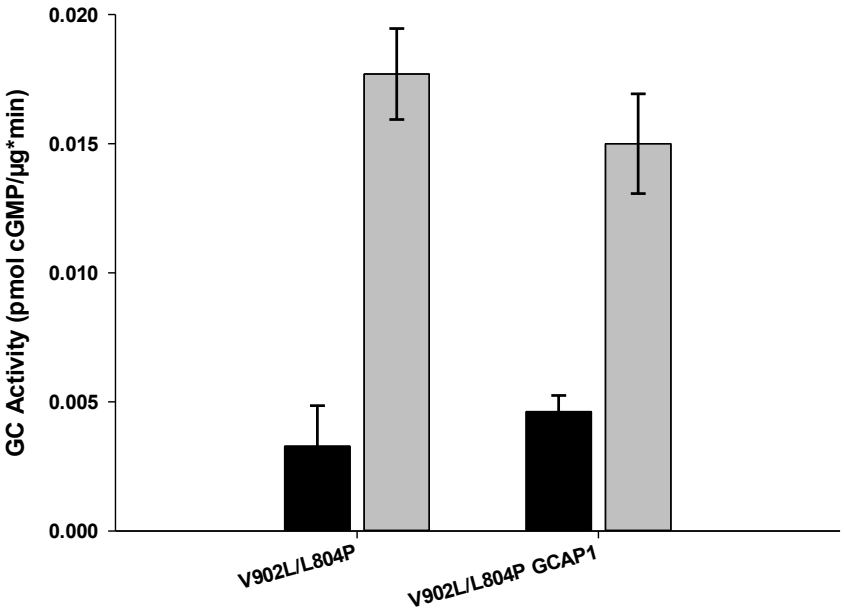

Figure S7. Activity profile of GC-E variant. Double mutant V902L/L804P was activated with GCAP1 at high (33 µM, black bars) or low (<10 nM, gray bars) free [Ca^{2+}]. The x-fold activation of double mutant without GCAP1 is 5.4 and is 3 in the presence of GCAP1. Error bars are s.d of technical replicates.

Figure S8

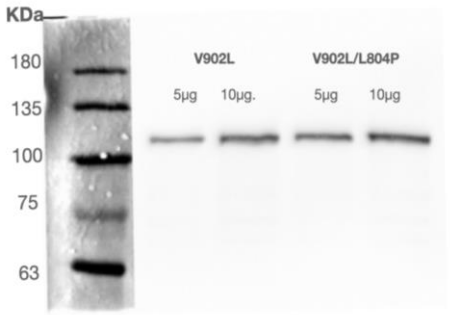

Figure S8. Expression of V902L and double mutant V902L/L804P in HEK293 cells. Expression level of mutants was compared in HEK293 cell membrane for its expression profile using immunoblotting. Five µg and ten µg of total protein amount for each membrane sample was analyzed by SDS-polyacrylamide gel electrophoresis. The samples were detected by the specific antibody anti-GC1#3 and ECL imaging (see Methods part in main text).

Figure S9.

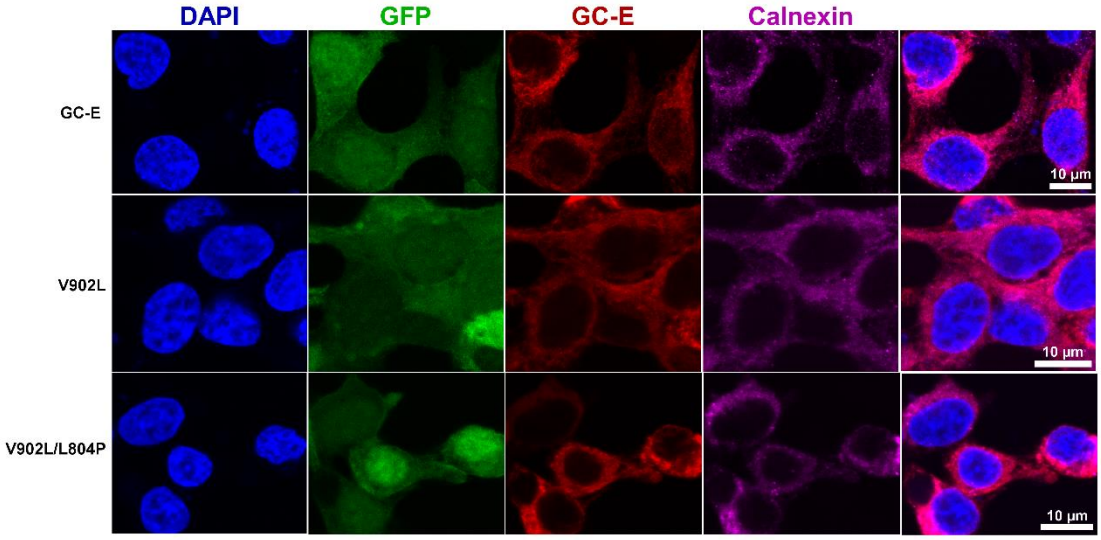

Figure S9. Heterologous expression of GC-E and mutants (V902L, V902L/L804P) in HEK293 cells. Confocal images of transfected cells probed with different antibodies. Transfected cells are visualized with GFP (green) and DAPI staining (nucleus), GC-E variants are recognized by an anti-GC-E specific antibody (#3, red), Endoplasmic reticulum (ER) is stained with the ER marker Calnexin (magenta). No difference has been observed in the localization of the mutants compared to the WT GC-E. An overlay is seen on the most right panels. Scale bar is 10 µm.

Chapter 4 : NMR and EPR-DEER structure of a dimeric Guanylate Cyclase Activator protein-5 from Zebrafish Photoreceptors

Published in final edited form as:
Biochemistry. 2021 October 19; 60(41): 3058–3070. doi:10.1021/acs.biochem.1c00612.

NMR and EPR-DEER Structure of a Dimeric Guanylate Cyclase Activator Protein-5 from Zebrafish Photoreceptors

Diana Cudia,
Department of Chemistry, University of California, Davis, California 95616, United States

Graham P. Roseman,
Department of Chemistry and Biochemistry, University of California, Santa Cruz, California 95064, United States

Tufa E. Assafa,
Department of Chemistry and Biochemistry, University of California, Santa Cruz, California 95064, United States

Manisha Kumari Shahu,
Division of Biochemistry, Department of Neuroscience, University of Oldenburg, 26129 Oldenburg, Germany

Alexander Scholten,
Division of Biochemistry, Department of Neuroscience, University of Oldenburg, 26129 Oldenburg, Germany

Sarah-Karina Menke-Sell,
Division of Biochemistry, Department of Neuroscience, University of Oldenburg, 26129 Oldenburg, Germany

Hiroaki Yamada,
Department of Chemistry, University of California, Davis, California 95616, United States

Karl-W. Koch,
Division of Biochemistry, Department of Neuroscience, University of Oldenburg, 26129 Oldenburg, Germany

Glenn Milhauser,

Corresponding Author: **James B. Ames** – *Department of Chemistry, University of California, Davis, California 95616, United States;* Phone: (530) 752-6358; jbames@ucdavis.edu.

Author Contributions
J.B.A. designed research and, with input from other authors, wrote the paper. D.C., G.P.R., T.E.A., M.K.S., A.S., S.-K.M.-S., H.Y., K.-W.K., G.M., and J.B.A. performed research. D.C., G.P.R., T.E.A., A.S., and J.B.A. analyzed data.

Supporting Information
The Supporting Information is available free of charge at https://pubs.acs.org/doi/10.1021/acs.biochem.1c00612.
HSQC NMR spectra of Mg^{2+}-free versus Mg^{2+}-bound GCAP5 (Figure S1), EPR-DEER data of all spin-labeled GCAP5 constructs and their corresponding distance distributions (Figure S2), HSQC NMR spectrum of $GCAP5^{H18A/Y21A}$ and MALS analysis of $GCAP5^{H18A/Y21A}$ and $GCAP5^{R22A}$ (Figure S3), and GCAP5 melting temperature analysis (Figure S4) (PDF)

Accession Codes
Atomic coordinates for GCAP5: PDB entry 7M2M.

Complete contact information is available at: https://pubs.acs.org/10.1021/acs.biochem.1c00612

The authors declare no competing financial interest.

Department of Chemistry and Biochemistry, University of California, Santa Cruz, California 95064, United States

James B. Ames
Department of Chemistry, University of California, Davis, California 95616, United States

Abstract

Retinal guanylate cyclases (RetGCs) are regulated by a family of guanylate cyclase-activating proteins (called GCAP1–7). GCAPs form dimers that bind to Ca^{2+} and confer Ca^{2+} sensitive activation of RetGC during visual phototransduction. The GCAP5 homologue from zebrafish contains two nonconserved cysteine residues (Cys15 and Cys17) that bind to ferrous ion, which stabilizes GCAP5 dimerization and diminishes its ability to activate RetGC. Here, we present NMR and EPR-DEER structural analysis of a GCAP5 dimer in the Mg^{2+}-bound, Ca^{2+}-free, Fe^{2+}-free activator state. The NMR-derived structure of GCAP5 is similar to the crystal structure of Ca^{2+}-bound GCAP1 (root-mean-square deviation of 2.4 Å), except that the N-terminal helix of GCAP5 is extended by two residues, which allows the sulfhydryl groups of Cys15 and Cys17 to become more solvent exposed in GCAP5 to facilitate Fe^{2+} binding. Nitroxide spin-label probes were covalently attached to particular cysteine residues engineered in GCAP5: C15, C17, T26C, C28, N56C, C69, C105, N139C, E152C, and S159C. The intermolecular distance of each spin-label probe in dimeric GCAP5 (measured by EPR-DEER) defined restraints for calculating the dimer structure by molecular docking. The GCAP5 dimer possesses intermolecular hydrophobic contacts involving the side chain atoms of H18, Y21, M25, F72, V76, and W93, as well as an intermolecular salt bridge between R22 and D71. The structural model of the GCAP5 dimer was validated by mutations (H18E/Y21E, H18A/Y21A, R22D, R22A, M25E, D71R, F72E, and V76E) at the dimer interface that disrupt dimerization of GCAP5 and affect the activation of RetGC. We propose that GCAP5 dimerization may play a role in the Fe^{2+}-dependent regulation of cyclase activity in zebrafish photoreceptors.

Graphical Abstract

Retinal guanylate cyclase-activating proteins (GCAP1[1] and GCAP2[2]) are EF-hand calcium sensor proteins in mammalian photoreceptor rod and cone cells[3] that control Ca^{2+} sensitive activation of retinal guanylate cyclases (RetGCs[4,5]), which regulates the recovery phase of vertebrate visual phototransduction.[6,7] Ca^{2+} binds to the second, third, and fourth EF-hands in the GCAP proteins[8,9] (shaded red, cyan, and yellow, respectively, in Figure 1), and the Ca^{2+}-bound GCAPs bind to and inhibit RetGCs in dark-adapted photoreceptors.[10,11] By contrast, Mg^{2+} binds to the second EF-hand in GCAP1,[12] and the Ca^{2+}-free, Mg^{2+}-bound GCAPs activate RetGCs in light-adapted photoreceptors.[10,11] Mutations in both GCAP1 and RetGCs that disrupt the Ca^{2+}-dependent cyclase activation are genetically linked to retinal degenerative diseases.[13–17] GCAP orthologues are also expressed in zebrafish photoreceptors (GCAP3–5 and -7[18]). *In situ* hybridization showed that expression of zebrafish specific GCs and GCAPs coincides with the onset of visual function.[19,20] The zebrafish GCAP5 homologue has the most divergent amino acid sequence (Figure 1), which contains two nonconserved cysteine residues (Cys15 and Cys17) that were shown recently to ligate ferrous ion,[21] and the binding of Fe^{2+} to GCAP5 greatly diminishes its ability to activate RetGC.[21] Ferrous ion has been shown to serve as a redox sensor in a variety of cell types,[22] and it is tempting to speculate that redox sensing by GCAP5 might control phototransduction in zebrafish photoreceptors. Indeed, the accumulation of iron levels in the retina has been correlated with age-related macular degeneration in humans, suggesting the involvement of redox sensitive processes in the pathogenesis of the disease.[23]

In this study, we present NMR structures of Mg^{2+}-bound, Ca^{2+}-free, Fe^{2+}-free GCAP5 (hereafter termed Mg^{2+}-bound GCAP5), which represents the first structure of a GCAP protein in an activator state that binds to and activates RetGC. Overall, Mg^{2+}-bound GCAP5 is structurally similar to the crystal structure of Ca^{2+}-bound GCAP1[9] [2.4 Å root-mean-square deviation (RMSD)]. However, the N-terminal and C-terminal helices, located outside of the EF-hand motifs of GCAP5, are structurally distinct from those of Ca^{2+}-bound GCAP1, and the Ca^{2+}-induced structural changes to these helices may play a role in regulating RetGC and may facilitate binding of Fe^{2+} to GCAP5. We also present an EPR-DEER structural analysis to determine intermolecular contacts in the GCAP5 dimer. Nitroxide spin-label probes were introduced at 10 different sites in GCAP5 [C15, C17, T26C, C29, N56C, C69, C105, N139C, E152C, and S159C (see Figure 1)], and intermolecular distances from each site in the GCAP5 dimer were measured. The DEER distance restraints define a GCAP5 dimer structure that contains key hydrophobic residues (H18, Y21, M25, F72, V76, and W93) as well as an intermolecular salt bridge between R22 and D71 at the dimer interface.

MATERIALS AND METHODS

Cloning, Expression, and Purification of GCAP5.

Recombinant myristoylated GCAP5 (hereafter termed GCAP5) was used throughout this study, and bacterial expression of myristoylated GCAP5 was accomplished by coexpressing the GCAP5 D3N mutant[24] and yeast *N*-myristoyl CoA transferase (NMT) in *Escherichia coli* strain BL21(DE3) as described previously[24] for GCAP1.[12] Acylation of the GCAP5 D3N mutant was originally confirmed in living cells by a click-chemistry approach.[24]

Cloning of all mutants used in this study was similar to that described for other point mutants of GCAPs.[25,26] Purification of GCAP5 (and mutants) was achieved using previously described methods.[21] The GCAP5 variants used in guanylate cyclase assays were purified by employing a HiTrap Q HP column (5 mL, Cytiva) in the anion exchange chromatography step (application of a gradient from 0 to 1 M NaCl in 20 column volumes).

Analytical Size Exclusion Chromatography (SEC).

The molar mass of GCAP5 in the presence of Mg^{2+} (5 mM) was measured using analytical SEC (Superdex 200 HR 10/30 column, GE Healthcare) as described previously.[21] A sample volume of 100 μL of GCAP5 (200 μM protein concentration) was applied to the column equilibrated with 30 mM MES (pH 6.6), 5 mM citrate, and 100 mM NaCl. The SEC measurements were taken at 4 °C with a flow rate of 0.5 mL/min.

NMR Spectroscopy.

GCAP5 samples for NMR experiments consisted of ^{15}N-labeled or doubly ^{15}N- and ^{13}C-labeled myristoylated and Ca^{2+}-free, Mg^{2+}-bound GCAP5 (0.50 mM) dissolved in 30 mM MES (pH 6.5) buffer containing 2 mM DTT-d_{10}, 5 mM $MgCl_2$, and 93:7 H_2O/D_2O. All NMR experiments were performed at 30 °C on a Bruker 800 MHz Avance III spectrometer equipped with a triple resonance cryogenic TCI probe and pulsed field gradients. Two-dimensional ^{15}N–^{1}H HSQC and IPAP-HSQC experiments were performed with 2048 (^{1}H) × 256 (^{15}N) data points using ^{15}N-labeled GCAP5. Three-dimensional NMR HSQC-NOESY and HCCH-TOCSY experiments were performed and analyzed as described previously.[12] Spectra were processed using NMRPipe software package[27] and analyzed using SPARKY.[28]

Residual dipolar couplings (RDCs[29]) of GCAP5 were determined as described previously.[30] Briefly, the filamentous bacteriophage Pf1 (Asla Biotech Ltd., Riga, Latvia) was used as an orienting medium. Pf1 (12 mg/mL) was added to ^{15}N-labeled GCAP5 (0.5 mM) to produce weak alignment. ^{1}H–^{15}N residual dipolar coupling constants (D_{NH}) were measured using a 2D IPAP (inphase/antiphase) ^{1}H–^{15}N HSQC.[31] The backbone N–H RDCs were calculated by measuring the difference in ^{15}N splitting for each amide resonance in the presence and absence of the orienting medium. The RDC *Q*-factor and analysis of RDC data were calculated by PALES.[32]

NMR Structure Calculation.

NMR-derived structures of GCAP5 were calculated using restrained molecular dynamics simulations within Xplor-NIH.[33] Residual dipolar couplings, NOE distances, dihedral angles from TALOS+,[34] and backbone hydrogen bonds were used as structural restraints. NOEs were obtained via ^{15}N-edited NOESY-HSQC and ^{13}C-edited NOESY-HSQC experiments. Backbone dihedral angles were calculated by TALOS+ using backbone chemical shifts (Hα, Cα, Cβ, CO, ^{15}N, and HN) as input. The Xplor-NIH structure calculation was performed as described previously for GCAP1.[12] From a total of 200 structures, the 10 lowest-energy structures were deposited in the RCSB Protein Data Bank (PDB entry 7M2M). The structure quality was assessed by PROCHECK-NMR[35] and MolProbity.[36]

Spin Labeling and DEER Sample Preparation.

Protein samples were dialyzed against 4 L of dialysis buffer in 20 mM Tris (pH 7.4) with 100 μM TCEP overnight at 4 °C and diluted to 10–20 μM. The (1-oxyl 2,2,5,5-tetramethyl Δ3-pyrroline-3-methyl) methanethiosulfonate spin-label (MTSSL, Toronto Research Chemicals Inc., Toronto, ON) was dissolved in dimethyl sulfoxide (DMSO) to a concentration of 40 mM. Excess MTSSL was added to the protein at a 30:1 molar ratio and then reacted on ice for 30 min. Unreacted spin-labels were removed by dialyzing overnight at 4 °C against 4 L of dialysis buffer containing 20 mM Tris (pH 7.4), which was repeated twice for >24 h. The protein was concentrated to a final concentration of ~300 μM by ultrafiltration using an Amicon spin concentrator. The final protein sample for DEER experiments was exchanged three times with 10 mM Tris-d_{11} (pH 7.4), 2 mM $MgCl_2$, and 99.9% D_2O. Before the sample was frozen, 25% glycerol-d_8 was added to the protein as a cryoprotectant.

EPR-DEER Measurements.

Four-pulse DEER data were collected on a Bruker ELEXSYS E580 spectrometer, capable of operation at both X-band and Q-band frequencies, equipped with an AWG bridge and a Q-band QT2 resonator. The pump pulse was fixed to the center peak in the field-swept nitroxide spectrum, and the probe frequency was set to be 100 MHz from this frequency. $\pi/2$ and π pulses were all 34 ns Gaussian pulses.[37] The delay between the first and second probe pulses was 400 ns, and dipolar evolution data were collected out to 1.5–8.0 μs. Experiments were performed at 50 K and were signal averaged for 4–16 h. The raw data were background-corrected and analyzed by Tikhonov regularization using DEERAnalysis.[38] CW-EPR spectra of the DEER samples were recorded at room temperature with a Bruker E500 CW-EPR spectrometer operating at the X-band frequency (~9.4 GHz) using an ER 4122SHQE resonator (Bruker).

Molecular Docking Calculation.

The web-based docking program HADDOCK[39] was used to generate a structural model of Mg^{2+}-bound GCAP5. The NMR structure of Mg^{2+}-bound GCAP5 was docked with itself to satisfy the intermolecular distance restraints measured by DEER. The docking calculation was initiated with a rigid body energy minimization that generated 1000 structures. The best 200 structures were subjected to a semiflexible simulated annealing step. In the final step, the 200 structures obtained from the previous simulated annealing step were refined in explicit waters. At the end of the HADDOCK dimer calculation, 10 structures formed a single cluster out of 200 water-refined structures. The coordinate file with the lowest HADDOCK score was chosen for the final structural model displayed in this study.

Guanylate Cyclase Assays.

To test the regulatory properties of wild type GCAP5 and it variants (mutants without C defined as 5A, H18A/Y21A, H18E/Y21E, R22A, R22D, M25E, N56C, N139C, and S159C), we reconstituted purified GCAP5 forms with cell membranes containing heterologously expressed human GC-E (orthologue of bovine and mice RetGC1) in HEK flip 293 cells essentially as described previously,[40,41] but using a cell line that stably expressed GC-E.

Cells were cultivated and harvested by centrifugation (300*g* for 5 min); the supernatant was discarded, and the pellet was resuspended in 100 μL of 50 mM HEPES-KOH (pH 7.4), 50 mM KCl, 20 mM NaCl, 1 mM DTT, and mammalian protease inhibitor cocktail (1:500). Cells were placed on ice for 20 min, disrupted by being passed several times through a syringe, and placed on ice again. Activities were measured according to a detailed protocol that was published previously[26,40] with the following modifications: GCAP5 was added at a final concentration of 3 μM, and GC activities were obtained by adjusting the free Ca^{2+} concentration using a K_2H_2EGTA/CaH_2EGTA buffer system as described previously.[26] The free Mg^{2+} concentration was 1 mM.

Light Scattering Experiments.

The molar mass of GCAP5 and mutants was assessed by using a multiangle light scattering (MALS) miniDawn instrument with a 690 nm laser (Wyatt Technologies, Inc.) coupled to a refractive index instrument (Optilab Rex, Wyatt Technologies, Inc.). The molar mass of chromatographed protein was calculated from the observed light scattering intensity and differential refractive index using ASTRA software (Wyatt Technologies, Inc.) based on a Zimm plot analysis using a refractive index increment ($dn/dc = 0.185$ L g^{-1}).[42,43]

RESULTS

NMR-Derived Structures of Mg^{2+}-Bound GCAP5.

NMR chemical shift assignments published previously for Mg^{2+}-bound GCAP5[44] were used in this study to determine NOESY-based distances, NMR-derived dihedral angle restraints, and residual dipolar coupling (RDC) restraints (Figure 2) that served as input for restrained molecular dynamics structure calculations (see Materials and Methods). The residual dipolar coupling magnitude and rhombicity were calculated by fitting the measured residual dipolar couplings to the calculated structure using the PALES program.[32] The RDC-refined structures have a quality *Q*-factor of 0.27 and an *R*-factor of 0.985 (Figure 2C). The NMR-derived structure of Mg^{2+}-bound GCAP5 (PDB entry 7M2M) was validated with PROCHECK: 90% of residues belonged to the most favorable region in the Ramachandran plot.

The NMR structures of Mg^{2+}-bound GCAP5 have a backbone RMSD of 1.0 Å (overlaid in Figure 3A), and structural statistics are listed in Table 1. The GCAP5 main chain structure (Figure 3B) contains a total of 11 α-helices and four β-strands: α1 (residues 8–15), α2 (19–27), α3 (35–41), α4 (50–62), α5 (72–82), α6 (88–97), α7 (108–121), α8 (130–140), α9 (151–160), α10 (162–172), α11 (175–182), β1 (32–34), β2 (69–71), β3 (105–107), and β4 (148–150). The secondary structure of the final NMR structure of Mg^{2+}-bound GCAP5 (Figure 3B) is slightly different from the secondary structure inferred from the chemical shift index.[44] In particular, the C-terminal helix (α11) defined by NOESY and RDC data was predicted to be a random coil based on chemical shift analysis.[44] The secondary structure elements of GCAP5 combine to form two separate domains: The N-terminal domain is formed by the N-terminal helix (α1), EF1 (green, residues 19–41), and EF2 (red, residues 50–82), and the C-terminal domain is formed by EF3 (cyan, residues 88–121), EF4 (yellow, residues 130–160), and C-terminal helices (α10 and α11 in Figure 3B). The

N-terminal helix (α1) of GCAP5 is extended by two residues compared to that of GCAP1 (Figure 1). This extension of α1 in GCAP5 causes the sulfhydryl side chains of Cys15 and Cys17 to become more solvent exposed compared to what they are in GCAP1, which may facilitate the binding of Fe^{2+} to GCAP5 (Figure 3C). The helix immediately adjacent to EF4 (α10, colored purple in Figure 3C) is one turn longer in Mg^{2+}-bound GCAP5 than in Ca^{2+}-bound GCAP1. Thus, α10 in GCAP5 is structurally identical to the Ca^{2+} switch helix reported for Ca^{2+}-free GCAP1.[12] The C-terminal helix (α11) is one-half turn shorter in Mg^{2+}-bound GCAP5 than in Ca^{2+}-bound GCAP1 (Figure 1). The Ca^{2+}-dependent structural differences in both α10 and α11 are consistent with a Ca^{2+}-myristoyl tug mechanism[45] seen previously for GCAP1.[12]

The NMR structure of GCAP5 contains Mg^{2+} bound at EF2 (orange sphere in Figure 3) as evidenced by characteristic Mg^{2+}-dependent amide chemical shift changes assigned to Gly68 in EF2.[44] Also, Mg^{2+}-induced NMR spectral changes for GCAP5 (Figure S1) further demonstrate binding of Mg^{2+} to GCAP5. The geometry of chelating amino acid residues in GCAP5 and the bound Mg^{2+} was not observed directly in our NMR study. Instead, the stereochemical geometry and chelation of Mg^{2+} bound at EF2 were modeled with structural constraints derived from the X-ray crystal structure of Mg^{2+}-bound CaM,[46] which closely resembles the Mg^{2+} binding site geometry conserved in other EF-hand proteins such as CaBP1[47] and CaBP4.[48] GCAP5 residues at positions 1, 3, and 5 of the EF-hand loop in EF2 were selected to chelate the bound Mg^{2+} (see D63, D65, and D67 in Figure 3A). Mutation of the corresponding residues in GCAP1 significantly weakens Mg^{2+} binding and prevents cyclase activation.[10] The four EF-hands of GCAP5 with one Mg^{2+} bound at EF2 (and no metal bound at EF1, EF3, or EF4) each adopt interhelical angles that are similar to those observed in the crystal structure of Ca^{2+}-bound GCAP1. The overall main chain structure of Mg^{2+}-bound GCAP5 is somewhat similar to that of the Ca^{2+}-bound GCAP1 crystal structure [RMSD = 2.4 Å (Figure 3D)]. For the Mg^{2+}-bound GCAP5 structure, the interhelical angles are 131° (EF1), 114° (EF2), 104° (EF3), and 107° (EF4). Thus, the three functional EF-hands in GCAP5 (EF2–EF4) each adopt a preformed open conformation in the Ca^{2+}-free state akin to that of calbindin D_{9k}[49] and other Ca^{2+} buffer proteins,[50] which may explain the very high nanomolar Ca^{2+} binding affinity for GCAP proteins.[51]

Intermolecular Distances of the GCAP5 Dimer Determined by EPR-DEER.

Previous studies demonstrated that GCAP5 forms a dimer in solution.[21] In the current study, we used EPR-DEER to measure intermolecular distances that were used as restraints to calculate a structural model of the GCAP5 dimer. The DEER data for GCAP5 (Figure 4) were analyzed to determine intermolecular distances between individual nitroxide spin-labels covalently attached to particular Cys residues on the protein surface (C15, C17, T26C, C28, N56C, C69, C105, N139C, E152C, and S159C). Wild type GCAP5 contains five native Cys residues (C15, C17, C28, C69, and C105), and single-Cys mutants were generated in each case by replacing the other four Cys residues with Ala. In addition, we introduced a non-native Cys at particular residues (T26C, N56C, N139C, E152C, and S159C) in a Cys-less background mutant of GCAP5 ($GCAP5^{CL}$) in which all five native Cys residues were replaced with Ala. A total of 10 single Cys mutants of GCAP5 were constructed for EPR-DEER: $GCAP5^{CL}$(A15C), $GCAP5^{CL}$(A17C), $GCAP5^{CL}$(T26C), $GCAP5^{CL}$(A28C),

GCAP5^{CL}(N56C), GCAP5^{CL}(A69C), GCAP5^{CL}(A105C), GCAP5^{CL}(N139C), GCAP5^{CL}(E152C), and GCAP5^{CL}(S159C).

Representative EPR-DEER data for GCAP5 with a nitroxide spin-label attached individually to each single-Cys mutant [G C A P 5$^{C L}$ (A 2 8 C), G C A P 5$^{C L}$ (N 5 6 C), and GCAP5^{CL}(A69C)] are shown in Figure 4 (Figure S2 shows DEER data for all 10 mutants). The DEER data in each case were modeled by a distance distribution with most probable intermolecular distances of 16 ± 4, 52 ± 5, and 43 ± 5 Å for GCAP1^{CL}(A28C), GCAP5^{CL}(N56C), and GCAP5^{CL}(A69C), respectively (Figure 4). The intermolecular DEER distances for all single Cys mutants of GCAP5 are listed in Table 2 and Figure S2.

Structural Model of a GCAP5 Dimer.

The intermolecular DEER distances for each spin-label attached to GCAP5 (Figure 5A and Table 2) were used as distance restraints within HADDOCK[52] to calculate the structure of the GCAP5 dimer as described in Materials and Methods. The measured DEER distances (Table 2) for the most part agree within experimental error with the calculated intermolecular distances in the GCAP5 dimer model (Figure 5A). The apparent deviation between the calculated versus observed distances for C15 and C17 (important for Fe^{2+} binding[21]) might reflect the dynamic disorder for these residues in the absence of Fe^{2+}. Much smaller distance deviations were observed for N56C, C69, N139C, and E152C because these residues are located in regions of regular secondary structure that are more rigidly held in place. The structure of the GCAP5 dimer (Figure 5A) contains intermolecular contacts between mostly hydrophobic residues (H18, Y21, M25, F72, V76, and W93) at the dimer interface. The closest contacts are formed between the hydrophobic side chain atoms of H18, M25, F72, V76, and W93 (colored red in Figure 5A). The intermolecular contacts with V76 are consistent with the previous observation that a V77E mutation abolished dimerization of GCAP1.[12] The aromatic side chain atoms of H18, Y21 (not shown), F72, and W93 make intermolecular contacts with each other at the dimer interface (Figure 5B). The GCAP5 dimer is also stabilized by an intermolecular salt bridge between the side chain atoms of R22 and D71 (Figure 5C). The GCAP5 dimer (Figure 5A) is structurally similar to the dimeric structural model reported recently for GCAP1.[53]

Mutant Lacking All Five Cys and DEER Mutants of GCAP5 Are Functionally Intact.

To verify whether the GCAP5 5A mutant (lacking all five Cys residues) and single-Cys mutants (N56C, N139C, and S159C) used in the DEER experiments are functionally intact, we measured the retinal guanylate cyclase activity in the presence of wild type GCAP5 and each mutant (Figure 6) in the presence and absence of Ca^{2+}. The data set includes two positive controls and one negative control. Incubation of cyclase activity with WT GCAP5 showed the activating property of GCAP5 and reproduced previous observations that WT GCAP5 lacks the Ca^{2+} dependence, which is typical for other GCAP isoforms.[21] The second positive control was the activity profile obtained with the 5A mutant that showed a canonical Ca^{2+} dependence of GC activation in which the cyclase activity at low Ca^{2+} activity levels was similar to that of WT GCAP5 but much lower at high Ca^{2+} concentrations. These results agree with our previous data showing that the presence of

Cys at positions 15 and 17 seems to interfere with the Ca^{2+} switch.[21] The negative control was the GC activity without addition of a GCAP variant (control in Figure 6), resulting in >10-fold lower basal GC activities. Activities of all other mutants were above the control level, showing that they were functionally intact. The guanylate cyclase activities in the presence of the Cys-less GCAP5 mutant (5A in Figure 6) and each of the DEER mutants (N56C, N139C, and S159C) are each qualitatively similar to that of wild type GCAP5 at low Ca^{2+} concentrations, demonstrating that these mutants are each capable of activating the cyclase and appear to be functionally intact. Furthermore, when the negatively charged amino acid in the H/Y-E and R22D mutants was replaced with Ala, activities increased, in the case of R22A to >5-fold higher than that of WT and 5A. Surprisingly, although the Ca^{2+} switch is operational in R22A, the Ca^{2+}-bound R22A activates the cyclase to a higher degree than the Ca^{2+}-bound wild type GCAP5 (see GC activation at high Ca^{2+} concentrations).

Mutations at the GCAP5 Dimer Interface.

The key amino acids that form intermolecular contacts at the GCAP5 interface (H18, Y21, R22, M25, D71, F72, V76, and W93) were mutated to form the following mutants: H18A/Y21A, H18E/Y21E, R22A, R22D, M25E, D71A, D71R, F72A, F72E, V76A, V76E, and W93E. The corresponding residues in GCAP1 are conserved (Figure 1), and the same mutations in GCAP1 (Y22E, M26E, F73E, V77E, and W94E) were shown previously to both weaken dimerization and abolish activation of the cyclase,[53] consistent with the idea that GCAP1 dimerization is necessary for cyclase activation. A similar result was seen for GCAP5. The GCAP5 dimerization site mutants (H18A/Y21A, H18E/Y21E, R22D, and M25E) each exhibited a >4-fold reduction in the level of activation of cyclase activity compared to that of the wild type (Figure 6). The GCAP5 dimerization site mutants (D71A, D71R, F72A, F72E, V76A, V76E, and W93E) were each expressed in the insoluble fraction of the bacterial lysate (called inclusion bodies), which prevented their characterization. The low solubility here suggests that these mutations may destabilize dimerization of GCAP5 that in turn could cause protein unfolding, which may explain the precipitation of the mutated proteins. A double mutant (H18E/Y21E and H81A/Y21A) and single mutants (R22A, R22D, and M25E) are somewhat more soluble, although a detectable fraction of each mutant could also be detected in inclusion bodies, in contrast to wild type GCAP5 that is not detected in inclusion bodies. The most soluble mutant (M25E) exhibited an NMR HSQC spectrum that was overall similar to that of the wild type (Figure 7A). However, a number of resonances assigned to residues near the dimer interface (H18, Y21, D71, and W93) and resonances near the center of the spectrum appear much broader in the M25E spectrum (Figure 7A, red). The observed peak broadening for the M25E mutant could be caused by chemical exchange broadening mechanisms associated with lower-affinity dimerization for M25E compared to wild type. The double mutants (H18E/Y21E and H18A/Y21A) each exhibited a highly heterogeneous NMR spectrum (Figure 7B for H18E/Y21E and Figure S3A for H18A/Y21A) in which at least four different amide peaks were assigned to G68 (circled in Figure 7B). This heterogeneity suggests a complex mixture of perhaps monomer, dimer, and higher-order oligomers, as evidenced by many broadened resonances in the center of the spectrum. A fraction of the H18E/Y21E mixture was isolated as a monomeric species (see chromatography elution profiles in panels C and D of Figure 7) with a molar mass of 24 ± 2 kDa determined by SEC-MALS for H18E/Y21E (Figure 7E)

and for H18A/Y21A (Figure S3B), in contrast to wild type GCAP5 that is mostly a dimer under the same conditions.[21] A similar monomeric fraction was isolated for R22D (see chromatography profiles in panels F and G of Figure 7) with a molar mass of 29 ± 4 kDa determined by SEC-MALS (Figures 7H). The same molar mass was determined for R22A (Figure S3C). Thus, the R22A, R22D, M25E, H18A/Y21A, and H18E/Y21E mutations each appear to weaken the dimerization of GCAP5 as predicted by the structure.

The protein folding melting temperature (T_m) was measured for the soluble GCAP5 dimerization site mutants (H18E/Y21E, R22D, and M25E) to probe the effect of these mutations on the protein folding stability (Figure S4). The T_m values of wild type GCAP5 and mutant proteins were determined by measuring NMR HSQC spectra at different temperatures. The NMR intensity of the downfield-shifted amide resonance assigned to Gly68 (characteristic of the folded protein, called I_{Gly68}) was monitored as a function of temperature. For wild type GCAP5, I_{Gly68} began to decrease as the temperature was increased above 47 °C and a T_m value (temperature at which I_{Gly68} decreased by 2-fold) was estimated to be 52 ± 1 °C. The T_m values for the H18E/Y21E, R22D, and M25E mutants were measured to be 48 ± 1, 49 ± 1, and 49 ± 1 °C, respectively. The lower T_m values for the dimerization site mutants compared to that of the wild type suggest that the intermolecular contacts at the dimer interface contribute to the overall protein folding stability.

DISCUSSION

In this study, we present the NMR structure of Mg^{2+}-bound GCAP5 (Figure 3) and EPR-DEER analysis (Figure 4) of the dimeric GCAP5 structure (Figure 5). The NMR structure of the Mg^{2+}-bound activator form of GCAP5 looks similar to that of the crystal structure of GCAP1 (Figure 3D, and RMSD = 2.4 Å).[9] However, an important structural difference is that the N-terminal helix in GCAP5 is elongated by two residues, which allows the nonconserved sulfhydryl side chain of Cys15 and Cys17 to both point outward and chelate Fe^{2+} that can bind to GCAP5 (Figure 3C). The solvent-exposed side chains of Cys15 and Cys17 are consistent with previous studies that report high-affinity binding of Fe^{2+} to GCAP5.[21] The 10th helix (α10) of GCAP5 (colored purple in Figure 3) is elongated by three residues compared to the corresponding helix in Ca^{2+}-bound GCAP1 (Figure 1). The Ca^{2+}-induced shortening of α10 may explain how binding of Ca^{2+} to EF4 (directly connected to α10) is allosterically transmitted to the N-terminal myristoyl group and surrounding residues in GCAP1 (Y22, R23, M26, F73, and V77) that are responsible for activating guanylate cyclase.[54] This is consistent with the Ca^{2+}-myristoyl tug model[12,45] in which the binding of Ca^{2+} to the fourth EF-hand of GCAP1 (EF4) causes Ca^{2+}-induced conformational changes that "tug" on the downstream C-terminal helix that contacts the N-terminal myristoyl group, which alter the exposure of residues that are believed to interact with RetGC. Binding of Mg^{2+} to GCAP1 does not initiate the tug mechanism, because Mg^{2+} binds only to the second EF-hand and does not bind to EF4. The Ca^{2+}-myristoyl tug mechanism explains how GCAP1 activates guanylate cyclase and appears to operate in GCAP5, as well.

The structure of the GCAP5 dimer (Figure 5) was determined by docking two molecules of the NMR structure of GCAP5 (Figure 3) according to intermolecular distance restraints

determined by EPR-DEER (Figure 4 and Table 2). The GCAP5 dimer structure looks somewhat similar to the structure of the GCAP1 dimer (RMSD = 2.4 Å).[53] The dimer interface in both GCAP1 and GCAP5 consists of the same exposed hydrophobic residues (H18, Y21, M25, F72, V76, and W93) colored red in Figure 5A. Mutations at the GCAP5 dimerization site (H18E/Y21E, H18A/Y21A, R22D, and M25E) disrupt dimerization of GCAP5 (Figure 7) and decrease the level of cyclase activation by >4-fold (Figure 6). Interestingly, the point mutation p.H19Y in human GCAP1 that is located in the dimer interface was identified in patients diagnosed with retinitis pigmentosa. Investigation of the molecular properties of the H19Y GCAP1 mutant protein revealed a disruption of Ca^{2+} binding, guanylate cyclase regulation, and dimer formation,[55] which points to the importance of a dynamic monomer–dimer equilibrium for the function of human GCAP1, as well.[56] However, the exposed hydrophobic residues at the GCAP5 dimerization site have also been suggested to mediate contacts with RetGC.[54] It is possible that the exposed dimerization site in GCAP5 might prefer to interact with RetGC rather than promote GCAP5 dimerization in the presence of a saturating level of RetGC. This scenario is consistent with the R22A mutant, which causes a 5-fold increase in the level of cyclase activation (Figure 6) even though GCAP5 dimerization is weakened by R22A (Figure S3C). Future studies are needed to determine whether the GCAP5 dimer structure will remain intact upon binding to RetGC and how it might stabilize the transition state of the cyclase reaction.

An important structural difference between GCAP1 and GCAP5 is that the GCAP5 dimer is stabilized by an intermolecular salt bridge between R22 and D71 (Figure 5C) that is not seen in the GCAP1 dimer structure, perhaps because R22 in GCAP5 is replaced with a lysine in GCAP1 (Figure 1). Slight differences in the quaternary structures of dimeric GCAP1 and GCAP5 may explain the 3 Å increase in the intermolecular distance between K22 and D71 in GCAP1[53] compared to the much shorter salt bridge distance in GCAP5 (Figure 5C). We suggest that this difference in quaternary structure for GCAP1 and GCAP5 might explain why GCAP1 is 3-fold more potent at activating guanylate cyclase.[21]

The structure of the Ca^{2+}-free, Fe^{2+}-free, Mg^{2+}-bound GCAP5 dimer (Figure 5) is quite different from a structural model of the Fe^{2+}-bound GCAP5 dimer proposed previously.[21] In the Fe^{2+}-bound GCAP5 dimer, a single Fe^{2+} is chelated by the sulfhydryl side chains of Cys15 and Cys17 from each subunit of the GCAP5 dimer so that the intermolecular distance of the sulfhydryl atoms for Cys15 is <8 Å (see the double arrow in Figure 8). By stark contrast, in the Fe^{2+}-free GCAP5 dimer, the intermolecular distance of the nitroxide spin-label attached to Cys15 is 24 Å. The much larger intermolecular distance for Cys15 in the Fe^{2+}-free GCAP5 dimer (Figure 5 and Table 2) suggests that binding of Fe^{2+} to the GCAP5 dimer may cause the two protein subunits within the dimer to rotate with respect to one another as illustrated in Figure 8. This Fe^{2+}-induced rotation of the two protein subunits in the GCAP5 dimer dramatically alters the exposure of residues (H18, Y21, M25, F73, V76, and W93 highlighted by red ovals in Figure 8) that have been implicated in binding to guanylate cyclase.[54,55] We propose that the Fe^{2+}-dependent exposure of the cyclase binding site residues may explain how binding of Fe^{2+} to GCAP5 prevents its activation of guanylate cyclase. Future studies are needed to determine the atomic resolution structures of Fe^{2+}-bound GCAP5 and GCAP5 bound to guanylate cyclase to further test our model.

Supplementary Material

Refer to Web version on PubMed Central for supplementary material.

ACKNOWLEDGMENTS

The authors thank Jeff Walton and Ping Yu for help with NMR experiments.

Funding

This work was supported by National Institutes of Health (NIH) Grant R01-EY012347 to J.B.A., NIH Grants R35-GM131781 and S10-OD024980 to G.M., and Deutsche Forschungsgemeinschaft Grants KO948/15-1 and GRK1885 to K.-W.K. and to the Research Training Group in Oldenburg.

ABBREVIATIONS

DEER	double electron electron resonance
HSQC	heteronuclear single quantum coherence
MALS	multiangle light scattering
NMR	nuclear magnetic resonance
NOESY	NOE spectroscopy
RetGC	retinal guanylate cyclase
SEC	size exclusion chromatography

REFERENCES

(1). Palczewski K; Subbaraya I; Gorczyca WA; Helekar BS; Ruiz CC; Ohguro H; Huang J; Zhao X; Crabb JW; Johnson RS; et al. Molecular cloning and characterization of retinal photoreceptor guanylyl cyclase-activating protein. Neuron 1994, 13, 395–404. [PubMed: 7520254]

(2). Dizhoor AM; Olshevskaya EV; Henzel WJ; Wong SC; Stults JT; Ankoudinova I; Hurley JB Cloning, sequencing and expression of a 24-kDa Ca^{2+}-binding protein activating photoreceptor guanylyl cyclase. J. Biol. Chem 1995, 270, 25200–25206. [PubMed: 7559656]

(3). Palczewski K; Polans AS; Baehr W; Ames JB Ca(2+)-binding proteins in the retina: structure, function, and the etiology of human visual diseases. BioEssays 2000, 22, 337–350. [PubMed: 10723031]

(4). Dizhoor AM; Lowe DG; Olsevskaya EV; Laura RP; Hurley JB The human photoreceptor membrane guanylyl cyclase, RetGC, is present in outer segments and is regulated by calcium and a soluble activator. Neuron 1994, 12, 1345–1352. [PubMed: 7912093]

(5). Lowe DG; Dizhoor AM; Liu K; Gu Q; Spencer M; Laura R; Lu L; Hurley JB Cloning and expression of a second photoreceptor-specific membrane retina guanylyl cyclase (RetGC), RetGC-2. Proc. Natl. Acad. Sci. U. S. A 1995, 92, 5535–5539. [PubMed: 7777544]

(6). Koch KW; Duda T; Sharma RK Photoreceptor specific guanylate cyclases in vertebrate phototransduction. Mol. Cell. Biochem 2002, 230, 97–106. [PubMed: 11952100]

(7). Koch KW; Stryer L Highly cooperative feedback control of retinal rod guanylate cyclase by calcium ions. Nature 1988, 334, 64–66. [PubMed: 2455233]

(8). Ames JB; Dizhoor AM; Ikura M; Palczewski K; Stryer L Three-dimensional structure of guanylyl cyclase activating protein-2, a calcium-sensitive modulator of photoreceptor guanylyl cyclases. J. Biol. Chem 1999, 274, 19329–19337. [PubMed: 10383444]

(9). Stephen R; Bereta G; Golczak M; Palczewski K; Sousa MC Stabilizing function for myristoyl group revealed by the crystal structure of a neuronal calcium sensor, guanylate cyclase-activating protein 1. Structure 2007, 15, 1392–1402. [PubMed: 17997965]

(10). Peshenko IV; Dizhoor AM Ca2+ and Mg2+ binding properties of GCAP-1. Evidence that Mg2+-bound form is the physiological activator of photoreceptor guanylyl cyclase. J. Biol. Chem 2006, 281, 23830–23841. [PubMed: 16793776]

(11). Peshenko IV; Dizhoor AM Activation and inhibition of photoreceptor guanylyl cyclase by guanylyl cyclase activating protein 1 (GCAP-1): the functional role of Mg2+/Ca2+ exchange in EF-hand domains. J. Biol. Chem 2007, 282, 21645–21652. [PubMed: 17545152]

(12). Lim S; Peshenko IV; Olshevskaya EV; Dizhoor AM; Ames JB Structure of Guanylyl Cyclase Activator Protein 1 (GCAP1) Mutant V77E in a Ca2+-free/Mg2+-bound Activator State. J. Biol. Chem 2016, 291, 4429–4441. [PubMed: 26703466]

(13). Behnen P; Dell' Orco D; Koch KW Involvement of the calcium sensor GCAP1 in hereditary cone dystrophies. Biol. Chem 2010, 391, 631–637. [PubMed: 20370318]

(14). Dell'Orco D; Behnen P; Linse S; Koch KW Calcium binding, structural stability and guanylate cyclase activation in GCAP1 variants associated with human cone dystrophy. Cell. Mol. Life Sci 2010, 67, 973–984. [PubMed: 20213926]

(15). Payne AM; Downes SM; Bessant DA; Taylor R; Holder GE; Warren MJ; Bird AC; Bhattacharya SS A mutation in guanylate cyclase activator 1A (GUCA1A) in an autosomal dominant cone dystrophy pedigree mapping to a new locus on chromosome 6p21.1. Hum. Mol. Genet 1998, 7, 273–277. [PubMed: 9425234]

(16). Sokal I; Li N; Surgucheva I; Warren MJ; Payne AM; Bhattacharya SS; Baehr W; Palczewski K GCAP1 (Y99C) mutant is constitutively active in autosomal dominant cone dystrophy. Mol. Cell 1998, 2, 129–133. [PubMed: 9702199]

(17). Wilkie SE; Li Y; Deery EC; Newbold RJ; Garibaldi D; Bateman JB; Zhang H; Lin W; Zack DJ; Bhattacharya SS; Warren MJ; Hunt DM; Zhang K Identification and functional consequences of a new mutation (E155G) in the gene for GCAP1 that causes autosomal dominant cone dystrophy. Am. J. Hum. Genet 2001, 69, 471–480. [PubMed: 11484154]

(18). Imanishi Y; Yang L; Sokal I; Filipek S; Palczewski K; Baehr W Diversity of guanylate cyclase-activating proteins (GCAPs) in teleost fish: characterization of three novel GCAPs (GCAP4, GCAP5, GCAP7) from zebrafish (Danio rerio) and prediction of eight GCAPs (GCAP1–8) in pufferfish (Fugu rubripes). J. Mol. Evol 2004, 59, 204–217. [PubMed: 15486694]

(19). Fries R; Scholten A; Saftel W; Koch KW Zebrafish guanylate cyclase type 3 signaling in cone photoreceptors. PLoS One 2013, 8, e69656. [PubMed: 23940527]

(20). Ratscho N; Scholten A; Koch KW Expression profiles of three novel sensory guanylate cyclases and guanylate cyclase-activating proteins in the zebrafish retina. Biochim. Biophys. Acta, Mol. Cell Res 2009, 1793, 1110–1114.

(21). Lim S; Scholten A; Manchala G; Cudia D; Zlomke-Sell SK; Koch KW; Ames JB Structural Characterization of Ferrous Ion Binding to Retinal Guanylate Cyclase Activator Protein 5 from Zebrafish Photoreceptors. Biochemistry 2017, 56, 6652–6661. [PubMed: 29172459]

(22). Crack JC; Green J; Thomson AJ; Le Brun NE Iron-sulfur clusters as biological sensors: the chemistry of reactions with molecular oxygen and nitric oxide. Acc. Chem. Res 2014, 47, 3196–3205. [PubMed: 25262769]

(23). Sterling J; Guttha S; Song Y; Song D; Hadziahmetovic M; Dunaief JL Iron importers Zip8 and Zip14 are expressed in retina and regulated by retinal iron levels. Exp. Eye Res 2017, 155, 15–23. [PubMed: 28057442]

(24). Sulmann S; Vocke F; Scholten A; Koch KW Retina specific GCAPs in zebrafish acquire functional selectivity in Ca2+-sensing by myristoylation and Mg^{2+}-binding. Sci. Rep 2015, 5, 11228. [PubMed: 26061947]

(25). Fries R; Scholten A; Saftel W; Koch KW Operation profile of zebrafish guanylate cyclase-activating protein 3. J. Neurochem 2012, 121, 54–65. [PubMed: 22212098]

(26). Scholten A; Koch KW Differential calcium signaling by cone specific guanylate cyclase-activating proteins from the zebrafish retina. PLoS One 2011, 6, e23117. [PubMed: 21829700]

(27). Delaglio F; Grzesiek S; Vuister GW; Zhu G; Pfeifer J; Bax A NMRPipe: a multidimensional spectral processing system based on UNIX pipes. J. Biomol. NMR 1995, 6, 277–293. [PubMed: 8520220]

(28). Lee W; Tonelli M; Markley JL NMRFAM-SPARKY: enhanced software for biomolecular NMR spectroscopy. Bioinformatics 2015, 31, 1325–1327. [PubMed: 25505092]

(29). Tjandra N; Bax A Direct measurement of disances and angles in biomolecules by NMR in a dilute liquid crystalline medium. Science 1997, 278, 1111–1114. [PubMed: 9353189]

(30). Peshenko IV; Yu Q; Lim S; Cudia D; Dizhoor AM; Ames JB Retinal degeneration 3 (RD3) protein, a retinal guanylyl cyclase regulator, forms a monomeric and elongated four-helix bundle. J. Biol. Chem 2019, 294, 2318–2328. [PubMed: 30559291]

(31). Ottiger M; Delaglio F; Marquardt JL; Tjandra N; Bax A Measurement of dipolar couplings for methylene and methyl sites in weakly oriented macromolecules and their use in structure determination. J. Magn. Reson 1998, 134, 365–369. [PubMed: 9761712]

(32). Zweckstetter M NMR: prediction of molecular alignment from structure using the PALES software. Nat. Protoc 2008, 3, 679–690. [PubMed: 18388951]

(33). Schwieters CD; Kuszewski JJ; Tjandra N; Clore GM The Xplor-NIH NMR molecular structure determination package. J. Magn. Reson 2003, 160, 65–73. [PubMed: 12565051]

(34). Shen Y; Delaglio F; Cornilescu G; Bax A TALOS+: a hybrid method for predicting protein backbone torsion angles from NMR chemical shifts. J. Biomol. NMR 2009, 44, 213–223. [PubMed: 19548092]

(35). Laskowski RA; Rullmann JA; MacArthur MW; Kaptein R; Thornton JM AQUA and PROCHECK-NMR: programs for checking the quality of protein structures solved by NMR. J. Biomol. NMR 1996, 8, 477–486. [PubMed: 9008363]

(36). Chen VB; Arendall WB 3rd; Headd JJ; Keedy DA; Immormino RM; Kapral GJ; Murray LW; Richardson JS; Richardson DC MolProbity: all-atom structure validation for macromolecular crystallography. Acta Crystallogr., Sect. D: Biol. Crystallogr 2010, 66, 12–21. [PubMed: 20057044]

(37). Teucher M; Bordignon E Improved signal fidelity in 4-pulse DEER with Gaussian pulses. J. Magn. Reson 2018, 296, 103–111. [PubMed: 30241017]

(38). Jeschke G; Chechik V; Ionita P; Godt A; Zimmermann H; Banham J; Timmel CR; Hilger D; Jung H DeerAnalysis2006-a comprehensive software package for analyzing pulsed ELDOR data. Appl. Magn. Reson 2006, 30, 473–498.

(39). van Zundert GC; Rodrigues JP; Trellet M; Schmitz C; Kastritis PL; Karaca E; Melquiond AS; van Dijk M; de Vries SJ; Bonvin AM The HADDOCK2.2 Web Server: User-Friendly Integrative Modeling of Biomolecular Complexes. J. Mol. Biol 2016, 428, 720–725. [PubMed: 26410586]

(40). Koch KW; Helten A Guanylate cyclase-based signaling in photoreceptors and retina. In Signal Transduction in the Retina; Taylor and Francis, CRC Press: Boca Raton, FL, 2008; pp 121–143.

(41). Zagel P; Dell'Orco D; Koch KW The dimerization domain in outer segment guanylate cyclase is a Ca(2)(+)-sensitive control switch module. Biochemistry 2013, 52, 5065–5074. [PubMed: 23815670]

(42). Meyer M; Morgenstern B Characterization of gelatine and acid soluble collagen by size exclusion chromatography coupled with multi angle light scattering (SEC-MALS). Biomacromolecules 2003, 4, 1727–1732. [PubMed: 14606902]

(43). Wyatt PJ Combined differential light scattering with various liquid chromatography separation techniques. Biochem. Soc. Trans 1991, 19, 485. [PubMed: 1889645]

(44). Cudia D; Ames J Chemical shift assignments of retinal guanylyl cyclase activating protein 5 (GCAP5). Biomol. NMR Assignments 2019, 13, 201–205.

(45). Peshenko IV; Olshevskaya EV; Lim S; Ames JB; Dizhoor AM Calcium-myristoyl Tug. J. Biol. Chem 2012, 287, 13972–13984. [PubMed: 22383530]

(46). Senguen FT; Grabarek Z X-ray structures of magnesium and manganese complexes with the N-terminal domain of calmodulin: insights into the mechanism and specificity of metal ion binding to an EF-hand. Biochemistry 2012, 51, 6182–6194. [PubMed: 22803592]

(47). Li C; Chan J; Haeseleer F; Mikoshiba K; Palczewski K; Ikura M; Ames JB Structural insights into Ca2+-dependent regulation of inositol 1,4,5-trisphosphate receptors by CaBP1. J. Biol. Chem 2009, 284, 2472–2481. [PubMed: 19008222]

(48). Park S; Li C; Haeseleer F; Palczewski K; Ames JB Structural Insights into Activation of the Retinal L-type Ca2+ Channel (Cav1.4) by Ca2+-binding Protein 4 (CaBP4). J. Biol. Chem 2014, 289, 31262–31273. [PubMed: 25258313]

(49). Skelton NJ; Kordel J; Chazin WJ Determination of the solution structure of Apo calbindin D9k by NMR spectroscopy. J. Mol. Biol 1995, 249, 441–462. [PubMed: 7783203]

(50). Ikura M Calcium binding and conformational response in EF-hand proteins. Trends Biochem. Sci 1996, 21, 14–17. [PubMed: 8848832]

(51). Lim S; Peshenko IV; Dizhoor AM; Ames JB Effects of Ca2+, Mg2+, and myristoylation on guanylyl cyclase activating protein 1 structure and stability. Biochemistry 2009, 48, 850–862. [PubMed: 19143494]

(52). de Vries SJ; van Dijk M; Bonvin AM The HADDOCK web server for data-driven biomolecular docking. Nat. Protoc 2010, 5, 883–897. [PubMed: 20431534]

(53). Lim S; Roseman G; Peshenko I; Manchala G; Cudia D; Dizhoor A; Millhauser G; Ames J Retinal Guanylyl Cyclase Activating Protein 1 Forms a Functional Dimer. PLoS One 2018, 13, e0193947. [PubMed: 29513743]

(54). Peshenko IV; Olshevskaya EV; Lim S; Ames JB; Dizhoor AM Identification of target binding site in photoreceptor guanylyl cyclase-activating protein 1 (GCAP1). J. Biol. Chem 2014, 289, 10140–10154. [PubMed: 24567338]

(55). Abbas S; Marino V; Weisschuh N; Kieninger S; Solaki M; Dell'Orco D; Koch KW Neuronal Calcium Sensor GCAP1 Encoded by GUCA1A Exhibits Heterogeneous Functional Properties in Two Cases of Retinitis Pigmentosa. ACS Chem. Neurosci 2020, 11, 1458–1470. [PubMed: 32298085]

(56). Boni F; Marino V; Bidoia C; Mastrangelo E; Barbiroli A; Dell'Orco D; Milani M Modulation of Guanylate Cyclase Activating Protein 1 (GCAP1) Dimeric Assembly by Ca(2+) or Mg(2+): Hints to Understand Protein Activity. Biomolecules 2020, 10, 1408.

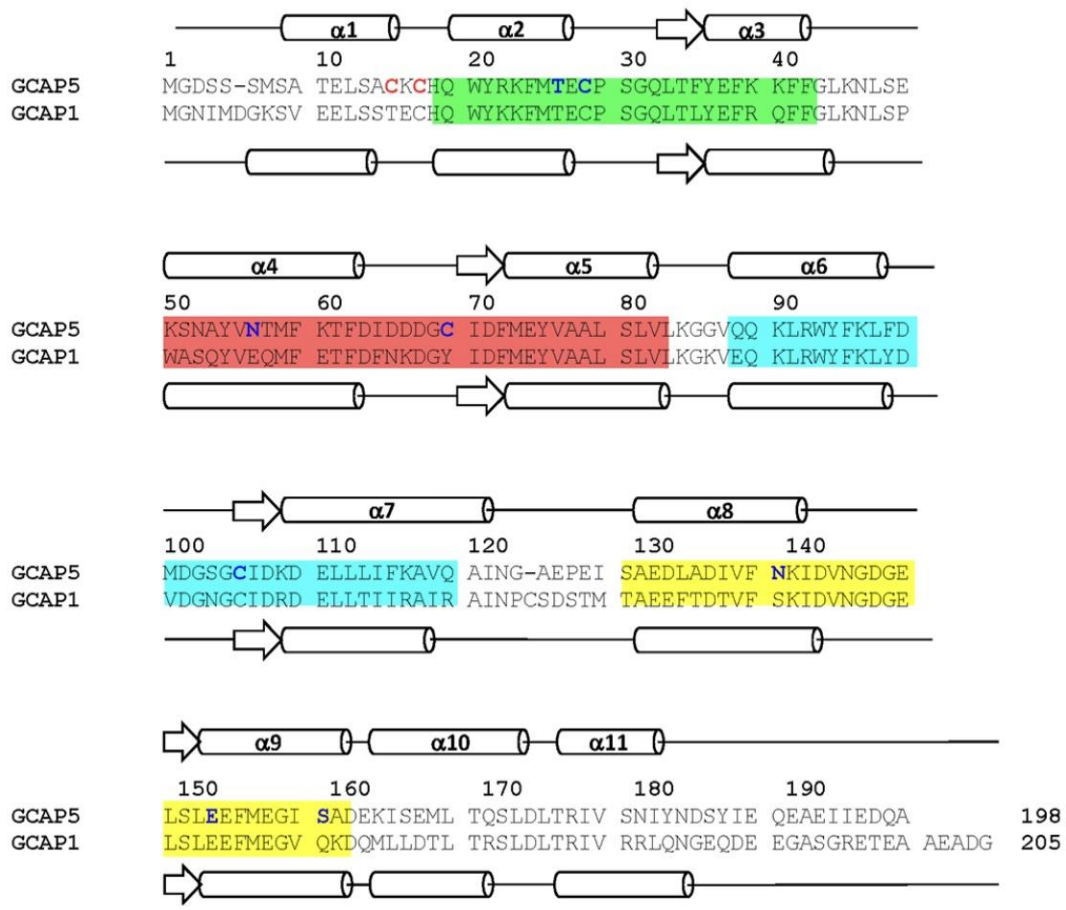

Figure 1.

Amino acid sequence alignment and secondary structure of GCAP1 and GCAP5. EF-hand motifs are shaded in color (green for EF1, red for EF2, cyan for EF3, and yellow for EF4). Nonconserved cysteine residues (C15 and C17) in GCAP5 are highlighted in red. Single cysteine residues (C15, C17, T26C, C28, N56C, C69, C105, N139C, E152C, and S158C) modified by nitroxide for DEER studies are highlighted in blue. α-Helices and β-strands are depicted by cylinders and arrows, respectively. Swiss Protein Database accession numbers are Q90WX4 (bovine GCAP1) and Q5MAC8 (zebrafish GCAP5).

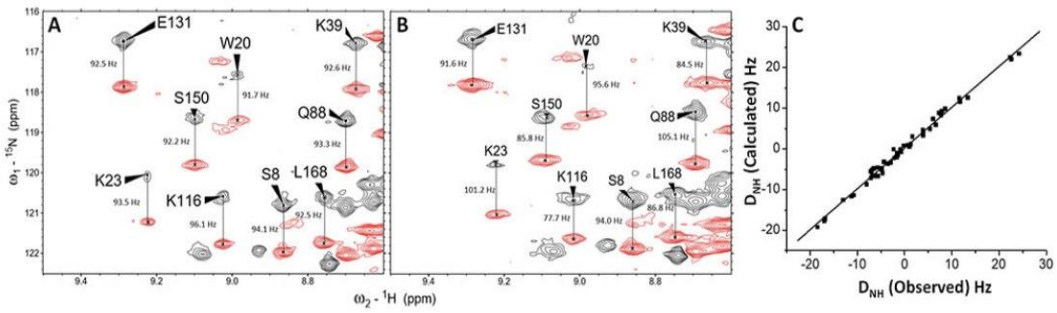

Figure 2.

Residual dipolar coupling (RDC) structural analysis of GCAP5. $^{1}H–^{15}N$ IPAP-HSQC spectra of Mg^{2+}-bound GCAP5 in the (A) absence and (B) presence of 12 mg/mL Pf1 phage. Observed spectral splittings in the absence of Pf1 (J_{NH}) and presence of Pf1 (J_{NH} + D_{NH}) are marked by vertical lines, and their difference was used to calculate RDCs as described in Materials and Methods. (C) RDCs calculated from the structure of Mg^{2+}-bound GCAP5 in Figure 3 plotted vs the RDCs measured in panel B show good agreement (Q-factor = 0.27, and R-factor = 0.985[32]).

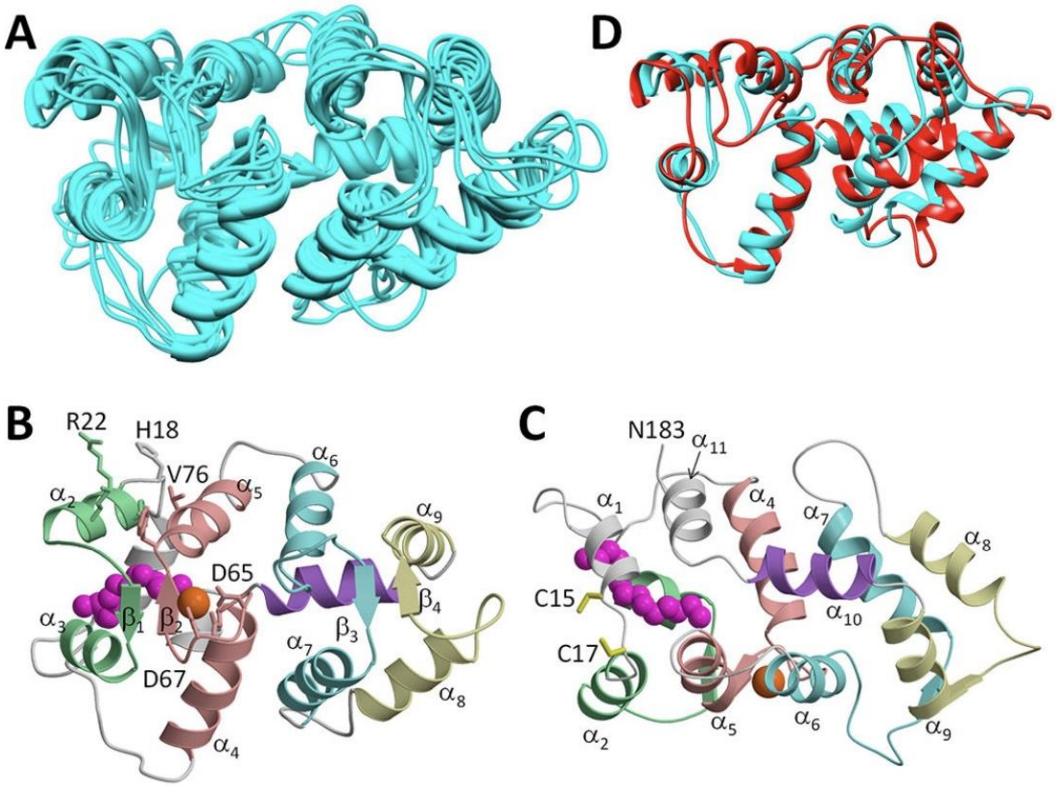

Figure 3.

NMR-derived structures of Mg^{2+}-bound GCAP5 (PDB entry 7M2M). (A) Ensemble of the 10 lowest-energy NMR structures. Structural statistics are listed in Table 1. (B) Average main chain structure of GCAP5 and (C) the same view rotated by 180° showing four EF-hands (colored as in Figure 1) packed in a globular arrangement very similar to what is seen for Ca^{2+}-bound GCAP1.[9] (D) Overlay of the main chain structure of GCAP5 (cyan) and the crystal structure of GCAP1 (red). The secondary structural elements are labeled as defined in Figure 1. The Ca^{2+} switch helix (α10) is colored purple. Cys15 and Cys17 side chain atoms are colored yellow. Bound Mg^{2+} is colored orange. The N-terminal myristoyl group is colored magenta. Side chain atoms of residues at the dimer interface (H18, Y21, M25, F72, and V76) and Mg^{2+} binding site (D63, D65, and D67) are indicated as sticks. (D) Overlay of main chain structures of Ca^{2+}-bound GCAP1 (red) and Ca^{2+}-free, Mg^{2+}-bound GCAP5 (cyan).

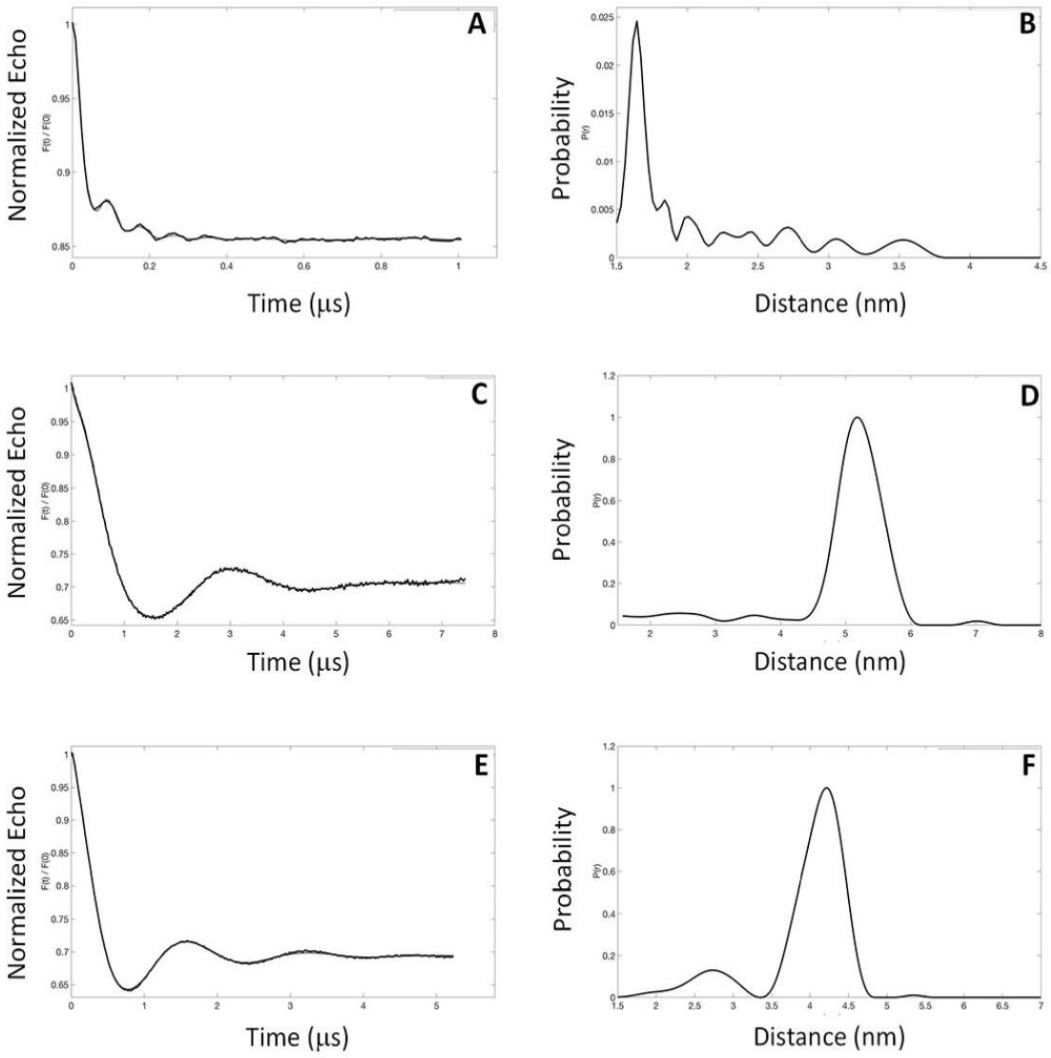

Figure 4.

EPR-DEER intermolecular distances for the GCAP5 dimer. Representative EPR-DEER data of (A) GCAP5^{CL}(A28C), (C) GCAP5^{CL}(N56C), and (E) GCAP5^{CL}(A69C) and corresponding distance distributions of (B) GCAP5^{CL}(A28C), (D) GCAP5^{cl}(N56C), and (F) GCAP5^{CL}(A69C). GCAP5 samples were in the Ca^{2+}-free, Mg^{2+}-bound state. Similar DEER data were observed for GCAP5 in the Ca^{2+}-bound state (not shown). A nitroxide spin-label (MTSSL) was covalently attached to the sole Cys residue in each mutant. The distance distributions and average intermolecular distances were calculated on the basis of the DEER data as described in Materials and Methods. The DEER intermolecular distances

were measured to be 16 ± 1 Å [GCAP5^{CL}(A28C) in panel B], 52 ± 3 Å [GCAP5^{CL}(N56C) in panel D], and 41 ± 3 Å [GCAP5^{CL}(A69C) in panel F].

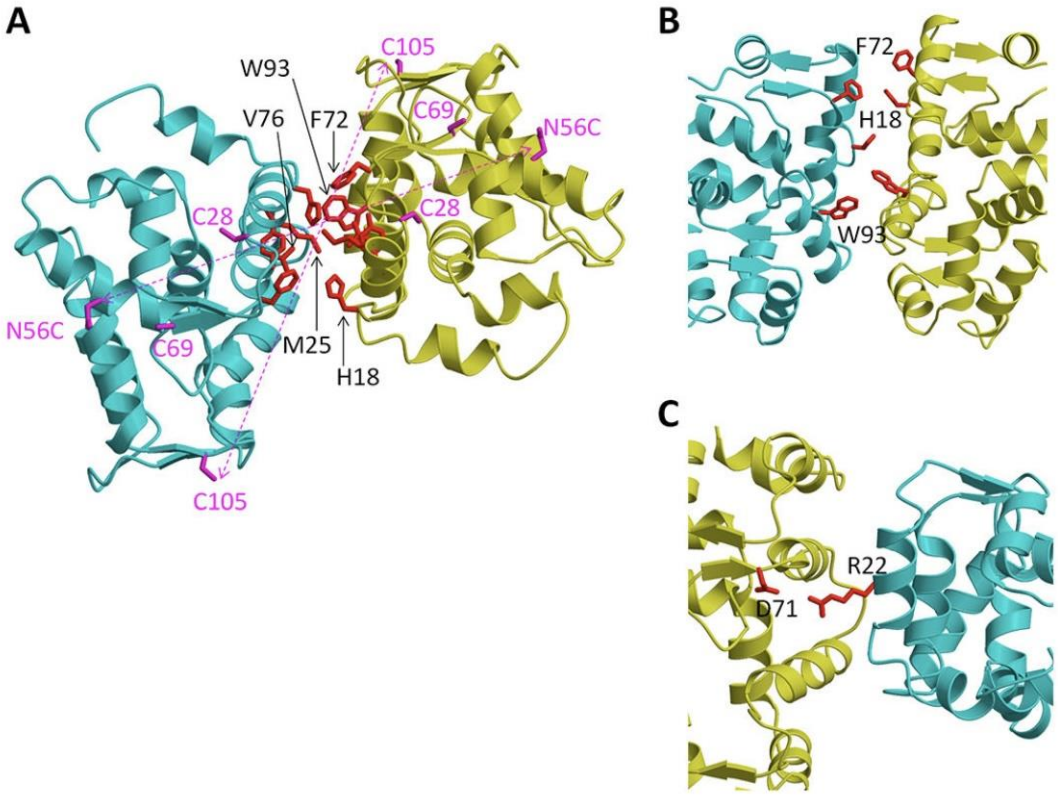

Figure 5.

Structural model of the GCAP5 dimer. (A) Ribbon diagram of the main chain structure of the GCAP5 dimer derived from DEER intermolecular distances listed in Table 2. The dimer subunits are colored cyan and yellow. Representative spin-labeled Cys residues for DEER studies (C28, N56C, C69, and C105) are colored magenta. Side chain atoms of residues at the dimer interface (H18, Y21, M25, F72, V76, and W93) are represented as sticks and are colored red. (B) Close-up of the dimer interface showing intermolecular contacts between aromatic residues. The side chain atoms of H18, F72, and W93 are colored red. (C) Close-up f the intermolecular salt bridge between R22 and D71.

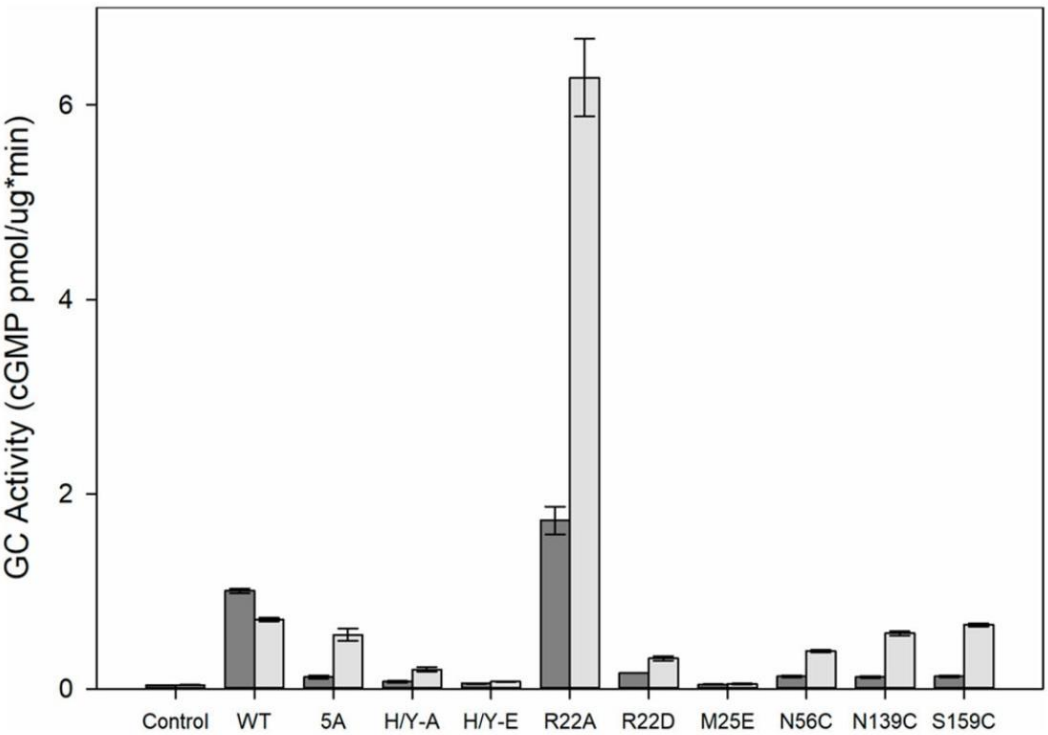

Figure 6.

Activation of photoreceptor guanylate cyclase by GCAP5 mutants. Purified myristoylated GCAP5 wild type (WT), Cys-less (5A), and variants (H18A/Y21A, H18E/Y21E, R22A, R22D, M25E, N56C, N139C, and S159C) were incubated with HEK293 cell membrane suspensions containing photoreceptor human guanylate cyclase (GC-E). The concentrations of wild type GCAP5 and variants were each 3 μM, and the free Ca^{2+} concentration was adjusted to 30 μM (dark gray bar) or 10 nM (light gray bar) using a Ca^{2+}/EGTA buffer system.

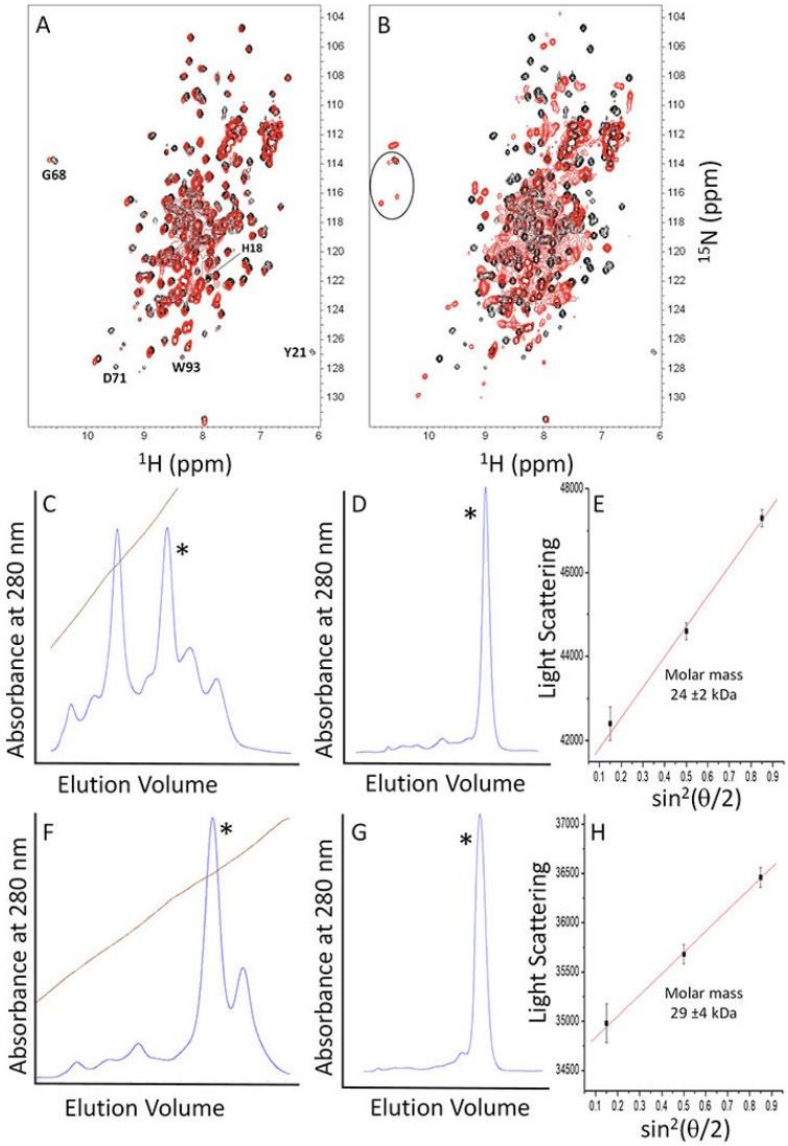

Figure 7.

NMR and SEC-MALS of GCAP5 dimerization site mutants. (A) ^{1}H–^{15}N HSQC spectra of ^{15}N-labeled GCAP5^{M25E} (red) and GCAP5^{WT} (black). (B) ^{1}H–^{15}N HSQC spectra of ^{15}N-labeled GCAP5$^{H18E/Y21E}$ (red) and GCAP5^{WT} (black). (C) Ion exchange chromatogram to isolate the monomeric fraction (marked by an asterisk) of GCAP5$^{H18E/Y21E}$. (D) Size exclusion chromatogram of GCAP5$^{H18E/Y21E}$. (E) MALS Zimm plot analysis of the monomeric fraction of GCAP5$^{H18E/Y21E}$ that determined a molar mass of 24 ± 2 kDa. (F) Ion exchange chromatogram to isolate a monomeric fraction (marked by an asterisk)

of GCAP5^{R22D}. (G) Size exclusion chromatogram of GCAP5^{R22D}. (H) MALS Zimm plot analysis of GCAP5^{R22D} that determined a molar mass of 29 ± 4 kDa. The experimental conditions for MALS are given in Materials and Methods.

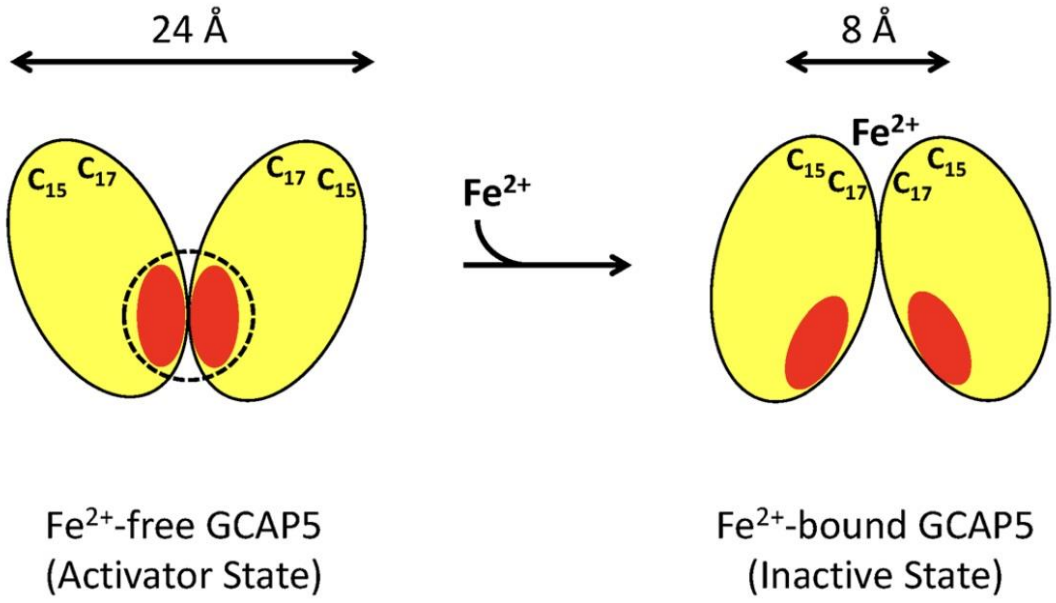

Figure 8.

Fe^{2+}-dependent structural changes in GCAP5. Schematic model of dimeric GCAP5 in the Fe^{2+}-free activator state (left) and Fe^{2+}-bound inactive state (right). A single bound Fe^{2+} is chelated by sulfhydryl side chains of Cys15 and Cys17 from both protein subunits of the GCAP5 dimer. The intermolecular distance between the Cys15 sulfhydryl group is depicted by a double arrow. GCAP5 residues (H18, Y21, M25, F73, V76, and W93) implicated previously in the binding to guanylate cyclase[54,55] are represented by red ovals, and the putative cyclase binding site is shown by a dotted circle.

Table 1.

NMR Structural Statistics for GCAP5

NMR restraints	**value (restraint violation)**
short-range NOEs	526 (0.0 ± 0.0)
long-range NOEs	145 (0.0 ± 0.0)
hydrogen bonds	144 (not used in water refinement)
dihedral angles	172 (0.1 ± 0.3)
$^{1}D_{HN}$ RDC	24 (0.0 ± 0.0)
RDC *Q*-factor	0.321
coordinate precision (Å)[a]	
RMSD for backbone atoms	1.0 ± 0.04
RMSD for all heavy atoms	1.6 ± 0.1
deviation from idealized geometry	
bonds (Å)	0.007 ± 0.001
angles (deg)	0.823 ± 0.015
impropers (deg)	0.925 ± 0.025
Ramachandran plot (%)	
favored region	78.1
allowed region	16.3
outlier region	5.6
structure quality[b]	
Clash score	80
Ramachandran outliers	5.6%
side chain outliers	6.1%

[a]Coordinate precision was calculated for residues 9–16, 20–41, 49–81, 89–120, 130–139, and 148–160.

[b]Structure quality metrics assessed by MolProbity.[36]

Table 2.

Molecular Docking Statistics for GCAP5

DEER distance restraint	C15 Sγ, 24 ± 6 Å
DEER distance restraint	C17 Sγ, 18 ± 2 Å
DEER distance restraint	T26C Sγ, 17 ± 2 Å
DEER distance restraint	C28 Sγ, 16 ± 1 Å
DEER distance restraint	N56C Sγ, 52 ± 3 Å
DEER distance restraint	C69 Sγ, 41 ± 3 Å
DEER distance restraint	C105 Sγ, 43 ± 11 Å
DEER distance restraint	N139C Sγ, 57 ± 4 Å
DEER distance restraint	E152C Sγ, 45 ± 4 Å
DEER distance restraint	S159C Sγ, 40 ± 3 Å
calculated distance	C15 Sγ, 32 Å
calculated distance	C17 Sγ, 28 Å
calculated distance	T26C Sγ, 16 Å
calculated distance	C28 Sγ, 21 Å
calculated distance	N56C Sγ, 52 Å
calculated distance	C69 Sγ, 39 Å
calculated distance	C105 Sγ, 52 Å
calculated distance	N139C Sγ, 57 Å
calculated distance	E152C Sγ, 42 Å
calculated distance	S159C Sγ, 42 Å
HADDOCK energy	−181.3 ± 5.8
RMSD (Å)[a]	0.9 ± 0.6
cluster size	11

[a]Root-mean-square deviation of backbone heavy atoms.

Chapter 5 : Unpublished results

The following section contains the results of experiments that were performed in the framework of Chapters 2 and 3, but were not published. These findings may be relevant for future research.

5.1 A putative rotation mechanism of the constitutive active mutant V902L- introduction of poly alanine segments

Following the poly alanine introduction to the transmembrane domain and checking the activity with wild type GC-E (see Chapter 2), we followed up introducing two and four poly alanine segments to the transmembrane domain (TMD) of the mutant V902L.

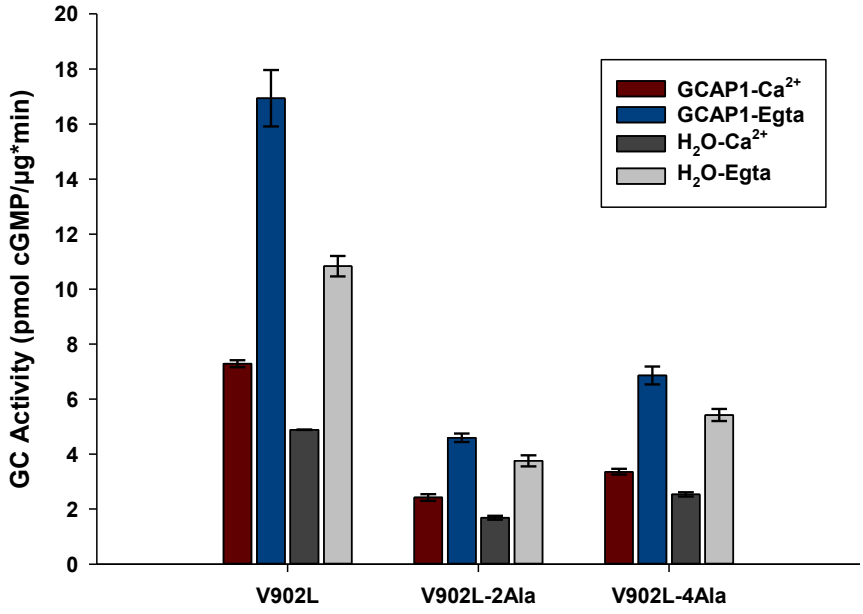

Figure 9: Catalytic activity of Ala mutants and mutant V902L.
Incubation of Ala mutants and mutant V902L in the presence of 5µM human GCAP1 at high (33 µM, maroon bars) and low (< 10 nM, blue bars) free [Ca^{2+}] and in the absence of GCAP1 at high (33 µM, black bars) and low (< 10 nM, grey bars) free [Ca^{2+}]. Results indicate an overall decrease in GC activity among different mutants, without affecting its Ca^{2+} dependency pattern among the different conditions used as seen by x-fold activation. The x-fold activation of control mutant V902L, V902L-2Ala and V902L-4Ala in the presence of GCAP1 is 2.3, 1.9, 2 and without GCAP1 is 2.2, 2.2, 2.1 respectively.

5.2 Truncated GCAP1

The importance of GCAP1 in the phototransduction has been viewed variedly above. Its structural studies are continually progressing to better understand its mechanism of action. A key objective in this field of research is to obtain high-quality crystals suitable for X-ray diffraction, which would enable the development of a reliable structural model. In this context, Francesco Bonì from the lab group of Prof. Mario Milani designed a truncated GCAP1

construct lacking the C-terminal region (residues Gly192-Gly201) and incorporating an engineered, putative disulfide bridge between the N-terminal and C-terminal cystein domains as seen in Figure 10.

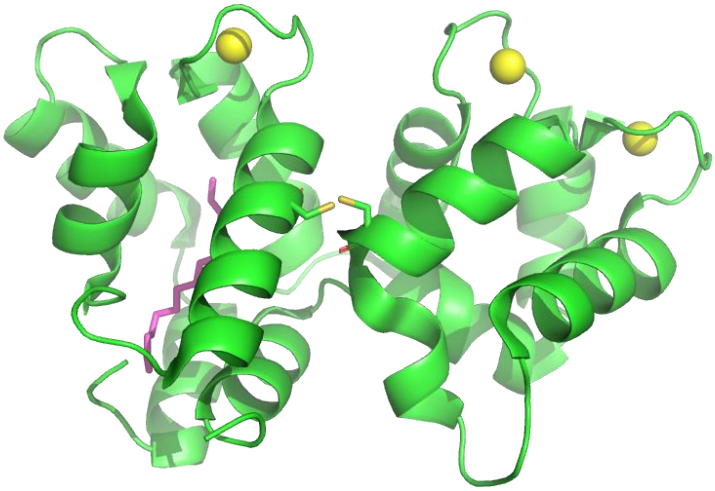

Figure 10: Structure of monomeric GCAP1
Monomeric GCAP1 with the two cysteins residue in the desired position (yellow stick), for creation of disulphide bond. Yellow round balls are the Ca^{2+} ions bound to EF 2,3,4 motif. Myristoyl group is highlighted with magenta. (Structure provided by Francesco Bonì)

The rationale behind this design was to reduce the intrinsic flexibility of the protein-particularly the reciprocal vibrational movement between the N-terminal (EF1-EF2) and C-terminal (EF3-EF4) lobes which often hinders crystallization. Additionally, they wanted to assessed whether this engineered construct retained functional activity in GC-E regulation, aiming to ensure the biological relevance of the structural insights. For this we had received the truncated protein sample from them and I further proceeded with an IC_{50} (half maximal inhibition) experiment to determine the activity profile of truncated GCAP1 and to compare it with the WT GCAP1.

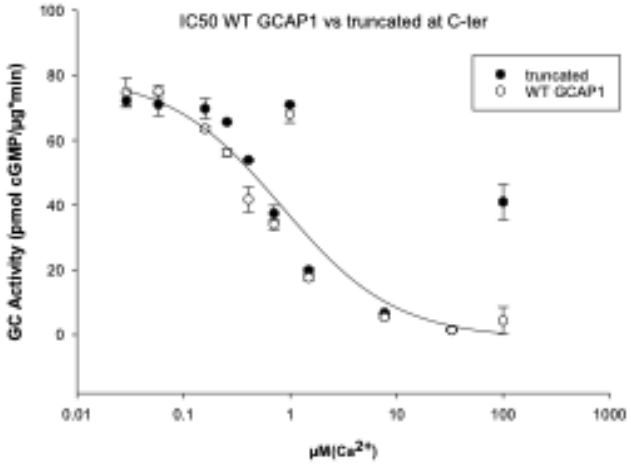

Figure 11: Half-maximal inhibition comparing truncated and WT GCAP1.
The GC-E was incubated with 10 µM of C-terminally truncated GCAP1 (black dot) or WT GCAP1 (white dots). Free [Ca^{2+}] was varied, as indicated and the analysis was performed. (Error bars are s.d., of technical duplicates).

The data presented here shows no principle difference between truncated and WT GCAP1. Unfortunately, despite these efforts, of generating a protein with reduced flexibility but being functionally active, diffracting crystals could not be obtained, and this result could not be used for any publication. However with this construct we could demonstrate that the C-terminus is not so essential in the regulation of the GC-E cyclase activity.

5.3 Guanylate cyclase activating protein 3 (GCAP3)

GCAP3 is a 23 kDa protein which is biochemically less characterized among other GCAPs isoforms. Therefore, this protein was used during my PhD work to some of the following experiments to elucidate its function and biochemical characteristic.

5.3.1 Ca^{2+} induced gel shifts in GCAP3

As seen in the gel images the expression and purification of GCAP3 was successful, however an increase in electrophoretic mobility was observed for GCAP3 upon electrophoresis. All known GCAP variants reacted to Ca^{2+} by adopting a different conformation, leading to the characteristic increase in electrophoretic mobility (Dell'Orco & Dal Cortivo, 2019), which is similar to other calcium sensors as well (Viviano et al., 2016). The presence of multiple bands could be due to protein oligomerization and/or residual Ca^{2+}-binding, is typical for calcium senosor proteins even after detergent-induced partial denaturation and the presence of a chelator in the buffer (Dell'Orco et al., 2012). The Ca^{2+} induced gel shift of the protein GCAP3 is reversed back by Ca^{2+} chelating ions (EDTA, EGTA) as illustrated in Figure 12.

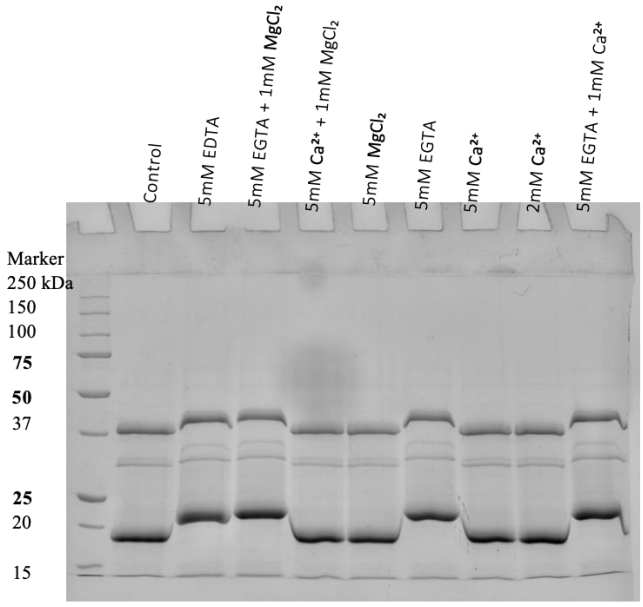

Figure 12: Ca^{2+} induced gel mobility shift
SDS-PAGE analysis of GCAP3. 5µg of protein was incubated for 30 min at RT in the presence and absence of respective ions and electrophorized in 12% SDS-PAGE gel and was stained with Coomassie blue.

5.3.2 GCAP3 and RD3 interaction with GC-E

We observed that GC-E is regulated by GCAP3 with less efficiency compared to GCAP1 as seen in Figure 1, Chapter 3. And as noted earlier, RD3 is known to inhibit cyclase activity. So we tested, whether RD3 could also inhibit cyclase activity regulated by GCAP3.

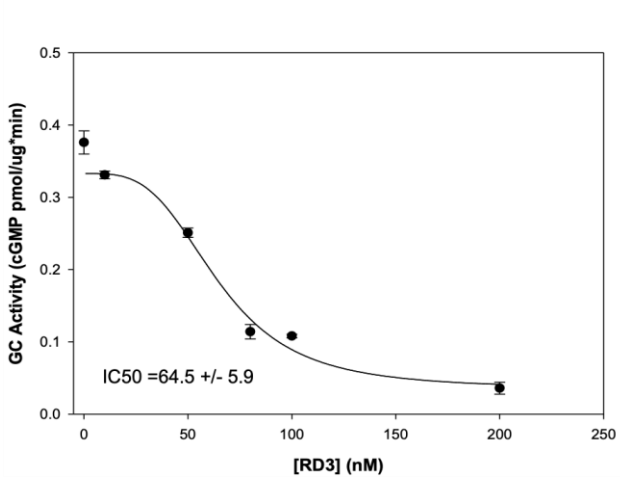

Figure 13: Inhibitory effect of RD3 on GC-E regulated by GCAP3
A titration of RD3 in the presence of 10 µM GCAP3 was performed. With increasing concentration of RD3, GC-E activity decreased with an IC_{50} value of 64.5 nM, which is closely similar to the inhibitory profile in the presence of GCAP1.

5.4 Does the binding of RD3 compete with the binding of GCAPs to the target GC-E?

RD3 is known to bind GC-E and is essential for its proper trafficking and function in photoreceptors (Azadi et al., 2010; Peshenko, et al., 2011). Importantly, RD3 has been shown to inhibit GC-E activation by GCAPs, helping keep the enzyme inactive during early photoreceptor development or mislocalization.

To expore whether the binding of RD3 competes with the binding of GCAP to GC-E, I conducted a functional assay using HEK293 cells expressing GC-E, WT and the mutant V902L and measured enzymatic activity upon stimulation with RD3 level near their respective IC_{50} value, in the presence of increasing GCAP1 concentration.

A

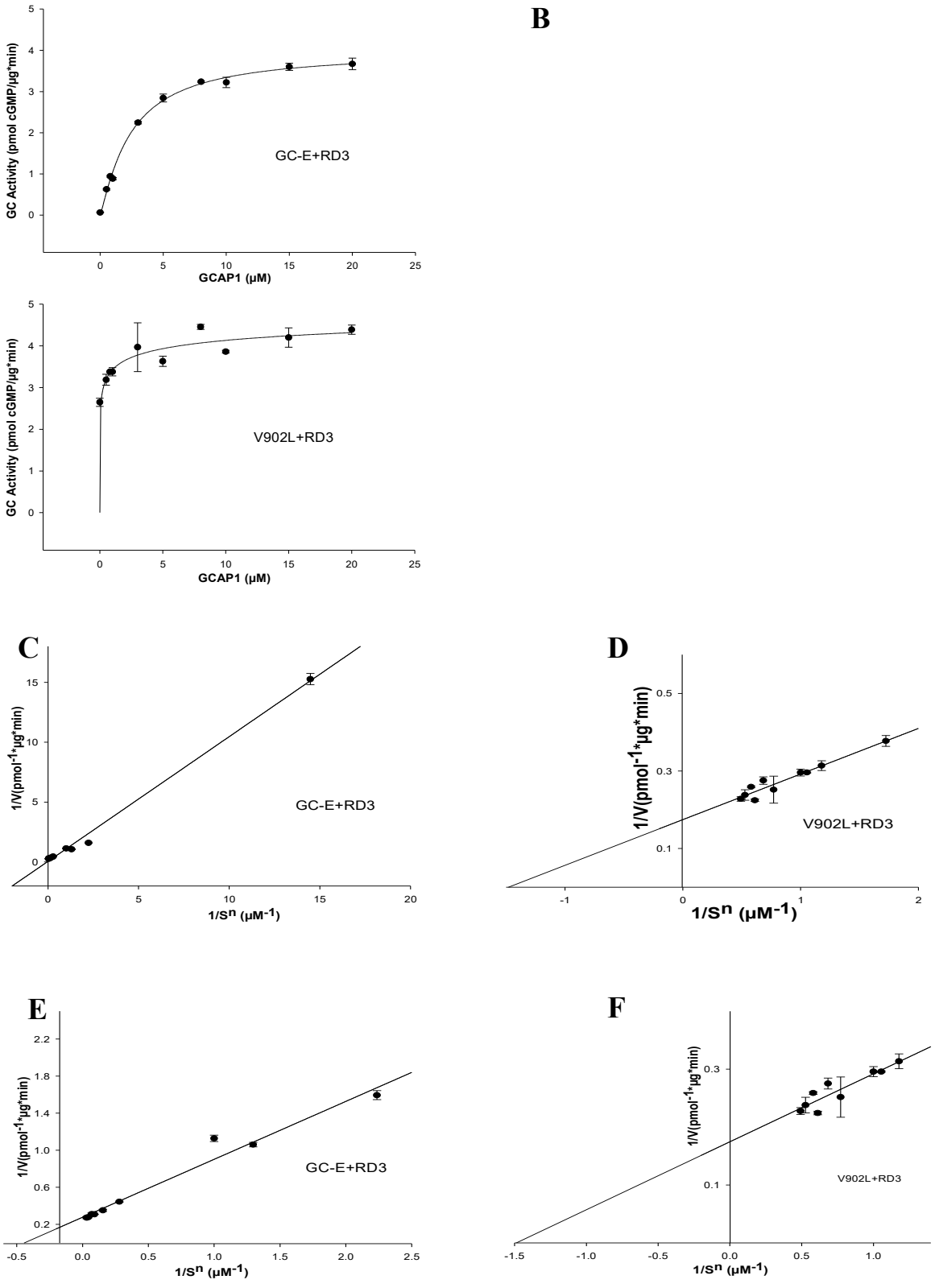

Figure 14: Competition of RD3 with GCAP1 in GC-E Activity assay.
GC-E was expressed in HEK293 cells, and its activity was stimulated by purified GCAP1 in the presence of RD3. The resulting data were fitted using a Sigmoidal 3Parameter model for the activity (**A-B**). Fitting of the curves to a Hill model and by analysis in Lineweaver -Burk plots, yielded values for Vmax (**C-D**). Because of the cooperative nature of substrate binding, the x-axis (1/[S]) can be adjusted using the Hill coefficient *n*, resulting in straight lines when plotted as 1/[S]^n. The maximal enzymatic GC-E activity at 68 nM RD3 was 18.62 pmol*µg-

$^{1}min^{-1}$ and V902L activity at 250 nM was 5.73 pmol*$\mu g^{-1}min^{-1}$, respectively, when activated by GCAP1. The half maximal effective concentrations (K½) for GCAP1 were 19.39 µM for GC-E and 0.67 µM for V902L respectively. (**E-F removing the 1st data value i.e 10**) The maximal enzymatic GC-E activity at 68 nM RD3 was 3.60 pmol*$\mu g^{-1}min^{-1}$ and V902L activity at 250 nM was 5.72 pmol*$\mu g^{-1}min^{-1}$ respectively when activated by GCAP1. The half maximal effective concentrations (K½) for GCAP1 were 2.25 µM for GC-E and 0.67 µM for V902L respectively.

Our data show that in the presence of RD3, the maximal GC-E activity stimulated by GCAP1 was noticeably reduced. Interestingly, the V902L mutant maintained higher activity even at a higher RD3 concentration. This suggests that the V902L mutation somehow makes the cyclase less sensitive to RD3 inhibition-possibly by disrupting RD3 binding or altering how RD3 influences the enzyme's structure.

Although this trend points to a potential interference by RD3 in GCAP1 mediated activation, however, it's important to note that we currently lack a direct control condition where GC-E was activated by GCAP1 in the absence of RD3 under the same experimental settings. Without this baseline, we cannot directly conclude that RD3 competes with GCAP1 for binding to GC-E. The reduced activity could also result from an independent regulatory effect of RD3 on GC-E, rather than direct competition at a shared binding site.

Still, our observations are consistent with the previous reports from the (Peshenko et al., 2011), where RD3 was shown to inhibit GCAP dependent activation of GC. Taken together our findings suggest that RD3 may modulate GC-E activation, possibly by interfering with GCAP1. However, to confidently demonstrate a competitive relationship, further experiments will be needed, especially including conditions with increasing GCAP1 concentration and stimulation in the absence of RD3 under conditions where the RD3 levels are well above the IC_{50} value.

Chapter 6 : Discussion

Retinal guanylate cyclases (GCs) and guanylate cyclase activating proteins (GCAPs) have long been recognised for their critical role in modulating visual phototransduction within retinal photoreceptor cells by synthesizing the second messenger cGMP in response to light stimuli. Despite their importance, the precise molecular mechanisms governing their regulation remain elusive. The structural complexity of GC-E protein, combined with persistent challenges in achieving reliable in vitro expression, of the full length protein in high yields, has hindered the determination of their crystal structures, limiting our understanding of their function. Mutation in GC-E and GCAPs are associated with various retinal disorders, further emphasizing the need to uncover the mechanism underlying their activation and regulation. Therefore, elucidating the activation mechanism of membrane-bound photoreceptor GCs which is regulated by GCAPs is the primary goal of my thesis. To support this investigation, recombinant protein production was carried out. The genes were cloned, expressed and purified and the resulting protein samples were then tested for biological activity and for interaction/regulation studies using various techniques. While the initial objective was to approach these problems experimentally, the study further extended in the direction of molecular dynamics. A computational approach was undertaken to explore the conformational changes that occur as the receptor transitions from its inactive to active state. Initial findings from this research have been addressed within the two publication **Chapter 2** and **Chapter 3.** During the course of my research, a side project emerged, focusing on understanding the conformational dynamics of GC regulator GCAP, specifically GCAP5 and the results are presented in a third publication, provided in **Chapter 4**. My thesis research work addressed two mechanisms that can be proposed for the catalytic operation of GC-E, ‘‘the rotation mechanism’’ and ‘‘the two metal ion catalytic mechanism’’. A brief description of the hypothetical mechanisms of the rotation mechanism is provided in the introduction, while the two metal ion catalytic mechanism is provided below, followed up by the detailed discussion.

6.1 Two metal ion catalytic mechanism

The two metal ion concept is a biochemical mechanism used to describe how certain enzymes, use two metal ions (such as Mg^{2+}, Mn^{2+}, Ca^{2+} or Zn^{2+}) in their active site to stabilize the transition state of the enzymatic reaction. The mechanism is widely applicable for enzymatic catalysis involving phosphate group transfer, where one metal ion interacts with ATP/GTP to form the substrate complex, while the other metal ion is primarily bound to the cyclase catalytic center. A similar mechanism has been reported in the case of adenylate cyclase (AC), showing the mechanism is likely to operate for the conversion of ATP to cAMP (Hurley, 1999). Tesmer et al. (1999) through crystallographic analysis determined the catalytic domains of AC’s in complexed with ATP analogs and divalent metal ions (Figure 15). These provided a model for the enzyme-substrate complex, conclusively demonstrating the two metal ions are essential for AC’s catalytic activity. A similar mechanism has been reported for soluble guanylate cyclase by Serfass et al. (2001).

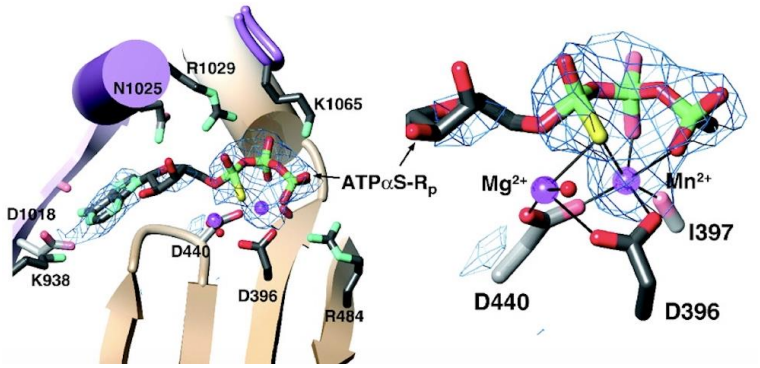

Figure 15: Two metal ion model
The active site of adenylate cyclase. AC·ATPαS-R_p·Mn (left) and a magnified view of its thiotriphosphate (right). Mn^{2+} is shown to bound with substrate ATP, while other metal ion Mg^{2+} is bound to the subunit of the catalytic center of AC (taken from Tesmer et al., 1999).

6.2 Activation of sensory GCs by a rotation mechanism?

Membrane-bound guanylate cyclases (GCs) share a common structural topology, comprising of an extracellular domain, a single spanning transmembrane domain connecting extracellular domain to an intracellular domain and a catalytic domain. Despite this shared architecture, the membrane-bound GCs reach their active state through distinct interaction processes. For instance, hormone receptor GCs are regulated by hormone peptides bound to the extracellular domain, whereas photoreceptor GCs have intracellular binding sites for Ca^{2+}- sensor proteins, called GCAPs. GCAPs operate in a stepwise activation mechanism that finely tunes the photoreceptor light response (Hwang et al., 2003; Koch & Dell'Orco, 2013). Despite these variations, the shared structural topology of membrane-bound GCs suggests the possibility of common conformational activation mechanisms.

Membrane bound hormone regulated GCs remain in a preformed dimeric, however in an inactive state prior to ligand binding. A rotation mechanism has been proposed for hormone-activated natriuretic peptide-receptor A (GC-A) that involves the juxtamembrane region located between the TM and KHD regions (Misono et al., 2011), where ligand binding induces an α-helix rotation that is transmitted to the catalytic domain, thereby switching the GC from its inactive to active state. Experimental evidence supporting this ligand-induced rotation mechanism was provided by Parat et al. (2010), who demonstrated that introducing a stretch of up to five alanine residues close to the N-terminal end of the TM region in rat GC-A triggered transmembrane helix rotation, transmitting the conformational change to the catalytic domain and switching the GC-A from the inactive to the active state.

However, whether this mechanism is conserved across all membrane GCs or even all transmembrane cell-surface receptors remain unclear (Maruyama, 2015). Sensory GCs, such as GC-E and GC-F, which are regulated by GCAPs acting as intracellular Ca^{2+} sensor proteins, require a change in free intracellular Ca^{2+} levels to transition into the active state. This mode of activation, which fundamentally differs from ligand-induced activation, raises the question of

whether GCAPs induce similar conformational changes through a comparable rotational mechanism in sensory GCs or not?

To investigate this possibility, a similar experimental approach to that of Parat et. al. (2010) was adopted. The incorporation of a single alanine residue into an α-helical secondary structure is predicted to induce a helix rotation of approximately 100°. Consequently, the insertion of four alanine residues into the primary sequence would result in a complete 360° rotation. If the rotation of the TM region or the other structural domains within GC-E is a requisite step for transitioning to the active state, it would be hypothesized that GC-E exhibits constitutive activity in the absence of GCAPs. Furthermore, such activation would likely render GC-E activity independent of Ca^{2+} regulation. To test this hypothesis, a stretch of one to five alanine residues was introduced close to the TM region (Figure 1, Chapter 2), in order to generate GC-E constructs, via site directed mutagenesis, and assessed the functional consequences through a GC-Assay. The results showed no evidence of any constitutive activation of GC-E, suggesting that the successive insertion of alanine residues does not trigger a conformational transition to the active state. These findings imply that photoreceptor guanylate cyclases differ fundamentally in their mode of action compared to the hormone- activated GC-A, suggesting that this rotation mechanism does not extend to all membrane bound GCs. Instead, minor disruptions in basal and GCAP-dependent activities observed in the alanine point mutants further raises critical questions about the structural determinants governing GC activation and their implications for retinal physiology.

6.3 The role of the V902L mutation in GC-E activation

The V902L mutation in human GC-E has provided key insights into the activation process of photoreceptor GCs. This V902L mutation is found in patients suffering from retinal cone-rod dystrophies is the only known human GC-E mutation which leads to constitutive activation, independent of GCAP regulation (Wimberg et al., 2018). In contrast, most GC-E mutations associated with visual impairment predominantly exhibit severely reduced activity or altered GCAP-mediated Ca^{2+} regulation, rather than increased basal activity (Sharon et al., 2018). The V902L mutation appears to induce a conformational shift to the active state of GC-E, eliminating the need for regulatory stabilization by GCAP Ca^{2+} sensors. This conformational transition mechanism resembles findings from alanine mutants of GC-A, where the integration of four alanine residues enforced a helix rotation, resulting in constitutive GC activation. Thus, the V902L mutant serves as a valuable tool for investigating GC-E activation mechanisms.

Previous biochemical characterization of V902L by Wimberg et al. (2018) primarily focused on the enzymatic activity profile of V902L in response to varying Ca^{2+} and GCAPs concentration, without detailed analysis of substrate dependency and the catalytic efficiency expressed in $kcat/K_M$. To address this gap, we extended our studies to determine the catalytic parameters involved as a function of the substrate (Mg-GTP) concentration both in the presence and absence of GCAP1 and GCAP2.

A sigmoidal curve (Figure 3, Chapter 2) plotting GC activity against Mg-GTP concentration suggested a cooperative process. GC-E in the presence of GCAP1 reached saturation at substrate concentrations above 1 mM GTP, with a Vmax of 11.33 pmol/µg x min. In contrast, GCAP2 regulated GC-E exhibited a 10-fold lower activation rate as noted previously and did not reach saturation within the tested Mg-GTP concentration range. The V902L mutant exhibited a saturation profile, with Vmax values ranging from 7 to 11 pmol/ µg x min of protein. Notably, the V902L mutant demonstrated constitutive activity in the absence of GCAPs, achieving half-maximal saturation at 0.37 mM GTP, a value comparable to wild type GC-E in the presence of GCAP1. Curve fitting to a Hill model yielded Vmax, EC50 (half-maximal saturation), and the apparent Hill coefficient, summarized in Table 1 (Chapter 2).

The analysis of catalytic parameters revealed that the constitutively active state of the V902L mutant closely resembled the active state of WT GC-E stabilized by GCAP1 and therefore could not originate from higher catalytic efficiency. Similar values of Vmax, K_M and Kcat, and catalytic efficiencies ranging between 2000 and 4000 M^{-1} x S^{-1} (Chapter 2) suggests that the V902L mutation induces a conformational change in GC-E that mimics the active state, even in the absence of GCAP1.

6.3.1 Structural transition from inactive to active state

Earlier studies identified the GCAP1 binding sites within the juxtamembrane and kinase homology regions of mammalian GC-E (Lange et al., 1999; Peshenko et al., 2015; Sulmann et al., 2017), suggesting a movement or conformational shift in the catalytic domain relative to the kinase homology domain during activation. The residue at position 902 is also in the catalytic domain, and the mutation could lead to a substantial rearrangement of the dimeric structure in this domain. To investigate this catalytic domain movement, the kinase homology domain of GC-E needed to be aligned with the mutant structure. Recently, a bovine GC-E 3D structure of IcD has been reported by Rehkamp et al. (2021). Since human and bovine orthologues share a high sequence homology, we therefore used this structure to follow up with our structural analysis based on molecular dynamic simulation. Notably, due to presence of five extra residues in the amino acid sequence in the bovine orthologue, the Valine position in bovine is at 907 and has been reported as V907L in Chapter 2 (in computational study part). Due to simplicity and since the numbering associated with the human CRD mutant is V902L, I therefore use and refer to V902L according to the human ortholog in the following description and discussion. Figure 16 illustrates the movement of the alpha-helical domain connected to the catalytic domain and its influence on residue at position 902. In the wild-type GC-E, both valines at this position were located close to the dimer interface and opposite to each other. However, in the V902L mutant, the substitution with leucine resulted in a more exposed side chain on the protein surface. Given that leucine contains an additional methylene group and is more hydrophobic than valine, the increased length and hydrophobicity might have induced a repulsive effect between leucines, leading to alterations in the dimer interface.

Furthermore, we depicted swinging movement of the dimerization domain representing a crucial conformational switch between low and high activity states in the cyclase. In GC-E,

this switch is normally triggered by GCAP1 interaction, whereas in the V902L mutant, the amino acid substitution alone was sufficient to drive the transition.

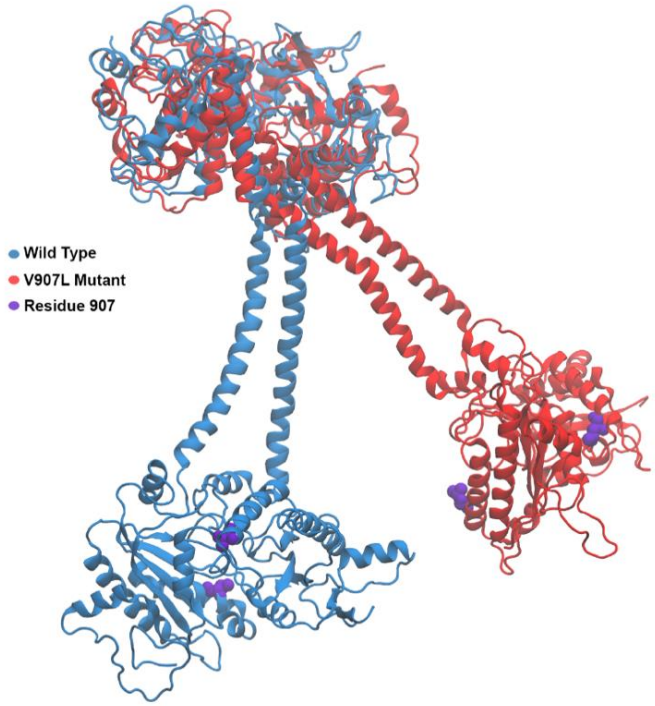

Figure 16: GC-E protein structure
GC-E protein structure depicting the intracellular domain, comprising of the kinase homology domain on top followed by the alpha-helical dimerization domain and concludes in the catalytic domain. The wildtype and the V902L mutant are shown in blue and red respectively. The residue 902 (907 in bovine GC-E) is highlighted in purple (taken from Shahu et al., 2022).

Another noticeable difference was highlighted on a Lys1051 position in Figure 17. In the catalytic center the GTP substrate-binding site is thought to comprise residues Asp890, Arg981, Ala1013, and Lys1051 in the cyclase catalytic domain (Liu et al., 1997; Tucker et al., 1998). This mutation caused the lysine residue to swing away from the dimer interface, suggesting that the increased flexibility might facilitate reaching the transition state in the catalytic center. Since GCAPs are known to activate photoreceptor guanylate cyclases (GCs) by stabilizing the transition state (Hwang & Koch, 2002), it is plausible that the V902L mutation leads to constitutive activation of GC-E by mimicking this stabilization effect. The structural changes observed in the mutant indicate that the mutation alone, without GCAP1 interaction, can induce the active conformation of the enzyme. This finding provides a fundamental distinction between the activation mechanisms of hormone receptor GCs and sensory GCs, shedding light on the molecular basis of retinal diseases.

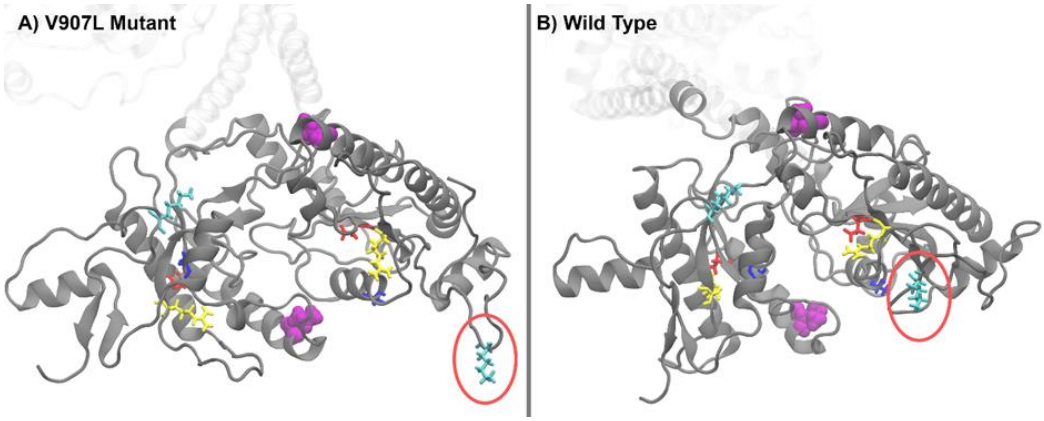

Figure 17: Differences observed in critical amino acid positions within the putative GTP substrate-binding site of GC-E.
The catalytic domain of V902L mutant (V907L) (**A**), and WT GC-E (**B**), residues 902 are highlighted in purple. The putative GTP binding site residues are highlighted in sticks as (blue=Ala, lime=Arg, red=Asp, cyan=Lys). In one of the subunits of WT GC-E, Lys1051 exhibits significant movement as it swings out (red ellipsoid) (taken from (Shahu et al., 2022).

6.3.2 Enzymatic efficiency across other GCAP variant (GCAP3)

GCAP3, a less characterized variant of GCAP in terms of its functional role in phototransduction, exhibits Ca^{2+} sensitive regulation of GC-E, albeit to a lesser extent than GCAP1. The V902L mutant, which remains constitutively active irrespective of the presence or absence of GCAP, was analyzed to determine whether the reduced efficiency of GCAP1 in activating GC-E also applied to GCAP3. The mutant V902L had significantly high activity at high and low [Ca^{2+}] in the absence of any GCAP variant exceeding the basal activity 6 to 16-fold in comparsion to GC-E. While GCAP3 activated GC-E in a Ca^{2+} dependent manner, its effect was weaker than that of GCAP1. V902L remained largely unaffected by GCAP3 (Figure 1, Chapter 3).

6.3.3 Ca^{2+} dependency and allosteric communication

Ca^{2+} is a vital metal ion in all organisms and as seen here, plays a crucial role as a second messenger in photoreceptor cells. Unlike the typical GC-GCAP system, where GC is regulated by GCAP in response to changes in intracellular Ca^{2+}, interestingly the V902L mutant exhibited Ca^{2+} dependent activity, although no Ca^{2+} sensor protein (GCAPs) was present to mediate this effect. This suggests an inherent Ca^{2+} mediated modulation of the catalytic site.

Experimental data (Figure 2A, Chapter 3) demonstrate that at high [Ca^{2+}] (above 10 µM), the activity declines and reached a plateau of lower activity at 100 µM free [Ca^{2+}] , supporting the idea of a two-metal ion catalytic mechanism (Hurley, 1999; Tesmer et al., 1999).

Apparently, type V adenylate cyclase (ACV), the fourth group of adenylate cyclase family belongs to the family of Ca^{2+} inhibited cyclases (Yoshimura & Cooper, 1992). The C-terminal region (C1b) of this ACV is responsible for Ca^{2+} binding and subsequently inhibition of the enzyme activity (Scholich et al., 1997). The guanylate cyclase which closely resembles adenylate cyclase, can be converted into an adenylate cyclase through just two amino acid

substitutions in GC-E (Tucker et al., 1998). Serfass et al. (2001) previously investigated a similar Ca^{2+} dependent inhibition affecting the catalytic properties of bovine lung derived in soluble guanylate cyclase. The authors described their findings as supporting a two-metal ion catalytic mechanism involving two Mg^{2+} ions, like the process observed above in adenylate cyclases. One Mg^{2+} ion interacts with GTP to form the substrate complex, while the other Mg^{2+} (more than substrate) is primarily bound to the cyclase at the catalytic center. This mechanism suggests that Ca^{2+}, when bound to the cyclase, can be displaced by increasing free Mg^{2+} beyond the concentration needed for the Mg^{2+} -GTP substrate.

The data obtained from Figure 2B (Chapter 3) demonstrate that the Mg^{2+} -dependent reversal of Ca^{2+} inhibition further corroborates this model, indicating that excess Mg^{2+} can counteract the inhibitory effects of Ca^{2+} on GC-E activity of the V902L mutant. These findings align with previous studies on soluble guanylate cyclases, suggesting the V902L mutant exhibit a competitive interaction between metal ions in enzyme regulation.

The swinging movement was hypothesized to occur at the dimerization domain site in the V902L mutant as shown in Figure 16, (s. above) which is taken from Shahu et al. (2022), a region typically static in the GC-E configuration. This motion, absent in the inactive state, appears to initiate from the CD and propagates upstream toward the αHD, suggesting that the point mutation at position 902 disrupts the native packing at the dimer interface. As a result, this mechanical shift influences upstream domains and provide direct evidence of an allosteric linkage between the αHD and the CD. The increased exposure and altered orientation of residue 902 (leucine vs valine) likely destabilizes local interactions, enabling structural flexibility and resembling the GCAP1 induced active conformation. Therefore, these observations support a model in which structural perturbation at the CD level alone is sufficient to induce global conformational changes, establishing a robust allosteric network within the intracellular domain of GC-E. This mechanism offers new insights into domain cooperation and intramolecular signaling relevant for cyclase activation in sensory phototransduction.

Lastly, although we reported no involvement of transmembrane rotational mechanism in photoreceptor GCs, we cannot rule out that the CD requires anchoring by the TMD to achieve its full activity. Our data with the poly-Ala mutants introduced in the V902L Figure 9 (presented under unpublished results Chapter 5), show a decrease in overall activity, indicating a key role of the TMD in enhancing the basal activity of the CD. This likely occurs by properly positioning all modular domains (JMD, KHD, αHD and CD) to create optimal condiions for catalysis, as previously reported by (Ravichandran, 2017). Interestingly, the Ca^{2+} dependency of the V902L mutant remains intact, in presence or absence of GCAP1 consistent with a two metal ion catalytic mechanism.

6.4 Impact of the double mutant L804P/V902L Mutation on Catalytic Efficiency

Restoring GC-E to its basal activity state is a key step in phototransduction. Our previous simulations suggested that a conformational change in the α-helical domain (αHD) is necessary for GC-E to shift between low- and high-activity states. Identifying the structural trigger within the helix-turn-helix motif led us to hypothesize that modifying or disrupting a critical α-helix could affect the catalytic center. To probe the regulatory architecture further, I generated a double mutant (L804P/V902L), targeting the αHD. The L804P mutation, introduced into the V902L background to explore conformational effects, resulted in reduced basal and Ca^{2+}-regulated activity. This supports the hypothesis that the helix-turn-helix motif in the αHD serves as a regulatory switch for GC-E activation. The substantial drop in catalytic efficiency observed in the double mutant underscores the critical role of this region in maintaining functional enzyme dynamics. Despite the retention of principal activation mechanisms, the altered catalytic efficiency suggests that the mutation disrupts an essential allosteric communication pathway between the αHD and the catalytic domain.

6.5 Computational connectivity analysis

The computational connectivity analysis of GC-E structural dynamics further revealed that the αHD acts as a conduit for allosteric signaling between the kinase homology domain and the catalytic domain. Our analysis emphasizing the network of amino acid interactions that underpin conformational transitions of GC-E. High-reach residues shifted from the catalytic domain in WT GC-E to the kinase homology domain in V902L, while betweenness analysis identified key residues in the α-helical region mediating allosteric communication. As seen with reach approach (Figure 5A, Chapter 3) of GC-E the positioning of residue S1011 within the catalytic domain, which lies adjacent to E1010-a residue known to coordinate with Mg^{2+} and the pyrophosphate moiety of GTP. This proximity likely plays a role in stabilizing the catalytic core during activation. In the V902L mutant (Figure 5B, Chapter 3), this connecting pathway shifted significantly, and this structural change may underlie the disruption in GCAP-mediated allosteric regulation of V902L mutant respectively.

Notably, some high-connectivity residues identified through this analysis correspond to known disease-associated mutations, such as D728N (LCA) and P873R (CRD), linking our findings to pathophysiological outcomes in inherited retinal disorders.

6.6 Conformational dynamics of GCAPs – GCAP5 and its role in regulating GCs

GCAPs (GCAP1-GCAP7) are a family of photoreceptor Ca^{2+} binding proteins that regulate retinal GCs in a Ca^{2+} dependent manner. In light activated photoreceptors, when cytosolic Ca^{2+} levels are low, Mg^{2+} bound, Ca^{2+} free GCAPs associate with GC and stimulate cGMP synthesis

(Peshenko & Dizhoor, 2006), whereas in dark adapted photoreceptors, when cytosolic Ca^{2+} levels are elvated Ca^{2+} bound GCAPs interact with GCs and supress cyclase activity. Unlike other GCAPs, the GCAP5 homologue from zebrafish is unique to its property as it has the most divergent amino acid sequence. This unique sequence contains two non-conserved cysteine residues (Cys15 and Cys17) which are known to bind ferrous ions (Fe^{2+}). Interestingly, the binding of the Fe^{2+} to the GCAP5 greatly diminishes its ability to activate the GC-E (Lim et al., 2017). In addition, it lacks the typical Ca^{2+} dependency as seen in other isoforms. In Chapter 4 our study determines the NMR structure of the Mg^{2+} bound activator form of GCAP5 (Ca^{2+} free, Fe^{2+} free, Mg^{2+} bound) that closely resembles the crystal structure of GCAP1. There are, however, key structural difference in the N-terminal helix of GCAP5, which is elongated by two residues. This elongation repositions the non-conserved sulfhydryl side chains of Cys15 and Cys17 to point outward and chelate Fe^{2+}. This finding aligns with the previous study by Lim et al. (2017) indicating high affintiy Fe^{2+} binding to GCAP5 (Fe^{2+} bound).

Lim et al., also found out that the GCAP5 in solvent remains in dimer form both in the Fe^{2+} free and Fe^{2+} bound state. The dimer interface found in GCAP5 is composed of the exposed hydrophobic residues H18, Y21, R22, M25, F72, V76 and W93 that are also present in the GCAP1 dimer (H19, Y22, M26, F73, V77, and W94). Dimerization is necessary for the cyclase activity as has been demonstrated for GCAP1 where mutations at the dimer interface of GCAP1 either diminished or completely suppressed the ability of GCAP1 to activate the cyclase (Lim et al., 2018; Peshenko et al., 2014). Therefore we checked if GCAP5 has similar properties by creating mutation at the GCAP5 dimerization site (H18A/Y21A, H18E/Y21E, R22A, R22D, and M25E). Our results presented in Chapter 4, Figure 6 and Figure 7 shows that the generated mutants, disrupt the dimerization (Figure 7) and significantly reduce GC activation by more than 4-fold (Figure 6). Notably R22A showed a 5-fold increase in cyclase activity, even though GCAP5 dimerization is weakened by the point mutation R22A. An explaination for this observation might be that the, GCAP5 dimerization site facilitates interactions with GC, suggesting that at higher GC concentrations, GCAP5 might preferentially bind to GC rather than forming dimers. These observations highlight the functional significance of the monomer-dimer equilibrium as has been seen with GCAP1 (Bonì et al., 2020; Olshevskaya et al., 1999).

Lastly, the structure of the Ca^{2+} free, Fe^{2+} free, Mg^{2+} bound GCAP5 dimer differs significantly from the one proposed Fe^{2+} bound GCAP5 dimer model by Lim et al. (2017). In the Fe^{2+} bound dimer, a single Fe^{2+} is chelated by Cys15 and Cys17 from each subunit, bringing the Cys15 atoms within 8Å distance. In contrast, the Fe^{2+} free dimer shows a much larger 24Å distance between the spin-labeled Cys15 residues, suggesting that Fe^{2+} binding induces a rotation of the dimer subunits. This rotation alters the exposure of key residues involved in GC binding, potentially explaining how Fe^{2+} binding inhibits GCAP5 activation of GCs.

6.7 Future perspective

Decades of intense research has been made in understanding the crucial role of the GC-GCAP system in phototransduction. Every small breakthrough raises new questions, and a complete understanding of membrane bound receptor-mediated signaling continues to evade scientists. From understanding the regulation of GC by GCAPs to evaluating the interaction/binding sites between GC and GCAPs, and involvement of other interacting proteins, numerous insights have emerged, revealing an increasing complexity in the models needed to explain these mechanisms. While some sensory or membrane bound receptors can be described using straightforward models, others require more intricate explanations. Given their crucial role in phototransduction and as such the whole interconnecting biochemical signaling cascade further transmitting to the second order neurons interactions are associated together and changes in this physiological homeostasis have been linked to various diseases. Therefore, advancing our understanding of these membrane bound receptor here guanylate cyclase is of paramount importance.

The combined insights from the three different Chapters of my PhD work underscore the intricate regulatory network governing photoreceptor GC activity. The involvement of KHD-CD interface and allosteric pathways along with the dynamic interplay between GCAPs, ensures precise control over cGMP synthesis, which is very much essential for phototransduction. As seen, disruptions in this network, whether due to mutations in GC-E or GCAPs, lead to severe retinal pathologies. Therefore, by unraveling the structural and functional basis of GC regulation, these studies paved the way for novel therapeutic interventions aimed at restoring photoreceptor homeostasis. As such, the identification of critical residues and domains involved in allosteric communication, as reported in Chapter 3, could be used as potential targets for pharmacological intervention. Small molecules or peptides that mimic GCAP function or restore normal allosteric signaling could offer promising avenues for treating retinal diseases. Most importantly the αHD offers a potential target and the network-based connectivity analysis conducted in this study identifies several key amino acid residues that play central roles in the allosteric regulation of GC-E. Importantly, some of these residues overlap with known pathogenic mutations, suggesting their potential as biomarkers or targets for therapeutic intervention. Others may represent novel candidates for further functional and genetic investigations in the context of inherited retinal diseases. Further cryo-EM or high-resolution crystallographic studies capturing intermediate conformations of GC-E, especially in the presence of different GCAP variants or Ca^{2+} concentrations, could clarify the nature of the conformational transitions inferred here. Additionally, in vivo transgenic animal models expressing for example constitutively active GC-E mutants like V902L could help to elucidate their long-term effects on photoreceptor function, calcium homeostasis, and visual cycle integrity. Future structural studies are needed to determine the Fe^{2+} bound state to elucidate whether the GCAP5 dimer structure will remain intact upon binding to GC-E and most importantly how it might stabilize the transition state of the cyclase activity.

References

Allerston, C. K., Von Delft, F., & Gileadi, O. (2013). Crystal Structures of the Catalytic Domain of Human Soluble Guanylate Cyclase. *PLoS ONE*, *8*(3), e57644. https://doi.org/10.1371/journal.pone.0057644

Ames, J. B. (2021). Structural Insights into Retinal Guanylate Cyclase Activator Proteins (GCAPs). *International Journal of Molecular Sciences*, *22*(16), 8731. https://doi.org/10.3390/ijms22168731

Ames, J. B., Dizhoor, A. M., Ikura, M., Palczewski, K., & Stryer, L. (1999). Three-dimensional Structure of Guanylyl Cyclase Activating Protein-2, a Calcium-sensitive Modulator of Photoreceptor Guanylyl Cyclases. *Journal of Biological Chemistry*, *274*(27), 19329–19337. https://doi.org/10.1074/jbc.274.27.19329

Ames, J. B., Ishima, R., Tanaka, T., Gordon, J. I., Stryer, L., & Ikura, M. (1997). Molecular mechanics of calcium–myristoyl switches. *Nature*, *389*(6647), 198–202. https://doi.org/10.1038/38310

Ames, J. B., & Lim, S. (2012). Molecular structure and target recognition of neuronal calcium sensor proteins. *Biochimica et Biophysica Acta (BBA) - General Subjects*, *1820*(8), 1205–1213. https://doi.org/10.1016/j.bbagen.2011.10.003

Aparicio, J. G., & Applebury, M. L. (1996). The Photoreceptor Guanylate Cyclase Is an Autophosphorylating Protein Kinase. *Journal of Biological Chemistry*, *271*(43), 27083–27089. https://doi.org/10.1074/jbc.271.43.27083

Applebury, M. L., Antoch, M. P., Baxter, L. C., Chun, L. L. Y., Falk, J. D., Farhangfar, F., Kage, K., Krzystolik, M. G., Lyass, L. A., & Robbins, J. T. (2000). The Murine Cone Photoreceptor. *Neuron*, *27*(3), 513–523. https://doi.org/10.1016/S0896-6273(00)00062-3

Ashman, D. F., Lipton, R., Melicow, M. M., & Price, T. D. (1963). Isolation of adenosine 3′,5′-monophosphate and guanosine 3′,5′-monophosphate from rat urine. *Biochemical and Biophysical Research Communications*, *11*(4), 330–334. https://doi.org/10.1016/0006-291X(63)90566-7

Astakhova, L. A., Samoiliuk, E. V., Govardovskii, V. I., & Firsov, M. L. (2012). cAMP controls rod photoreceptor sensitivity via multiple targets in the phototransduction cascade. *Journal of General Physiology*, *140*(4), 421–433. https://doi.org/10.1085/jgp.201210811

Avesani, A., Bielefeld, L., Weisschuh, N., Marino, V., Mazzola, P., Stingl, K., Haack, T. B., Koch, K.-W., & Dell'Orco, D. (2022). Molecular Properties of Human Guanylate Cyclase-Activating Protein 3 (GCAP3) and Its Possible Association with Retinitis Pigmentosa. *International Journal of Molecular Sciences*, *23*(6), 3240. https://doi.org/10.3390/ijms23063240

Azadi, S., Molday, L. L., & Molday, R. S. (2010). RD3, the protein associated with Leber congenital amaurosis type 12, is required for guanylate cyclase trafficking in photoreceptor cells. *Proceedings of the National Academy of Sciences*, *107*(49), 21158–21163. https://doi.org/10.1073/pnas.1010460107

Baylor, D. A., Lamb, T. D., & Yau, K. W. (1979). Responses of retinal rods to single photons. *The Journal of Physiology*, *288*, 613–634.

Behnen, P., Dell'Orco, D., & Koch, K.-W. (2010). Involvement of the calcium sensor GCAP1 in hereditary cone dystrophies. *Biological Chemistry*, *391*(6). https://doi.org/10.1515/bc.2010.063

Bereta, G., & Palczewski, K. (2011). Heterogeneous N-Terminal Acylation of Retinal Proteins Results from the Retina's Unusual Lipid Metabolism. *Biochemistry*, *50*(18), 3764–3776. https://doi.org/10.1021/bi200245t

Bereta, G., Wang, B., Kiser, P. D., Baehr, W., Jang, G.-F., & Palczewski, K. (2010). A Functional Kinase Homology Domain Is Essential for the Activity of Photoreceptor Guanylate Cyclase 1. *Journal of Biological Chemistry*, *285*(3), 1899–1908. https://doi.org/10.1074/jbc.M109.061713

Bilotta, J., & Saszik, S. (2001). The zebrafish as a model visual system. *International Journal of Developmental Neuroscience*, *19*(7), 621–629. https://doi.org/10.1016/S0736-5748(01)00050-8

Bonì, F., Marino, V., Bidoia, C., Mastrangelo, E., Barbiroli, A., Dell'Orco, D., & Milani, M. (2020). Modulation of Guanylate Cyclase Activating Protein 1 (GCAP1) Dimeric Assembly by Ca2+ or Mg2+: Hints to Understand Protein Activity. *Biomolecules*, *10*(10), 1408. https://doi.org/10.3390/biom10101408

Bredt, D. S., & Snyder, S. H. (1994). NITRIC OXIDE: A Physiologic Messenger Molecule. *Annual Review of Biochemistry*, *63*(1), 175–195. https://doi.org/10.1146/annurev.bi.63.070194.001135

Burns, M. E., & Pugh, E. N. (2010). Lessons from Photoreceptors: Turning Off G-Protein Signaling in Living Cells. *Physiology*, *25*(2), 72–84. https://doi.org/10.1152/physiol.00001.2010

Chao, Y., Chen, C., Lin, Y., Breer, H., Fleischer, J., & Yang, R. (2015). Receptor guanylyl cyclase- G is a novel thermosensory protein activated by cool temperatures. *The EMBO Journal*, *34*(3), 294–306. https://doi.org/10.15252/embj.201489652

Cote, R. (2006). Photoreceptor Phosphodiesterase (PDE6): A G-Protein-Activated PDE Regulating Visual Excitation in Rod and Cone Photoreceptor Cells. In S. Francis, J. Beavo, & M. Houslay (Eds.), *Cyclic*

Nucleotide Phosphodiesterases in Health and Disease. CRC Press. https://doi.org/10.1201/9781420020847.ch8
Curcio, C. A., Sloan, K. R., Kalina, R. E., & Hendrickson, A. E. (1990). Human photoreceptor topography. *Journal of Comparative Neurology*, *292*(4), 497–523. https://doi.org/10.1002/cne.902920402
Dell'Orco, D., Behnen, P., Linse, S., & Koch, K.-W. (2010). Calcium binding, structural stability and guanylate cyclase activation in GCAP1 variants associated with human cone dystrophy. *Cellular and Molecular Life Sciences*, *67*(6), 973–984. https://doi.org/10.1007/s00018-009-0243-8
Dell'Orco, D., & Dal Cortivo, G. (2019). Normal GCAPs partly compensate for altered cGMP signaling in retinal dystrophies associated with mutations in GUCA1A. *Scientific Reports*, *9*(1), 20105. https://doi.org/10.1038/s41598-019-56606-5
Dell'Orco, D., Sulmann, S., Linse, S., & Koch, K.-W. (2012). Dynamics of Conformational Ca^{2+} -Switches in Signaling Networks Detected by a Planar Plasmonic Device. *Analytical Chemistry*, *84*(6), 2982–2989. https://doi.org/10.1021/ac300213j
Derbyshire, E. R., & Marletta, M. A. (2012). Structure and Regulation of Soluble Guanylate Cyclase. *Annual Review of Biochemistry*, *81*(1), 533–559. https://doi.org/10.1146/annurev-biochem-050410-100030
Dizhoor, A. (1994). The human photoreceptor membrane guanylyl cyclase, RetGC, is present in outer segments and is regulated by calcium and a soluble activator. *Neuron*, *12*(6), 1345–1352. https://doi.org/10.1016/0896-6273(94)90449-9
Dizhoor, A. M., Olshevskaya, E. V., Henzel, W. J., Wong, S. C., Stults, J. T., Ankoudinova, I., & Hurley, J. B. (1995). Cloning, Sequencing, and Expression of a 24-kDa Ca2+-binding Protein Activating Photoreceptor Guanylyl Cyclase. *Journal of Biological Chemistry*, *270*(42), 25200–25206. https://doi.org/10.1074/jbc.270.42.25200
Dowling, J. E. (1987). *The retina: An approachable part of the brain.* Harvard University Press.
Dowling, J. E. (2012). The Retina: An Approachable Part of the Brain. *Harvard University Press.*
Duda, T., Fik-Rymarkiewicz, E., Venkataraman, V., Krishnan, R., Koch, K.-W., & Sharma, R. K. (2005). The Calcium-Sensor Guanylate Cyclase Activating Protein Type 2 Specific Site in Rod Outer Segment Membrane Guanylate Cyclase Type 1. *Biochemistry*, *44*(19), 7336–7345. https://doi.org/10.1021/bi050068x
Duda, T., Goraczniak, R. M., & Sharma, R. K. (1996). Molecular Characterization of S100A1-S100B Protein in Retina and Its Activation Mechanism of Bovine Photoreceptor Guanylate Cyclase. *Biochemistry*, *35*(20), 6263–6266. https://doi.org/10.1021/bi960007m
Duda, T., Koch, K. W., Venkataraman, V., Lange, C., Beyermann, M., & Sharma, R. K. (2002). Ca2+ sensor S100beta-modulated sites of membrane guanylate cyclase in thephotoreceptor-bipolar synapse. *The EMBO Journal*, *21*(11), 2547–2556. https://doi.org/10.1093/emboj/21.11.2547
Duda, T., & Koch, K.-W. (2002). Calcium-modulated membrane guanylate cyclase in synaptic transmission? In R. K. Sharma (Ed.), *Guanylate Cyclase* (pp. 107–116). Springer US. https://doi.org/10.1007/978-1-4615-0927-1_8
Duda, T., Pertzev, A., & Sharma, R. K. (2012). Differential Ca^{2+} Sensor Guanylate Cyclase Activating Protein Modes of Photoreceptor Rod Outer Segment Membrane Guanylate Cyclase Signaling. *Biochemistry*, *51*(23), 4650–4657. https://doi.org/10.1021/bi300572w
Duda, T., & Sharma, R. K. (2004). S100B-modulated Ca^{2+} -dependent ROS-GC1 transduction machinery in the gustatory epithelium: A new mechanism in gustatory transduction. *FEBS Letters*, *577*(3), 393–398. https://doi.org/10.1016/j.febslet.2004.09.089
Elbers, D., Scholten, A., & Koch, K.-W. (2018). Zebrafish Recoverin Isoforms Display Differences in Calcium Switch Mechanisms. *Frontiers in Molecular Neuroscience*, *11*. https://doi.org/10.3389/fnmol.2018.00355
Endres, N. F., Barros, T., Cantor, A. J., & Kuriyan, J. (2014). Emerging concepts in the regulation of the EGF receptor and other receptor tyrosine kinases. *Trends in Biochemical Sciences*, *39*(10), 437–446. https://doi.org/10.1016/j.tibs.2014.08.001
Ermilov, A. N., Olshevskaya, E. V., & Dizhoor, A. M. (2001). Instead of Binding Calcium, One of the EF-hand Structures in Guanylyl Cyclase Activating Protein-2 Is Required for Targeting Photoreceptor Guanylyl Cyclase. *Journal of Biological Chemistry*, *276*(51), 48143–48148. https://doi.org/10.1074/jbc.m107539200
Erofeeva, N., Meshalkina, D., & Firsov, M. (2023). Multiple Roles of cAMP in Vertebrate Retina. *Cells*, *12*(8), 1157. https://doi.org/10.3390/cells12081157
Fesenko, E. E., Kolesnikov, S. S., & Lyubarsky, A. L. (1985). Induction by cyclic GMP of cationic conductance in plasma membrane of retinal rod outer segment. *Nature*, *313*(6000), 310–313. https://doi.org/10.1038/313310a0

Fitzpatrick, D. A., O'Halloran, D. M., & Burnell, A. M. (2006). Multiple lineage specific expansions within the guanylyl cyclase gene family. *BMC Evolutionary Biology*, *6*(1), 26. https://doi.org/10.1186/1471-2148-6-26

Fleischman, D., & Denisevich, M. (1979). Guanylate cyclase of isolated bovine retinal rod axonemes. *Biochemistry*, *18*(23), 5060–5066. https://doi.org/10.1021/bi00590a006

Friedman, J. S., Chang, B., Kannabiran, C., Chakarova, C., Singh, H. P., Jalali, S., Hawes, N. L., Branham, K., Othman, M., Filippova, E., Thompson, D. A., Webster, A. R., Andréasson, S., Jacobson, S. G., Bhattacharya, S. S., Heckenlively, J. R., & Swaroop, A. (2006). Premature Truncation of a Novel Protein, RD3, Exhibiting Subnuclear Localization Is Associated with Retinal Degeneration. *The American Journal of Human Genetics*, *79*(6), 1059–1070. https://doi.org/10.1086/510021

Fries, R., Scholten, A., Säftel, W., & Koch, K. (2012). Operation profile of zebrafish guanylate cyclase-activating protein 3. *Journal of Neurochemistry*, *121*(1), 54–65. https://doi.org/10.1111/j.1471-4159.2011.07643.x

Frins, S., Bönigk, W., Müller, F., Kellner, R., & Koch, K.-W. (1996). Functional Characterization of a Guanylyl Cyclase-activating Protein from Vertebrate Rods. *Journal of Biological Chemistry*, *271*(14), 8022–8027. https://doi.org/10.1074/jbc.271.14.8022

Fu, Y., & Yau, K.-W. (2007). Phototransduction in mouse rods and cones. *Pflügers Archiv - European Journal of Physiology*, *454*(5), 805–819. https://doi.org/10.1007/s00424-006-0194-y

Gajiwala, K. S., & Burley, S. K. (2000). Winged helix proteins. *Current Opinion in Structural Biology*, *10*(1), 110–116. https://doi.org/10.1016/S0959-440X(99)00057-3

Goraczniak, R., Duda, T., & Sharma, R. K. (1997). Structural and Functional Characterization of a Second Subfamily Member of the Calcium-Modulated Bovine Rod Outer Segment Membrane Guanylate Cyclase, ROS-GC2. *Biochemical and Biophysical Research Communications*, *234*(3), 666–670. https://doi.org/10.1006/bbrc.1997.6579

Goraczniak, R. M., Duda, T., Sitaramayya, A., & Sharma, R. K. (1994). Structural and functional characterization of the rod outer segment membrane guanylate cyclase. *Biochemical Journal*, *302*(2), 455–461. https://doi.org/10.1042/bj3020455

Gorczyca, W. A., Polans, A. S., Surgucheva, I. G., Subbaraya, I., Baehr, W., & Palczewski, K. (1995). Guanylyl Cyclase Activating Protein. *Journal of Biological Chemistry*, *270*(37), 22029–22036. https://doi.org/10.1074/jbc.270.37.22029

Haeseleer, F., Sokal, I., Li, N., Pettenati, M., Rao, N., Bronson, D., Wechter, R., Baehr, W., & Palczewski, K. (1999). Molecular Characterization of a Third Member of the Guanylyl Cyclase-activating Protein Subfamily. *Journal of Biological Chemistry*, *274*(10), 6526–6535. https://doi.org/10.1074/jbc.274.10.6526

Hallett, M. A., Delaat, J. L., Arikawa, K., Schlamp, C. L., Kong, F., & Williams, D. S. (1996). Distribution of guanylate cyclase within photoreceptor outer segments. *Journal of Cell Science*, *109*(7), 1803–1812. https://doi.org/10.1242/jcs.109.7.1803

Hayashi, F., & Yamazaki, A. (1991). Polymorphism in purified guanylate cyclase from vertebrate rod photoreceptors. *Proceedings of the National Academy of Sciences*, *88*(11), 4746–4750. https://doi.org/10.1073/pnas.88.11.4746

Hecht, S., Shlaer, S., & Pirenne, M. H. (1942). ENERGY, QUANTA, AND VISION. *Journal of General Physiology*, *25*(6), 819–840. https://doi.org/10.1085/jgp.25.6.819

Helten, A., Säftel, W., & Koch, K. (2007). Expression level and activity profile of membrane bound guanylate cyclase type 2 in rod outer segments. *Journal of Neurochemistry*, *103*(4), 1439–1446. https://doi.org/10.1111/j.1471-4159.2007.04923.x

Hoon, M., Okawa, H., Della Santina, L., & Wong, R. O. L. (2014). Functional architecture of the retina: Development and disease. *Progress in Retinal and Eye Research*, *42*, 44–84. https://doi.org/10.1016/j.preteyeres.2014.06.003

Hurley, J. H. (1999). Structure, Mechanism, and Regulation of Mammalian Adenylyl Cyclase. *Journal of Biological Chemistry*, *274*(12), 7599–7602. https://doi.org/10.1074/jbc.274.12.7599

Hwang, J., Lange, C., Helten, A., Höppner-Heitmann, D., Duda, T., Sharma, R. K., & Koch, K. (2003). Regulatory modes of rod outer segment membrane guanylate cyclase differ in catalytic efficiency and Ca^{2+} -sensitivity. *European Journal of Biochemistry*, *270*(18), 3814–3821. https://doi.org/10.1046/j.1432-1033.2003.03770.x

Hwang, J.-Y., & Koch, K.-W. (2002). Calcium- and Myristoyl-Dependent Properties of Guanylate Cyclase-Activating Protein-1 and Protein-2. *Biochemistry*, *41*(43), 13021–13028. https://doi.org/10.1021/bi026618y

Imanishi, Y., Yang, L., Sokal, I., Filipek, S., Palczewski, K., & Baehr, W. (2004). Diversity of Guanylate Cyclase-Activating Proteins (GCAPs) in Teleost Fish: Characterization of Three Novel GCAPs (GCAP4, GCAP5, GCAP7) from Zebrafish (Danio rerio) and Prediction of Eight GCAPs (GCAP1-8)

in Pufferfish (Fugu rubripes). *Journal of Molecular Evolution*, *59*(2), 204–217. https://doi.org/10.1007/s00239-004-2614-y

Iribarne, M., & Masai, I. (2017). Neurotoxicity of cGMP in the vertebrate retina: From the initial research on *rd* mutant mice to zebrafish genetic approaches. *Journal of Neurogenetics*, *31*(3), 88–101. https://doi.org/10.1080/01677063.2017.1358268

Jacobson, S. G., Cideciyan, A. V., Peshenko, I. V., Sumaroka, A., Olshevskaya, E. V., Cao, L., Schwartz, S. B., Roman, A. J., Olivares, M. B., Sadigh, S., Yau, K.-W., Heon, E., Stone, E. M., & Dizhoor, A. M. (2013). Determining consequences of retinal membrane guanylyl cyclase (RetGC1) deficiency in human Leber congenital amaurosis en route to therapy: Residual cone-photoreceptor vision correlates with biochemical properties of the mutants. *Human Molecular Genetics*, *22*(1), 168–183. https://doi.org/10.1093/hmg/dds421

Jankowska, A., Sharma, R. K., & Duda, T. (2014). Ca2+-modulated ROS-GC1 transduction system in testes and its presence in the spermatogenic cells. *Frontiers in Molecular Neuroscience*, *7*. https://doi.org/10.3389/fnmol.2014.00034

Karan, S., Frederick, J. M., & Baehr, W. (2010). Novel functions of photoreceptor guanylate cyclases revealed by targeted deletion. *Molecular and Cellular Biochemistry*, *334*(1–2), 141–155. https://doi.org/10.1007/s11010-009-0322-z

Katsuki, S., Arnold, W., Mittal, C., & Murad, F. (1977). Stimulation of guanylate cyclase by sodium nitroprusside, nitroglycerin and nitric oxide in various tissue preparations and comparison to the effects of sodium azide and hydroxylamine. *Journal of Cyclic Nucleotide Research*, *3*(1), 23–35.

Koch, K., Stecher, P., & Kellner, R. (1994). Bovine retinal rod guanyl cyclase represents a new N-glycosylated subtype of membrane-bound guanyl cyclases. *European Journal of Biochemistry*, *222*(2), 589–595. https://doi.org/10.1111/j.1432-1033.1994.tb18901.x

Koch, K. W. (1991). Purification and identification of photoreceptor guanylate cyclase. *Journal of Biological Chemistry*, *266*(13), 8634–8637. https://doi.org/10.1016/S0021-9258(18)93021-8

Koch, K.-W. (2013). The guanylate cyclase signaling system in zebrafish photoreceptors. *FEBS Letters*, *587*(13), 2055–2059. https://doi.org/10.1016/j.febslet.2013.04.023

Koch, K.-W. (2023). Molecular tuning of calcium dependent processes by neuronal calcium sensor proteins in the retina. *Biochimica et Biophysica Acta (BBA) - Molecular Cell Research*, *1870*(6), 119491. https://doi.org/10.1016/j.bbamcr.2023.119491

Koch, K.-W., & Dell'Orco, D. (2013). A Calcium-Relay Mechanism in Vertebrate Phototransduction. *ACS Chemical Neuroscience*, *4*(6), 909–917. https://doi.org/10.1021/cn400027z

Koch, K.-W., & Dell'Orco, D. (2015). Protein and Signaling Networks in Vertebrate Photoreceptor Cells. *Frontiers in Molecular Neuroscience*, *8*. https://doi.org/10.3389/fnmol.2015.00067

Koch, K.-W., Duda, T., & Sharma, R. K. (2002). Photoreceptor specific guanylate cyclases in vertebrate phototransduction. *Molecular and Cellular Biochemistry*, *230*(1–2), 97–106.

Koch, K.-W., & Stryer, L. (1988). Highly cooperative feedback control of retinal rod guanylate cyclase by calcium ions. *Nature*, *334*(6177), 64–66. https://doi.org/10.1038/334064a0

Körschen, H. G., Beyermann, M., Müller, F., Heck, M., Vantler, M., Koch, K.-W., Kellner, R., Wolfrum, U., Bode, C., Hofmann, K. P., & Kaupp, U. B. (1999). Interaction of glutamic-acid-rich proteins with the cGMP signalling pathway in rod photoreceptors. *Nature*, *400*(6746), 761–766. https://doi.org/10.1038/23468

Kuhn, M. (2016). Molecular Physiology of Membrane Guanylyl Cyclase Receptors. *Physiological Reviews*, *96*(2), 751–804. https://doi.org/10.1152/physrev.00022.2015

Kukekova, A. V., Goldstein, O., Johnson, J. L., Richardson, M. A., Pearce-Kelling, S. E., Swaroop, A., Friedman, J. S., Aguirre, G. D., & Acland, G. M. (2009). Canine RD3 mutation establishes rod-cone dysplasia type 2 (rcd2) as ortholog of human and murine rd3. *Mammalian Genome*, *20*(2), 109–123. https://doi.org/10.1007/s00335-008-9163-4

Lange, C., Duda, T., Beyermann, M., Sharma, R. K., & Koch, K.-W. (1999). Regions in vertebrate photoreceptor guanylyl cyclase ROS-GC1 involved in Ca^{2+} -dependent regulation by guanylyl cyclase-activating protein GCAP-1. *FEBS Letters*, *460*(1), 27–31. https://doi.org/10.1016/S0014-5793(99)01312-5

Laura, R. P., Dizhoor, A. M., & Hurley, J. B. (1996). The Membrane Guanylyl Cyclase, Retinal Guanylyl Cyclase-1, Is Activated through Its Intracellular Domain. *Journal of Biological Chemistry*, *271*(20), 11646–11651. https://doi.org/10.1074/jbc.271.20.11646

Lavorgna, G., Lestingi, M., Ziviello, C., Testa, F., Simonelli, F., Manitto, M. P., Brancato, R., Ferrari, M., Rinaldi, E., Ciccodicola, A., & Banfi, S. (2003). Identification and characterization of C1orf36, a transcript highly expressed in photoreceptor cells, and mutation analysis in retinitis pigmentosa. *Biochemical and Biophysical Research Communications*, *308*(3), 414–421. https://doi.org/10.1016/S0006-291X(03)01410-4

Lim, S., Peshenko, I., Dizhoor, A., & Ames, J. B. (2009). Effects of Ca^{2+} , Mg^{2+} , and Myristoylation on Guanylyl Cyclase Activating Protein 1 Structure and Stability. *Biochemistry*, *48*(5), 850–862. https://doi.org/10.1021/bi801897p

Lim, S., Roseman, G., Peshenko, I., Manchala, G., Cudia, D., Dizhoor, A. M., Millhauser, G., & Ames, J. B. (2018). Retinal guanylyl cyclase activating protein 1 forms a functional dimer. *PLOS ONE*, *13*(3), e0193947. https://doi.org/10.1371/journal.pone.0193947

Lim, S., Scholten, A., Manchala, G., Cudia, D., Zlomke-Sell, S.-K., Koch, K.-W., & Ames, J. B. (2017). Structural Characterization of Ferrous Ion Binding to Retinal Guanylate Cyclase Activator Protein 5 from Zebrafish Photoreceptors. *Biochemistry*, *56*(51), 6652–6661. https://doi.org/10.1021/acs.biochem.7b01029

Liu, Y., Ruoho, A. E., Rao, V. D., & Hurley, J. H. (1997). Catalytic mechanism of the adenylyl and guanylyl cyclases: Modeling and mutational analysis. *Proceedings of the National Academy of Sciences*, *94*(25), 13414–13419. https://doi.org/10.1073/pnas.94.25.13414

López-Begines, S., Plana-Bonamaisó, A., & Méndez, A. (2018). Molecular determinants of Guanylate Cyclase Activating Protein subcellular distribution in photoreceptor cells of the retina. *Scientific Reports*, *8*(1), 2903. https://doi.org/10.1038/s41598-018-20893-1

Lowe, D. G., Dizhoor, A. M., Liu, K., Gu, Q., Spencer, M., Laura, R., Lu, L., & Hurley, J. B. (1995). Cloning and expression of a second photoreceptor-specific membrane retina guanylyl cyclase (RetGC), RetGC-2. *Proceedings of the National Academy of Sciences*, *92*(12), 5535–5539. https://doi.org/10.1073/pnas.92.12.5535

Marino, V., Sulmann, S., Koch, K.-W., & Dell'Orco, D. (2015). Structural effects of Mg2+ on the regulatory states of three neuronal calcium sensors operating in vertebrate phototransduction. *Biochimica et Biophysica Acta (BBA) - Molecular Cell Research*, *1853*(9), 2055–2065. https://doi.org/10.1016/j.bbamcr.2014.10.026

Maruyama, I. N. (2015). Activation of transmembrane cell-surface receptors via a common mechanism? The "rotation model." *BioEssays*, *37*(9), 959–967. https://doi.org/10.1002/bies.201500041

Matthews, E. E., Zoonens, M., & Engelman, D. M. (2006). Dynamic Helix Interactions in Transmembrane Signaling. *Cell*, *127*(3), 447–450. https://doi.org/10.1016/j.cell.2006.10.016

Mendez, A., Burns, M. E., Sokal, I., Dizhoor, A. M., Baehr, W., Palczewski, K., Baylor, D. A., & Chen, J. (2001). Role of guanylate cyclase-activating proteins (GCAPs) in setting the flash sensitivity of rod photoreceptors. *Proceedings of the National Academy of Sciences*, *98*(17), 9948–9953. https://doi.org/10.1073/pnas.171308998

Misono, K. S., Philo, J. S., Arakawa, T., Ogata, C. M., Qiu, Y., Ogawa, H., & Young, H. S. (2011). Structure, signaling mechanism and regulation of the natriuretic peptide receptor guanylate cyclase. *The FEBS Journal*, *278*(11), 1818–1829. https://doi.org/10.1111/j.1742-4658.2011.08083.x

Nakatani, K., Chen, C., Yau, K.-W., & Koutalos, Y. (2002). Calcium and Phototransduction. In W. Baehr & K. Palczewski (Eds.), *Photoreceptors and Calcium* (Vol. 514, pp. 1–20). Springer US. https://doi.org/10.1007/978-1-4615-0121-3_1

Oliveira, L., Miniou, P., Viegas-Pequignot, E., Rozet, J.-M., Dollfus, H., & Pittler, S. J. (1994). Human Retinal Guanylate Cyclase (GUC2D) Maps to Chromosome 17p13.1. *Genomics*, *22*(2), 478–481. https://doi.org/10.1006/geno.1994.1415

Olshevskaya, E. V., Ermilov, A. N., & Dizhoor, A. M. (1999). Dimerization of Guanylyl Cyclase-activating Protein and a Mechanism of Photoreceptor Guanylyl Cyclase Activation. *Journal of Biological Chemistry*, *274*(36), 25583–25587. https://doi.org/10.1074/jbc.274.36.25583

Olshevskaya, E. V., Hughes, R. E., Hurley, J. B., & Dizhoor, A. M. (1997). Calcium Binding, but Not a Calcium-Myristoyl Switch, Controls the Ability of Guanylyl Cyclase-activating Protein GCAP-2 to Regulate Photoreceptor Guanylyl Cyclase. *Journal of Biological Chemistry*, *272*(22), 14327–14333. https://doi.org/10.1074/jbc.272.22.14327

Otto-Bruc, A., Fariss, R. N., Haeseleer, F., Huang, J., Surgucheva, J. B., Irina, Baehr, W., Milam, A. H., & Palczewski, K. (1997). Localization of guanylate cyclase-activating protein 2 in mammalian retinas. *Proceedings of the National Academy of Sciences*, *94*(9), 4727–4732. https://doi.org/10.1073/pnas.94.9.4727

Palczewski, K., Sokal, I., & Baehr, W. (2004). Guanylate cyclase-activating proteins: Structure, function, and diversity. *Biochemical and Biophysical Research Communications*, *322*(4), 1123–1130. https://doi.org/10.1016/j.bbrc.2004.07.122

Palczewski, K., Subbaraya, I., Gorczyca, W. A., Helekar, B. S., Ruiz, C. C., Ohguro, H., Huang, J., Zhao, X., Crabb, J. W., Johnson, R. S., Walsh, K. A., Gray-Keller, M. P., Detwiler, P. B., & Baehr, W. (1994). Molecular cloning and characterization of retinal photoreceptor guanylyl cyclase-activating protein. *Neuron*, *13*(2), 395–404. https://doi.org/10.1016/0896-6273(94)90355-7

Parat, M., Blanchet, J., & De Léan, A. (2010). Role of Juxtamembrane and Transmembrane Domains in the Mechanism of Natriuretic Peptide Receptor A Activation. *Biochemistry*, *49*(22), 4601–4610. https://doi.org/10.1021/bi901711w

Payne, A. (1998). A mutation in guanylate cyclase activator 1A (GUCA1A) in an autosomal dominant cone dystrophy pedigree mapping to a new locus on chromosome 6p21.1. *Human Molecular Genetics*, *7*(2), 273–277. https://doi.org/10.1093/hmg/7.2.273

Peshenko, I. V., & Dizhoor, A. M. (2006). Ca2+ and Mg2+ Binding Properties of GCAP-1. *Journal of Biological Chemistry*, *281*(33), 23830–23841. https://doi.org/10.1074/jbc.M600257200

Peshenko, I. V., Olshevskaya, E. V., Azadi, S., Molday, L. L., Molday, R. S., & Dizhoor, A. M. (2011). Retinal Degeneration 3 (RD3) Protein Inhibits Catalytic Activity of Retinal Membrane Guanylyl Cyclase (RetGC) and Its Stimulation by Activating Proteins. *Biochemistry*, *50*(44), 9511–9519. https://doi.org/10.1021/bi201342b

Peshenko, I. V., Olshevskaya, E. V., & Dizhoor, A. M. (2015). Dimerization Domain of Retinal Membrane Guanylyl Cyclase 1 (RetGC1) Is an Essential Part of Guanylyl Cyclase-activating Protein (GCAP) Binding Interface. *Journal of Biological Chemistry*, *290*(32), 19584–19596. https://doi.org/10.1074/jbc.M115.661371

Peshenko, I. V., Olshevskaya, E. V., & Dizhoor, A. M. (2016). Functional Study and Mapping Sites for Interaction with the Target Enzyme in Retinal Degeneration 3 (RD3) Protein. *Journal of Biological Chemistry*, *291*(37), 19713–19723. https://doi.org/10.1074/jbc.M116.742288

Peshenko, I. V., Olshevskaya, E. V., Lim, S., Ames, J. B., & Dizhoor, A. M. (2012). Calcium-Myristoyl Tug Is a New Mechanism for Intramolecular Tuning of Calcium Sensitivity and Target Enzyme Interaction for Guanylyl Cyclase-activating Protein 1. *Journal of Biological Chemistry*, *287*(17), 13972–13984. https://doi.org/10.1074/jbc.M112.341883

Peshenko, I. V., Olshevskaya, E. V., Lim, S., Ames, J. B., & Dizhoor, A. M. (2014). Identification of Target Binding Site in Photoreceptor Guanylyl Cyclase-activating Protein 1 (GCAP1). *Journal of Biological Chemistry*, *289*(14), 10140–10154. https://doi.org/10.1074/jbc.M113.540716

Peshenko, I. V., Olshevskaya, E. V., Savchenko, A. B., Karan, S., Palczewski, K., Baehr, W., & Dizhoor, A. M. (2011). Enzymatic Properties and Regulation of the Native Isozymes of Retinal Membrane Guanylyl Cyclase (RetGC) from Mouse Photoreceptors. *Biochemistry*, *50*(25), 5590–5600. https://doi.org/10.1021/bi200491b

Peshenko, I. V., Olshevskaya, E. V., Yao, S., Ezzeldin, H. H., Pittler, S. J., & Dizhoor, A. M. (2010). Activation of Retinal Guanylyl Cyclase RetGC1 by GCAP1: Stoichiometry of Binding and Effect of New LCA-Related Mutations. *Biochemistry*, *49*(4), 709–717. https://doi.org/10.1021/bi901495y

Pettelkau, J., Thondorf, I., Theisgen, S., Lilie, H., Schröder, T., Arlt, C., Ihling, C. H., & Sinz, A. (2013). Structural Analysis of Guanylyl Cyclase-Activating Protein-2 (GCAP-2) Homodimer by Stable Isotope-Labeling, Chemical Cross-Linking, and Mass Spectrometry. *Journal of the American Society for Mass Spectrometry*, *24*(12), 1969–1979. https://doi.org/10.1007/s13361-013-0734-6

Pugh, E. N., Duda, T., Sitaramayya, A., & Sharma, R. K. (1997). Photoreceptor Guanylate Cyclases: A Review. *Bioscience Reports*, *17*(5), 429–473. https://doi.org/10.1023/A:1027365520442

Pugh, E. N., & Lamb, T. D. (2000). Chapter 5 Phototransduction in vertebrate rods and cones: Molecular mechanisms of amplification, recovery and light adaptation. In *Handbook of Biological Physics* (Vol. 3, pp. 183–255). Elsevier. https://doi.org/10.1016/S1383-8121(00)80008-1

Ramamurthy, V., Tucker, C., Wilkie, S. E., Daggett, V., Hunt, D. M., & Hurley, J. B. (2001). Interactions within the Coiled-coil Domain of RetGC-1 Guanylyl Cyclase Are Optimized for Regulation Rather than for High Affinity. *Journal of Biological Chemistry*, *276*(28), 26218–26229. https://doi.org/10.1074/jbc.M010495200

Rätscho, N., Scholten, A., & Koch, K.-W. (2009). Expression profiles of three novel sensory guanylate cyclases and guanylate cyclase-activating proteins in the zebrafish retina. *Biochimica et Biophysica Acta (BBA) - Molecular Cell Research*, *1793*(6), 1110–1114. https://doi.org/10.1016/j.bbamcr.2008.12.021

Rätscho, N., Scholten, A., & Koch, K.-W. (1/2010b). Diversity of sensory guanylate cyclases in teleost fishes. *Molecular and Cellular Biochemistry*, *334*(1–2), 207–214. https://doi.org/10.1007/s11010-009-0320-1

Ravichandran, S. (2017). Membrane Guanylate Cyclase catalytic Subdomain: Structure and Linkage with Calcium Sensors and Bicarbonate. *Frontiers in Molecular Neuroscience*, *10*. https://doi.org/10.3389/fnmol.2017.00173

Rehkamp, A., Tänzler, D., Tüting, C., Kastritis, P. L., Iacobucci, C., Ihling, C. H., Kipping, M., Koch, K.-W., & Sinz, A. (2021). First 3D-Structural Data of Full-Length Guanylyl Cyclase 1 in Rod-Outer-Segment Preparations of Bovine Retina by Cross-Linking/Mass Spectrometry. *Journal of Molecular Biology*, *433*(10), 166947. https://doi.org/10.1016/j.jmb.2021.166947

Rieke, F. (2000). Mechanisms of single-photon detection in Rod photoreceptors. In *Methods in Enzymology* (Vol. 316, pp. 186–202). Elsevier. https://doi.org/10.1016/S0076-6879(00)16724-2

Rosenzweig, D. H., Saidas Nair, K., Levay, K., Peshenko, I. V., Crabb, J. W., Dizhoor, A. M., & Slepak, V. Z. (2009). Interaction of retinal guanylate cyclase with the α subunit of transducin: Potential role in transducin localization. *Biochemical Journal*, *417*(3), 803–812. https://doi.org/10.1042/BJ20081513

Russwurm, M., & Koesling, D. (2002). Isoforms of NO-sensitive guanylyl cyclase. *Molecular and Cellular Biochemistry*, *230*(1/2), 159–164. https://doi.org/10.1023/A:1014252309493

Saha, S., Biswas, K. H., Kondapalli, C., Isloor, N., & Visweswariah, S. S. (2009). The Linker Region in Receptor Guanylyl Cyclases Is a Key Regulatory Module. *Journal of Biological Chemistry*, *284*(40), 27135–27145. https://doi.org/10.1074/jbc.M109.020032

Scholich, K., Barbier, A. J., Mullenix, J. B., & Patel, T. B. (1997). Characterization of soluble forms of nonchimeric type V adenylyl cyclases. *Proceedings of the National Academy of Sciences*, *94*(7), 2915–2920. https://doi.org/10.1073/pnas.94.7.2915

Scholten, A., & Koch, K. W. (2011). Differential calcium signaling by cone specific guanylate cyclase-activating proteins from the zebrafish retina. *PLoS ONE*, *6*(8), e23117. https://doi.org/10.1371/journal.pone.0023117

Schrem, A., Lange, C., Beyermann, M., & Koch, K.-W. (1999). Identification of a Domain in Guanylyl Cyclase-activating Protein 1 That Interacts with a Complex of Guanylyl Cyclase and Tubulin in Photoreceptors. *Journal of Biological Chemistry*, *274*(10), 6244–6249. https://doi.org/10.1074/jbc.274.10.6244

Seebacher, T., Beitz, E., Kumagami, H., Wild, K., Ruppersberg, J. P., & Schultz, J. E. (1999). Expression of membrane-bound and cytosolic guanylyl cyclases in the rat inner ear. *Hearing Research*, *127*(1–2), 95–102. https://doi.org/10.1016/S0378-5955(98)00176-2

Seno, K., Kishigami, A., Ihara, S., Maeda, T., Bondarenko, V. A., Nishizawa, Y., Usukura, J., Yamazaki, A., & Hayashi, F. (1998). A Possible Role of RGS9 in Phototransduction. *Journal of Biological Chemistry*, *273*(35), 22169–22172. https://doi.org/10.1074/jbc.273.35.22169

Serfass, L., Carr, H. S., Aschenbrenner, L. M., & Burstyn, J. N. (2001). Calcium Ion Downregulates Soluble Guanylyl Cyclase Activity: Evidence for a Two-metal Ion Catalytic Mechanism. *Archives of Biochemistry and Biophysics*, *387*(1), 47–56. https://doi.org/10.1006/abbi.2000.2090

Shahu, M. K., Schuhmann, F., Scholten, A., Solov'yov, I. A., & Koch, K. W. (2022). The Transition of Photoreceptor Guanylate Cyclase Type 1 to the Active State. *International Journal of Molecular Sciences*, *23*(7), 4030. https://doi.org/10.3390/ijms23074030

Sharma, R. K., & Duda, T. (2012). Ca2+-sensors and ROS-GC: Interlocked sensory transduction elements: a review. *Frontiers in Molecular Neuroscience*, *5*. https://doi.org/10.3389/fnmol.2012.00042

Sharon, D., Wimberg, H., Kinarty, Y., & Koch, K.-W. (2018). Genotype-functional-phenotype correlations in photoreceptor guanylate cyclase (GC-E) encoded by GUCY2D. *Progress in Retinal and Eye Research*, *63*, 69–91. https://doi.org/10.1016/j.preteyeres.2017.10.003

Sokal, I., Li, N., Surgucheva, I., Warren, M. J., Payne, A. M., Bhattacharya, S. S., Baehr, W., & Palczewski, K. (1998). GCAP1(Y99C) Mutant Is Constitutively Active in Autosomal Dominant Cone Dystrophy. *Molecular Cell*, *2*(1), 129–133. https://doi.org/10.1016/S1097-2765(00)80121-5

Stenkamp, D. L. (2015). Development of the Vertebrate Eye and Retina. In *Progress in Molecular Biology and Translational Science* (Vol. 134, pp. 397–414). Elsevier. https://doi.org/10.1016/bs.pmbts.2015.06.006

Stephen, R., Bereta, G., Golczak, M., Palczewski, K., & Sousa, M. C. (2007). Stabilizing Function for Myristoyl Group Revealed by the Crystal Structure of a Neuronal Calcium Sensor, Guanylate Cyclase-Activating Protein 1. *Structure*, *15*(11), 1392–1402. https://doi.org/10.1016/j.str.2007.09.013

Stone, J. R., & Marletta, M. A. (1995). Heme Stoichiometry of Heterodimeric Soluble Guanylate Cyclase. *Biochemistry*, *34*(45), 14668–14674. https://doi.org/10.1021/bi00045a007

Subbaraya, I., Ruiz, C. C., Helekar, B. S., Zhao, X., Gorczyca, W. A., Pettenati, M. J., Rao, P. N., Palczewski, K., & Baehr, W. (1994). Molecular characterization of human and mouse photoreceptor guanylate cyclase-activating protein (GCAP) and chromosomal localization of the human gene. *The Journal of Biological Chemistry*, *269*(49), 31080–31089.

Sulmann, S., Kussrow, A., Bornhop, D. J., & Koch, K.-W. (2017). Label-free quantification of calcium-sensor targeting to photoreceptor guanylate cyclase and rhodopsin kinase by backscattering interferometry. *Scientific Reports*, *7*(1), 45515. https://doi.org/10.1038/srep45515

Surguchov, A., Bronson, J. D., Banerjee, P., Knowles, J. A., Ruiz, C., Subbaraya, I., Palczewski, K., & Baehr, W. (1997). The Human GCAP1 and GCAP2 Genes Are Arranged in a Tail-to-Tail Array on the Short Arm of Chromosome 6 (p21.1). *Genomics*, *39*(3), 312–322. https://doi.org/10.1006/geno.1996.4513

Tesmer, J. J. G., Sunahara, R. K., Gilman, A. G., & Sprang, S. R. (1997). Crystal Structure of the Catalytic Domains of Adenylyl Cyclase in a Complex with $G_{s\alpha}$ ·GTPγS. *Science*, *278*(5345), 1907–1916. https://doi.org/10.1126/science.278.5345.1907

Tesmer, J. J. G., Sunahara, R. K., Johnson, R. A., Gosselin, G., Gilman, A. G., & Sprang, S. R. (1999). Two-Metal-Ion Catalysis in Adenylyl Cyclase. *Science*, *285*(5428), 756–760. https://doi.org/10.1126/science.285.5428.756

Theisgen, S., Thomas, L., Schröder, T., Lange, C., Kovermann, M., Balbach, J., & Huster, D. (2011). The presence of membranes or micelles induces structural changes of the myristoylated guanylate-cyclase activating protein-2. *European Biophysics Journal*, *40*(4), 565–576. https://doi.org/10.1007/s00249-011-0680-9

Tucker, C. L., Hurley, J. H., Miller, T. R., & Hurley, J. B. (1998). Two amino acid substitutions convert a guanylyl cyclase, RetGC-1, into an adenylyl cyclase. *Proceedings of the National Academy of Sciences*, *95*(11), 5993–5997. https://doi.org/10.1073/pnas.95.11.5993

Venkataraman, V., Duda, T., Ravichandran, S., & Sharma, R. K. (2008). Neurocalcin δ Modulation of ROS-GC1, a New Model of Ca^{2+} Signaling. *Biochemistry*, *47*(25), 6590–6601. https://doi.org/10.1021/bi800394s

Vinberg, F., Peshenko, I. V., Chen, J., Dizhoor, A. M., & Kefalov, V. J. (2018). Guanylate cyclase–activating protein 2 contributes to phototransduction and light adaptation in mouse cone photoreceptors. *Journal of Biological Chemistry*, *293*(19), 7457–7465. https://doi.org/10.1074/jbc.ra117.001574

Viviano, J., Krishnan, A., Wu, H., & Venkataraman, V. (2016). Electrophoretic mobility shift in native gels indicates calcium-dependent structural changes of neuronal calcium sensor proteins. *Analytical Biochemistry*, *494*, 93–100. https://doi.org/10.1016/j.ab.2015.11.005

Walls, G. L. (1942). *The vertebrate eye and its adaptive radiation [by] Gordon Lynn Walls.* Cranbrook Institute of Science,. https://doi.org/10.5962/bhl.title.7369

Wässle, H. (2004). Parallel processing in the mammalian retina. *Nature Reviews Neuroscience*, *5*(10), 747–757. https://doi.org/10.1038/nrn1497

Wen, X.-H., Dizhoor, A. M., & Makino, C. L. (2014). Membrane guanylyl cyclase complexes shape the photoresponses of retinal rods and cones. *Frontiers in Molecular Neuroscience*, *7*. https://doi.org/10.3389/fnmol.2014.00045

Wen, X.-H., Duda, T., Pertzev, A., Venkataraman, V., Makino, C. L., & Sharma, R. K. (2012). S100B Serves as a Ca^{2+} Sensor for ROS-GC1 Guanylate Cyclase in Cones but not in Rods of the Murine Retina. *Cellular Physiology and Biochemistry*, *29*(3–4), 417–430. https://doi.org/10.1159/000338496

Wilkie, S. E., Li, Y., Deery, E. C., Newbold, R. J., Garibaldi, D., Bateman, J. B., Zhang, H., Lin, W., Zack, D. J., Bhattacharya, S. S., Warren, M. J., Hunt, D. M., & Zhang, K. (2001). Identification and Functional Consequences of a New Mutation (E155G) in the Gene for GCAP1 That Causes Autosomal Dominant Cone Dystrophy. *The American Journal of Human Genetics*, *69*(3), 471–480. https://doi.org/10.1086/323265

Wimberg, H., Lev, D., Yosovich, K., Namburi, P., Banin, E., Sharon, D., & Koch, K. W. (2018). Photoreceptor Guanylate Cyclase (GUCY2D) Mutations Cause Retinal Dystrophies by Severe Malfunction of Ca2+-Dependent Cyclic GMP Synthesis. *Frontiers in Molecular Neuroscience*, *11*. https://doi.org/10.3389/fnmol.2018.00348

Winger, J. A., Derbyshire, E. R., Lamers, M. H., Marletta, M. A., & Kuriyan, J. (2008). The crystal structure of the catalytic domain of a eukaryotic guanylate cyclase. *BMC Structural Biology*, *8*(1), 42. https://doi.org/10.1186/1472-6807-8-42

Yoshimura, M., & Cooper, D. M. (1992). Cloning and expression of a Ca(2+)-inhibitable adenylyl cyclase from NCB-20 cells. *Proceedings of the National Academy of Sciences*, *89*(15), 6716–6720. https://doi.org/10.1073/pnas.89.15.6716

Zägel, P., Dell'Orco, D., & Koch, K.-W. (2013). The Dimerization Domain in Outer Segment Guanylate Cyclase Is a Ca^{2+} -Sensitive Control Switch Module. *Biochemistry*, *52*(30), 5065–5074. https://doi.org/10.1021/bi400288p

Zulliger, R., Naash, M. I., Rajala, R. V. S., Molday, R. S., & Azadi, S. (2015). Impaired Association of Retinal Degeneration-3 with Guanylate Cyclase-1 and Guanylate Cyclase-activating Protein-1 Leads to Leber Congenital Amaurosis-1. *Journal of Biological Chemistry*, *290*(6), 3488–3499. https://doi.org/10.1074/jbc.M114.616656

List of publications and conference

Published:

1. Shahu, M. K., Schuhmann, F., Scholten, A., Solov'yov, I. A., & Koch, K. W. (2022). The Transition of Photoreceptor Guanylate Cyclase Type 1 to the Active State. *International journal of molecular sciences*, *23*(7), 4030. https://doi.org/10.3390/ijms23074030

2. Shahu, M. K., Schuhmann, F., Wong, S. Y., Solov'yov, I. A., & Koch, K. W. (2024). Allosteric Communication of the Dimerization and the Catalytic Domain in Photoreceptor Guanylate Cyclase. *Biochemistry*, *63*(17), 2131–2140. https://doi.org/10.1021/acs.biochem.4c00170

3. Cudia, D., Roseman, G. P., Assafa, T. E., Shahu, M. K., Scholten, A., Menke-Sell, S. K., Yamada, H., Koch, K. W., Milhauser, G., & Ames, J. B. (2021). NMR and EPR-DEER Structure of a Dimeric Guanylate Cyclase Activator Protein-5 from Zebrafish Photoreceptors. *Biochemistry*, *60*(41), 3058–3070. https://doi.org/10.1021/acs.biochem.1c00612

Conference:

Poster presentation:

1. Kick-off and farewell meeting 2019. Activity control of membrane bound guanylate cyclase. Uol, Germany
2. FENS Forum 2022. The Transition of photoreceptor guanylate cyclase 1 to the active state. Paris

Oral presentation:

1. RTG Summer- Symposium 2022. Regulatory features of GCAP-dependent control of guanylate cyclase activity. Berlin
2. ENCODS 2023. Primary steps in seeing-second messenger homeostasis in photoreceptor cells. Faro

Orga event:

Christmas Party
 Meet the postdoc- online networking event
 RTG- Summer Symposium

Participation in the following Research Training Group events:
 RTG SensoryBio Lecture: Basic Principles and Concepts in Physics, Chemistry and Biology
 RTG SensoryBio Lecture: The physics and biology of sensory stimuli and systems
 Group seminar: Biochemistry of Signaltransduction?

 Weekly Seminar of the RTG SensoryBio
 Kick-off and farewell meeting of the DFG research training group molecular basis of sensory biology 1885
(2019)
 Oltech: Scientific Image Processing and Analysis (Biovoxxel- Dr. Jan Brocher) March 24-25,2020
 How to publish in peer-reviewed journals by Tress and Tress (Ferdinand Esser) July 1-3,2020
 Oltech: Welcome workshop June 11,2020
 Oltech: Good Scientific Practice- Protecting Scientific Integrity, June 24-25,2020

 Good Imaging Practice webinar for Fluorescence microscopy Jan 14,2021.
 RTG Workshop: Networking skills and self-marketing skills for women in academia (Sibyl Schädeli) Feb 5-9,
2021.
 Latex Workshop.
 Online symposium of cell sorting (Dr. rer. nat. Helge Meyer)
 RTG workshop: Basic Statistics with R
 Oltech: Advanced presentation techniques.

Acknowledgement

First and foremost, I would like to express my deepest gratitude to my supervisor, Prof. Dr. Karl-Wilhelm Koch, for giving me the opportunity to conduct my PhD research in this beautiful city of Oldenburg. His depth of knowledge, commitment to excellence, and invaluable support, constant guidance, and encouragement have been instrumental in shaping my research experience which has allowed to groom myself.

Secondly, I extend my sincere thanks to Prof. Dr. Michael Winkelhofer for his presence, guidance and being my second reviewer. I am truly honored. My thanks would not be enough for my collaborators Prof. Dr. Ilia Solov'yov, Dr. Fabian Schuhmann and Dr. Siu Ying Wong from the Institute of Physics (quant biolab) at University of Oldenburg for their valuable contributions and support during the collaboration and preparing the publication and further beyond.

Further my gratitude to the DFG for funding within the Research Training Group 1885, ''Molecular basis of sensory biology''. Without which I would have not got the Opportunity to do my research and meet my lovely fellow PhD batchmates. A special thanks to Dr. Kristin Tietje for being an amazing scientific coordinator and for immense support which she always ready to help even outside her comfort zone.

Further I would like to thank the backbones of Biochemistry group, Dr. Alexander Scholten to whom I go for my every doubts and learning all the techniques, Maike Möller for her help in cell culture and beyond and Uwe Maschmann to whom I always trouble with HPLC repairing and I extend my gratitude to former members (Jutta Appelt and Werner Säftel) for their help, guidance and support. I deeply thank all of them for the technical support and valuable advice related to scientific and personal- which extended far beyond the professional sphere.

Writing this acknowledgment brings back countless memories- arriving in Germany, the devastating loss of my father, and soon after, the world was struck by the COVID-19 pandemic, making life as a foreign in a new country even more challenging. However, the unwavering support from my family, my wonderful Biochemistry group and my dear friend, helped me navigate this difficult time. Dr. Sarah-Karina Zlomke, thank you for welcoming my first arrival to Oldenburg and patiently waiting for me until 2 AM despite the delays cause by Deutsche Bahn. A special mention to Dr. Katharina Görtemaker, who stood by me in my darkest moments. She made sure to take me out and distract me from my pain, and for that I will always be grateful. While Vanessa Schnarre really helped me navigate the exhausting room search. I am also deeply grateful to Dr. Chad Yee for assisting with paperwork and Dr. Nicole Ahrens for her unforgettable cakes- I miss them deeply. I would like to thank former members Dr. Yaoyu Chen, Dr. Haijia Wu, Dr. Charlotte Beelen, Dr. Seher Abbas, and Dr. Lena Dübbel, I appreciate our time together in lab. I wish the current fellow PhD students, Luisa Hintze, Patryk Bielski, Srdan Vujinovic, Ümmügülsüm Güzelsoy and Lars-Oliver Peters to do their best, I had a good time interacting with you all. I am thankful to all the bachelor and master students

with special mention to Annika Janßen, Eva Maria Breuer, Christina Kramer for being my late evening work buddies and shared wonderful experiences.

I am deeply aware that this achievement is the result of consistent support and motivation from many people over the years. I cannot forget to thank all my dear ones from CCMB, India – a big thank you.

A love filled thanks goes to my lovely batchmates and friends, Domna Zourelidou, Matteo Spinelli, Malien Laurien, Alejandra Acevedo Harnecker, Faiza Altaf, Dipti Ranjan Pradhan, and Anders Frederiksen for the wonderful time we spent together, laughter and the unforgettable memories we have created from the start of this journey, and I hope to carry them with me into the future.

Finally, my deepest gratitude goes to my family. Your love, patience, and countless sacrifices have been my greatest source of strength. The pain of not being able to attend my father's funeral- Late Shri Phulchand Prasad, still weighs heavily on my heart. I deeply regret not being there for my family during such a difficult time, yet, I know his blessings have guided me throughout this journey, lighting my path during the darkest moments. Despite the physical distance, the love and sacrifices of my father, Shri Phulchand Prasad, my mother, Ram Sundari Devi, my brothers, Ravinder Kumar Shah and Prasant Kumar, my sister-in-law, Sweety Devi, my sister Rima Devi, and my brother-in-law, Rakesh Prasad, and the love and best wishes from the kids and entire family have been a constant source of support which inspire me every single day. For that, I am forever grateful. This achievement is as much dedicated to my parents- it is theirs as much as it is mine.

Erklärung

Hiermit erkläre ich, dass ich die vorliegende Arbeit selbständig verfasst und keine anderen als die angegebenen Quellen und Hilfsmittel benutzt habe. Ich versichere, dass diese Arbeit weder als Ganzes noch in Teilen an einer anderen Universität zur Begutachtung in einem Promotionsverfahren vorgelegen hat und dass ich die Regeln guter wissenschaftlicher Praxis der Carl von Ossietzky Universität Oldenburg eingehalten habe. Weiterhin versichere ich, dass ich im Zusammenhang mit dem Promotionsvorhaben keine gewerblichen Vermittlungs- oder Beratungsleistungen (Promotionsberatung) in Anspruch genommen habe.

(Ort, Datum) (Manisha Kumari Shahu)